Homology and periods of algebraic varieties

Eric Pichon-Pharabod

September 12, 2024

Introduction

Historically, periods see their birth with the study of *elliptic integrals*

$$x \mapsto \int_a^x \frac{\mathrm{d}t}{\sqrt{P(t)}}\,, \tag{1}$$

where P is a polynomial of degree 3 or 4 without double roots. Such integrals have been of great interest to mathematicians, dating back to the 18th century with works of Giulio Fagnano, Leonhard Euler and Carl Friedrich Gauss. In particular, the latter showed that the inverse of a specific elliptic integral, the lemniscate function, had the remarkable property of having two periods. This turned out to be related to a general phenomenon appearing with elliptic curves: the inverse of an elliptic integral is a Weierstrass $\mathcal{P}$-function, which also show this biperiodic property. In fact, its periods ω_1, ω_2 are precisely given by the integral of the holomorphic 1-form ω on a basis of the 1-cycles γ_1, γ_2 of the elliptic curve:

$$\omega_i = \int_{\gamma_i} \omega\,. \tag{2}$$

In particular, one may realise the elliptic curve E as a complex torus obtained by taking the quotient the complex plane by the *lattice of periods*

$$\Lambda = \left\{ \int_\gamma \omega \mid \gamma \text{ is a 1-cycle of } E \right\} = \omega_1\mathbb{Z} \oplus \omega_2\mathbb{Z}\,. \tag{3}$$

This quotient space $\mathbb{C}/\Lambda$ is the *Jacobian* of the elliptic curve. Notably, it turns out that E and $\mathrm{Jac}(E)$ are isomorphic as abelian varieties.

For a complex algebraic curve C of arbitrary genus $g \geq 2$, the space of holomorphic forms $\Omega^1(C)$ is higher dimensional. One may nonetheless define the period lattice in a similar fashion

$$\Lambda = \left\{ \left(\int_\gamma \omega_1, \ldots, \int_\gamma \omega_g \right) \right\} \subset \mathbb{C}^g\,, \tag{4}$$

where $\omega_1, \ldots, \omega_g$ is a basis of $\Omega^1(C)$. Similarly, one may define the Jacobian $\mathrm{Jac}(C)$ of C as

$$\mathrm{Jac}(C) = \mathbb{C}^g/\Lambda\,. \tag{5}$$

One may see that, after choosing a base point $O \in C$, we have a well defined analytic map

$$C \to \mathrm{Jac}(C) : P \mapsto \left(\int_O^P \omega_1, \ldots, \int_O^P \omega_g \right)\,, \tag{6}$$

called the *Abel-Jacobi map*. The following theorem due to Torelli (1913) shows that the Jacobian of a curve, and thus its periods, characterise it entirely.

Theorem 1 (Torelli theorem for curves)**.** *Let C_1, C_2 be two smooth complex curves of genus g. Then* $\mathrm{Jac(C_1)}$ *and* $\mathrm{Jac(C_2)}$ *are isomorphic as polarised complex polytori if and only if C_1 and C_2 are isomorphic.*

This shows that the relation between the topological data of the singular homology and the algebraic data of the cohomology of the curves encoded in the integration pairing contains very precise information about the geometry of the curves. The numerical computation of periods gives access to an approximate representation of the Jacobian, which in turn leads to interesting invariants. This has for instance been used to compute some of the data related to genus 2 curves in the LMFDB (Booker et al., 2016), such as the endomorphism rings (Costa et al., 2019) or the Sato–Tate groups (Fité et al., 2012), which can be obtained by recovering integer relations between the periods.

In fact, this phenomenon generalises beyond curves to certain classes of higher dimensional varieties. In this setting, we define the k-th period matrix of a smooth complex variety $\mathcal{X}$ to be the matrix of the De Rham pairing $H_k(\mathcal{X}) \times H^k_{\mathrm{DR}}(\mathcal{X}) \to \mathbb{C}$ between singular homology and (algebraic) De Rham cohomology.

Theorem 2 (De Rham's theorem, de Rham (1931))**.** *Let $\mathcal{X}$ be a smooth compact manifold. The integration pairing between De Rham cohomology $H^k_{\mathrm{DR}}(\mathcal{X})$ and singular homology $H_k(\mathcal{X})$*

$$([\gamma], [\omega]) \mapsto \int_\gamma \omega,$$

is perfect. In particular it expresses $H^k_{\mathrm{DR}}(\mathcal{X})$ and $H_k(\mathcal{X})$ as duals of each other.

For curves, the De Rham cohomology splits in two subspaces of equal dimension, consisting respectively of *holomorphic* and *anti-holomorphic* differential 1-forms. Similarly, for a smooth complex projective variety $\mathcal{X}$ of dimension n, the middle algebraic DeRham cohomology admits a *Hodge decomposition*

$$H^n_{\mathrm{DR}}(\mathcal{X}) = H^{0,n}(\mathcal{X}) \oplus H^{1,n-1}(\mathcal{X}) \oplus \cdots \oplus H^{n,0}(\mathcal{X})\,. \tag{7}$$

When $H^k_{\mathrm{DR}}(\mathcal{X})$ is endowed with this additional Hodge-theoretical structure, the period matrix defines a remarkable continuous invariant of X which reflects the interplay between the complex algebraic structure and the topological one (P. A. Griffiths, 1968; Carlson et al., 2017).

For curves, the periods relate cycles of singular homology to holomorphic forms of De Rham cohomology, yielding the Jacobian. In higher dimensions, this relation similarly gives a polarisation to the Hodge structure of $\mathcal{X}$. As a generalisation to Torelli's theorem, so called *Torelli-type theorems* state that two algebraic varieties in the same class are isomorphic if and only if their polarised Hodge structures are. Here "class" is meant to be taken broadly: an example of a class would be smooth projective hypersurfaces of a given degree and dimension in $\mathbb{P}^n$ (see Donagi (1983)). Another example, which will be relevant in this thesis, is the class of complex algebraic K3 surfaces (Huybrechts, 2016).

Theorem 3 (Torelli-type theorem for K3 surfaces)**.** *Let $\mathcal{X}_1$ and $\mathcal{X}_2$ be two K3 algebraic surfaces. Then $\mathcal{X}_1$ is isomorphic $\mathcal{X}_2$ if and only if their polarised Hodge structures are isomorphic.*

Note that there are exceptions to Torelli-type theorems. Notably, smooth cubic surfaces are all isomorphic to $\mathbb{P}^2$ blown up at 6 points. In particular, they are rational surfaces, and their Hodge structure is thus contained in the middle piece $H^{1,1}(\mathcal{X})$. In particular all cubic surfaces have the same polarised Hodge structure.

Similarly to curves, periods of surfaces also lead to interesting invariants that are hard to compute by other means. For example, for an algebraic surface $\mathcal{X}$, Lefschetz's theorem on $(1,1)$-classes

(P. Griffiths and Harris (1978, p. 163), see also Theorem 55 below) relates the integer relations between the periods of $\mathcal{X}$ with the algebraic curves lying on $\mathcal{X}$. Integer relations can be recovered from numerical approximations of the periods thanks to lattice reduction algorithms (Lenstra et al., 1982, 1982; Håstad et al., 1989; Ferguson & Bailey, 1992). This leads to a practical algorithm for computing, heuristically, the Néron–Severi group of a surface in $\mathbb{P}^3(\mathbb{C})$ (Lairez & Sertöz, 2019). The appearance of explicit algebraic varieties in various fields of mathematics, such as Diophantine approximation (Beukers & Peters, 1984) or mathematical physics (Bloch et al., 2015), is a strong incentive for developing automatic methods to compute algebraic invariants. In a nutshell, periods linearise some aspects of algebraic varieties, at the cost of introducing transcendental functions through integration. This transcendental nature makes it difficult to compute exactly with periods, but large precision (typically hundreds or thousands of decimal digits) may allow to recover exact invariants (D. V. Chudnovsky & Chudnovsky, 1989).

Monodromy representation of families of varieties

Among these invariants, one we may recover exactly is the monodromy representation of a family of smooth varieties over the punctured projective line. This is a key ingredient in the reconstruction of the topological cycles necessary to compute the periods. It is also a relevant discrete invariant on its own, providing insight into the variation of the Hodge structure of the generic fibre induced by the fibration. A method, in some sense dual to the one presented in this thesis, for its computation up to a global sign was developed in Dettweiler and Wewers (2006b, 2006a), where the focus was to provide an algorithmic way to compute the *parabolic cohomology* using *braid computations*. This method was built upon in Kostiuk (2018) and Doran and Kostiuk (2023) to investigate the Hodge structures of certain towers of fibrations, in particular allowing for the study of the variations of Hodge structures of some polarised elliptic K3 surfaces. As an application of our methods, we will in this thesis compute the monodromy representation of certain K3-fibered Landau–Ginzburg models appearing in homological mirror symmetry.

Complex multiplication of K3 surfaces

Another invariant we will consider is whether a variety has complex multiplication. For a complex elliptic curve E, viewed as abelian varieties, this amounts to the existence of a non-trivial endomorphism $E \to E$ respecting both the group structure and the complex analytic structure. In terms of periods, having complex multiplication is equivalent to the τ-invariant (the ratio of the two holomorphic periods of E) being in a quadratic extension of $\mathbb{Q}$. This may be checked numerically. In higher dimensional Calabi–Yau manifolds, for K3 surfaces (which are no longer abelian varieties), the notion of complex multiplication is generalised to mean that the Hodge structure has non-trivial endomorphism, which again may be checked numerically in terms of periods. Such methods were already developed in Lairez and Sertöz (2019) and Elsenhans and Jahnel (2022) — in this thesis we apply them on new K3 surfaces for which the computations of periods were previously out of reach.

Feynman integrals

Periods appear in mathematical physics, and more precisely in perturbative quantum field theory, as Feynman integrals. Feynman diagrams are graphs modelling the ways in which particles may interact with each other. To each possible graph G, i.e., each possible interaction, is associated an amplitude quantifying the probability that this specific interaction effectively happens. This amplitude is given by a Feynman integral $\mathcal{I}_G$, of the form

$$\mathcal{I}_G = \int_{\mathbb{R}_+^n} \frac{\mathcal{U}_G^\nu}{\mathcal{F}_G^s} \Omega_0 \,, \tag{8}$$

where n is the number of *internal edges* of G and $\mathcal{U}_G$ and $\mathcal{F}_G$ are certain polynomials associated to G, called *Symanzik polynomials*, Ω_0 is the volume form of the ambiant space, and s and n are parameters. Presented as such, these integrals are not proper periods: first, the integration cycle has a boundary; second, in many cases, the variety defined by $\mathcal{U}_G$ and $\mathcal{F}_G$ is highly singular. Nonetheless, work of Bloch et al. (2006) and Brown (2017) show that one may obtain an understanding as a period by using a series of linear blow-ups in the ambiant projective space. While we will not focus on this aspect of Feynman integrals further in this thesis, we will showcase how our methods may apply to certain Feynman graphs by recovering geometric invariants of the Feynman integral associated to the a certain graph, the Tardigrade graph.

Related works

Algorithms for computing period matrices of curves (also known as Riemann matrices) are well established, with work by Deconinck and van Hoeij (2001), Swierczewski (2017), Bruin et al. (2019), Molin and Neurohr (2019), and Neurohr (2018), to name a few. The papers by Cynk and van Straten (2019) and Elsenhans and Jahnel (2022) are the first to tackle higher dimensions in some particular cases: double covers of $\mathbb{P}^3(\mathbb{C})$ ramified along 8 planes, and double covers of $\mathbb{P}^2(\mathbb{C})$ ramified along 6 lines, respectively. The algorithm by Sertöz (2019) is the first and only algorithm to tackle the case of smooth hypersurfaces in any dimension. It proceeds in the following way. Assume you wish to compute the period

$$\int_\gamma \frac{\Omega_2}{x^3+y^3+z^3+xyz} \,, \tag{9}$$

where γ is a cycle of the complement in $\mathbb{P}^2$ of the elliptic curve $E = V(x^3+y^3+z^3+xyz) \subset \mathbb{P}^2$ and $\Omega_2 = x\mathrm{d}y \wedge \mathrm{d}z - y\mathrm{d}x \wedge \mathrm{d}z + z\mathrm{d}y \wedge \mathrm{d}z$ is the volume form of $\mathbb{P}^2$. One way to proceed is to instead consider the *relative period*

$$\pi(t) = \int_{\gamma(t)} \frac{\Omega_3}{x^3+y^3+z^3+txyz} \,, \tag{10}$$

where $\gamma(t)$ is the deformation of γ with respect to t. Then the intial value we wanted to compute is $\pi(1)$. One may show that π is solution to a differential operator in t, its *Picard–Fuchs equation*

$$\mathcal{L} = (t^3+27)\partial_t^2 + 3t^2\partial_t + t \,. \tag{11}$$

Furthermore, the value of $\pi(0)$ is a period of the Fermat elliptic curve $V(x^3+y^3+z^3)$. From work of Pham (1965) and Sertöz (2019) formulae for the periods of Fermat hypersurfaces have been worked out in terms of values of Gamma functions. Therefore, using numerical analytic continuation software, one may obtain a numerical approximation with certified precision bounds of the period (9) from the data of the values of π at 0, as well as its derivatives' (which are also periods of the Fermat elliptic curve), and the Picard–Fuchs equation.

In practice, this method faces computational challenges when trying to compute the periods of hypersurfaces *far* (in terms of the defining equation) from the Fermat hypersurfaces. Indeed, for the case of quartic K3 surfaces in $\mathbb{P}^3$, the operators that need to be integrated have order 21 and, in practice, high degree, and current numerical analytic continuation software does not allow to integrate such operators in reasonable time. Furthermore, generalising this method to other types of varieties, say complete intersections, would require the equivalent of the Fermat variety in this setting — that is, a variety for which the periods are known, and from which the goal variety is attainable by deformation.

In a nutshell, the method presented in this text answers these two points. The main idea is to have a general way to obtain an effective description of the cycles, so that the periods may be integrated *ad hoc*. This is more efficient than deforming, in most cases, because the Picard–Fuchs equation related to the integration step that is internal to the variety is generally much smaller than the Picard–Fuchs differential equation associated to its deformation. For example, for a quartic K3 surface, the order drops from 21 to 4, or even 2 when the K3 surface is elliptic. This method is also more intrinsic, which gives it the potential to study varieties beyond smooth projective hypersurfaces.

Computing a period matrix of an algebraic variety requires to address, in one way or another, three computational problems reflecting the very definition of a period matrix: first, compute a basis of the homology, second, compute a basis of the cohomology, and, third, compute the coefficients of the pairing of (2) by numerical integration. Each of these problems is related to a different research field.

Singular homology

Computing a basis of the singular homology is a major obstacle. While there are algorithms for computing the homology of submanifolds of $\mathbb{R}^n$ from sample points (Niyogi et al., 2008; Cucker et al., 2018) they seem challenging to implement and exploit. A complex surface in $\mathbb{P}^3(\mathbb{C})$ is already a 4-dimensional real manifold in a 6-dimensional ambient space. Recent experiments suggest that the number of samples required to compute rigorously the homology is rather large (Di Rocco et al., 2020) compared to the Betti numbers. Furthermore, we do not know how to use such a data structure (homology computed from sample points) to efficiently compute periods.

In the case of curves, the problem reduces to computing the monodromy action on the roots of a univariate polynomial depending on a parameter (Tretkoff & Tretkoff, 1984). In the case of projective hypersurfaces, Sertöz' algorithm deals with the problem indirectly and only need a description of the homology of Fermat hypersurface, which has been worked out by (Pham, 1965).

De Rham cohomology

The algebraic De Rham cohomology, in the case of projective hypersurfaces, is well described by the Griffiths–Dwork reduction (P. A. Griffiths, 1969), both theoretically and computationally (see Section 3.1). There are also algorithms for the affine case (Oaku & Takayama, 1999), but we are not aware of any algorithm for the general case of a projective variety (not to mention that there are also projective varieties that are not naturally embedded in a projective space, like multiprojective varieties, or fibrations). In the case case of elliptic surfaces, work of Stiller (1987) allows to obtain a description of a piece of the cohomology of the surface together with the Hodge filtration from the Picard–Fuchs equation. Conveniently, this piece is sufficient to recover the full Hodge structure in the case of elliptic K3 surfaces.

Numerical integration

For the integration step, a direct approach seems possible. If the homology basis is sufficently explicit, and if we can numerically evaluate the differential forms defining the cohomology basis at any given point, we can certainly compute the pairing of (2).

However we aim for high precision, so all finite-order quadrature methods (like Simpson's rule or Monte-Carlo algorithms) are ruled out because they have exponential complexity with respect to precision. The periods are n-dimensional integrals of algebraic functions, where n is the complex dimension of X. Assuming that we can formulate them as integrals over a n-simplex, or $[0,1]^n$, we can compute them with the Gauss–Legendre quadrature formula. We expect a $p^{n+1+o(1)}$ complexity with respect to the precision p. For computing the periods of curves, this is a $p^{2+o(1)}$ complexity and this method is the most commonly used. In our method, we use numerical analytic continuation of differentially finite functions to compute integrals. The complexity is quasilinear with respect to precision, $p^{1+o(1)}$, thanks to binary splitting. Numerical analytic continuation is also what we use to compute monodromy actions, so it is natural to use it for integration as well. Note however that, in our typical computations (involving large degree differential operators and large but not extreme precision), we are far from the threshold where binary splitting gets better than $p^{2+o(1)}$ methods.

Contributions

We provide a general framework for computing numerical approximations of the period matrices of certain projective varieties, and detail the application to the case of complete intersections and elliptic surfaces. Let $\mathcal{X} \subset \mathbb{P}^n(\mathbb{C})$ be a projective variety. A major obstacle in the computation of the period matrices for $\mathcal{X}$ is the lack of algorithms for computing an explicit description of the singular homology of $\mathcal{X}$. By "explicit", we mean explicit enough to be able to perform numerical integration over a basis of cycles. We provide an algorithm for computing at the same time:

1. an explicit basis of the singular homology of X;
2. a numerical approximation, with rigorous error bounds, of the period matrix of $\mathcal{X}$ with respect to this homology basis, and the Griffiths–Dwork cohomology basis.

With respect to precision only, the complexity of the algorithm is quasilinear: computing twice as many digits takes roughly twice as much time. Note that, as a specificity of projective complete intersections, only the n-th period matrix of $\mathcal{X}$ is interesting, the other ones are trivial (1×1 or 0×0 matrices).

The algorithm may be used to compute the period matrix of any complete intersection. The algorithm relies on a fibration of the variety $\mathcal{X} \to \mathbb{P}^1$ over the projective line, where the periods of the generic fibre $\mathcal{X}_t = f^{-1}(t)$can be computed. In the case of elliptic surfaces, this fibration is part of input data. In the other considered cases, it is obtained by considering a one-parameter family of hyperplane sections $X \cap H_t$, following the principles of Picard–Lefschetz theory (Lefschetz, 1924; Lamotke, 1981). An important step of the algorithm is the computation of the monodromy action induced by this family of sections on the homology $H_{n-1}(\mathcal{X}_b)$ of one section (above a chosen basepoint $b \in \mathbb{P}^1$). We perform this computation through duality with De Rham cohomology, using the period matrix of $\mathcal{X}_b$ which can be obtained by induction on dimension as $\dim \mathcal{X}_b = \dim \mathcal{X} - 1$.

To perform the numerical integration, we reduce to one-variable contour integrals of rational multiples of the periods of $H_{n-1}(\mathcal{X}_t)$. Since these periods are solutions of a Picard–Fuchs differential equation, which we can compute explicitly, we can perform the integration using general algorithms for integration of *differentially finite functions* (van der Hoeven, 1999; Mezzarobba, 2010). These algorithms provide rigorous error bounds with quasilinear complexity with respect to precision.

On the practical side, we have implemented the above algorithm in SageMath (The Sage Developers, 2023), together with the computation of related invariants (Picard rank, Néron–Severi group, endomorphism ring) for the cases of hypersurfaces, elliptic surfaces, and double covers of a projective space ramified along a smooth hypersurface. This implementation can be found in the package `lefschetz-family`[1]. We are able to compute the periods of the holomorphic form of a smooth quartic K3 surface in $\mathbb{P}^3(\mathbb{C})$ defined over $\mathbb{Q}$ in, typically, about an hour on a laptop, with 300 decimal digits of precision. The computation is much faster for elliptic K3 surface, taking

[1] https://gitlab.inria.fr/epichonp/lefschetz-family

around 15 seconds to obtain the same result, but the method is restricted to the computation of the holomorphic periods. For K3 surfaces given as double covers of $\mathbb{P}^2$ ramified along a sextic, the same computation takes around 2 minutes.

Naturally, the actual running time depends on many parameters, including the bitsize of the coefficients of the defining equation, and the conditioning of some numerical steps, see Section 5.2 for concrete examples. The computation of the holomorphic periods of quartic K3 surfaces was not feasible in reasonable time with the previously known algorithm (Sertöz, 2019), except for some quartic surfaces defined by sparse polynomials.

We then apply this method to reproduce recent results and provide evidence, both numerical and exact, of conjectures in mirror symmetry and arithmetic geometry. This showcases how this tool may be used to study phenomenology in algebraic geometry, and hopefully bring insight into open questions.

Content

Let $f\colon \mathcal{X} \to \mathbb{P}^1(\mathbb{C})$ be a morphism of smooth projective varieties. Let $b \in \mathbb{P}^1$ be a generic base point. Let $\Sigma \subset \mathbb{P}^1$ be the set of all t such that $\mathcal{X}_t = f^{-1}(t)$ is singular. The fibration induces an action of $\pi_1(\mathbb{P}^1 \setminus \Sigma, b)$ on $H_{n-1}(\mathcal{X}_b)$. In Chapter 2, we show, mostly following Lamotke (1981), how this monodromy action determines the homology of $\mathcal{X}$ in an explicit way in terms of the homology groups of $\mathcal{X}_b$. Chapter 3 describes the computational methods that are used to turn the results of Chapter 2 into a working algorithm. Chapter 4, Chapter 6, Chapter 7 provide the details pertaining to the cases of respectively complete intersections, elliptic surfaces and double cover of $\mathbb{P}^2$ ramified along a smooth sextic. Chapter 5 details explicit computations in the case of quartic surfaces, and provides insight into the computational complexity. Chapter 8 and Chapter 9 provide examples of application to respectively mirror symmetry and arithmetic geometry. Finally, Chapter 10 gives a way to compute the monodromy representation of a fibration relying on braids, as a more combinatorial alternative to the methods of Chapter 3.

Contents

M. Picard a donné à ces intégrales le nom de périodes; je ne saurais l'en blâmer puisque cette dénomination lui a permis d'exprimer dans un langage plus concis les intéressants résultats auxquels il est parvenu. Mais je crois qu'il serait fâcheux qu'elle s'introduisît définitivement dans la science et qu'elle serait propre à engendrer de nombreuses confusions.

Mr. Picard gave to these integrals the name of periods; I cannot blame him as this denomination allowed him to express in a more concise language the interesting results which he reached. However I believe it would be unfortunate if it were to be definitively introduced into science, and would be likely to generate many confusions.

Henri Poincaré
Sur les résidus d'intégrales doubles, 1886

Part I

Computation of periods

Chapter 1

Preliminaries

In the entirety of the thesis, unless explicitly stated otherwise, $H_n(\mathcal{X})$ will denote the singular homology with integral coefficients, while $H^n_{\mathrm{DR}}(\mathcal{X})$ will designate the algebraic DeRham cohomology with complex coefficients.

1.1 Local systems and the Gauss-Manin connection

In this section we recall the formalism of local systems, which conveniently encodes the data of the fibration that is necessary for our investigation. To the interested reader, we recommend checking Doran and Kostiuk (2023) and Kostiuk (2018) for further reading on the topic, notably in the case of elliptic surfaces.

Let U be a topological space and R a commutative ring.

Definition 1. *A* local system *of R-modules on U is a locally constant sheaf of free R-modules of finite rank.*

We denote by $\mathcal{V}_x$ the stalk at $x \in U$, and by s its rank. Given a basepoint $b \in U$, the fundamental group $\pi_1(U, b)$ acts on $\mathcal{V}_b$.

Definition 2. *The* monodromy representation *of $\mathcal{V}$ is the group representation $\rho : \pi_1(U, b) \to \mathrm{GL}(\mathcal{V}_b)$.*

In practice we will be interested in cases where U is the projective line punctured at finitely many points $c_1, \dots, c_r$. In that case $\pi_1(U, b)$ is a free group generated by $r - 1$ elements $\gamma_1, \dots, \gamma_{r-1}$ consisting of simple counterclockwise loops around $c_1, \dots, c_{r-1}$ respectively. To preserve the symmetry, we will also consider the simple loop around γ_r, and we assume that these loops are chosen so that their composition is trivial:

$$\ell_r \dots \ell_1 = 1 \,, \tag{1.1}$$

where the product is the element that goes through ℓ_1, then ℓ_2, etc. up to ℓ_r.

Then, fixing a basis $\gamma_1, \dots, \gamma_s$ of $\mathcal{V}_b$, the monodromy representation can be encoded into a r-tuple of $s \times s$ matrices $M_1, \dots, M_r$, such that

$$M_r \dots M_1 = I_s \,, \tag{1.2}$$

where I_s is the identity matrix of size s. M_s acts by multiplication on the left on vectors $(a_1, \dots, a_s)$ representing an element $\gamma = a_1\gamma_1 + \cdots + a_s\gamma_s \in \mathcal{V}_b$.

The Gauss-Manin connection and Picard–Fuchs equations

Local systems are very closely related to flat connections. Let $U = \mathbb{P}^1 \setminus \Sigma$ denote the projective line punctured at finitely many points $\Sigma = \{c_1, \dots, c_r\}$. Let $\mathcal{V}$ be a locally constant sheaf on U.

Definition 3. *A* connection *on $\mathcal{F}$ is a $\mathbb{C}$-linear homomorphism*

$$\nabla \colon \mathcal{F} \to \mathcal{F} \otimes \Omega^1_U \tag{1.3}$$

satisfying the Leibniz rule

$$\nabla(fs) = \mathrm{d}f \otimes s + f\nabla s\,. \tag{1.4}$$

A connection extends to a $\mathbb{C}$-linear map $\nabla_i : \mathcal{F} \otimes \Omega^i_U \to \mathcal{F} \otimes \Omega^{i+1}_U$; it is said to be flat *(or* integrable*) when $\nabla_1 \circ \nabla = 0$*

If $\mathcal{F}$ is a local system on U, then we can define a flat connection on $\mathcal{O}_U \otimes \mathcal{F}$ by setting $\nabla(f \otimes s) = \mathrm{d}f \otimes s$. This is known as the *Gauss-Manin connection* associated to the local system $\mathcal{F}$. Conversely a flat connection ∇ defines a local system $\mathcal{F}$ by $\mathcal{F} = \ker \nabla$.

Let ω be a section of $\mathcal{O}_U \otimes \mathcal{V}_t$. As $\mathcal{V}_t$ has finite rank, there exist an integer s and rational functions $f_0, \dots, f_s \in \mathcal{O}_U$ such that

$$f_0\omega + f_1\nabla\omega + \cdots + f_s\nabla^s\omega = 0\,. \tag{1.5}$$

When s is minimal, when the f_i's are polynomials and coprime, then the differential operator $\mathcal{L} = f_0 + f_1\nabla + \cdots + f_s\nabla^s$ is called the *Picard–Fuchs operator* or *Picard–Fuchs equation* of ω. As we will see in Section 3.4, the Picard–Fuchs operator of a well chosen section ω encodes a lot of information about the local system. In particular, it will provide us with a means to efficiently compute the monodromy representations $\mathcal{H}^n(\mathcal{X}/U, \mathbb{Z})$. For now, let us simply state a regularity theorem for Picard–Fuchs operators:

Theorem 4. *Any Picard–Fuchs operator stemming from a variation of Hodge structure is Fuchsian, i.e., at every point $s \in \mathbb{P}^1$ admits a basis of solutions of the form*

$$(t-s)^\nu(\sigma_0(t) + \sigma_1(t)\log(t-s) + \cdots + \sigma_r(t)\frac{\log(t-s)^k}{k!}) \quad \text{with } \nu \in \mathbb{Q}\,, \tag{1.6}$$

where the σ_i's are holomorphic functions around s.

Variation of local systems

We will also be interested in the varying a local system with respect to a parameter: the configuration of the points $c_1, \dots, c_r$ will vary with the parameter, and this will induce a monodromy action on $\pi_1(U, b)$, and thus on $\mathcal{V}$. This is formalised by the notion of *variation of local systems*.

Let A be a connected complex manifold and $r \geq 3$.

Definition 4. *An r-configuration over A is a smooth proper morphism $f \colon T \to A$ of complex manifolds together with a smooth relative divisor $D \subset \mathcal{X}$ such that the fibres $T_t = f^{-1}(t)$ are isomorphic to $\mathbb{P}^1$ and $D \cap T_t$ consists of r pairwise distinct points.*

Definition 5. *Fix an r-configuration (T, D) over A and a basepoint $a_0 \in A$. Define $U = T \setminus D$ and set $U_t = (T \setminus D) \cap \mathcal{X}_t$ and assume $U_0 \simeq \mathbb{P}^1 \setminus \{c_1, \dots, c_r\}$. Let $\mathcal{V}_0$ be a local system on U_{a_0}. A* variation of the local system $\mathcal{V}_0$ over (T, D) *is a local system $\mathcal{V}$ on U whose restriction to U_{a_0} is identified with $\mathcal{V}_0$.*

In practice we will be interested in the following construction: We will be considering a one parameter algebraic family $\mathcal{X}_u$ of varieties equipped with a projection $f_u : \mathcal{X}_u \to \mathbb{P}^1$. For a fixed generic u, the critical values of f_u will be the roots of a minimal squarefree polynomial P. The coefficients of P are themselves polynomial in the parameter u. We thus consider $P \in \mathbb{Q}[u, t]$. Let $\tilde{\Sigma}$ be the set of $u \in \mathbb{C}$ such that the polynomial $t \mapsto P(u, t)$ has distinct roots. In other words, $\tilde{\Sigma}$ is the union of the set of roots of the discriminant $\operatorname{discr}_u P$ in u of P with the set of roots of the leading coefficient in t of P. We then set $A = \mathbb{C} \setminus \tilde{\Sigma}$, $T = \mathbb{P}^1 \times A$ and $D = \{(u, t) \in \mathbb{P}^1 \times A \mid P(u, t) = 0\}$. The projection $D \to A$ is a locally trivial fibration. The deformation of the fibre D_u with respect to u will induce a braid on r strands, which in turn will induce an automorphism of the local system $\mathcal{V}$: the monodromy. This will be the topic of Chapter 10.

1.2 Hodge structure

Let n be an integer.

Definition 6. *A* Hodge structure *of weight n is a free $\mathbb{Z}$-module of finite rank $H_\mathbb{Z}$ together with a decomposition of its complexification $H_\mathbb{C} \stackrel{\text{def}}{=} H_\mathbb{Z} \otimes \mathbb{C}$ in a direct sum of subspaces $H_\mathbb{C} = \bigoplus_{k=0}^n H^{k,n-k}$ such that*

$$\forall p, q \in \mathbb{Z}, \qquad p + q = n \implies H^{p,q} = \overline{H^{q,p}} \tag{1.7}$$

We will denote the dimension of these vector spaces as $h^{p,q} = \dim H^{p,q}$.

Equivalently, we may consider Hodge filtrations:

Definition 7. *A* Hodge filtration *of weight n is a $\mathbb{Z}$-module $H_\mathbb{Z}$ together with a finite decreasing filtration of its complexification $H_\mathbb{C}$ by subspaces $\mathcal{F}^i H$ such that*

$$\forall p, q \in \mathbb{Z}, \qquad p + q = n + 1 \implies H_\mathbb{C} = \mathcal{F}^p H \oplus \overline{\mathcal{F}^q H}\,. \tag{1.8}$$

One may check that these two concepts are equivalent with the relationship

$$H^{p,q} = \mathcal{F}^p H \cap \overline{\mathcal{F}^q H} \qquad \text{and} \qquad \mathcal{F}^p H = \bigoplus_{i=p}^{n} H^{p,n-p}\,. \tag{1.9}$$

Definition 8. *A* polarized Hodge structure *of weight n is the data of a Hodge structure $H_\mathbb{Z}, H^{p,q}$ of weight n together with a bilinear form $\langle \cdot, \cdot \rangle : H_\mathbb{Z} \times H_\mathbb{Z} \to \mathbb{Z}$, such that:*

- $\langle \gamma_1, \gamma_2 \rangle = (-1)^n \langle \gamma_2, \gamma_1 \rangle'$ *for all γ_1, γ_2 in $\mathcal{H}_Z$*
- $\langle \gamma_1, \gamma_2 \rangle = 0$ *for $\gamma_1 \in H^{p,n-p}$ and $\gamma_2 \in H^{n-q,q}$ with $p \neq q$*

The middle De Rham cohomology of an n-dimensional complex projective variety $\mathcal{X}$ inherits a Hodge filtration from its Kähler manifold structure. The De Rham theorem embeds the complexification of the dual of the singular homology $H_n(\mathcal{X}, Z) \otimes \mathbb{C}$ in $H^n_{\mathrm{DR}}(\mathcal{X}, \mathbb{C})$ and the intersection product induces a polarisation. It turns out that the polarised Hodge structure often carries lots of information about the $\mathcal{X}$. This is the content of Torelli-type theorems. In order to be more precise, we first need to define *Hodge isometries.* Let ${}^1H_\mathbb{Z}$ and ${}^2H_\mathbb{Z}$ be two polarised Hodge structures.

Definition 9. *A* Hodge isometry *between ${}^1H_\mathbb{Z}$ and ${}^2H_\mathbb{Z}$ is a $\mathbb{Z}$-linear map $h\colon {}^1H_\mathbb{Z} \to {}^2H_\mathbb{Z}$ such that*

- *it respects the polarization: $\langle h(\gamma_1), h(\gamma_2) \rangle_2 = \langle \gamma_1, \gamma_2 \rangle_1$;*
- *the induced map $h_\mathbb{C}\colon {}^1H_\mathbb{C} \to {}^2H_\mathbb{C}$ respect the Hodge structure: for all p, q $h({}^1H^{p,q}) = {}^2H^{p,q}$*

We also define *Hodge bases*, which are bases respecting the Hodge filtration. Let $r = \dim H_{\mathbb{C}}$ and $r_p = \dim \mathcal{F}^p H$.

Definition 10. *A* Hodge basis *of $H_{\mathbb{C}}$ is a basis $\omega_1, \dots, \omega_r$ of $H_{\mathbb{C}}$ such that*

$$\langle \omega_1, \dots, \omega_{r_p} \rangle = \mathcal{F}^p H \,. \tag{1.10}$$

1.3 Variation of Hodge structures

We will now consider a smooth map between projective varieties $\pi\colon \mathcal{X} \to U$ and set $n = \dim \mathcal{X} - \dim U$. The deformation of a smooth fibre with respect to the parameter in U will be of major relevance to the work presented in this thesis. In particular we will be interested in the *variation of the Hodge structure* of the middle cohomology group of the fibre.

Definition 11. *A* polarized variation of Hodge structure *on U of weight n is the data of:*

- *a local system $\mathcal{H}_{\mathbb{Z}}$ of free $\mathbb{Z}$-modules of finite rank on U,*
- *a finite decreasing filtration $\mathcal{F}^*$ of $H_{\mathbb{Z}} \otimes \mathcal{O}_U$ by holomorphic subvectormodules such that $\mathcal{F}^*$ induces a Hodge filtration on each fibre $\mathcal{H}_t$ of $\mathcal{H}_{\mathbb{Z}}$,*
- *a flat non-degenerate integral bilinear form on $\mathcal{H}_{\mathbb{Z}}$ inducing a polarisation of each fibre $\mathcal{H}_t$,*

further satisfying Griffiths transversality:

$$\nabla \mathcal{F}^p \subset \mathcal{F}^{p-1} \otimes \Omega^1_U \,, \tag{1.11}$$

where ∇ is the Gauss-Manin connection on $\mathcal{H}_{\mathbb{Z}}$. The flatness of the bilinear form means that $\mathrm{d}\langle s, s' \rangle = \langle \nabla s, s' \rangle + \langle s, \nabla s' \rangle$.

The fibration π can induces a variation of Hodge structure on the *middle relative De Rham cohomology group of $\mathcal{X}$*. The middle De Rham cohomology groups of the fibres of π can be encoded into a sheaf $\mathcal{H}(\mathcal{X}/U)$ of $\mathcal{O}_U$-modules, called the relative De Rham cohomology of the fibration. It can be defined in general as the n-th derived functor on the sheaf of U-differentials on $\mathcal{X}$ (Katz & Oda, 1968). In all the cases we will consider, U will be a subset of the complex projective line. When relevant, we will offer a more explicit (i.e., less categorical) definition of this sheaf of $\mathbb{C}(t)$-modules.

Remark 5. *This should not be confused with the* relative homology of a pair (X, A)*, which does not concern fibrations. Both are relevant and will be used throughout the thesis. It should be most of the time clear when one is meant instead of the other. We will be careful to be clear when ambiguity may arise.*

1.4 De Rham cohomology

We now have the vocabulary to state everything we want about De Rham cohomology. We first start by defining it.

Definition

Let $\mathcal{X}$ be a smooth complex projective variety of dimension n and denote by $\mathcal{O}_{\mathcal{X}}$ its ring of regular functions. We may define its sheaf $\Omega^1_{\mathcal{X}}$ of differential 1-forms, dual to the tangent bundle of $\mathcal{X}$

Further define the sheaves of differential i-th forms $\Omega^i_{\mathcal{X}} = \bigwedge^i \Omega^1_{\mathcal{X}}$ (the i-th exterior power of $\Omega^1_{\mathcal{X}}$). Finally, define $d : \Omega^i_{\mathcal{X}} \to \Omega^{i+1}_{\mathcal{X}}$ the exterior differential. This gives rise to the *De Rham complex* of $\mathcal{X}$

$$0 \to \mathcal{O}_{\mathcal{X}} \to \Omega^1_{\mathcal{X}} \to \cdots \to \Omega^{2n}_{\mathcal{X}} \to 0\,. \tag{1.12}$$

The cohomology of this complex gives rise to the *De Rham cohomology groups* $H^i_{\mathrm{DR}}(\mathcal{X})$ of $\mathcal{X}$, which are finitely generated $\mathbb{Q}$-vector spaces.

The complex structure of $\mathcal{X}$ provides it with the structure of a Kähler $2n$-manifold. In particular, $\Omega^1_{\mathcal{X}}$ is generated by *holomorphic* differentials $\mathrm{d}z_1, \ldots, \mathrm{d}z_n$ and their *antiholomorphic* counterparts $\overline{\mathrm{d}z_1}, \ldots, \overline{\mathrm{d}z_n}$. In particular this gives rise to a decomposition

$$\Omega^k_{\mathcal{X}} = \Omega^{0,k}_{\mathcal{X}} \oplus \Omega^{1,k-1}_{\mathcal{X}} \oplus \cdots \oplus \Omega^{k,0}_{\mathcal{X}}\,, \tag{1.13}$$

where $\Omega^{k,0}_{\mathcal{X}}$ is the space of holomorphic differential k-forms, $\Omega^{0,k}_{\mathcal{X}}$ that of antiholomorphic k-forms, and $\Omega^{k,k'}_{\mathcal{X}} = \Omega^{k,0}_{\mathcal{X}} \wedge \Omega^{0,k'}_{\mathcal{X}}$.

This induces a similar decomposition, called the *Hodge decomposition* on the cohomology groups:

$$H^k_{\mathrm{DR}}(\mathcal{X}) = H^{0,k}_{\mathrm{DR}}(\mathcal{X}) \oplus \cdots \oplus H^{k,0}_{\mathrm{DR}}(\mathcal{X})\,. \tag{1.14}$$

This decomposition equips the k-th De Rham cohomology group with a Hodge structure of weight k.

Singular homology and the De Rham theorem

The singular homology of $\mathcal{X}$ can be similarly defined from the complex of singular chains on X. A *singular n-simplex* is a continuous map $\sigma : \Delta^n \to \mathcal{X}$, where Δ^n is the standard n-simplex. The space $C_n(\mathcal{X})$ of n-chains on $\mathcal{X}$ is then defined to be space of formal sums of singular simplices with integral coefficients.

Simplices come with a boundary, denoted $\delta\sigma$. It is the formal sum of the singular $(n-1)$-simplices induced by the ordered faces of Δ^n, with a certain sign. It induces a differential $\partial\colon C_n(X) \to C_{n-1}(\mathcal{X})$, and one may show that $\partial \circ \partial = 0$. We thus obtain the *singular complex* of $\mathcal{X}$

$$0 \to C_{2n}(\mathcal{X}) \to \cdots \to C_0(\mathcal{X}) \to 0\,. \tag{1.15}$$

We derive the *singular homology groups* $H_n(\mathcal{X})$ from this complex, which again can be proven to be finitely generated $\mathbb{Z}$-modules. Elements of $H_n(\mathcal{X})$ are called *n-cycles.*

One may integrate an n-form $\omega \in \Omega^n_{\mathcal{X}}$ on an n-simplex σ using to the following formula:

$$\int_\sigma \omega \stackrel{\mathrm{def}}{=} \int_{\Delta^n} \sigma^*\omega \in \mathbb{C}\,, \tag{1.16}$$

where $\sigma^*\omega$ is the pullback of ω by σ. By linearity this extends to a bilinear map $C_n(\mathcal{X}) \times \Omega^n_{\mathcal{X}} \to \mathbb{C}$. One may show as a consequence of Stokes' theorem that this map induces a bilinear pairing between the singular homology and De Rham cohomology groups of $\mathcal{X}$:

$$H_n(\mathcal{X}) \times H^n_{\mathrm{DR}}(\mathcal{X}) \to \mathbb{C} : (\gamma, \omega) \mapsto \int_\gamma \omega\,. \tag{1.17}$$

We then have the following theorem due to Georges de Rham:

Theorem 6 (De Rham theorem, de Rham (1931))**.** *The integration pairing $H_n(\mathcal{X}) \times H^n_{\mathrm{DR}}(\mathcal{X}) \to \mathbb{C}$, $\gamma, \omega \to \int_\gamma \omega$ is perfect. In other words, it establishes $H^n_{\mathrm{DR}}(\mathcal{X})$ as the dual of (the complexification of) $H_n(\mathcal{X})$.*

Remark 7. *More precisely, De Rham proved that this pairing was perfect for the* analytic *De Rham cohomology, derived from the complex of* smooth *differential forms; Grothendieck later proved that the algebraic and analytic De Rham cohomology were naturally isomorphic.*

We will denote by $H^n(\mathcal{X}, \mathbb{Z}) \subset H^n_{\mathrm{DR}}(\mathcal{X})$ the embedding of the singular homology of $\mathcal{X}$ in (the complexification of) its De Rham cohomology.

The intersection product

Let $\gamma_1, \gamma_2 \in H_n(\mathcal{X})$. Assume we may find n-chains A_1 and A_2 representing γ_1 and γ_2, such that their intersection is transverse. We then define the intersection product $\langle A_1, A_2 \rangle \in \mathbb{Z}$ to be their number of intersection points, counted with orientation. One may show that this number does not depend on the choice of representatives A_1 and A_2 but only on their homology class. In particular, it extends to a bilinear pairing

$$\langle \cdot, \cdot \rangle \colon H_n(\mathcal{X}) \times H_n(\mathcal{X}) \to \mathbb{Z} \tag{1.18}$$

called the *intersection product* of $H_n(\mathcal{X})$. It equips $H_n(\mathcal{X})$ (and *a fortiori* $H^n(\mathcal{X}, \mathbb{Z})$) with the structure of a *non-degenerate unimodular integral lattice.* Furthermore, the embedding of $H_n(\mathcal{X})$ in $H^n_{\mathrm{DR}}(\mathcal{X})$ equips it with the structure of a polarised Hodge structure.

Relative De Rham cohomology

When $\pi \colon \mathcal{X} \to U$ is a *projective family* (meaning that $\mathcal{X}$ locally embeds into $\mathbb{P}^1 \times U$, with the family given by the projection onto the second factor), one may similarly define the sheaf of *relative De Rham cohomology groups* $\mathcal{H}^*(\mathcal{X}/U)$: it is a locally constant sheaf of $\mathcal{O}_U$-modules of finite rank. The fibre above u is given by De Rham cohomology groups $H^*_{\mathrm{DR}}(\pi^{-1}(u))$. Furthermore, the inclusion $H^n(\mathcal{X}, \mathbb{Z}) \subset H^n_{\mathrm{DR}}(\mathcal{X})$ glues to yield a subsheaf $\mathcal{H}^n(\mathcal{X}/U, \mathbb{Z}) \subset \mathcal{H}^n(\mathcal{X}/U)$ of $\mathbb{Z}$-modules: it defines a local system. We may thus define the Gauss-Manin connection of $\mathcal{H}^n(\mathcal{X}/U)$ as the unique connection ∇ such that $\ker \nabla = \mathcal{H}_n(\mathcal{X}/U, \mathbb{Z})$.

All in all, we see that $\mathcal{H}^n(\mathcal{X}/U)$ is equipped with a variation of polarised Hodge structures, where the polarisation is induced by the intersection product on $\mathcal{H}^n(\mathcal{X})$.
The monodromy representation of $\mathcal{H}(\mathcal{X}/U)$ at b is contained in the subgroup of $\mathrm{GL}(H^n(\mathcal{X}_b, Z))$ fixing the intersection product. In particular, the eigenvalues of the monodromy maps are all roots of unity.

1.5 K3 surfaces

Among algebraic curves, elliptic curves are the ones exhibiting the most structure. Their set of points have a natural group structure, the Mordell–Weil group. Their moduli space is well understood.

Thus one may naturally be inclined to find a generalisation of such varieties to higher dimensions. One possible direction which we will not expand on is that of abelian varieties, i.e., varieties equipped with a group structure. Another one that is of interest to us is that of *Calabi-Yau* varieties.

Along with complex tori, K3 surfaces are the Calabi-Yau varieties of dimension 2. Their topology is well studied. They are all diffeomorphic, and their middle homology has rank 22. Its lattice structure has signature $19, 3$, and is even. By the classification of unimodular indefinite even lattices, it is isomorphic to the *standard K3 lattice.*

Definition 12. *The* standard K3 lattice *is the unimodular even lattice*

$$\Lambda_{K3} = E_8(-1) \oplus E_8(-1) \oplus H \oplus H \oplus H\,. \tag{1.19}$$

Beyond their topology, K3 surfaces exhibit interesting algebro-geometric invariants. Let $\mathcal{X}$ be a complex K3 surface. Its middle Hodge numbers are $h^{2,0} = h^{0,2} = 1$ and (consequently) $h^{1,1} = 20$. In particular its polarised Hodge structure is entirely determined by its holomorphic periods. Let $\omega \in H^{2,0}_{\mathrm{DR}}(\mathcal{X})$ be a generator of the space of rational holomorphic 2-forms.

Definition 13. *The* holomorphic period map *of $\mathcal{X}$ is the map*

$$\pi_\omega \colon H_n(\mathcal{X}) \to \mathbb{C} : \gamma \mapsto \int_\gamma \omega\,. \tag{1.20}$$

It is only defined up to the choice of ω, i.e., up to multiplication by a scalar in $\mathbb{C}^\times$.

Definition 14. *The* Néron–Severi group *or* Picard lattice *of $\mathcal{X}$ is the subspace*

$$\mathrm{NS}(\mathcal{X}) = H^2(\mathcal{X}, \mathbb{Z}) \cap H^{1,1}(\mathcal{X})\,. \tag{1.21}$$

Its rank ρ is called the Picard rank *of $\mathcal{X}$.*

The Picard lattice is an algebraic invariant of the K3 surface, which may be recovered by computing the periods It is equipped with a lattice structure, which by the Hodge index theorem has signature $1, \rho - 1$ By the Lefschetz $(1,1)$ theorem, this subspace is precisely the kernel of the holomorphic period map. In particular this will provide us with a means to recover the Néron–Severi group from numerical approximations of periods of $\mathcal{X}$.

Theorem 8 (Lefschetz $(1,1)$ theorem for K3 surfaces)**.**

$$\mathrm{NS}(\mathcal{X}) = \ker \pi_\omega\,. \tag{1.22}$$

The Torelli theorem for K3 surface (see Huybrechts (2016)) states that the polarised Hodge structure of a K3 surface determines its isomorphism class. In particular, this means that, given a choice of an isometry $H_2(\mathcal{X}) \simeq \Lambda_{K3}$, we may associate a point in

$$\Omega_{K3} \overset{\mathrm{def}}{=} \{[\omega] \in \mathbb{P}(\Lambda_{K3} \otimes \mathbb{C}) \mid \langle \omega, \omega \rangle = 0, \langle \omega, \overline{\omega} \rangle > 0\}\,, \tag{1.23}$$

where the conditions on $\langle \omega, \omega \rangle$ and $\langle \omega, \overline{\omega} \rangle$ follow from Hodge theoretic reasons. The 20-dimensional complex manifold Ω_{K3} is the *period space* of K3 surfaces. The Torelli theorem can then be restated as such:

Theorem 9 (Torelli theorem for K3 surfaces)**.** *Two K3 surfaces $\mathcal{X}_1$ and $\mathcal{X}_2$ are isomorphic if and only if there exist a choice of isometries $H_2(\mathcal{X}_1) \simeq \Lambda_{K3}$ and $H_2(\mathcal{X}_2) \simeq \Lambda_{K3}$ that send the holomorphic forms to the same point in Ω_{K3}.*

The tools we will develop in this thesis allow to compute a numerical approximation of the point in the period space corresponding to a K3 surface given by its defining equation. These will appear in three different forms throughout this thesis, in decreasing computational complexity:

- as quartic surfaces in $\mathbb{P}^3$, yielding a genus 3 fibration;
- as double covers of $\mathbb{P}^2$ ramified along a sextic curve (or equivalently complete intersections of degree $(2,3)$ in $\mathbb{P}^4$), yielding a genus 2 fibration;
- or finally as elliptic surfaces, i.e., genus 1 fibrations.

For (much!) more thorough overview of K3 surfaces, we encourage the interested reader to turn to Huybrechts (2016) and the very nice exposition of Harder and Thompson (2015).

Chapter 2

The homology of fibrations

In this chapter, we leave the realms of algebraic geometry and focus on algebraic topology. Our goal is to obtain an effective description of the homology of the total space of certain families of algebraic varieties to allow for the integration of periods. We do so by following the now 100-years-old groundbreaking ideas of Solomon Lefschetz in his book *"L'analyse in situs et la géométrie algébrique"*, which would lead to the developments of algebraic topology in the following decades. The reason why this approach is particularly interesting to us is that it is *effective* — in particular they will provide us with an explicit description of the cycles of homology on which we will be able to effectively and efficiently integrate the periods. This is the content of Chapter 3.

2.1 Monodromy and extensions

We first recall the concepts of monodromy and extensions, following closely Lamotke (1981, §6.4). Let $f\colon \mathcal{X} \to \mathbb{P}^1$ be a smooth proper map . The fibre above a point $t \in \mathbb{P}^1$ is denote $\mathcal{X}_t = f^{-1}(t)$. We assume that for all but finitely many $t \in \mathbb{P}^1$, $\mathcal{X}_t$ is smooth. The values $c_1, \dots, c_r$ above which X_{c_i} is not smooth are called *critical values*. We denote by $\Sigma = \{c_1, \dots, c_r\}$ the set of critical values.

2.1.1 Monodromy

By Ehresmann's theorem, the restriction of f to $f^{-1}(\mathbb{P}^1 \setminus \Sigma)$ is a smooth fibre bundle: for any simply connected open set $U \subseteq \mathbb{P}^1 \setminus \Sigma$ and any $b \in U$, there is a diffeomorphism $\Phi_U\colon f^{-1}(U) \to \mathcal{X}_b \times U$ with the compatibility $\mathrm{pr}_2 \circ \Phi_U = f|_{f^{-1}(U)}$ and $\mathrm{pr}_1 \circ \Phi_U|_{\mathcal{X}_b} = \mathrm{id}_{\mathcal{X}_b}$. Such a diffeomorphism is called a *trivialisation.*

In particular, for any continuous path $\ell : [0,1] \to \mathbb{P}^1 \setminus \Sigma$ without self intersection from a point $b = \ell(0)$ to another $b' = \ell(1)$, we obtain a continuous deformation of X_b into $X_{b'}$. Namely, we pick a simply connected neighbourhood U of $\ell([0,1])$ and we have an induced diffeomorphism

$$\mathcal{X}_b \to \mathcal{X}_{b'}, \quad x \mapsto \Phi_U^{-1}(x, b')\,, \tag{2.1}$$

depending on the choice of a trivialisation. This diffeomorphism is uniquely determined up to homotopy. Thus, it induces a well-defined determined isomorphism $\ell_* : H_q(\mathcal{X}_b) \to H_q(\mathcal{X}_{b'})$, for any q. This map depends only on the homotopy class of ℓ in $\mathbb{P}^1 \setminus \Sigma$. This is the *action of monodromy along ℓ on homology.* To extend this notion to self-intersecting paths, we cut the paths into non-self-intersecting pieces and compose the actions of each piece. For any paths ℓ and ℓ', with $\ell(1) = \ell'(0)$, let $\ell'\ell$ denote the composition (go through ℓ then ℓ'). Then

$$(\ell'\ell)_* = \ell'_*\ell_*\,. \tag{2.2}$$

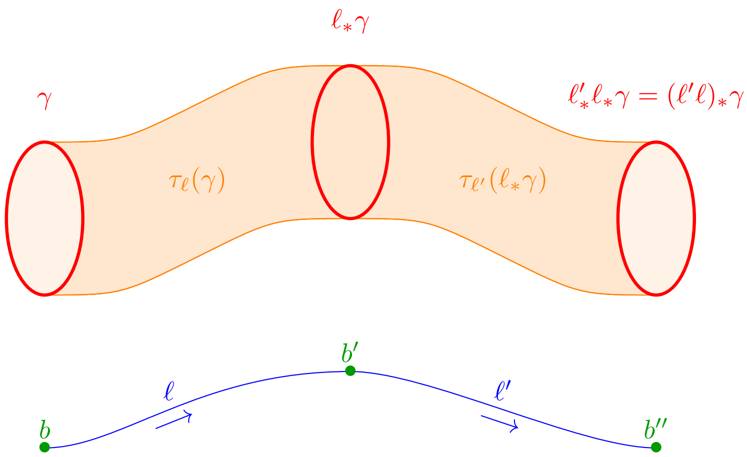

Figure 2.1: *The monodromy and extensions of a cycle γ along two composable paths ℓ and ℓ'. The extension of γ along $\ell\ell'$ is the sum of the extensions of γ along ℓ and of $\ell_*\gamma$ along ℓ'. As stated in* (2.7)*, the border of $\tau_\ell(\gamma)$ is $\ell_*\gamma - \gamma$.*

This defines the monodromy action of $\pi(\mathbb{P}^1 \setminus \Sigma, b)$ on $H_q(\mathcal{X}_b)$. The application

$$\pi_1(\mathbb{P}^1 \setminus \Sigma, b) \to \mathrm{GL}(H_q(\mathcal{X}_b)) : \ell \mapsto \ell_* \,. \tag{2.3}$$

is a group representation of $\pi_1(\mathbb{P}^1 \setminus \Sigma, b)$. It is the monodromy representation.

2.1.2 Extensions

In the same setting, given a q-chain A in $\mathcal{X}_b$, we may consider the $q+1$-chain $A \times [0,1]$ in $\mathcal{X}_b \times [0,1]$ and its image $\Phi_U(A \times [0,1])$ in $\mathcal{X}$. Given any open set V containing $f^{-1}(U)$, this induces a map

$$\tau_\ell \colon H_q(\mathcal{X}_b) \to H_{q+1}(V, \mathcal{X}_b \cup \mathcal{X}_{b'}) \tag{2.4}$$

called the *extension along* ℓ. (This map also follows from the Künneth formula for the pairs $(\mathcal{X}_b, \varnothing)$ and $([0,1], \{0,1\})$ since $f^{-1}(\ell([0,1])) \simeq \mathcal{X}_b \times [0,1]$.) The map τ_ℓ depends only on the homotopy class of ℓ. Given two paths ℓ and ℓ' with $\ell(1) = \ell'(0)$ we have (Fig. 2.1)

$$\tau_{\ell'\ell} = \tau_\ell + \tau_{\ell'} \circ \ell_* \,. \tag{2.5}$$

Using this composition rule one may define extensions along paths with self intersections. When the path ℓ is a loop from b to b, we obtain a map

$$\tau_\ell \colon H_q(\mathcal{X}_b) \to H_{q+1}(V, \mathcal{X}_b), \tag{2.6}$$

for any neighbourhood $V \subseteq \mathcal{X}$ of $f^{-1}(\ell([0,1]))$.

These two concepts, extensions and monodromy, are related by the formula

$$(-1)^{n-1}\partial \circ \tau_\ell = \ell_* - \mathrm{id}\,, \tag{2.7}$$

where $\partial \colon H_q(\mathcal{X}, \mathcal{X}_b \cup \mathcal{X}'_b) \to H_{q-1}(\mathcal{X}_b) \oplus H_{q-1}(\mathcal{X}_{b'})$ is the border map (Lamotke, 1981, §6.4.6).

2.1.3 The extension sublattice

Our goal is to recover a description of $H_n(\mathcal{X})$ in terms of $H_{n-1}(\mathcal{X}_b)$ and the monodromy representation of $\pi_1(\mathbb{P}^1 \setminus \Sigma, b)$. First, recall the long exact sequence of relative homology of the pair $(\mathcal{X}, \mathcal{X}_b)$:

$$\cdots \to H_k(\mathcal{X}_b) \to H_k(\mathcal{X}) \to H_k(\mathcal{X}, \mathcal{X}_b) \to H_{k-1}(\mathcal{X}_b) \to \cdots \tag{2.8}$$

The first and second arrow are induced by inclusion of chains, and the last is the boundary map ∂. In particular this long exact sequence establishes an isomorphism

Lemma 10.

$$\ker \partial \simeq H_n(\mathcal{X})/H_n(\mathcal{X}_b)\,. \tag{2.9}$$

In Section 3.3, we will provide a means to compute the periods of extensions. We thus define a relevant lattice of $H_n(\mathcal{X}, \mathcal{X}_b)$, as well as a sublattice corresponding to extensions that may be lifted to yield cycles in $H_n(\mathcal{X})$.

Definition 15. *The* relative extension lattice $\mathcal{T}(\mathcal{X}, \mathcal{X}_b)$ *is the sublattice of* $H_n(\mathcal{X}, \mathcal{X}_b)$ *generated by the images* $\operatorname{im} \tau_{\ell_i}$ *for* $1 \le i \le r$*. The* extension lattice *is the sublattice* $\mathcal{T}(\mathcal{X}) = \mathcal{T}(\mathcal{X}, \mathcal{X}_b) \cap \ker \partial$*.*

Remark 11. *Despite not being apparent, both* $\mathcal{T}(\mathcal{X}, \mathcal{X}_b)$ *and* $\mathcal{T}(\mathcal{X})$ *depend not just on* $\mathcal{X}$*, but also on the fibration* $\mathcal{X} \to \mathbb{P}^1$*.*

The following lemma implies that we may restrict our study locally around the critical values to recover $H_*(\mathcal{X}, \mathcal{X}_b)$. First chose a generic point $\infty \in \mathbb{P}^1 \setminus \Sigma$ to remove, which we call the *point at infinity.* We identify (topologically) $\mathbb{C} \simeq \mathbb{P}^1 \setminus \{\infty\}$ and denote $\mathcal{X}^* = f^{-1}(\mathbb{C})$. We pick a basepoint $b \in \mathbb{C} \setminus \Sigma$. We then define disjoint disks $B_1, \dots, B_r \subset \mathbb{C}$ such that $c_i \in B_i$ and $b \notin B_i$ for every i. Finally we chose a *local basepoint* $b_i \in \partial B_i$, as well as a path $p_i : [0,1] \to \mathbb{C} \setminus \bigcup_{i=1}^r B_i \setminus \{b_i\}$ connecting $p(0) = b$ to $p(1) = b_i$ for every i, and such that they do not intersect: $\operatorname{im} p_i \cap \operatorname{im} p_j = \emptyset$ for $i \neq j$.

We define $T_i = f^{-1}(B_i)$.

Lemma 12. *The inclusion yields an isomorphism*

$$\bigoplus_{c \in \Sigma} H_*(T_i, \mathcal{X}_{b_i}) \to H_*(\mathcal{X}^*, \mathcal{X}_b)\,, \tag{2.10}$$

where the identification $\mathcal{X}_{b_i} \simeq \mathcal{X}_b$ *is given by* p_i*.*

Proof. The main line of the argument is that the retraction of $\mathbb{C}$ to $\bigcup_{i=0}^r B_i \cup \operatorname{im} p_i$ lifts through f. For more details, see Lamotke (1981, §5.3). ☐

Finally, we make the link between $H_*(\mathcal{X}^*, \mathcal{X}_b)$ and $H_*(\mathcal{X}, \mathcal{X}_b)$. The long exact sequence of the triple $(\mathcal{X}, \mathcal{X}^*, \mathcal{X}_b)$ is

$$\cdots \to H_{q+1}(\mathcal{X}, \mathcal{X}_b) \to H_{q+1}(\mathcal{X}, \mathcal{X}^*) \to H_q(\mathcal{X}^*, \mathcal{X}_b) \to H_q(\mathcal{X}^*, \mathcal{X}_b) \to \cdots\,, \tag{2.11}$$

As $(\mathcal{X}, \mathcal{X}^*) \simeq \mathcal{X}_b \times (D, S^1)$, the Künneth formula reads

$$H_q(\mathcal{X}, \mathcal{X}^*) \simeq H_{q-2}(\mathcal{X}_b)\,, \tag{2.12}$$

and combining with Lemma 12, we obtain

$$\cdots \to H_{q+1}(\mathcal{X}, \mathcal{X}_b) \to H_{q-1}(\mathcal{X}_b) \to \bigoplus_{c \in \Sigma} H_q(T_i, \mathcal{X}_{b_i}) \to H_q(\mathcal{X}, \mathcal{X}_b) \to \cdots\,. \tag{2.13}$$

In this sequence, the first map is the intersection with $\mathcal{X}_b$, the last map is the inclusion, and the second map is the extension along a clockwise loop ℓ_∞ around ∞, which we denote $\tau_\infty = \tau_{\ell_\infty}$.

In general not much can be said about $H_*(T_i, \mathcal{X}_{b_i})$. However, for certain fibrations, called *Lefschetz fibrations*, we have an explicit description of this group. This is the content of the following section.

2.2 Lefschetz fibrations

Certain fibrations are of interest to us as their monodromy representation is quite simple, and their topology is fully understood. These correspond to the "most generic" fibration, where the singular fibres are the "least" singular — we will make this genericity statement precise in Chapter 4. Such fibrations were introduced by Solomon Lefschetz in his now 100 years-old seminal book Lefschetz (1924) to study the topology of complex hypersurfaces. Lefschetz established the ideas which would in time lead to the field of algebraic topology. They thus inherited the name of *Lefschetz fibrations*, and the theory that was developed to study them is called Picard–Lefschetz theory. It is the equivalent of real Morse theory in the holomorphic setting. In fact, Picard–Lefschetz theory even predates Morse theory, as the former first appeared in Lefschetz (1924), whereas the latter was introduced in Morse (1929).

Definition 16. *A critical value $c_i \in \Sigma$ is called* Lefschetz *or* non-degenerate *if the fibre $\mathcal{X}_{c_i}$ has a single singular point x_i, and the Hessian matrix of f is invertible at this point.*

In this case we may give an explicit coordinate description of a neighbourhood of the critical point. More precisely, we may choose be local holomorphic coordinates $z_1, \dots, z_n$ in a neighbourhood B of x_i such that $f|_B$ has the coordinate description

$$f(z) = c_i + z_1^2 + \cdots + z_n^2 \,. \tag{2.14}$$

Definition 17. *A fibration is called Lefschetz if all its critical fibres are Lefschetz.*

2.2.1 Vanishing cycles and thimbles

Vanishing cycles

The monodromy around a Lefschetz fibre is fully understood. The action on $H_{n-1}(\mathcal{X}_b)$ along a simple loop ℓ_i around a Lefschetz critical value c_i is given by the *Picard–Lefschetz formula* (Lamotke, 1981, §6.3.3):

$$\ell_{i*}(\eta) = \eta + (-1)^{n(n+1)/2} \langle \eta, \delta_i \rangle \delta_i \tag{2.15}$$

where $\langle \cdot, \cdot \rangle$ is the intersection product on $H_{n-1}(\mathcal{X}_b)$ and δ_i is a cycle in $H_{n-1}(\mathcal{X}_b)$, called the *vanishing cycle* at c_i, determined up to sign. Note that the vanishing cycle not only depends on c_i, but also on the choice of the homotopy class of ℓ_i. Note also, as a consequence of (2.15), that the map $\ell_{i*} - \mathrm{id}$ is of rank 1, and its image is generated by δ_i.

Thimbles

Similarly, the extension map $\tau_{\ell_i} : H_{n-1}(X_b) \to H_n(Y_+, X_b)$ around ℓ_i (see Section 2.1) has rank one, and there is a uniquely determined element $\Delta_i \in H_n(Y_+, X_b)$, the *Lefschetz thimble* associated to the critical value t_i, such that (Lamotke, 1981, (6.7.1))

$$\tau_{\ell_i}(\eta) = -(-1)^{\frac{n(n-1)}{2}} \langle \eta, \delta_i \rangle \Delta_i \in H_n(\mathcal{X}, \mathcal{X}_b), \tag{2.16}$$

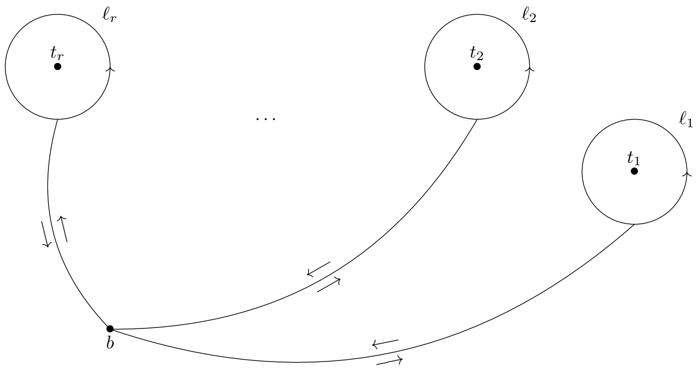

Figure 2.2: *The simple loops ℓ_i's around the critical points represent a basis of the homotopy group $\pi_1(\mathbb{C} \setminus \Sigma, b)$.*

which combined with (2.7) gives back the Picard–Lefschetz formula (2.15).

The thimble Δ_i is also dependent on the choice of the homotopy class of ℓ_i. By definition, it can be obtained as the extension $\tau_{\ell_i}(p_i)$ of some cycle $p_i \in H_{n-1}(\mathcal{X}_b)$. It generates $H_n(T_i, \mathcal{X}_b)$. In particular, note that

$$\partial \Delta_i = \delta_i. \tag{2.17}$$

Remark 13. *The thimble can also can be obtained as the geometric extension of δ_i along a path from b to the singular value c_i (Fig. 2.3). Indeed, the vanishing cycle contracts to a point as the fibre gets deformed from b to c_i (which justifies the name). We will not be using this description of vanishing cycles in the remainder of this text.*

2.2.2 Homology of Lefschetz fibrations

In order to recover a description of the homology of $\mathcal{X}$, we start from the explicit description of the relative homology group $H_n(\mathcal{X}, \mathcal{X}_b)$ in terms of the Lefschetz thimbles.

Lemma 14 (Main lemma, Lamotke, 1981, §5)**.** *With the notations above,*

(i) $H_q(\mathcal{X}, \mathcal{X}_b) = 0$ if $q \neq n$;

(ii) $H_n(\mathcal{X}, \mathcal{X}_b)$ is free of rank r and $\Delta_1, \dots, \Delta_r$ is a basis.

Proof. We recall the main line of the proof. For further details, see Lamotke (1981, §5). Recall the decomposition of Section 2.1.3, i.e.

$$H_*(\mathcal{X}, \mathcal{X}_b) \simeq \bigoplus_{i=1}^{r} H_*(T_i, \mathcal{X}_{b_i}). \tag{2.18}$$

Let B be a small neighbourhood of x_i, and define $T = T_i \cap B$ and $F = \mathcal{X}_{b_i} \cap B$. By excision we may show that the inclusion induces an isomorphism $H_*(T_i, \mathcal{X}_{b_i}) \simeq H_*(T, F)$. Then, as T can be linearly contracted to the origin, the boundary yields an isomorphism $H_q(T, F) \simeq H_{q-1}(F)$ for $q \neq 0, 1$. Furthermore, we have $H_0(T, F) \simeq 0$. Finally, a study using the local coordinates of 2.14 shows that F is diffeomorphic to the space of tangential vectors to the sphere, with norm ≤ 1:

$$Q = \{(u, v) \in \mathbb{R}^n \times \mathbb{R}^n \mid \|u\| = 1, \|v\| \leq 1 \text{ and } u \cdot v = 0\}, \tag{2.19}$$

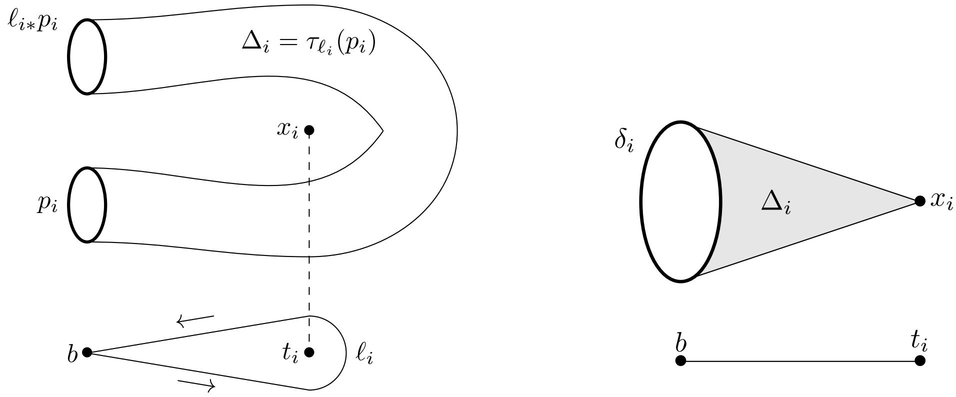

(a) *There is a unique cycle $\Delta_i \in H_n(\mathcal{X}, \mathcal{X}_b)$ stemming from extensions along the simple loop ℓ_i around t_i. It is called the* Lefschetz thimble at t_i. *It is dependent on the homotopy class of ℓ_i.*

(b) *The border $\delta_i = \ell_{i*}p_i - p_i$ of Δ_i is the* vanishing cycle at t_i. *This name comes from the fact that the geometric representative of δ_i collapses when deforming towards t_i. Δ_i is the extension of δ_i along a path connecting b to t_i.*

Figure 2.3: *Thimbles and vanishing cycles.*

which is contractible to an $n-1$-sphere S^{n-1}. Thus $H_q(F) = 0$ if $q \neq 0, n-1$, and we recover the statement of the lemma for $q \neq 1$. For $q = 1$, the long exact sequence of the pair (T, F) yields

$$0 \to H_1(T, F) \to H_0(F) \to H_0(T)\,, \tag{2.20}$$

and the inclusion $H_0(F) \to H_0(T)$ is surjective as T is connected. ☐

Remark 15. *The proof in Lamotke (1981) is wrong for $q = 1$, as there is no isomorphism $H_1(T, F) \to H_0(F)$ as is claimed in (5.5.4) (and in fact, if there was, we would obtain a different result than (5,5,8)). Nevertheless the result remains true because of the above observations.*

As a first consequence of this lemma we have the following lemma

Lemma 16. *We have short exact sequence*

$$H_{n-1}(\mathcal{X}_b) \to^{\tau_\infty} \bigoplus_{i=1}^{r} \Delta_i \mathbb{Z} \to H_n(\mathcal{X}, \mathcal{X}_b) \to H_{n-2}(\mathcal{X}_b) \to 0\,. \tag{2.21}$$

Proof. This is the exact sequence from (2.13), where $H_{n-2}(\mathcal{X}, \mathcal{X}_b) = 0$ from Lemma 14. ☐

As all thimbles are extensions, and conversely any extension is a combination of thimbles per (2.5), $\mathcal{T}(\mathcal{X}, \mathcal{X}_b)$ is generated by the inclusion of thimbles in $H_n(\mathcal{X}, \mathcal{X}_b)$. However $\ell_1, \ldots, \ell_r$ do not generate $\pi_1(\mathbb{P}^1 \setminus \Sigma, b)$ freely: we have the relation $\ell_\infty = \ell_r \cdots \ell_1 = 1$. Thus the thimbles do not generate $\mathcal{T}(\mathcal{X}, \mathcal{X}_b)$ freely. In particular extensions along ℓ_∞ are contractible and thus trivial. It turns out that these are the only trivial extensions, which gives the following description of $\mathcal{T}(\mathcal{X})$.

Lemma 17. *We have an isomorphism induced by inclusion*

$$\mathcal{T}(\mathcal{X}, \mathcal{X}_b) \simeq \bigoplus_{i=1}^{r} \Delta_i \mathbb{Z} / \operatorname{im} \tau_\infty\,. \tag{2.22}$$

Intersecting with $\ker \partial$, *we obtain*

$$\mathcal{T}(\mathcal{X}) \simeq \frac{\ker\left(\partial\colon H_n(\mathcal{X}^*, \mathcal{X}_b) \to H_{n-1}(\mathcal{X}_b)\right)}{\operatorname{im}\left(\tau_\infty\colon H_{n-1}(\mathcal{X}_b) \to H_n(\mathcal{X}^*, \mathcal{X}_b)\right)}\,. \tag{2.23}$$

Proof. As thimbles generate $\mathcal{T}(\mathcal{X}, \mathcal{X}_b)$, we have the short exact sequence

$$H_{n-1}(\mathcal{X}_b) \xrightarrow{\tau_\infty} H_n(\mathcal{X}^*, \mathcal{X}_b) \to \mathcal{T}(\mathcal{X}, \mathcal{X}_b) \to 0 \tag{2.24}$$

stemming from the long exact sequence of the pair $(\mathcal{X}, \mathcal{X}_b)$. □

Before proceeding further, let us describe informally the nature of this isomorphism. By Lemma 14, elements of $H_n(\mathcal{X}^*, \mathcal{X}_b)$ are linear combinations of thimbles. Thimbles have boundary in $\mathcal{X}_b$ (Fig. 2.3), but the boundary of a linear combinations of thimbles may be homologically 0 in $\mathcal{X}_b$. These linear combinations form a subspace which is exactly $\ker(\partial\colon H_n(\mathcal{X}^*, \mathcal{X}_b) \to H_{n-1}(\mathcal{X}_b))$. Let C be a chain representing such a linear combination. By definition, ∂C is homologically 0 in $\mathcal{X}_b$, so we can add a n-chain C' in $\mathcal{X}_b$ such that $\partial(C + C') = 0$. Then, the n-chain $C + C'$ is an n-cycle in $\mathcal{X}$. Since C' is determined only up to n-cycles in $\mathcal{X}_b$, we obtain a well defined element in $H_n(\mathcal{X})/H_n(\mathcal{X}_b)$.

Combinations of thimbles produced by the extension map $\tau_\infty : H_{n-1}(\mathcal{X}_b) \to H_n(\mathcal{X}^*, \mathcal{X}_b)$ are irrelevant, because the equator is contractible in $\mathbb{P}^1 \setminus \Sigma$, so these extensions are homologically zero in $(\mathcal{X}, \mathcal{X}_b)$. This explains why we have a map

$$\mathcal{T}(\mathcal{X}) \to H_n(\mathcal{X})/H_n(\mathcal{X}_b)\,. \tag{2.25}$$

From a computational perspective this is very convenient: we can represent classes in $\mathcal{T}(\mathcal{X})$ by the coefficients of a decomposition over the thimbles, and checking equality amount to simply checking whether an element is in $\operatorname{im} \tau_\infty$, for which we can compute a basis.

Finally, this last result explains how $\mathcal{T}(\mathcal{X})$ relates to the full homology lattice $H_n(\mathcal{X})$.

Theorem 18. *We have an exact sequence*

$$0 \to \mathcal{T}(\mathcal{X}) \to H_n(\mathcal{X})/H_n(\mathcal{X}_b) \to H_{n-2}(\mathcal{X}_b) \to 0,$$

where the arrow from $\mathcal{T}(\mathcal{X})$ is (2.25)*, and the arrow to $H_{n-2}(\mathcal{X}_b)$ is given by intersecting with $\mathcal{X}_b$.*

Proof. Consider the commutative diagram

$$\begin{tikzcd}
 & & H_n(\mathcal{X}_b) \arrow[d, "\iota_*"] & & \\
 & & H_n(\mathcal{X}) \arrow[d] & & \\
H_{n-1}(\mathcal{X}_b) \arrow[r, "\tau_\infty"] & H_n(\mathcal{X}^*, \mathcal{X}_b) \arrow[r] \arrow[dr, "\partial"] & H_n(\mathcal{X}, \mathcal{X}_b) \arrow[r] \arrow[d, "\partial"] & H_{n-2}(\mathcal{X}_b) \arrow[r] & 0 \\
 & & H_{n-1}(\mathcal{X}_b) & &
\end{tikzcd} , \tag{2.26}$$

where:

- The horizontal line is the long exact sequence of the triple $(\mathcal{X}, \mathcal{X}^*, \mathcal{X}_b)$ where $H_n(\mathcal{X}, \mathcal{X}^*)$ is identified to $H_{n-2}(\mathcal{X}_b)$ using (2.12). The last term is 0 because of Lemma 14.
- The column is the long exact sequence of the pair $(\mathcal{X}, \mathcal{X}_b)$.

Now, the exact sequence we aim to prove follows from diagram chasing in (4.6). □

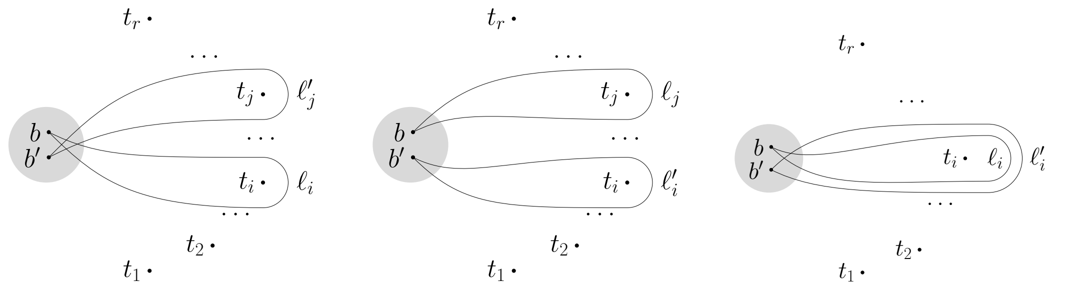

Figure 2.4: *The three possible configurations of extensions paths. Their intersection can be reduced to intersection products of cycles of the fibre at the fibres above the intersections of ℓ_i and ℓ'_j.*

2.2.3 The intersection product of extensions

We now show that we may compute the intersection product between lifts of extensions despite them being determined only modulo $H_n(\mathcal{X}_b)$.

Lemma 19. *The intersection product on $H_n(\mathcal{X}^*)$ induced by ι_* induces an intersection product on $\mathcal{T}(\mathcal{X})$ through the surjective inclusion $\phi\colon H_s(\mathcal{X}) \to \mathcal{T}(\mathcal{X})$.*

Proof. The inclusion $\iota : \mathcal{X}^* \to \mathcal{X}$ induces an intersection product on $H_n(\mathcal{X}^*)$ from that on $H_n(\mathcal{X})$. We aim to prove that this product induces a well-defined defined product on $\mathcal{T}(\mathcal{X})$. From the long exact sequence of the pair $(\mathcal{X}^*, \mathcal{X}_b)$, $H_n(\mathcal{X}^*)$ can be identified with $\ker\delta \oplus H_n(\mathcal{X}_b)$.

Let $\Gamma_1, \Gamma_2 \in H_n(\mathcal{X}^*)$ and assume that the class of $\phi(\Gamma_2) = 0$. Then $\Gamma_2 \in \operatorname{im}\tau_\infty \oplus H_n(\mathcal{X}_b)$. In particular, as $\operatorname{im}\tau_\infty \subset \ker\iota_*$ from the second line of (4.6), $\iota_*\Gamma_2 = h$ for some integer $h \in H_n(\mathcal{X}_b)$. We thus have

$$\langle \Gamma_1, \Gamma_2 \rangle = \langle \iota_*\Gamma_1, h \rangle = 0\,, \tag{2.27}$$

as h can be deformed to the fibre $H_n(\mathcal{X}_\infty)$, and thus not intersect $\iota_*\Gamma_1$. □

Let $\Gamma_i = \sum_j a_{ij}\Delta_j \in \mathcal{T}(\mathcal{X})$ be two extensions, described as a linear combination of thimbles for $i = 1, 2$. The previous lemma implies that the intersection product $\langle \Gamma_1, \Gamma_2 \rangle$ is well defined.

In order to compute this intersection product, we may deform the geometric representatives of the thimbles for Γ_2 slightly, in a way that the basepoint is no longer the same for Γ_1 and Γ_2, as is represented in Fig. 2.4. We then notice that the intersection between Δ_i and Δ'_j (where the latter is the aforementioned deformation of Δ_j) is contained in at most 4 fibres. This means that in order to compute the intersection product $\langle \Gamma_1, \Gamma_2 \rangle$, we may simply consider the intersection of pairs of thimbles (which we will also denote $\langle \Delta_i, \Delta_j \rangle$ by abuse of notation) and use bilinearity. More precisely, we see that

- if $i > j$, then $\langle \Delta_i, \Delta_j \rangle = 0$,
- if $i < j$, then $\langle \Delta_i, \Delta_j \rangle = \langle \delta_i, \delta_j \rangle$,
- if $i = j$, then $\langle \Delta_i, \Delta_j \rangle = -\langle p_i, \delta_i \rangle$,

where δ_i and p_i are respectively the vanishing cycle and a permuting cycle of Δ_i, i.e. $\delta_i = \ell_{i*}p_i - p_i = \partial\Delta_i$. We can then recover the intersection product with the formula $\langle \Gamma_1, \Gamma_2 \rangle = \sum_{i,j} a_{1i}a_{2j}\langle \Delta_i, \Delta_j \rangle$.

Remark 20. *The space of thimbles with this bilinear pairing is called a* pseudolattice.

2.2.4 Projective complete intersections

From now on, we assume that $\mathcal{X} \subset \mathbb{P}^N \times \mathbb{P}^1$ such that the map $\mathcal{X} \to \mathbb{P}^1$ is the projection onto the second coordinate, and that the general fibre $\mathcal{X}_b \subseteq \mathbb{P}^N$ is a complete intersection. In particular, all the homology groups that appear are free, so the exact sequences split, due to the following lemma which gathers some well known facts.

Lemma 21. *Let $\mathcal{V}$ be a n-dimensional smooth complete intersection of $\mathbb{P}^N$.*

(i) For $k < n$, the inclusion $\mathcal{V} \hookrightarrow \mathbb{P}^N$ induces isomorphisms $H_k(\mathcal{V}) \simeq H_k(\mathbb{P}^N)$ and $H^k(\mathcal{V}) \simeq H^k(\mathbb{P}^N)$.

(ii) All the homology groups $H_k(\mathcal{V}, \mathbb{Z})$ are free.

(iii) For $k < n$ even, $H_k(\mathcal{V})$ is generated by the homology class $\frac{1}{\deg \mathcal{V}}[\mathcal{V} \cap L]$ where L is a projective subspace of complex codimension $n - \frac{k}{2}$.

(iv) For $n < k \leq 2n$ even, $H_k(\mathcal{V})$ is is generated by the homology class $[\mathcal{V} \cap L]$ where L is a projective subspace of complex codimension $n - \frac{k}{2}$.

Proof. The first point is a consequence of Lefschetz's hyperplane theorem. Poincaré duality implies $H_k(\mathcal{V}) \simeq H_{2N-2n+k}(\mathbb{P}^N)$ for $k > n$. In particular, $H_k(\mathcal{V})$ is free for any $k \neq n$. For the second point, see Hirzebruch (1956, §2.2). For convenience, we recall the main line of the argument. By the first point and Poincaré duality, it only remains to check that $H_n(\mathcal{V})$ is free. By the universal coefficient theorem (Hatcher, 2002, Corollary 3.3), we have

$$H_n(\mathcal{V}) \simeq H^n(\mathcal{V}) \simeq \mathrm{Free}(H_n(\mathcal{V})) \oplus \mathrm{Tor}(H_{n-1}(\mathcal{V})) = \mathrm{Free}(H_n(\mathcal{V})), \tag{2.28}$$

where Free denotes the free part and Tor the torsion part.

For the third point, consider the inclusion $\mathcal{V} \hookrightarrow \mathbb{P}^N$, which, by the first point, induces an isomorphism $H_k(\mathcal{V}) \simeq H_k(\mathbb{P}^N)$. It maps a linear section of $\mathcal{V}$ by a projective subspace $L^{n-\frac{k}{2}}$ of codimension $n - \frac{k}{2}$ to the class of $\mathcal{V} \cap L$ in $\mathbb{P}^N$. But in $\mathbb{P}^N$, $\mathcal{V}$ is homologous to $\deg(\mathcal{V})L^{N-n}$ so $[\mathcal{V} \cap L]$ is homologous to $\deg(\mathcal{V})L^{N-\frac{k}{2}}$. So in $H_k(\mathcal{V})$, $[\mathcal{V} \cap L]$ is divisible by $\deg(\mathcal{V})$ and the quotient is a generator.

For the last point, we consider the *umkehr* homorphism $i_! : H_{2N-2n+k}(\mathbb{P}^N) \to H_k(\mathcal{V})$ obtained by Poincaré duality from the morphism $H^{2n-k}(\mathbb{P}^N) \to H^{2n-k}(\mathcal{V})$ induced by inclusion. As the latter is an isomorphism by the first point, $i_!$ is an isomorphism too. We check easily that it maps a projective subspace $L^{n-\frac{k}{2}}$, which generates $H_{2N-2n+k}(\mathbb{P}^N)$, to the linear section $\mathcal{V} \cap L^{n-\frac{k}{2}}$ of $\mathcal{V}$. □

In the case of complete intersections, is it convenient to study the homology of $\mathcal{X}$ without the part coming from the homology of $\mathbb{P}^N$. In particular, when n is even, the homology group $H_n(\mathcal{X})$ contains the class of a linear section h of $\mathcal{X}$ by a codimension $\frac{n}{2}$ linear space. We thus define the primitive homology

$$PH_n(\mathcal{X}) = \begin{cases} H_n(\mathcal{X})/\mathbb{Z}h & \text{if } n \text{ is even} \\ H_n(\mathcal{X}) & \text{if } n \text{ is odd.} \end{cases} \tag{2.29}$$

In the case where n is odd, we define $h = 0 \in H_n(\mathcal{X})$. h can be identified as a generator of the *tubular* mapping $T : H_n(\mathcal{X}) \to H_{n+1}(\mathcal{X}^{\complement})$ which sends a cycle to the boundary of a tubular neighbourhood of one of its representative.

We can also be slightly more precise about $H_n(\mathcal{X})$ and obtain a filtration. There is not a canonical decomposition associated to this filtration, but when we will study the intersection product, natural choices will appear.

Theorem 22. *Let $\mathcal{X} \to \mathbb{P}^1$ be a smooth variety with a fibration by projective complete intersections. Then there is a canonical filtration $\mathcal{F}^0 \subset \mathcal{F}^1 \subset \mathcal{F}^2 = H_n(\mathcal{X})$ such that*

- $\mathcal{F}^0 \simeq H_n(\mathcal{X}_b)$ *,*
- $\mathcal{F}^1/\mathcal{F}^0 \simeq \mathcal{T}(\mathcal{X})$ *, and*
- $\mathcal{F}^2/\mathcal{F}^1 \simeq H_{n-2}(\mathcal{X}_b)$ *.*

Note that $H_n(\mathcal{X}_b) \simeq H_{n-2}(\mathcal{X}_b) \simeq \mathbb{Z}$

Proof. Since $H_{n-2}(\mathcal{X}_b)$ is free, the exact sequence in Theorem 18 splits. Moreover, the map $\iota : H_n(\mathcal{X}_b) \to H_n(\mathcal{X})$ is injective. Indeed, let $L_n \in H_n(\mathcal{X}_b)$ and $L_{n-2} \in H_{n-2}(\mathcal{X}_b)$ be the classes of linear sections. Then $\langle L_n, L_{n-2}\rangle_{\mathcal{X}_b} = 1$ and thus $\langle L_n, L_{n-2} \times \mathbb{P}^1\rangle_{\mathcal{X}} = -1$. As all these groups are free, we obtain the claim. □

Finally, we provide two results providing insight into the structure of the homology of the fibre in terms of the vanishing cycles when n is odd (when it is even, these results are trivial):

Lemma 23. *The kernel K of the inclusion $H_{n-1}(\mathcal{X}_b) \to H_{n-1}(\mathcal{X})$ is generated by vanishing cycles, i.e.*

$$K = \operatorname{im}\left(\partial\colon \mathcal{T}(\mathcal{X}, \mathcal{X}_b) \to H_{n-1}(\mathcal{X}_b)\right) . \tag{2.30}$$

Furthermore, K is the orthogonal complement of the linear class $h_{\mathcal{X}_b}$ of $H_{n-1}(\mathcal{X}_b)$

$$K = h_{\mathcal{X}_b}^{\perp} \tag{2.31}$$

and for any $\gamma \in H_{n-1}(\mathcal{X}_b)$ such that $\langle h_{\mathcal{X}_b}, \gamma\rangle = 1$,

$$H_{n-1}(\mathcal{X}_b) = K \oplus \langle\gamma\rangle \tag{2.32}$$

Proof. The first statement is the long exact sequence of relative homology

$$\cdots \to H_n(\mathcal{X}, \mathcal{X}_b) \to H_{n-1}(\mathcal{X}_b) \to H_{n-1}(\mathcal{X}) \to \dots ,$$

which in this instance, using Lemma 14, simplifies to

$$0 \to K \to H_{n-1}(\mathcal{X}_b) \to H_{n-1}(\mathcal{X}) \to 0 .$$

Here, $H_{n-1}(\mathcal{X}_b)$ is free and thus the exact sequence splits. As $h_{\mathcal{X}_b}^{\perp}$ does not have monodromy, it follows from (2.15) that K is included in $h_{\mathcal{X}_b}^{\perp}$. As the intersection product on $H_{n-1}(\mathcal{X}_b)$ is unimodular and $h_{\mathcal{X}_b}$ is primitive in $H_{n-1}(\mathcal{X}_b)$, there exists $\gamma \in H_{n-1}(\mathcal{X}_b)$ such that $\langle \gamma, h_{\mathcal{X}_b}\rangle = 1$. In particular we have that $K \oplus \langle\gamma\rangle = H_{n-1}(\mathcal{X}_b)$. Let $\eta \in h_{\mathcal{X}_b}^{\perp}$. Then $\eta = \alpha\kappa + \beta\gamma$ for some $\kappa \in K$ and $\alpha, \beta \in \mathbb{Z}$. But taking the intersection product with $h_{\mathcal{X}_b}$ yields that $b = 0$ and so $h_{\mathcal{X}_b}^{\perp} \subset K$. □

As a direct consequence we also have the following.

Lemma 24. *The inclusion $[\gamma]$ of γ in $H_{n-1}(\mathcal{X})$ generates $H_{n-1}(\mathcal{X})$. In particular* $\deg \mathcal{X}[\gamma] = h$.

Intersection product

We now explain how to obtain the intersection product on all of $H_n(\mathcal{X})$ from the intersection product on $\mathcal{T}(\mathcal{X})$ computed in Section 2.2.3, using methods similar to those of Shiga (1979, §2) or Narumiya and Shiga (2001, §3).

When n is odd, $H_n(\mathcal{X})$ and $\mathcal{T}(\mathcal{X})$ coincide so we are done. Assume n even. By the same argument as that of Lemma 19, h is orthogonal to the image of $H_n(\mathcal{X}^*)$ in $H_n(\mathcal{X})$. All that remains it to compute the intersection products of the generator of $H_{n-2}(\mathcal{X}_b)$, which we denote S. From

Lemma 21, S is the class $\frac{1}{\deg \mathcal{X}}[\mathcal{X} \cap (L_{n+2} \times \mathbb{P}^1)]$, and h is the class $[\mathcal{X} \cap L_n]$, where L_k is a projective linear subspace of (real) codimension k. In particular the intersection $\mathcal{X} \cap L_n \cap L_{n-2}$ consists of $\deg \mathcal{X}$ points, and thus

$$\langle h, S\rangle = 1\,. \tag{2.33}$$

Let $\Gamma_1, \ldots, \Gamma_s \in H_n(\mathcal{X}^*)$ induce a basis of $\mathcal{T}(\mathcal{X})$ through ϕ. Up to adding multiples of h, we may assume the Γ_i's to be orthogonal to S. These observations allow us to recover the full intersection matrix of $H_n(\mathcal{X})$. We summarise these results with the following lemma.

Lemma 25. *There exist $\Gamma_1, \ldots, \Gamma_s \in H_n(\mathcal{X}_+)$, $h \in H_n(\mathcal{X}_b)$ and $S \in H_{n-2}(\mathcal{X})$ such that*

- *$\phi(\Gamma_1), \ldots, \phi(\Gamma_s)$ is a basis of $\mathcal{T}(\mathcal{X})$ (where we recall ϕ is the inclusion $H_2(\mathcal{X}) \to \mathcal{T}(\mathcal{X})$),*
- *S is a section of $\mathcal{H}_{n-2}(\mathcal{X}_t)$,*
- *$h, \iota_*\Gamma_1, \ldots, \iota_*\Gamma_s, S$ is a basis of $H_n(\mathcal{X})$.*

Define the coefficients a_{ij} to be so that $\phi(\Gamma_i) = \sum_j a_{ij}\Delta_j$. The intersection products are given by

- *$\langle \iota_*\Gamma_i, \iota_*\Gamma_j\rangle = \sum_{k,l} a_{ik}a_{jl}\langle \Delta_k, \Delta_l\rangle$ for all i, j,*
- *$\langle \iota_*\Gamma_i, h\rangle = 0$ for all i,*
- *$\langle \iota_*\Gamma_i, S\rangle = 0$ for all i,*
- *$\langle h, h\rangle = 0$,*
- *$\langle h, S\rangle = 1$.*

The intersection matrix in the aforementioned basis of $H_2(Y)$ is therefore given by

$$\begin{bmatrix} 0 & \boldsymbol{0} & 1 \\ \boldsymbol{0} & M & \boldsymbol{0} \\ 1 & \boldsymbol{0} & \langle S, S\rangle \end{bmatrix}, \tag{2.34}$$

where M is the matrix given coefficient-wise by $M_{ij} = \sum_{k,l} a_{ik}a_{jl}\langle \Delta_k, \Delta_l\rangle$.

Remark 26. *We have not yet specified $\langle S\rangle$. Up to adding h to S, its value is only defined modulo 2. The parity of self-intersection $\langle S, S\rangle$ depends on the specific cases. We will specify the correct values in the cases considered in upcoming sections.*

2.3 The non-Lefschetz case

We have seen in the previous section that the data of the monodromy matrices of the family is sufficient to recover the homology of $\mathcal{X}$ in the Lefschetz case. With more general fibrations, things may not be so easy. It is possible that certain cycles of $\mathcal{X}$ are "hidden" within the singular fibres of the fibration. Such cycles are called *singular components*.

Definition 18. *The* singular components lattice of the fibre above c_i *is the sublattice of* $H_n(T_i, \mathcal{X}_{b_i})$

$$\Theta_i = \ker\left(\partial\colon H_n(T_i, \mathcal{X}_{b_i}) \to H_{n-1}(\mathcal{X}_{b_i})\right)\,. \tag{2.35}$$

In some cases, we may still recover such cycles by the means of a *morsification*. In a nutshell, our goal is to deform $\mathcal{X}$ in a way that splits the non-Lefschetz singular fibres into several Lefschetz fibres. It would then be possible to compute the homology of the deformed variety from its monodromy matrices, which is by construction diffeomorphic to the original one.

More precisely, let $V \subset \mathbb{P}^1$ be open and $D = \{z \in \mathbb{C} \mid |z| \leq 1\}$ denote the unit disk.

Definition 19. *Let $\mathcal{X} \to V$ be a fibration of complex manifolds. Consider a commutative diagram of proper surjective holomorphic maps between complex manifolds*

$$\begin{tikzcd} \tilde{\mathcal{X}} \arrow[r, "\tilde{f}"] \arrow[dr, "\eta"'] & V \times D \arrow[d, "p"] \\ & D \end{tikzcd}, \tag{2.36}$$

where p is the projection onto the second coordinate. For $u \in D$, denote $\tilde{\mathcal{X}}_u = \eta^{-1}(u)$ and $f_u = \tilde{f}|_{\tilde{\mathcal{X}}_u} : \tilde{\mathcal{X}}_u \to V$ where we identify $\tilde{\mathcal{X}} \times \{u\} \simeq V$. Such a diagram is a morsification *of $\mathcal{X} \to V$ if*

- *$\eta : \tilde{\mathcal{X}} \to D$ has no critical values;*
- *$f_0 : \tilde{\mathcal{X}}_0 \to V$ is identified with $\mathcal{X} \to V$;*
- *for $u \in D \setminus \{0\}$, $f_u : \tilde{\mathcal{X}}_u \to V$ is a Lefschetz fibration.*

Remark 27. *Such a deformation is sometimes also called a* splitting deformation *of the elliptic surface.*

Remark 28. *Note that by Ehresmann's fibration theorem (Ehresmann, 1951), there is a trivialisation $\tilde{\mathcal{X}} \simeq S \times V$. In particular this implies that for every $u \in D$, $\mathcal{X}_t$ is diffeomorphic to $\mathcal{X}$, but not necessarily biholomorphic.*

Morsifications are useful as they allow use of the results for Lefschetz fibrations to obtain information about more general fibrations. Indeed as η is a trivial fibration, it induces an isometry $H_n(\mathcal{X}_0) \simeq H_n(\mathcal{X}_u)$ for all $u \in D \setminus \{0\}$, and we may apply the results of Section 2.2 to the describe the latter.

We now focus on a single critical value c_i. To ease the notations, we denote $c = c_i$, $B = B_i$, $b = b_i$ and $T = T_i$. Assume we have a morsification $\tilde{T}$ of $T \to B$. Pick $t \in D \setminus \{0\}$. If the fibre above c_i is not of Lefschetz type, the morsification will split c_i into several critical values $\alpha_1, \dots, \alpha_s$ of $\tilde{T}_t$, the fibres above which are of Lefschetz type. Define $\tilde{T}_{t,b} = \tilde{T}_t \cap \tilde{f}^{-1}(\{b_i\} \times D)$ to be the fibre above the basepoint b_i of the fibre above t of the morsification. Finally choose a path p connecting 0 to t. This path induces an isomorphism between the homology groups of $\mathcal{X}_{b_i}$ and $\tilde{T}_{t,b}$

$$p_* \colon H_q(\mathcal{X}_{b_i}) \to H_q(\tilde{T}_{t,b}),$$

as well as

$$p_* \colon H_q(T_i, \mathcal{X}_{b_i}) \to H_q(\tilde{T}_t, \tilde{T}_{tb}).$$

The fundamental group $\pi_1(B \setminus \{\alpha_1, \dots, \alpha_s\}, b)$ is bigger than $\pi_1(B_i \setminus \{c_i\}, b)$. In particular there may be more extensions, and we may have a proper inclusion

$$\mathcal{T}(T_i, \mathcal{X}_{b_i}) \to \mathcal{T}(\tilde{T}_t, \tilde{T}_{tb}), \tag{2.37}$$

induced by p_*.

Chapter 3

Numerical methods for period computations

In the previous chapter, we developed an algebraic topology framework to recover the homology of the total space of a fibration. In order to turn this into a working algorithm that may be used on concrete examples, we describe the effective tools that take advantage of this topological analysis.

The content of this chapter is based on Lairez et al. (2024).

3.1 The De Rham cohomology of hypersurfaces

We now focus on the cohomology of a smooth projective hypersurface $\mathcal{X} = V(P) \subset \mathbb{P}^{n+1}$, where n is an integer and P a homogeneous polynomial in $n+2$ variables. In particular $\mathcal{X}$ has dimension n. The condition that $\mathcal{X}$ is smooth amounts to saying that the Jacobian ideal of P, $J_P = \langle \partial_0 P, \dots, \partial_{n+1} P\rangle$, is trivial.

We had defined the hyperplane class h and the primitive homology of $\mathcal{X}$ in Section 2.2.4. We can similarly decompose the De Rham cohomology in two pieces. The first piece comes from the ambient projective space and is the Poincaré dual h^* of h. The associated periods are given by $\int_\gamma h^* = \langle h, \gamma\rangle$.

The second piece is called the *primitive De Rham cohomology*, or simply the *primitive cohomology.*

Definition 20. *The middle* primitive cohomology *group* $PH^n_{\mathrm{DR}}(\mathcal{X})$ *of* $\mathcal{X}$ *is the subspace of* $H^n_{\mathrm{DR}}(\mathcal{X})$ *of classes* ω *which evaluate to* 0 *when integrated on* h*, i.e.*

$$PH^n_{\mathrm{DR}}(\mathcal{X}) \overset{\mathrm{def}}{=} \left\{\omega \in H^n_{\mathrm{DR}}(\mathcal{X}) \mid \int_h \omega = 0\right\}. \tag{3.1}$$

As we will see in this section, primitive cohomology classes can be represented in terms of residue classes of cohomology classes of the projective complement of $\mathcal{X}$.

Primitive cohomology and the Griffiths-Dwork reduction

The understanding of the De Rham cohomology of $\mathcal{X}$ is made simpler by looking at the cohomology of the complement $\mathcal{X}^{\complement} = \mathbb{P}^{n+1} \setminus X$ in projective space (P. A. Griffiths, 1969, §2; Cox & Katz, 1999, §5.3). There is a natural injective morphism $\mathrm{Res} : H^{n+1}_{\mathrm{DR}}(\mathcal{X}^{\complement}) \to H^n_{\mathrm{DR}}(\mathcal{X})$ called the *residue mapping.* Its image is the *primitive De Rham cohomology of* $\mathcal{X}$,

$$PH^n_{\mathrm{DR}}(\mathcal{X}) \overset{\mathrm{def}}{=} \mathrm{Res}\left(H^{n+1}_{\mathrm{DR}}(\mathcal{X}^{\complement})\right) = \left\{\omega \in H^n_{\mathrm{DR}}(\mathcal{X}) \;\middle|\; \int_h \omega = 0\right\}. \tag{3.2}$$

The residue map is dual to the tubular mapping T of Section 2.2.4: for any $\omega \in H^{n+1}(\mathcal{X}^{\complement})$ and $\gamma \in H_n(\mathcal{X})$,

$$2\pi i \int_\gamma \operatorname{Res}\omega = \int_{T(\gamma)} \omega. \tag{3.3}$$

The kernel of T is generated by h and we have $PH_n(\mathcal{X}) = \operatorname{coker}(T) = H_n(\mathcal{X})/\mathbb{Z}h$. Equation (3.3) shows that the pairing $PH_n(\mathcal{X}) \times PH^n_{\mathrm{DR}}(\mathcal{X})$ is well defined.

The cohomology classes in $H^{n+1}(\mathcal{X}^{\complement})$ have an explicit description. Recall that $P \in \mathbb{C}[x_0, \dots, x_{n+1}]$ denotes the defining polynomial of X. The algebraic differential $(n+1)$-forms on $\mathcal{X}^{\complement}$ can be written uniquely as

$$\omega = \frac{A}{P^k}\Omega_{n+1}, \tag{3.4}$$

where $\Omega_{n+1} = \sum_{i=0}^{n+1}(-1)^i x_i \mathrm{d}x_1 \cdots \mathrm{d}x_{i-1}\mathrm{d}x_{i+1}\cdots \mathrm{d}x_{n+1}$ is the projective volume form, k is a positive integer and $A \in \mathbb{C}[\mathbf{x}]_{kd-n-2}$ is a homogeneous polynomial of degree $kd-n-2$. Since the variety $\mathcal{X}^{\complement}$ is affine, its De Rham cohomology can be computed using algebraic forms directly (Grothendieck, 1966). Explicitly, we have

$$H^{n+1}_{\mathrm{DR}}(\mathcal{X}^{\complement}) \simeq \frac{\operatorname{Vect}_{\mathbb{C}}\left\{\frac{A}{P^k}\Omega_{n+1} \;\middle|\; k \geq 0 \text{ and } A \in \mathbb{C}[\mathbf{x}]_{kd-n-2}\right\}}{\operatorname{Vect}_{\mathbb{C}}\left\{\frac{\partial}{\partial x_i}\left(\frac{B}{P^k}\right)\Omega_{n+1} \;\middle|\; k \geq 0 \text{ and } 0 \leq i \leq n+1 \text{ and } B \in \mathbb{C}[\mathbf{x}]_{kd-n-1}\right\}}. \tag{3.5}$$

This is the quotient of homogeneous rational functions, regular outside of X, of degree $-n-2$ modulo sums of partial derivatives of homogeneous rational functions, regular outside of X, of degree $-n-1$.

In this representation, a basis of $H^{n+1}_{\mathrm{DR}}(\mathcal{X}^{\complement})$ can be described in terms of the Jacobian ideal of f, namely

$$J = \left\langle \frac{\partial P}{\partial x_0}, \dots, \frac{\partial P}{\partial x_{n+1}} \right\rangle \subseteq \mathbb{C}[\mathbf{x}]. \tag{3.6}$$

We fix any monomial ordering on $\mathbb{C}[\mathbf{x}]$. A basis of the cohomology space is given by the forms $\frac{m}{P^k}\Omega_{n+1}$, where m is a monomial in the variables $\mathbf{x}$ such that:

- $kd = \deg(m) + n + 2$;
- m is not the leading monomial of any element of J.

The monomials m are precisely the monomials under the staircase of a Gröbner basis of J, with degree congruent to $n+2$ modulo d. The process of computing the coefficients in this basis of a given equivalence class of a $n+1$-form on $\mathcal{X}^{\complement}$ is called *Griffiths–Dwork reduction*. In short, it relies on the observation that

$$\frac{A\partial_i P}{P^k} = \frac{1}{k-1}\frac{\partial_i A}{P^{k-1}} - \frac{1}{k-1}\partial_i\left(\frac{A}{P^{k-1}}\right), \tag{3.7}$$

where $k > 1$, $A \in \mathbb{C}[\mathbf{x}]_{kd-n-2}$, and ∂_i denotes $\frac{\partial}{\partial x_i}$ for readability. Typical Gröbner bases computation allow to rewrite any homogeneous monomial A of degree $kd-n-2$ for certain $k \geq 1$ as

$$c_1 m_1 + \cdots + c_s m_s + A_1\partial_1 P + \cdots + A_1 \partial_1 P\,, \tag{3.8}$$

where the c_i's are rational coefficients, m_s are the basis monomials of the same degree as A, and the A_i are homogenenous polynomials of degree $\deg A - d + 1$. Then (3.7) allows to inductively compute the decomposition of any rational form $\frac{A}{P^k}\Omega_{n+1}$ as a linear combination of the $\frac{m}{P^k}\Omega_{n+1}$'s. For more details, we refer to Cox and Katz (1999, §5.3).

The Hodge filtration

The space

$$\frac{\operatorname{Vect}_{\mathbb{C}}\left\{\frac{A}{P^k}\Omega_{n+1} \;\middle|\; k \geq 0 \text{ and } A \in \mathbb{C}[\mathbf{x}]_{kd-n-2}\right\}}{\operatorname{Vect}_{\mathbb{C}}\left\{\frac{\partial}{\partial x_i}\left(\frac{B}{P^k}\right)\Omega_{n+1} \;\middle|\; k \geq 0 \text{ and } 0 \leq i \leq n+1 \text{ and } B \in \mathbb{C}[\mathbf{x}]_{kd-n-1}\right\}} \tag{3.9}$$

appearing on the right hand-side of (3.5) is equipped by an decreasing filtration given by the pole order k, namely

$$\mathcal{F}^p = \frac{\operatorname{Vect}_{\mathbb{C}}\left\{\frac{A}{P^k}\Omega_{n+1} \;\middle|\; n-p \geq k \geq 0 \text{ and } A \in \mathbb{C}[\mathbf{x}]_{kd-n-2}\right\}}{\operatorname{Vect}_{\mathbb{C}}\left\{\frac{\partial}{\partial x_i}\left(\frac{B}{P^k}\right)\Omega_{n+1} \;\middle|\; k \geq 0 \text{ and } 0 \leq i \leq n+1 \text{ and } B \in \mathbb{C}[\mathbf{x}]_{kd-n-1}\right\}}\,. \tag{3.10}$$

This equips $H^{n+1}_{\mathrm{DR}}(\mathcal{X}^{\complement})$, and in turn $PH^n_{\mathrm{DR}}(\mathcal{X})$, with a filtration. A result of P. A. Griffiths (1969) shows that this coincides with the Hodge filtration induced on $PH^n_{\mathrm{DR}}(\mathcal{X})$. In particular we obtain the following corollary.

Corollary 29. *The basis induced by the monomials $m_1, \ldots, m_r$ above, sorted by increasing degree, is a Hodge basis.*

This is convenient for two reasons. First we obtain information about the Hodge structure. Second, for K3 surfaces, the holomorphic period will be given by a rational form with a single order pole at P. From computations, it appears that the degree of the Picard–Fuchs equations that need to be integrated (see the next section) increases with the pole order. Thus the Picard–Fuchs equation of the holomorphic form is arguably easier to integrate than that of a general form, and is sufficient to recover the Hodge structure on $PH^n_{\mathrm{DR}}(\mathcal{X})$. The same is in general: it is sufficient to integrate the periods of the first $n/2$ Hodge pieces of the cohomology to recover the full Hodge structure, and these are arguably easier to obtain than the general ones.

Primitive periods

Finally, we end this section with the definition of a primitive period matrix

Definition 21. *A* primitive period matrix *is the data of a basis $\gamma_1, \ldots, \gamma_r$ of $PH_n(\mathcal{X})$, a basis $\omega_1, \ldots, \omega_r$ of $PH^n(\mathcal{X})$, and of the period pairing matrix*

$$\Pi_{ij} = \int_{\gamma_i} \omega_j\,. \tag{3.11}$$

Informally, the primitive period matrix contains the part of the periods that are difficult to compute. In odd dimension, it is equal to the full period matrix. In even dimensions, to obtain the full period matrix, it is sufficient to add the homology class h and any cohomology class not vanishing when evaluated against h. In particular, we may take the dual h^* of h, as $\langle h, h\rangle = \deg \mathcal{X} \neq 0$. Then the missing entries to obtain the full period matrix are simply 0 when evaluating a primitive cohomology class against h, and the intersection product $\langle h, \gamma\rangle$ when evaluating h^* against a cycle γ.

3.2 Computing the Gauss-Manin connection

In this section, we give a method for computing the Gauss-Manin connection of a family of projective hypersurfaces. Let $f\colon \mathcal{X} \to \mathbb{P}^1$ be such a family, i.e., there is an embedding $\mathcal{X} \subset \mathbb{P}^n \times \mathbb{P}^1$ such that the map to $\mathbb{P}^1$ is the projection onto the second component, and the general fibre $\mathcal{X}_t = f^{-1}(t)$ is a hypersurface given by a polynomial equation $\mathcal{X}_t = V(P_t)$ that is homogeneous in the projective coordinates $x_0, \dots, x_n$ and with coefficients in $\mathbb{Q}(t)$. Further assume that the $\mathcal{X}_t$ is smooth for generic (i.e., all but finitely many) values of $t \in \mathbb{P}^1$.

Similarly to the previous section, Griffiths-Dwork reduction can be used to compute the Gauss-Manin connection of the relative primitive cohomology of a family of projective hypersurfaces. Following Section 3.1, the residue mapping induces an isomorphism

$$PH^{n-1}_{\mathrm{DR}}(\mathcal{X}_t) \simeq \frac{\mathrm{Vect}_{\mathbb{C}}\left\{ \frac{A}{P_t^k}\Omega_n \;\middle|\; k \geq 0 \text{ and } A \in \mathbb{C}[x_0, \dots, x_n]_{kd-n-1} \right\}}{\mathrm{Vect}_{\mathbb{C}}\left\{ \frac{\partial}{\partial x_i}\left(\frac{B}{P_t^k}\right)\Omega_n \;\middle|\; k \geq 0 \text{ and } 0 \leq i \leq n \text{ and } B \in \mathbb{C}[x_0, \dots, x_n]_{kd-n} \right\}}. \tag{3.12}$$

By extending the scalars from $\mathbb{C}$ to $\mathbb{C}(t)$, we can define the *relative primitive De Rham cohomology* $\mathcal{PH}$ of $\mathcal{X}$ to be the space of sections of $PH^{n-1}_{\mathrm{DR}}(\mathcal{X}_t)$

$$\mathcal{PH}(\mathbb{P}^1 \setminus \Sigma) = \frac{\mathrm{Vect}_{\mathbb{C}(t)}\left\{ \frac{A}{P_t^k}\Omega_n \;\middle|\; k \geq 0 \text{ and } A \in \mathbb{C}(t)[x_0, \dots, x_n]_{kd-n-1} \right\}}{\mathrm{Vect}_{\mathbb{C}(t)}\left\{ \frac{\partial}{\partial x_i}\left(\frac{B}{P_t^k}\right)\Omega_n \;\middle|\; k \geq 0 \text{ and } 0 \leq i \leq n \text{ and } B \in \mathbb{C}(t)[x_0, \dots, x_n]_{kd-n} \right\}}. \tag{3.13}$$

It is a subsheaf of the sheaf of the relative De Rham cohomology $\mathcal{H}$. For a given $\beta \in \mathcal{H}$ and a generic $t \in \mathbb{P}^1$, evaluation at t gives an element $\beta(t)$ of $PH^n_{\mathrm{DR}}(\mathcal{X}_t)$. Because $\frac{\partial}{\partial t}$ commutes with $\frac{\partial}{\partial x_i}$, we see that differentiation with respect to the parameter t induces a derivation ∇ of $\mathcal{H}$. This is the *Gauss–Manin connection.*

Let $\beta \in \mathcal{H}$. For $\eta \in H_{n-1}(\mathcal{X}_b)$, let $\eta(t) \in H_{n-1}(\mathcal{X}_t)$ be the cycle uniquely determined by transporting η in $\mathcal{Y}_t$, following a path in some simply connected neighbourhood of b. The Gauss–Manin connection is uniquely determined by the property

$$\frac{d}{dt}\int_{\eta(t)} \beta(t) = \int_{\eta(t)} \nabla\beta(t). \tag{3.14}$$

Using Griffiths–Dwork reduction, we can compute a basis of $\mathcal{H}$, say $\beta_1, \dots, \beta_s$, and the matrix $A(t) = (a_{ij}) \in \mathbb{C}(t)^{s\times s}$ of the Gauss–Manin connection (for details on its computation, see Bostan et al. (2013)), defined by

$$\nabla\beta_i = \sum_j a_{ij}\beta_j. \tag{3.15}$$

Typically, β_i will be in the form $\frac{m}{P_t^k}\Omega_n$, for some monomial m, and so $\nabla\beta_i$ will be given by the Griffiths–Dwork reduction of $-k\frac{m}{P_t^{k+1}}\frac{\partial P_t}{\partial t}\Omega_n$. We can also choose β_1 to be a cyclic vector and $\beta_i = \nabla^{i-1}\beta_1$ so that the differential system is encoded in a single scalar equation which is well adapted to the *ore_algebra* package (see Section 3.3). Finally, the evaluations $\beta_i(b)$ yield a basis of $PH^n_{\mathrm{DR}}(\mathcal{X}_b)$ for generic values of b.

3.3 Numerical analytic continuation

We now briefly present the algorithms underlying our numerical computations. Consider a linear differential system, in the complex plane, with rational coefficients – that is an equation

$$Y'(t) = A(t)Y(t), \tag{3.16}$$

where $A(t) \in \mathbb{C}(t)^{s\times s}$, and Y is a unknown vector or matrix of functions. A point $t \in \mathbb{C}$ is *ordinary* if A is continuous at t and *singular* otherwise. At any ordinary point $b \in \mathbb{C}$, there is a uniquely determined $s \times s$ solution matrix Y_b with $Y_b(b) = I_s$, the $r \times r$ identity matrix (Haraoka, 2020, Theorem 3.1). Let us call it the *fundamental solution at* b. Any other solution matrix $\tilde{Y}$ of (3.16) in a neighbourhood of b can be written as $\tilde{Y}(t) = Y_b(t)U$ for some constant matrix U.

Consider a continuous path $\gamma : [0,1] \to \mathbb{C}$ which avoids singular values. From the computational point of view, we assume that γ is polygonal with ordinary vertices in $\mathbb{Q}[i]$ (results in the more general setting where the vertices are singular points or given numerically exist, but we will not need them). The analytic continuation along γ of the fundamental solution at $\gamma(0)$ gives a new solution, denoted $\gamma_* Y$ in the neighbourhood of $\gamma(1)$ (Haraoka, 2020, Theorem 3.2). In particular, there is a unique matrix $\Lambda_\gamma \in \mathbb{C}^{r\times r}$, the *transition matrix along* γ, such that

$$\gamma_* Y = Y_{\gamma(1)} \Lambda_\gamma. \tag{3.17}$$

Since $Y_{\gamma(1)}(\gamma(1)) = \mathrm{id}$, we have $\Lambda_\gamma = \gamma_* Y(\gamma(1))$. The map $\gamma \to \Lambda_\gamma$ is a morphism from the fundamental groupoid of $\mathbb{C} \setminus \Sigma$ to $\mathrm{GL}(\mathbb{C}^r)$: Λ_γ depends on γ only up to homotopy, and if $\gamma\eta$ is the composition of two paths (going through η first then γ), then $\Lambda_{\gamma\eta} = \Lambda_\gamma \Lambda_\eta$.

Theorem 30 (D. V. Chudnovsky and Chudnovsky, 1990; van der Hoeven, 1999; Mezzarobba, 2010)**.** *Given $p > 0$, we can compute an approximation of Λ_γ up to 2^{-p} (for any norm on $\mathbb{C}^{r\times r}$). When the differential system* (3.16) *and the path γ are fixed, and $p \to \infty$, we need $O(M(p(\log p)^2)) = p^{1+o(1)}$ bit operations, where $M(n)$ is the complexity of n-bit integer multiplication.*

The main idea behind this method is the following observation. Let $\mathcal{L}$ be a differential operator of order r, and let f be a solution in a neighbourhood of an ordinary point a of $\mathcal{L}$. Assume we know the values $f(a), \ldots, f^{(r-1)}(a)$. As f is solution to $\mathcal{L}$, we may inductively recover $f^{(m)}(a)$ for any $m \in \mathbb{N}$.

Furthermore, assume that f is holomorphic in the disk $D(a, R)$ of center a and radius $R > 0$. The Taylor formula states that for $z \in D\left(a, \frac{R}{2}\right)$, we have

$$\left| f(z) - f(a) + (z-a)f'(a) + \cdots + (z-a)^m \frac{f^{(m)}(a)}{m!} \right| \leq P(m) 2^{-m}\,, \tag{3.18}$$

where P is a polynomial that may be effectively computed. In fact, we know a lower bound for the radius of convergence R: it is greater than the distance between a and the closest singularity of $\mathcal{L}$, which we denote $R(a)$. In particular, if we pick a piecewise linear path γ avoiding the singularities of $\mathcal{L}$, there exists an $\varepsilon > 0$ such that $R(\gamma(t)) > \epsilon$ for all $t \in [0,1]$. In particular, is possible to recover $f(\gamma(t))$ for all $t \in [0,1]$ by decomposing γ in finitely many linear paths of length $\varepsilon/2$. This is illustrated in Fig. 3.1.

We will use this result in two different ways. First, when γ is a loop, the transition matrix along γ is the monodromy matrix of the differential system (3.16) along γ. Second, we use this result to integrate the solutions of (3.16) along a path. Let $R(t) \in \mathbb{C}(t)^{1\times r}$ be a vector of rational functions. Consider the differential system of dimension $r+1$

$$Z' = \left(\begin{array}{c|c} A & 0 \\ \hline R & 0 \end{array}\right) Z. \tag{3.19}$$

The vector solutions are exactly of the form $Z(t) = (Y(t),\ g(t))^t$ where $Y(t)$ is a solution of (3.16) and $g(t)$ is a primitive integral of $R(t) \cdot Y(t)$. More precisely, the fundamental solution at a point b has the form

$$Z_b(t) = \left(\begin{array}{c|c} Y_b(t) & 0 \\ \hline \int_b^t R(t) \cdot Y_b(t) & 1 \end{array}\right). \tag{3.20}$$

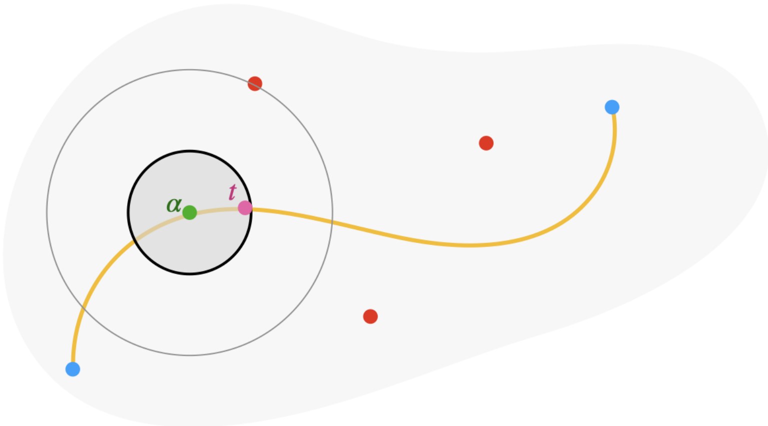

Figure 3.1: *Assuming we know numerical approximations of the values of a function f and its n first derivatives at the point α, the Taylor expansion allows to recover the value at t with precision exponential in m. We may analytically continue f along the orange path by iterating this step.*

The last row of the transition matrix Λ_γ associated to the augmented system (3.19) is therefore $\int_\gamma R(t) \cdot Y_b(t)$ (and the coefficient 1). This gives an algorithm for computing integrals over γ of rational function multiples of the coefficients of vector solutions of (3.16).

As for the practical aspects, we used the implementation of numerical analytic continuation provided in SageMath by Mezzarobba (2016) in the *ore_algebra* package (Kauers et al., 2015). This package deals with scalar differential equations. This has practical implications, but from the mathematical point of view, scalar differential equations and differential systems are equivalent (Haraoka, 2020, Chapter 2).

3.4 Computation of the monodromy matrices of a Lefschetz fibration

Monodromy on the primitive homology

We consider the monodromy action of $\pi_1(\mathbb{P}^1 \setminus \Sigma)$ on $H_{n-1}(\mathcal{X}_b)$. Let ℓ be a loop $\mathbb{P}^1 \setminus \Sigma$, starting from the base point b. As t runs along ℓ, $\mathcal{X}_t$ is continously deformed and there is a uniquely determined continuation $\eta(t)$ of η in $H_{n-1}(\mathcal{X}_t)$. The action of ℓ on η, denoted $\ell_*\eta$ is defined as the determination of $\eta(b)$ after t has travelled along ℓ. It is clear that a linear section of $\mathcal{X}_b$ has trivial monodromy, thus the monodromy action on $H_{n-1}(\mathcal{X}_b)$ induces an action on $PH_{n-1}(\mathcal{X}_b)$.

Computation of a monodromy matrix given a path

Let $\Pi(t)$ be a primitive period matrix of $\mathcal{X}_t$ defined by

$$\Pi_{ij}(t) = \int_{\eta_j(t)} \beta_i(t), \tag{3.21}$$

for some basis η_j of $PH_{n-1}(\mathcal{X}_b)$, and where the $\beta_i(t)$'s form a basis of $\mathcal{PH}$, see Section 3.2. It depends holomorphically on t (on some neighbourhood of b). Combining (3.14) and (3.15), we obtain the first-order linear differential system

$$\Pi'(t) = A(t)\Pi(t). \tag{3.22}$$

In particular, the matrix Π extends holomorphically along the path ℓ and gives another determination, denoted $\ell_*\Pi$, of Π in a neighbourhood of b. Naturally,

$$\ell_*\Pi_{ij}(t) = \int_{\ell_*\eta_j(t)} \beta_i(t). \tag{3.23}$$

In particular, the matrix of the action of ℓ on $H_{n-1}(\mathcal{X}_b)$ in the basis (η_j) is given by

$$\mathrm{Mat}(\ell_*) = \Pi^{-1}(b) \cdot \ell_*\Pi(b) = \Pi^{-1}(b)\Lambda_\ell\Pi(b), \tag{3.24}$$

where Λ_ℓ is the transition matrix introduced in Section 3.3, associated to the differential system (3.22) and the loop ℓ. It is possible to compute Δ_ℓ numerically with arbitrary precision and rigorous error bounds using the differential system (3.22), see Theorem 30. Together with the data of $\Pi(b)$, we compute the entries of $\mathrm{Mat}(\ell_*)$, which are integers, exactly.

Computation of appropriate paths

It only remains to compute a set of generators of $\pi_1(\mathbb{P}^1 \setminus \Sigma)$, which we compute as piecewise linear paths. To do this, we compute the Voronoi diagram of Σ in $\mathbb{C}$. Each critical point $c_i \in \Sigma$ lies in a unique Voronoi cell. Up to adding additional points around the convex hull of Σ, we may assume that the boundary of that cell is a polygon that describes a loop ℓ'_i around the critical point (although not pointed at b). We pick the loop to be anticlockwise.

For each i, we pick a vertex v_i of ℓ'_i. We can then consider the Voronoi graph V, for which the vertices and edges are those of the Voronoi cells. We also add the basepoint b, and an edge connecting the basepoint to the closest other vertex in V. We compute a subtree T of V covering all the v_i and rooted at b. In T there is a unique path p_i connecting b to a given v_i. A simple loop around c_i pointed at b is then given by the composition $\ell_i = p_i^{-1}\ell'_i p_i$.

For the sake of computing the extension around the equator τ_∞ (see (3.29) below), we need to order these paths so that the composition of them is the loop around ∞. We define a supertree T' of T by adding a child corresponding to ℓ'_i at v_i, for each i. For a given node of T', we order its children in anticlockwise order starting from the parent. Finally the ordering on the loops is simply the ordering induced by the prefix ordering of the nodes of T'. This can be achieved with a depth-first search throughout T, illustrated in Fig. 3.2.

3.5 Computation of a homology basis

We seek a description of $H_n(\mathcal{X})$ given the matrices of the monodromy action of $\pi_1(\mathbb{P}^1 \setminus \Sigma)$ on $PH_{n-1}(X_b)$.

Basis of $\mathcal{T}(\mathcal{X})$

Recall the setting of Section 2.1: we have a generating set $\ell_1, \dots, \ell_r$ of $\pi_1(\mathbb{P}^1 \setminus \Sigma, b)$ and we further assume that $\ell_r \cdots \ell_1 = 1$ is the loop at ∞. Each ℓ_i induces an automorphism of $PH_{n-1}(X_b)$, denoted ℓ_{i*}. Thanks to the algorithm given in Section 3.4, we can compute the matrix M_i of ℓ_{i*} with respect to some fixed basis $\beta_1, \dots, \beta_s$ of $PH_{n-1}(\mathcal{X}_b)$.

The linear section h (which is nonzero when n is even) is fixed by ℓ_{i*} By the Picard–Lefschetz formula (2.15), this implies that $\langle h, \delta_i\rangle = 0$. In particular, $\langle h, h\rangle = \deg X \neq 0$, and therefore h is not a vanishing cycle. These two observations show that monodromy action on the quotient is well defined, and the corresponding matrices still satisfy $\operatorname{rk} M_i - I_s = 1$. Thus there are vectors $d_i \in \mathbb{Z}^{s\times 1}$ and $m_i \in \mathbb{Z}^{1\times s}$ such that

$$M_i = I_s + d_i m_i \in \mathbb{Z}^{s\times s}. \tag{3.25}$$

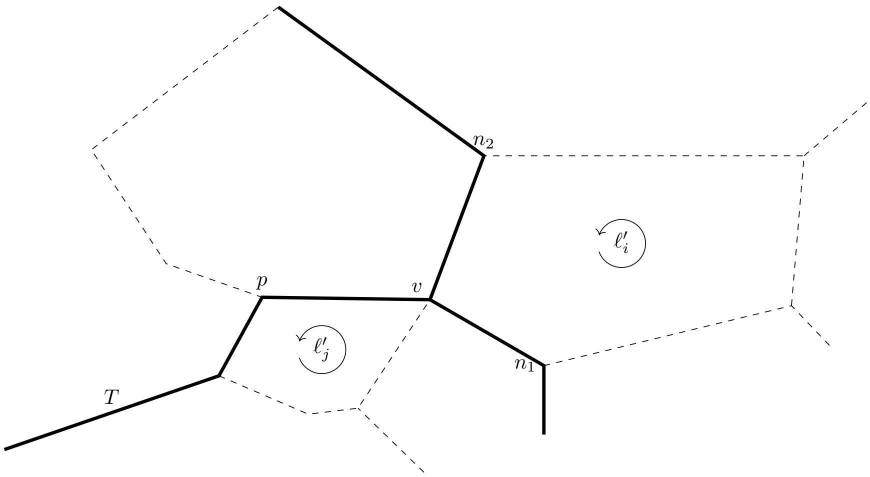

Figure 3.2: *The tree T (bold) is a subtree of the Voronoi graph (dashed) that connects all the points on which the polygonal loops are pointed. Assume we are visiting vertex v, coming from vertex p, and that two polygonal loops ℓ'_i and ℓ'_j are pointed at v. v has three neighbours p, n_1 and n_2. The sorting algorithm will yield j, the result of visiting n_1, i, and finally the result of visiting n_2, in this order. Applying this sorting algorithm from the vertex b gives an order on the loops pointed at b such that their composition is the loop around ∞.*

The vectors d_i and m_i are uniquely determined, up to sign, by M_i. The vector d_i is the coordinates of the vanishing cycle δ_i (see §2.1) in the basis $\beta_1, \ldots, \beta_s$ of $PH_{n-1}(\mathcal{X}_b)$, and m_i is the linear form $\eta \mapsto (-1)^{\frac{n(n+1)}{2}} \langle \eta, \delta_i \rangle$, which is well defined on $PH_{n-1}(\mathcal{X}_b)$ since $\langle h, \delta_i \rangle = 0$.

The extension map $\tau_{\ell_i} : H_{n-1}(\mathcal{X}_b) \to H_n(\mathcal{X}^*, \mathcal{X}_b)$ is described by (2.16) in terms of the linear maps $\langle -, \delta_i \rangle$. In particular, it factors through $PH_{n-1}(\mathcal{X})$, and in the bases $(\beta_j)_{1 \le j \le s}$ for $PH_{n-1}(\mathcal{X}_b)$ and $(\Delta_i)_{1 \le i \le r}$ for $H_n(\mathcal{X}^*, \mathcal{X}_b)$, the matrix T_i of the induced map is given by

$$T_i = (-1)^{n-1} \left(\begin{array}{c} \mathbf{0} \\ \hline m_i \\ \hline \mathbf{0} \end{array} \right) \in \mathbb{Z}^{r \times s}\,, \text{ where } m_i \text{ is the } i\text{-th line.} \tag{3.26}$$

Finally, the boundary map $\delta : H_n(\mathcal{X}^*, \mathcal{X}_b) \to H_{n-1}(\mathcal{X}_b)$ mapping Δ_i to δ_i induces a map $\tilde{\delta} : H_n(\mathcal{X}^*, \mathcal{X}_b) \to PH_{n-1}(\mathcal{X}_b)$. The matrix B of $\tilde{\delta}$ is given by

$$B = \operatorname{Mat}(\tilde{\delta}) = \left(\begin{array}{c|c|c} d_1 & \cdots & d_r \end{array} \right) \in \mathbb{Z}^{s \times r}. \tag{3.27}$$

Recall that τ_∞ is the extension map $H_{n-1}(\mathcal{X}_b) \to H_n(\mathcal{X}^*, \mathcal{X}_b)$ along the equator, which is homotopically equivalent to the composition $\ell_r \cdots \ell_1$. By (2.5), it follows that

$$\tau_\infty = \sum_{i=1}^{r} \tau_{\ell_i} \ell_{i-1*} \cdots \ell_{1*}, \tag{3.28}$$

and therefore, in terms of the notations above, the matrix of the map $PH_{n-1}(\mathcal{X}_b) \to H_n(\mathcal{X}^*, \mathcal{X}_b)$ induced by τ_∞ is

$$T_\infty = T_1 + T_2 M_1 + T_3 M_2 M_1 + \cdots + T_r M_{r-1} \cdots M_1. \tag{3.29}$$

With these matrices in hands, we obtain a basis of $\mathcal{T}(\mathcal{X})$ as $\ker(B)/\operatorname{im}(T_\infty)$.

3.6 Integrating the period matrix

We now explain how to integrate the periods of a form $\omega = \omega_t \wedge \mathrm{d}t$ on the basis of $\mathcal{T}(\mathcal{X})$ obtained in the previous section. We will explain how to obtain such a description of cohomology classes of $\mathcal{X}$ in the specific instances of a hypersurface (Chapter 4) and elliptic surfaces (Chapter 6), as well as some ideas for how to deal with the general case (Chapter 9). However there is to my knowledge no known general way to compute such a representation of cohomology classes of $\mathcal{X}$. In order to compute the period matrix of $H_n(\mathcal{X})$, we first compute the matrix $P_{\mathcal{X}}$ of the pairing $\mathcal{T}(\mathcal{X}) \times PH^n_{\mathrm{DR}}(X) \to \mathbb{C}$

$$(\gamma, \omega) \mapsto \int_{\pi_*(\gamma)} \omega. \tag{3.30}$$

To recover a primitive period matrix of X, it is then sufficient to compute a basis of $\mathcal{T}(Y)/\ker \pi_*$ and extract from $P_{Y,X}$ the relevant submatrix.

Integrating periods

Let $\gamma = \tau_\ell(\eta) \in \mathcal{T}(\mathcal{X})$ be an extension along some path ℓ in $\mathbb{P}^1 \setminus \Sigma$ of some cycle $\eta \in H_{n-1}(\mathcal{X}_b)$. Assume for now that we can write $\omega = \beta \wedge \mathrm{d}f$, for some $(n-1)$-form β on $\mathcal{X}$. Then

$$\int_\gamma \omega = \int_{\tau_\ell(\eta)} \beta \wedge \mathrm{d}f = \int_\ell \left(\int_{\eta_t} \beta|_{X_t} \right) \mathrm{d}t, \tag{3.31}$$

where η_t is the uniquely determined continuation of $\eta \in H_{n-1}(\mathcal{X}_t)$. This expresses the period $\int_\gamma \omega$ as an integral of a period of the fiber $\mathcal{X}_t$, varying with the parameter.

The computations can be more explicitly carried out using the isomorphism between $PH^n_{\mathrm{DR}}(\mathcal{X})$ and $H^{n+1}_{\mathrm{DR}}(\mathcal{X}^{\mathsf{C}})$. Recall that $\mathcal{X}^{\mathsf{C}}$ denotes the complement $\mathbb{P}^{n+1} \setminus X$. Let $\mathcal{X}^* = \mathcal{X} \setminus \mathcal{X}_\infty$, where $\mathcal{X}_\infty$ is the fibre of $f\colon \mathcal{X} \to \mathbb{P}^1$ above the point at infinity. By choice of coordinates, the hyperplane family $(H_t)_{t \in \mathbb{P}^1}$ is given by $H_t = V(x_{n+1} - tx_0)$, and we check that

$$Y' \simeq \{(x,t) \in \mathbb{P}^n \times \mathbb{C} \mid P_t(x_0, \ldots, x_n) = 0\},$$

where $P_t(x_0, \ldots, x_n) = P(x_0, \ldots, x_n, tx_0)$ is the equation of X_t in $\mathbb{P}^n$. Let Y^{C} be the complement of Y', that is

$$Y^{\mathsf{C}} = \{(x,t) \in \mathbb{P}^n \times \mathbb{C} \mid P_t(x_0, \ldots, x_n) \neq 0\}.$$

The map

$$([x_0 : \cdots : x_n], t) \mapsto [x_0 : \cdots : x_n : tx_0]$$

induces a map $\pi\colon Y^{\mathsf{C}} \to X^{\mathsf{C}}$. The Leray residue maps $H^{n+1}(Y^{\mathsf{C}}) \to H_n(Y')$ and $H^{n+1}(X^{\mathsf{C}}) \to H^n(X)$ commute with π. Therefore, given a form $\omega \in PH^n_{\mathrm{DR}}(X)$, which we write as $\mathrm{Res}(\frac{A}{P^k}\Omega_{n+1})$ following Section 3.1, we have

$$\int_{\pi_*\gamma} \omega = \int_\gamma \pi^* \mathrm{Res}\left(\frac{A}{P^k}\Omega_{n+1}\right) = \int_{T(\gamma)} \pi^* \left(\frac{A}{P^k}\Omega_{n+1}\right) = \int_{T(\gamma)} \frac{x_0 A_t}{P_t^k} \Omega_n \wedge \mathrm{d}t \tag{3.32}$$

$$= \int_\ell \left(\int_{T(\eta_t)} \frac{x_0 A_t}{P_t^k} \Omega_n \right) \mathrm{d}t. \tag{3.33}$$

The form $\frac{x_0 A_t}{P_t^k}\Omega_n$ defines an element of the space $\mathcal{H}$ of sections of $PH^n_{\mathrm{DR}}(X_t^{\mathsf{C}})$. In particular, we can write, in $\mathcal{H}$,

$$\frac{x_0 A_t}{P_t^k}\Omega_n = \sum_{i=1}^s r_i(t)\beta_i(t)$$

for some rational functions $r_i(t)$, which we can compute explicitly using the Griffiths–Dwork reduction. The vector $Y' = (y_i(t))_{1\le i\le s}$ defined by $y_i(t) = \int_{\eta_t} \beta_i(t)$ is a solution to the differential system $Y'(t) = A(t)Y(t)$ coming from the Gauss–Manin connection, see (3.15) and (3.22). Moreover, (4.9) gives

$$\int_{\pi_*\gamma} \omega = \int_\ell \sum_{i=1}^{s} r_i(t) y_i(t) \mathrm{d}t. \tag{3.34}$$

We can compute $Y(0)$ from the primitive period matrix of X_b (which we assume is given as input data), and then we can use numerical analytic continuation to compute the integral in (4.11) efficiently (Section 3.3).

Chapter 4

Application : smooth complex projective complete intersections

The methods described in the previous section rely on the knowledge of the primitive period matrix of the fibre above the basepoint $\mathcal{X}_b$. In this instance $\mathcal{X}_b$, is assumed to be a complete intersection. The goal of this section is to provide a way to compute these periods. This will in particular relevant in the next section, which is dedicated to elliptic surfaces, and where the general fibre is thus a smooth cubic curve.

The content of this chapter is in major parts based on Lairez et al. (2024).

Lefschetz pencils and modifications

Let $\mathbb{P}^N$ denote the N-dimensional complex projective space. Let $A \subset \mathbb{P}^N$ be an $N-2$-dimensional projective subspace. The *pencil of axis* A is the one-dimensional family of hyperplanes of $\mathbb{P}^N$ that contain A. It is parametrised by $\mathbb{P}^1$. Concretely, if A is the vanishing locus of two linear forms λ and μ, then for $t \in \mathbb{P}^1$, we define $H_t = V(\lambda - t\mu)$ (and $H_\infty = V(\mu)$).

We consider an irreducible, closed complex complete intersection $\mathcal{X} \subset \mathbb{P}^N$, with dimension $\dim \mathcal{X} = n$. We aim at studying the topology of $\mathcal{X}$ through the intersections of $\mathcal{X}$ with the hyperplanes H_t. For $t \in \mathbb{P}^1$, let

$$\mathcal{X}_t \stackrel{\text{def}}{=} \mathcal{X} \cap H_t. \tag{4.1}$$

For any $x \in \mathcal{X} \setminus A$, there is a unique $t \in \mathbb{P}^1$ such that $x \in H_t$. This defines a rational map $\mathcal{X} \dashrightarrow \mathbb{P}^1$. It is useful to consider a *modification* $\mathcal{Y}$ of $\mathcal{X}$:

$$\mathcal{Y} \stackrel{\text{def}}{=} \{(x,t) \in \mathcal{X} \times \mathbb{P}^1 \mid x \in H_t\}. \tag{4.2}$$

The projection on the first coordinate induces a proper map $\pi \colon \mathcal{Y} \to \mathcal{X}$, which is an isomorphism above $\mathcal{X} \setminus A$. The projection on the second coordinate induces a regular map $f \colon \mathcal{Y} \to \mathbb{P}^1$ which resolves the indeterminacies of the map $\mathcal{X} \dashrightarrow \mathbb{P}^1$. The map π is the blowup of X at the base locus $\mathcal{X}' \stackrel{\text{def}}{=} \mathcal{X} \cap A$ of $\mathcal{X} \dashrightarrow \mathbb{P}^1$. The fibre $f^{-1}(t)$ above some $t \in \mathbb{P}^1$ is isomorphic to $\mathcal{X}_t$. Indeed, by definition, $f^{-1}(t) = \{x \in \mathcal{X} \mid x \in H_t\} = \mathcal{X} \cap H_t$.

Let $\Sigma \stackrel{\text{def}}{=} \{f(x) \mid x \in \mathcal{Y} \text{ and } \mathrm{d}f = 0\}$ be the set of critical values. It is also the set of all $t \in \mathbb{P}^1$ such that $\mathcal{X}_t$ is singular. It is well known that Σ is finite (since f is locally constant on the subvariety $\{\mathrm{d}f = 0\} \subseteq \mathcal{Y}$). We will work under the hypothesis that the fibration is a Lefschetz fibration — i.e., that all the critical points of f are nondegenerate (meaning the Hessian matrix at the critical point is nonsingular) and the critical values associated to different critical points are distinct, see Section 2.2. This condition is mild: it is satisfied for a generic choice of A (Lamotke, 1981, §1.6).

The exposition of Chapter 2 provides a way to recover a description of the homology of $\mathcal{Y}$ in terms of extensions and compute certain of its periods. In order to recover the periods of $\mathcal{X}$, we have two things to do:

- Specify the self-intersection of the section S in Lemma 25.
- Obtain a description of the algebraic DeRham cohomology $H^n_{\mathrm{DR}}(\mathcal{X})$ (together with the Hodge filtration) in terms of the relative DeRham cohomology of the fibration $\mathcal{H}(\mathcal{Y}/\mathbb{P}^1)$ so we may use the methods of Chapter 3 to compute their associated periods.
- Recover a description of the homology of $\mathcal{X}$ from that of $\mathcal{Y}$.

Once these points are addressed, we obtain an algorithm for computing the periods of a complete intersection, by induction on the dimension of $\mathcal{X}$. Let $H \subseteq \mathbb{P}^{n+1}$ be a generic hyperplane. A primitive period matrix of $\mathcal{X}$ is computed from a primitive period matrix of $\mathcal{X} \cap H$ (as a complete intersection in $H \simeq \mathbb{P}^n$). To this end, we choose a pencil of hyperplanes $\{H_t\}_{t\in\mathbb{P}^1}$ and a base point b such that $H_b = H$ and which induces a Lefschetz fibration, as defined in Section 2.2.

Up to a change of coordinates, we may assume that the pencil is given by $H_t = V(x_{n+1} - tx_0)$. As in the previous sections, we consider the rational map $f\colon \mathcal{X} \dashrightarrow \mathbb{P}^1$ given by $[\mathbf{x}] \mapsto [x_0 : x_{n+1}]$. We consider the blowup $\pi\colon \mathcal{Y} \to \mathcal{X}$ of $\mathcal{X}$ along the base locus $\mathcal{X}' = \mathcal{X} \cap V(x_0, x_1)$ of the pencil. The composition $f \circ \pi\colon \mathcal{Y} \to \mathbb{P}^1$ extends to a regular map on Y, also denoted f. The fibre $\mathcal{X}_t \overset{\text{def}}{=} f^{-1}(t)$ is isomorphic to the intersection $\mathcal{X} \cap H_t$. The set of critical values is denoted Σ, it is the set of all t such that $\mathcal{X}_t$ is singular.

The main steps of the algorithms are:

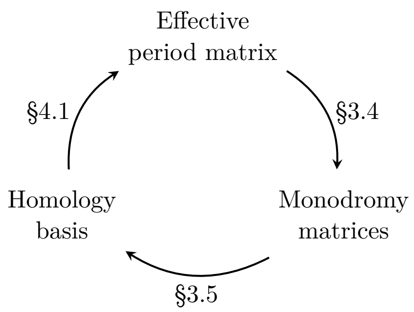

1. derive the action of monodromy of $\pi_1(\mathbb{P}^1 \setminus \Sigma)$ on $H_{n-1}(\mathcal{X}_b)$ from the primitive period matrix of $\mathcal{X}_b$, see Section 3.4;
2. compute a basis of homology of $H_n(\mathcal{Y})$ from the action of monodromy, see Section 4.1;
3. compute a primitive period matrix of $\mathcal{X}$ by integrating the varying periods of $\mathcal{X}_t$ in an appropriate way, see Section 4.1.

The base case for this induction is the case of 0-dimensional varieties, where a description of homology and the effective period matrix can be obtained directly. We will deal with this case right below in the case of hypersurfaces. From then on, steps (1), (2), (3) allow to recover the effective period matrix of a curve, another iteration the one of surfaces, and so on.

Primitive period matrix of a 0-dimensional hypersurface

Let P be a homogeneous polynomial in two variables defining a smooth variety $\mathcal{X} = V(P)$ in $\mathbb{P}^1$. In this case we obtain the primitive period matrix of $\mathcal{X}$ explicitly from the usual residue formula for rational functions.

More precisely, the middle homology group $H_0(\mathcal{X})$ is freely generated by d points. The cohomology space $H^0_{\mathrm{DR}}(\mathcal{X})$ is the set of functions $\mathcal{X} \to \mathbb{C}$. The linear section h is the sum of all points. In particular $PH^0_{\mathrm{DR}}(\mathcal{X})$ is the set of functions $r\colon X \to \mathbb{C}$ with $\sum_{x\in\mathcal{X}} r(x) = 0$. A basis of the middle primitive cohomology space $H^1_{\mathrm{DR}}(\mathcal{X}^{\complement})$ is given by the rational forms $\omega_k = \frac{x^k y^{d-k-2}}{P}\Omega_1$ for

$0 \leq k \leq d-2$, where $\Omega_1 = y\mathrm{d}x - x\mathrm{d}y$ is the volume form of $\mathbb{P}^1$. The residue mapping $H^1_{\mathrm{DR}}(\mathcal{X}^\complement) \to H^0(\mathcal{X})$ is the classical residue

$$\frac{A}{P}\Omega_1 \mapsto \left(z \in X \mapsto \mathrm{Res}_z\left(\frac{A}{P}\Omega_1\right)\right), \tag{4.3}$$

the tube map $T\colon H_0(\mathcal{X}) \to H_1(\mathcal{X}^\complement)$ maps a point of $\mathcal{X}$ to a loop around it, and Equation (3.3) is Cauchy's residue theorem. Since the sum of residues is zero, the image of the residue mapping is indeed included in $PH^0_{\mathrm{DR}}(\mathcal{X})$.

We choose $d-1$ roots $z_1, \ldots, z_{d-1}$ of P in X in the affine chart $y = 1$, they give a basis of $PH_0(X)$ and a primitive period matrix of X is given by the coefficients

$$z_i^j \frac{\partial P}{\partial x}(z_i)^{-1}, \tag{4.4}$$

for $1 \leq i \leq d-1$ and $0 \leq j \leq d-2$.

4.1 Computation of the primitive period matrix

In this section, we provide a method to compute the period matrix $P_{\mathcal{Y},\mathcal{X}}$ of the pairing between $PH^n_{\mathrm{DR}}(\mathcal{X})$ and the pushforward $\mathcal{T}(\mathcal{Y})$, From the knowledge of this matrix and the exceptional divisors in $\mathcal{T}(\mathcal{Y})$, a primitive period matrix of $\mathcal{X}$ can then be recovered. We start with the following theorem, showing that the primitive homology of $\mathcal{X}$ is entirely described by pushforwards of extensions of $\mathcal{Y}$.

Theorem 31. *Let K be the kernel of the map $H_{n-2}(\mathcal{X}') \to H_{n-2}(\mathcal{X}_b)$ induced by inclusion. We have an exact sequence*

$$0 \to K \to \mathcal{T}(\mathcal{Y}) \to PH_n(\mathcal{X}) \to 0. \tag{4.5}$$

Proof. We extend the commutative diagram of Theorem 18 by including the exact sequence from Lamotke (1981, (3.1.2)). The dashed arrow is induced by inclusion. Indeed, let A be a closed $n-2$-chain in $H_{n-2}(\mathcal{X}')$. It is sent to $A \times \mathbb{P}^1$ in $H_n(\mathcal{Y})$, which is then included in $H_n(\mathcal{Y}, \mathcal{X}_b)$ and then $H_n(\mathcal{Y}, \mathcal{Y}_+) \cap H_{n-2}(\mathcal{X}_b)$, where the identification is given by intersecting with $\mathcal{X}_b$, which yields A again.

$$\begin{tikzcd}
 & & H_n(\mathcal{X}_b) \arrow[d, "\iota_*"] \arrow[dr, "\iota_*"] & & \\
0 \arrow[r] & H_{n-2}(\mathcal{X}') \arrow[r] \arrow[drr, dashed] & H_n(\mathcal{Y}) \arrow[r, "\pi_*"] \arrow[d] & H_n(\mathcal{X}) \arrow[r] & 0 \\
H_{n-1}(\mathcal{X}_b) \arrow[r, "\tau_\infty"] & H_n(\mathcal{Y}_+, \mathcal{X}_b) \arrow[r] \arrow[dr, "\partial"'] & H_n(\mathcal{Y}, \mathcal{X}_b) \arrow[r] \arrow[d, "\partial"] & H_{n-2}(\mathcal{X}_b) \arrow[r] & 0 \\
 & & H_{n-1}(\mathcal{X}_b) & &
\end{tikzcd}, \tag{4.6}$$

Importantly, the dashed arrow $H_{n-2}(X') \to H_{n-2}(X_b)$ is surjective, by Lefschetz' hyperplane theorem, since X' is a hyperplane section of X_b. Now, the exact sequence follows from diagram chasing in (4.6). □

With the methods of Chapter 2 and Chapter 3, we may obtain a description of a basis of $\mathcal{T}(\mathcal{Y})$ and, by Theorem 31, $\pi\colon \mathcal{Y} \to \mathcal{X}$ induces a surjective map $\mathcal{T}(\mathcal{Y}) \to PH_n(\mathcal{X})$. In order to compute the period matrix of $H_n(\mathcal{X})$, we first compute the matrix $P_{\mathcal{Y},\mathcal{X}}$ of the pairing $\mathcal{T}(\mathcal{Y}) \times PH^n_{\mathrm{DR}}(\mathcal{X}) \to \mathbb{C}$

$$(\gamma, \omega) \mapsto \int_{\pi_*(\gamma)} \omega. \tag{4.7}$$

To recover a primitive period matrix of $\mathcal{X}$, it is then sufficient to compute a basis of $\mathcal{T}(\mathcal{Y}) / \ker \pi_*$ and extract from $P_{\mathcal{Y},\mathcal{X}}$ the relevant submatrix.

Integrating periods

Let $\omega \in PH^n_{\mathrm{DR}}(\mathcal{X})$ and $\gamma \in \mathcal{T}(\mathcal{Y})$. By definition, γ is the extension along some path ℓ in $\mathbb{P}^1 \setminus \Sigma$ of some cycle $\eta \in H_{n-1}(\mathcal{X}_b)$. Assume for now that we can write $\pi^*\omega = \beta \wedge \mathrm{d}f$, for some $n-1$-form β on $\mathcal{Y}$. Then

$$\int_{\pi_*\gamma} \omega = \int_\gamma \pi^*\omega = \int_{\tau_\ell(\eta)} \beta \wedge \mathrm{d}f = \int_\ell \left(\int_{\eta_t} \beta|_{\mathcal{X}_t} \right) \mathrm{d}t, \tag{4.8}$$

where η_t is the uniquely determined continuation of $\eta \in H_{n-1}(\mathcal{X}_t)$ along ℓ. This expresses the period $\int_{\pi_*\gamma} \omega$ as an integral of a period of the fiber $\mathcal{X}_t$, varying with the parameter t.

The computations can be more explicitly carried out using the isomorphism between $PH^n_{\mathrm{DR}}(\mathcal{X})$ and $H^{n+1}_{\mathrm{DR}}(\mathcal{X}^\complement)$. Recall that $X^\complement$ denotes the complement $\mathbb{P}^{n+1} \setminus \mathcal{X}$. Let $\mathcal{Y}' = \mathcal{Y} \setminus \mathcal{Y}_\infty$, where $\mathcal{Y}_\infty$ is the fibre of $f\colon \mathcal{Y} \to \mathbb{P}^1$ above the point at infinity. By choice of coordinates, the hyperplane family $(H_t)_{t\in\mathbb{P}^1}$ is given by $H_t = V(x_{n+1} - tx_0)$, and we check that

$$\mathcal{Y}' \simeq \{(x,t) \in \mathbb{P}^n \times \mathbb{C} \mid P_t(x_0, \ldots, x_n) = 0\},$$

where $P_t(x_0, \ldots, x_n) = P(x_0, \ldots, x_n, tx_0)$ is the equation of $\mathcal{X}_t$ in $\mathbb{P}^n$. Let $\mathcal{Y}^\complement$ be the complement of Y', that is

$$\mathcal{Y}^\complement = \{(x,t) \in \mathbb{P}^n \times \mathbb{C} \mid P_t(x_0, \ldots, x_n) \neq 0\}.$$

The map

$$([x_0 : \cdots : x_n], t) \mapsto [x_0 : \cdots : x_n : tx_0]$$

induces a map $\pi\colon \mathcal{Y}^\complement \to X^\complement$. The Leray residue maps $H^{n+1}(\mathcal{Y}^\complement) \to H_n(Y')$ and $H^{n+1}(X^\complement) \to H^n(\mathcal{X})$ commute with π. Therefore, given a form $\omega \in PH^n_{\mathrm{DR}}(\mathcal{X})$, which we write as $\mathrm{Res}(\frac{A}{P^k}\Omega_{n+1})$ following Section 3.1, we have

$$\int_{\pi_*\gamma} \omega = \int_\gamma \pi^* \mathrm{Res}\left(\frac{A}{P^k}\Omega_{n+1}\right) = \int_{T(\gamma)} \pi^*\left(\frac{A}{P^k}\Omega_{n+1}\right) = \int_{T(\gamma)} \frac{x_0 A_t}{P_t^k}\Omega_n \wedge \mathrm{d}t \tag{4.9}$$

$$= \int_\ell \left(\int_{T(\eta_t)} \frac{x_0 A_t}{P_t^k}\Omega_n \right) \mathrm{d}t. \tag{4.10}$$

The form $\frac{x_0 A_t}{P_t^k}\Omega_n$ defines an element of the space $\mathcal{H}$ of sections of $PH^n_{\mathrm{DR}}(\mathcal{X}_t^\complement)$. In particular, we can write, in $\mathcal{H}$,

$$\frac{x_0 A_t}{P_t^k}\Omega_n = \sum_{i=1}^s r_i(t)\beta_i(t)$$

for some rational functions $r_i(t)$, which we can compute explicitly using the Griffiths–Dwork reduction. The vector $Y' = (y_i(t))_{1\leq i\leq s}$ defined by $y_i(t) = \int_{\eta_t} \beta_i(t)$ is a solution to the differential system $Y'(t) = A(t)Y(t)$ coming from the Gauss–Manin connection, see (3.15) and (3.22). Moreover, (4.9) gives

$$\int_{\pi_*\gamma} \omega = \int_\ell \sum_{i=1}^s r_i(t) y_i(t) \mathrm{d}t. \tag{4.11}$$

We can compute $Y(0)$ from the primitive period matrix of $\mathcal{X}_b$ (which we assume is given as input data), and then we can use numerical analytic continuation to compute the integral in (4.11) efficiently (Section 3.3).

Kernel of $\mathcal{T}(\mathcal{Y}) \to PH_n(\mathcal{X})$

The final step to get the primitive period pairing $PH_n(\mathcal{X}) \times PH^n_{\mathrm{DR}}(\mathcal{X})$ is to identify the cycles stemming from the blowup of the base locus of the fibration $\mathcal{Y} \to \mathcal{X}$. We present here a heuristic method relying on finding linear integer relations between the periods, which has the advantage of being computationally cheap. This method uses the duality between $PH_n(\mathcal{X})$ and $PH^n_{\mathrm{DR}}(\mathcal{X})$ to obtain that

$$\ker\left(\pi_* : \mathcal{T}(\mathcal{Y}) \to PH_n(\mathcal{X})\right) = \left\{ \gamma \in \mathcal{T}(\mathcal{Y}) \;\middle|\; \forall \omega \in PH^n_{\mathrm{DR}}(\mathcal{X}), \int_{\pi_*(\gamma)} \omega = 0 \right\}. \tag{4.12}$$

This amounts to computing the kernel of a full-rank matrix with complex coefficients, knowing that it is generated by integer-coefficient vectors. This is numerically stable as the matrix we consider has full rank. In practice, the coefficients are small and we can compute them using lattice-reduction algorithms. However, we cannot certify this computation. In Section 4.2.1 we give a certified method for finding the coefficients of the blowups in terms of the thimbles in the case of surfaces. This method generalises to higher dimensions but we did not implement it.

Since the matrix of the pairing $PH_n(\mathcal{X}) \times PH^n_{\mathrm{DR}}(\mathcal{X})$ is non-degenerate, the kernel of π_* is exactly the left-kernel of the full-rank matrix $P_{\mathcal{Y},\mathcal{X}}$. This is a sublattice of $\mathcal{T}(\mathcal{Y})$, so $\ker \pi_*$ is generated by integer-coefficient vectors. We present an alternative rigorous way of computing $\ker \pi_*$ in Section 4.2.1.

4.2 Removing blow-ups

In addition to the effective period matrix, we wish to recover the intersection product of $H_n(\mathcal{X})$ in the basis we have computed. This is the focus of this section.

4.2.1 Exceptional divisors as thimbles

We begin with the case of surfaces to develop intuition, and then generalise to complete intersections.

The case of surfaces

The exceptional locus $\mathcal{X}'$ of the map $\mathcal{X} \dashrightarrow \mathbb{P}^1$ is the intersection of $\mathcal{X}$ with a (generic) line. It is therefore a set of d points $s_1, \dots, s_d$, where $d = \deg \mathcal{X}$. The modification $\pi \colon \mathcal{Y} \to \mathcal{X}$ is the blowup of $\mathcal{X}$ along $\mathcal{X}'$. Let $E_1, \dots, E_d \subset Y$ denote the d components of the exceptional divisor, that is $E_k = \pi^{-1}(s_k)$. They are all isomorphic to $\mathbb{P}^1$, and linearly independent. The E_k's define classes in $H_2(\mathcal{Y})$ and we have the exact sequence (Lamotke, 1981, (3.1.2))

$$0 \to \bigoplus_{k=1}^{d} \mathbb{Z}E_k \to H_2(\mathcal{Y}) \to H_2(\mathcal{X}) \to 0. \tag{4.13}$$

For any two E_k and E_j, the intersection $(E_k - E_j) \cap \mathcal{X}_b$ is the difference of two points, which is homologous to 0 in $H_0(\mathcal{X}_b)$. Therefore, by Theorem 18, the homology class of $E_k - E_j$ comes from a uniquely determined element in $\mathcal{T}(\mathcal{Y})$. In particular, we obtain the exact sequence

$$0 \to \bigoplus_{k=2}^{d} \mathbb{Z}(E_k - E_1) \to \mathcal{T}(\mathcal{Y}) \to PH_2(\mathcal{X}) \to 0. \tag{4.14}$$

We can compute the image of $E_k - E_1$ in $\mathcal{T}(Y)$ in terms of the Lefschetz thimbles as follows. Let $p_1, \ldots, p_r$ be non-intersecting paths in $\mathbb{P}^1$ connecting b to the critical points $t_1, \ldots, t_r$ respectively. Consider $T = \cup_{i=1}^r p_i \subset \mathbb{P}^1$. It defines an oriented tree covering the critical points of f. Finally let $U = \mathbb{P}^1 \setminus T$. It is a simply connected subset of $\mathbb{P}^1 \setminus \Sigma$, above which f has no critical point. From Thom's isotopy lemma (Mather, 2012) applied to the pair $(Y, \pi^{-1}(\mathcal{X}'))$ we obtain a trivialisation of the fibration $f^{-1}(U) \to U$ where the points s_k are fixed in the fibres. In other words, there is a homeomorphism $\phi\colon f^{-1}(U) \to X_{b'} \times U$, where $b' \in U$, such that the following diagram is commutative

$$\begin{tikzcd}
\mathcal{X}' \times U \arrow[d, "\iota"] \arrow[dr, "\iota_2"] & \\
f^{-1}(U) \arrow[r, "\phi"] \arrow[d, "f"] & \mathcal{X}_b \times U \arrow[dl, "p_2"] , \\
U &
\end{tikzcd} \tag{4.15}$$

where ι and ι_2 are inclusions.

Take a 1-chain α_k in $\mathcal{X}_{b'}$ such that $\partial\alpha_k = s_k - s_1$ (in other words, α_k is the relative homology class of a path connecting s_k to s_1 in $\mathcal{X}_{b'}$). For $u \in U$, let $\alpha_k(u) = \phi^{-1}(\{u\} \times \alpha_k)$. Note that

$$\partial\alpha_k(u) = \iota_*(s_k, u) - \iota_*(s_1, u) = s_k - s_1. \tag{4.16}$$

For $t \in T$ not a vertex, that is $t \neq b$ and $t \notin \Sigma$, define $\alpha_k(t^+)$ and $\alpha_k(t^-)$ as the left and right limit of $\alpha_k(u)$ as $u \to t$ for $t \in T$ (where the direction is given by the orientation of T). Since s_k and s_1 are fixed, $\partial(\alpha_k(t^+) - \alpha_k(t^-)) = 0$, and this chain defines a cycle $v_k(t) \in H_1(X_t)$. Let $v_{kj} \in H_1(\mathcal{X}_b)$ be the limit of $v_k(t)$ as $t \to b$ along the j-th branch of T.

Lemma 32. *With the above notations, the cycle $v_{kj} \in H_1(\mathcal{X}_b)$ is a multiple of δ_j, the vanishing cycle associated to the critical value t_j.*

Proof. Consider a small enough ball B in Y around the critical point associated to the critical value t_j. Let $t \in T$ be very close to t_j. The paths $\alpha_k(t^+)$ and $\alpha_k(t^-)$ define an element of $H_1(\mathcal{X}_t, \mathcal{X}_t \setminus B)$. Following a loop from t around t_i transforms $\alpha_k(t^-)$ into $\alpha(t^+)$. By (Lamotke, 1981, (6.5.1)), the extension of $\alpha_k(t^+)$ along a loop around t_j gives a multiple of the j-th thimble. In particular the boundary of this extension, which is just $\alpha_k(t^+) - \alpha_k(t^-)$, is a multiple of the vanishing cycle δ_j. Since v_{kj} is the deformation of $\alpha_k(t^+) - \alpha_k(t^-)$ along the j-th branch, we obtain the claim. □

Let $m_{kj} \in \mathbb{Z}$ such that $v_{kj} = m_{kj}\delta_j$.

Lemma 33. *With the above notations, $E_k - E_1 = \sum_{j=1}^r m_{kj}\Delta_j$ in $\mathcal{T}(\mathcal{Y})$.*

Proof. Consider in $\mathcal{Y}$ the 3-chain

$$B = \overline{\phi^{-1}(\alpha_k \times U)} = -\overline{\cup_{u\in U}\alpha_k(u)}. \tag{4.17}$$

The border ∂B defines an element of $H_2(Y)$. It decomposes into a part coming from the border of α_k and another coming from the border of U. The part coming from $\partial\alpha_k$ is the closure of all $\partial\alpha_k(u)$, which is $E_k - E_1$ by (4.16). The part coming from ∂U is $\cup_{t\in T}(\alpha_k(t^+) - \alpha_k(t^-))$. For

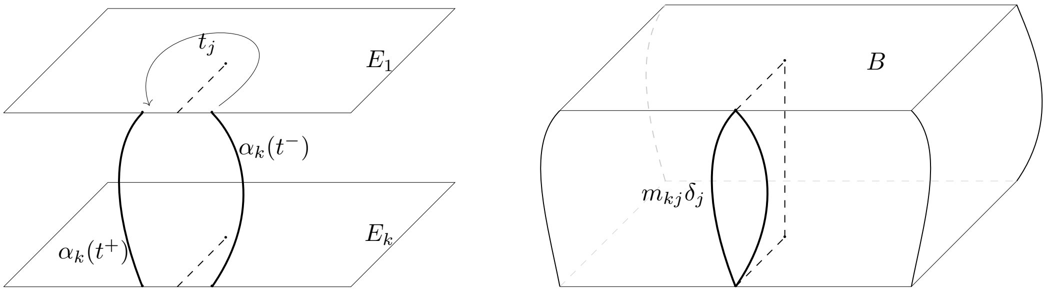

(a) *A 1-chain α_k connecting s_0 to s_1 in one of the fibres may have monodromy around the critical values t_j. Above T the chain $\alpha_k(t^+) - \alpha_k(t^-)$ has no boundary, and thus represents a 1-cycle.*

(b) *We obtain a 3-chain B by extending A to all of $\mathbb{P}^1 \setminus T$. The boundary of B is the sum of $E_k - E_1$ with the 2-chain $\cup_{t\in T}(\alpha_k(t^+) - \alpha_k(t^-))$. Since the intersection of this 2-chain with p_j has boundary only in X_b, $\alpha_k(t^+) - \alpha_k(t^-)$ is a multiple of the vanishing cycle δ_j.*

Figure 4.1: *The action of monodromy on relative homology and total transforms*

a given edge p_j of T, the union $\cup_{t\in p_j}(\alpha_k(t^+) - \alpha_k(t^-))$ is the extension along p_j of the cycle v_{kj}. Since v_{kj} is a multiple of the vanishing cycle $m_{kj}\delta_j$, the boundary of $\cup_{t\in p_j}(\alpha_k(t^+) - \alpha_k(t^-))$ is $m_{kj}\delta_j$. In particular this extension is a multiple of the Lefschetz' thimble Δ_j with the same factor. □

An illustration of this construction is given in Fig. 4.1.

Higher dimensions

In the general case, we have the exact sequence

$$0 \to H_{n-2}(\mathcal{X}') \to H_n(\mathcal{Y}) \to H_n(\mathcal{X}) \to 0. \tag{4.18}$$

Recall from Lemma 23 the decomposition $H_{n-1}(\mathcal{X}') = K \oplus \langle \eta \rangle$ where K is the kernel of the inclusion $H_{n-2}(\mathcal{X}') \to H_{n-2}(\mathcal{X}_b)$ and the intersection of $\eta \in H_{n-2}(\mathcal{X}')$ with the linear class $h_{\mathcal{X}'}$ of $H_{n-2}(\mathcal{X}')$ is $\langle \eta, h_{\mathcal{X}'} \rangle = 1$. Again, by Theorem 18, for $\gamma \in K$, the homology class of $[\gamma \times \mathbb{P}^1]$ in $H_n(\mathcal{X})$ comes from a uniquely determined element in $\mathcal{T}(\mathcal{Y})$. In particular, we obtain the exact sequence

$$0 \to K \to \mathcal{T}(\mathcal{Y}) \to PH_n(\mathcal{X}) \to 0. \tag{4.19}$$

From Lemma 23, K is generated by the vanishing cycles of the fibration of $\mathcal{X}_b$. Let $\gamma_1, \dots, \gamma_s \in K$ be a basis of K, of which the elements are vanishing cycles of the modification of $\mathcal{X}_b$. Each γ_k induces a total transform $[\gamma_k \times \mathbb{P}^1]$ in $H_n(\mathcal{Y})$, denoted Γ_k.

As γ_k is a vanishing cycle, it is the boundary of a thimble of the modification $\mathcal{X}_b \to \mathbb{P}^1$. This thimble is represented by an n-chain $[A_k]$ (obtained from an extension along a loop)

$$\partial[A_k] = \gamma_k \in H_{n-2}(\mathcal{X}')\,. \tag{4.20}$$

Again, we may recover Γ_k in terms of the thimbles of $\mathcal{Y}$. Consider the restriction $\tilde{f}$ of the fibration $f\colon \mathcal{Y} \to \mathbb{P}^1$ to $\mathcal{Y} \setminus (\mathcal{X}' \times \mathbb{P}^1)$. Let $T \subset \mathbb{P}^1$ be the union of non-intersecting paths $\ell_1, \dots, \ell_r$ connecting the basepoint b to the critical points $t_1, \dots, t_r$ of f. In particular T is an oriented covering tree of the critical points of $\tilde{f}$. Define $U = \mathbb{P}^1 \setminus T$. Similarly to the 2-dimensional case, Thom's isotopy lemma yields a trivialisation $\phi\colon \tilde{f}^{-1}(U) \simeq (\mathcal{X}_b \setminus \mathcal{X}') \times U$.

For $u \in U$, let $A_k(u) = \phi^{-1}(\{u\} \times A_k)$ and see that

$$\partial A_k(u) = \gamma_k \,. \tag{4.21}$$

Define $A_k^+(t)$ and $A_k^-(t)$ the left and right limits of $A_k(u)$ as $u \to t$, for $t \in T$ not a vertex. Then

$$\partial \left(A_k^+(t) - A_k^-(t)\right) = 0\,, \tag{4.22}$$

and the homology class of $A_k^+(t) - A_k^-(t)$ defines a cycles $v_k(t) \in H_{n-1}(\mathcal{X}_t)$. Finally define v_{kj} the transportation of $v_k(t)$ as $t \to b$ along the j-th branch of T.

Lemma 34. *With the above notations, the cycle $v_{kj} \in H_{n-1}(\mathcal{X}_b)$ is a multiple of δ_j, the vanishing cycle associated to the critical value t_j.*

Proof. The proof is the same as that of Lemma 32 □

Let $m_{kj} \in \mathbb{Z}$ such that $v_{kj} = m_{kj}\delta_j$.

Lemma 35. *With the above notations, $\Gamma_k = \sum_{j=1}^r m_{kj}\Delta_j$ in $\mathcal{T}(\mathcal{Y})$ where Δ_j is the thimble corresponding to the path p_j.*

Proof. Again, the proof is essentially the same as that of Lemma 33 □

Both in the 2-dimensional case and higher, the recovery of the exceptional divisors relies on the knowledge of the action of monodromy on the thimbles. The next section describes a way to compute it.

4.2.2 Monodromy action on relative homology

Consider the relative homology space $H_{n-1}(\mathcal{X}_b, \mathcal{X}')$, where $\mathcal{X}'$ is the exceptional locus. As in the previous section, let $\gamma_1, \dots, \gamma_r$ be a basis of vanishing cycles generating K, and let $\alpha_1, \dots, \alpha_r$ be the corresponding thimbles. It follows directly from the long exact sequence of relative homology of the pair $(\mathcal{X}_b, \mathcal{X}')$ that

$$H_{n-1}(\mathcal{X}_b, \mathcal{X}') \simeq H_{n-1}(\mathcal{X}_b) \oplus \bigoplus_{i=2}^{d} \mathbb{Z}\gamma_k. \tag{4.23}$$

Following the construction in the previous section, we have a monodromy action of $\pi_1(\mathbb{P}^1 \setminus \Sigma, b)$ on $H_{n-1}(\mathcal{X}_b, \mathcal{X}')$ which extends the monodromy action on $H_{n-1}(\mathcal{X}_b)$.

In view of Lemma 35, the problem of computing the exceptional divisors in $\mathcal{T}(Y)$ reduces to the computation of the coefficients m_{kj}, which are determined by the monodromy action on $H_{n-1}(\mathcal{X}_b, \mathcal{X}')$.

Lemma 36. *The integers m_{kj} in Lemma 35 satisfy*

$$\ell_{j*}\alpha_k = \alpha_k + m_{kj}\delta_j.$$

Proof. This is simply a reformulation of the definition of m_{kj}. □

The method described in Section 3.4 to compute the matrices of the monodromy action on $H_{n-1}(\mathcal{X}_b)$ extends to the relative case to compute the action on $H_{n-1}(\mathcal{X}_b, \mathcal{X}')$. We provide detail in the case of hypersurfaces.

We choose a basis $\omega_1, \dots, \omega_r$ of $\mathcal{H}$ in the form

$$\omega_i = \operatorname{Res} \frac{B_i}{P_t^{k_i}} \Omega_2. \tag{4.24}$$

Recall the period matrix $\Pi(t)$ defined by the coefficients

$$\Pi_{ij}(t) = \int_{\eta_j(t)} \omega_i(t) = \int_{T(\eta_j(t))} \frac{B_i}{P_t^{k_i}} \Omega_2, \tag{4.25}$$

where $T : H_1(\mathcal{X}_t) \to H_2(\mathbb{P}^2 \setminus \mathcal{X}_t)$ is the Leray tube map. Recall that $\Pi(t)$ satisfies a differential equation $\Pi'(t) = A(t)\Pi(t)$, see (3.22), and that the monodromy action on the solution space of this differential equation is dual to the monodromy action on $H_1(X_b)$.

We can extend the matrix $\Pi(t)$ with integrals related to the paths $\alpha_k(t)$. For each k, we define a Leray tube $T(\alpha_k(t))$ around $\alpha_k(t)$ as follows. For each point p of $\alpha_k(t)$, we choose, continuously with respect to p, a line L_p in $\mathbb{P}^2$ passing through p and not tangent to X_t. Then, for ε small enough, we define $T(\alpha_k(t))$ as the union over all points $p \in \alpha_k(t)$ of the ε-circle in L_p with center p. Up to homotopy, $T(\alpha_k(t))$ only depends on the choice of L_{s_1} and L_{s_k}, which determine the border. Indeed, for each p, the space of possible lines L_p is contractible, so the choice of L_p is irrelevant. We assume that L_{s_1} and L_{s_k} are fixed, so that the border of $T(\alpha_k(t))$ is constant.

Let

$$\Theta_{ik}(t) = \int_{T(\alpha_k(t))} \frac{B_i}{P_t^{k_i}} \Omega_2. \tag{4.26}$$

It is an analytic function of t, in a neighbourhood of b. Indeed, if t is close enough to b, then $T(\alpha_k(t))$ deforms into $T(\alpha_k(b))$ in $X_t^{\complement}$, with fixed boundary. So the integral (4.26) may be taken over the fixed domain $T(\alpha_k(b))$. Since the integrand depends analytically on the parameter t, this shows that $\Theta_{ik}(t)$ depends analytically on t. By following the deformation of the path $\alpha_k(t)$, the function Θ_{ik} extends meromorphically on any simply connected open subset of the complex plane avoiding the singular values Σ. (There may be poles at points t where L_{s_1} or L_{s_k} are tangent to X_t.) After extending $\Theta_{ik}(t)$ over a loop ℓ_j, we obtain a new determination ${\ell_j}_* \Theta_{ik}$ which satisfies

$${\ell_j}_* \Theta_{ik}(t) = \int_{T(\alpha_k(t) + v_{kj}(t))} \frac{B_i}{P_t^{k_i}} \Omega_2 = \Theta_{ik}(t) + m_{kj} \int_{\delta_j(t)} \omega_i(t). \tag{4.27}$$

In particular, the monodromy action on the functions Θ_{ik} determine the coefficients m_{kj}, and therefore the monodromy action on $H_1(X_b, X')$.

It remains to see that the Θ_{ik} are solutions of a differential system, so that the monodromy action can be recovered by numerical integration. Indeed, by definition of $\mathcal{H}$, there are some β_i 1-forms on $X_t^{\complement}$ such that

$$\frac{\partial}{\partial t} \frac{B_i}{P_t^{k_i}} \Omega_2 = \sum_j a_{ij}(t) \frac{B_j}{P_t^{k_i}} \Omega_2 + \mathrm{d}\beta_i. \tag{4.28}$$

After integrating over $T(\alpha_k(t))$, we obtain

$$\Theta'_{ik}(i) = \sum_j a_{ij}(t) \Theta_{ik}(t) + \int_{T(\alpha_k(t))} \mathrm{d}\beta_i. \tag{4.29}$$

The boundary of $T(\alpha_k(t))$ is two circles, one in L_{s_k} and one in L_{s_1} (with a minus sign), so by Stokes' and Cauchy's formulae,

$$\int_{T(\alpha_k(t))} \mathrm{d}\beta_i = \int_{\partial T(\alpha_k(t))} \beta_i = \mathrm{Res}_{s_k}(\beta_i|_{L_{s_k}}) - \mathrm{Res}_{s_1}(\beta_i|_{L_{s_1}}). \tag{4.30}$$

Since s_1 and s_k are fixed, this is simply a rational function in t, which we denote $R_{ik}(t)$, defining a matrix $R \in \mathbb{C}(t)^{r \times (d-1)}$.

So we can consider the following differential system, of dimension $r + d - 1$,

$$Z' = \left(\begin{array}{c|c} A & R \\ \hline 0 & 0 \end{array}\right) Z, \tag{4.31}$$

which admits the fundamental solution

$$\tilde{\Pi} = \left(\begin{array}{c|c} \Pi & \Theta \\ \hline 0 & \mathbf{1} \end{array}\right). \tag{4.32}$$

The monodromy of this differential system is conjugate to the monodromy action on $H_{n-1}(\mathcal{X}_b, \mathcal{X}')$. Namely, considering the matrix $\mathrm{Mat}(\ell_*)$ of the action of a path ℓ in the basis $\eta_1, \dots, \eta_r, \alpha_2, \dots, \alpha_d$ of $H_{n-1}(\mathcal{X}_b, \mathcal{X}')$, we have similarly to (3.24)

$$\mathrm{Mat}(\ell_*) = \tilde{\Pi}(b)^{-1} \cdot \ell_* \tilde{\Pi}(b) = \tilde{\Pi}(b)^{-1} \tilde{\Lambda}_\ell \tilde{\Pi}(b), \tag{4.33}$$

where $\tilde{\Lambda}_\ell$ is the transition matrix associated to the system (4.32). This gives the desired algorithm for computing the monodromy action on relative homology. From the knowledge of these monodromy matrices we may recover the m_{kj}'s using equation (3.29), with an algorithm similar to that of Section 3.5.

Remark 37. *The order of the differential operators that need to be integrated is larger than those of Section 3.4, so the computation is expensive in practice, even for quartic surfaces. An alternative approach relying on braid computation is provided in Chapter 10.*

4.2.3 Intersection product

The intersection product of $H_n(\mathcal{Y})$

Let $n \leq 2$ and d be respectively the dimension and degree of $\mathcal{X}$.

We begin with a lemma characterising $H_n(\mathcal{X})$ as a subspace of $H_n(\mathcal{Y})$.

Lemma 38. *The Poincaré dual of the pullback π^* embeds $H_n(\mathcal{X})$ to the orthogonal complement of $H_{n-2}(\mathcal{X}')$ in $H_n(\mathcal{Y})$ isometrically (i.e. the intersection product is preserved).*

Proof. Let $\alpha, \beta \in H^n(\mathcal{X})$. As π^* preserves cup products, we have that

$$\langle \pi^*\alpha, \pi^*\beta \rangle = \langle \alpha, \beta \rangle. \tag{4.34}$$

For $1 \leq i \leq d$, let $\tilde{E}_i \in H^n(\mathcal{Y})$ be the Poincaré dual of the exceptional divisor E_i. The projection formula (Hartshorne, 1977, p. 256, A4) yields that

$$\pi_*(\tilde{E}_i \cdot \pi^*\alpha) = \pi_*\tilde{E}_i \cdot \alpha = 0, \tag{4.35}$$

as $\pi_*\tilde{E}_i = 0$. Poincaré duality yields the desired result. □

In particular we may recover the intersection product of $H_n(\mathcal{X})$ from the one of $H_n(\mathcal{Y})$.

The intersection product of $H_n(\mathcal{X})$

Once again, let $\gamma_1, \dots, \gamma_r$ be a basis of K consisting of vanishing cycles. If n is even, let $\gamma \in H_{n-2(\mathcal{X})}$ be such that $\langle \gamma, h_{\mathcal{X}'} \rangle = 1$. In particular, by Lemma 24, we may choose the $H_{n-2}(\mathcal{X}_b)$ piece of the filtration of Theorem 22 to be generated by $S = \gamma \times \mathbb{P}^1$.

In order to recover the intersection product on $H_n(\mathcal{X})$, it only remains to remove the exceptional divisors $\Gamma_i = [\gamma_i \times \mathbb{P}^1]$ for $i = 1, \dots, r$. We begin with the following lemma which allows us to compute the intersection product of the Γ_i.

Lemma 39. $\langle \Gamma_i, \Gamma_j \rangle = -\langle \gamma_i, \gamma_j \rangle$

Proof. This follows from Voisin (2002, Theorem 3.71). □

In particular we may answer specify the value of the missing entry in for the intersection matrix of $\mathcal{Y}$, see Lemma 25.

Lemma 40. $\langle S, S \rangle = -\langle \gamma, \gamma \rangle$

We can also get rid of the indeterminacy of the quotient $\mathcal{T}(\mathcal{Y}) \subset H_n(\mathcal{Y})/H_n(\mathcal{X}_b)$ which is present when n is even.

Lemma 41. *For $1 \le i \le s$, $\Gamma_i = \sum_{j=1}^{s} m_{ij}\tilde{\Gamma}_j + \langle \gamma, \gamma_k \rangle h$, where the m_{ij} are the integers computed in section 4.2.1 and the $\tilde{\Gamma}_j$'s are the Γ_j's of Lemma 25.*

Proof. Per Section 4.2.1, we have for every i the equality

$$\Gamma_i = \sum_{j=1}^{s} m_{ij}\tilde{\Gamma}_j + k_i h \,, \tag{4.36}$$

where the m_{ij}'s are known integers, and $k_i \in \mathbb{Z}$. Taking the intersection product with S makes it clear that $k_i = \langle \Gamma_i, \Gamma \rangle = -\langle \gamma_i, \gamma \rangle$. □

We thus have the image of $H_{n-2}(\mathcal{X}')$ in $H_n(\mathcal{Y})$, and Lemma 38 allows us to recover the intersection product of $H_n(\mathcal{X})$.

4.3 Wrapup

Let us summarise the main steps of the algorithm for computing a primitive period matrix of a projective hypersurface $\mathcal{X}$ in $\mathbb{P}^{n+1}$ given:

- the defining polynomial $P(x_0, \dots, x_{n+1})$ of $\mathcal{X}$;
- a generic hyperplane family $H_t = V(x_{n+1} - t x_0)$;
- a generic base point b;
- a primitive period matrix $\Pi(b)$ of $\mathcal{X}_b = \mathcal{X} \cap H_b$, for a well-specified basis of $PH^n_{\mathrm{DR}}(\mathcal{X}_b)$.

1. Using Griffiths–Dwork reduction, compute a basis $\beta_1(t), \dots, \beta_s(t)$ of $\mathcal{H}$ (as a $\mathbb{C}(t)$-linear space), the space of sections of $PH^{n-1}_{\mathrm{DR}}(\mathcal{X}_t)$ defined in Section 3.2, and the matrix $A(t) \in \mathbb{C}(t)^{s\times s}$ of the Gauss–Manin connection over it (§§3.1 and 3.2).

2. If necessary, perform a change of basis so that the primitive period matrix $\Pi(b)$ of $\mathcal{X}_b$ is given with respect to the basis $(\beta_i(b))$ of $PH^n_{\mathrm{DR}}(\mathcal{X}_b)$.

3. Compute the critical values $\Sigma \subset \mathbb{P}^1$ and polygonal loops $\ell_1, \dots, \ell_r$ generating the fundamental group of $\mathbb{P}^1 \setminus \Sigma$ (§3.4).

4. For each ℓ_i, integrate numerically the differential system $\Pi'(t) = A(t)\Pi(t)$, with given initial value $\Pi(b)$ along ℓ_i to obtain the value $\ell_{i*}\Pi(b)$, with rigorous error bounds. Compute the matrix $M_i = \Pi(b)^{-1} \cdot \ell_{i*}\Pi(b)$. It is an integer matrix, so we only need to compute the coefficients of M_i with a coefficient-wise error bounded by $\frac{1}{2}$ (§3.4).

5. Using Equations (3.27) and (3.29), compute the integer matrices $B \in \mathbb{Z}^{s\times r}$ and $T_\infty \in \mathbb{Z}^{r\times s}$. Compute bases of $\ker(B)$ and $\mathrm{im}(T_\infty)$ in $\bigoplus_{i=1}^{r} \mathbb{Z}\Delta_i$ and a basis of a sublattice $T \subseteq \ker(B)$ such that $\ker(B) = T \oplus \mathrm{im}(T_\infty)$. This sublattice is isomorphic to $\mathcal{T}(\mathcal{Y})$ (§3.5).

6. Compute a basis $\omega_1, \dots, \omega_e$ of $PH^n_{\mathrm{DR}}(\mathcal{X})$, using Griffiths–Dwork reduction, and compute the integrals $\int_{\pi^*(\Delta_i)} \omega_j$ (§4.1). This amounts to
   (a) Computing the coefficients of $\omega_j|_{X_t}$ in the basis (β_i) of $\mathcal{H}$;
   (b) Computing a Picard–Fuchs differential equation for the partial integral $y(t) = \int_{\delta_i(t)} \omega_j|_{\mathcal{X}_t}$, using the coefficients above and the matrix $A(t)$ of the Gauss–Manin connection, where $\delta_i(t)$ is the vanishing cycle associated to the i-th critical value, transported in X_t;
   (c) Computing initial conditions $y^{(k)}(b)$ using the matrix $\Pi(b)$;
   (d) Computing $\int_{\ell_i} y(t)\mathrm{d}t$ using the method given in Section 3.3.
7. With appropriate linear combinations, compute $\int_{\pi^*(\tau_i)} \omega_j$ for some basis (τ_i) of $T \simeq \mathcal{T}(\mathcal{Y})$ computed at Step 5, which gives the matrix P of the pairing $\mathcal{T}(\mathcal{Y}) \times PH^n_{\mathrm{DR}}(\mathcal{X})$.
8. Identify the exceptional divisors in $\mathcal{T}(\mathcal{Y})$. Restrict the matrix P to the orthogonal complement of this kernel, to obtain a primitive period matrix of $\mathcal{X}$.

Complexity aspects

Let d be the degree of P. We can perform Step 1 using $d^{5n+O(1)}$ operations (Bostan et al., 2013). The dimension s of $\mathcal{H}$ is bounded by d^n and the entries of the $s \times s$ matrix A are rational functions with numerators and denominators of degree at most $n3^n d^{n+1}$ (Bostan et al., 2013, Proposition 8).

In Step 3, the set Σ of critical values has $d(d-1)^n$ elements (by genericity of the hyperplane family). We can compute them by solving a system of $n+1$ homogeneous equations of degree at most d in $\mathbb{P}^{n+1}$. The algebraic complexity is bounded by $d^{O(n)}$ (Giusti et al., 2001), and we should also consider the cost of numerical approximation in the complex plane. In practice, the computational cost is negligible. The polynomial systems we have can be considered as toy examples.

In Step 5, we reduce to integrating a differential operator of order at most d^n and coefficients of degree $d^{O(n)}$. As an optimization, Steps 5 and 6d can be performed simultaneously. The complexity depends on the size of the differential operator, the desired precision but also numerical parameters. No complete description is known. With respect to precision only, when everything else is fixed, Theorem 30 guarantees a quasilinear complexity.

Chapter 5

Practical aspects for hypersurfaces

In this chapter, we present practical details of the computations that need to be carried out with the methods presented in the previous chapters on quartic surfaces. The computations were done using the SageMath implementation `lefschetz-family`[1]. We also quantify the efficiency of the method on a large number of sample varieties, and compare to the other known algorithm for computing such periods, of Sertöz (2019).

The content of this chapter is based on the paper Lairez et al. (2024).

5.1 An explicit example: quartic surface

Let $P = w^4 + x^4 + y^4 + z^4$ and define the Fermat quartic surface $\mathcal{X} = V(P) \subset \mathbb{P}^3$. It is a smooth quartic projective surface. Thus it is a K3 surface, its middle cohomology group has rank 22 and its holomorphic subgroup has rank 1. In this section, we give an explicit description of the computation of the periods of $\mathcal{X}$.

A static SAGE worksheet reproducing the computations of this section can be found at *Fermat_periods.ipynb*[2]. The computation of this notebook took a bit less than 18 minutes on a laptop.

5.1.1 Constructing the Lefschetz fibration

Let $\lambda = w$ and $\mu = 2x + 3y + z$, and for $t \in \mathbb{P}^1$, define $H_t = V(\lambda - t\mu)$. This defines a hyperplane pencil $\{H_t\}_{t\in\mathbb{P}^1}$ with axis $A = V(\lambda, \mu)$. Then the modification of $\mathcal{Y}$ along $\mathcal{X}$ is the blowup of X along A which resolves the indeterminacies of the rational map $\frac{\lambda}{\mu} : \mathcal{X} \dashrightarrow \mathbb{P}^1$ into a map $f : \mathcal{Y} \to \mathbb{P}^1$. The fibre $f^{-1}(t)$ is isomorphic to $\mathcal{X}_t \overset{\text{def}}{=} \mathcal{X} \cap H_t$. The defining equation for $\mathcal{X}_t$ when $t \neq \infty$ is

$$P_t = t^4(2x + 3y + z)^4 + x^4 + y^4 + z^4\,. \tag{5.1}$$

The map f has 36 critical values $t_1, \ldots, t_{36}$. We chose a basepoint b and a value which will serve as ∞, both regular.

[1] https://gitlab.inria.fr/epichonp/lefschetz-family

[2] https://nbviewer.org/urls/gitlab.inria.fr/epichonp/eplt-support/-/raw/main/Fermat_periods.ipynb

5.1.2 Computing cohomology

The primitive cohomology $PH^2(\mathcal{X})$ is computed thanks to the Griffiths–Dwork reduction (see Section 3.1). $PH^2(\mathcal{X})$ has rank 21 and a basis is given by the residues of rational forms

$$\frac{1}{P}\Omega_3, \frac{A_1}{P^2}\Omega_3, \dots, \frac{A_{19}}{P^2}\Omega_3, \frac{w^2x^2y^2z^2}{P^3}\Omega_3 \in H^3(\mathbb{P}^2 \setminus \mathcal{X}), \tag{5.2}$$

where $A_1, \dots, A_{19}$ are all the monomials of degree 4 in w, x, y, z with exponents at most 2, and $\Omega_3 = w\mathrm{d}x\mathrm{d}y\mathrm{d}z - x\mathrm{d}w\mathrm{d}y\mathrm{d}z + y\mathrm{d}w\mathrm{d}x\mathrm{d}z - z\mathrm{d}w\mathrm{d}x\mathrm{d}y$ is the volume form of $\mathbb{P}^3$. The 21 monomials 1, $w^2x^2y^2z^2$ and $A_1, \dots, A_{19}$ are all the monomials whose degree is a multiple of 4 and that are not divisible by the leading term of any element of the Jacobian ideal of P, which is in this case, the monomial ideal $\langle w^3, x^3, y^3, z^3\rangle$.

Similarly, a basis of $\mathcal{H}$, defined as the space of sections of $PH_1(X_t)$ (which, since 1 is odd, is just $H_1(\mathcal{X}_t)$) is given by the residues of the forms

$$\frac{x}{P_t}\Omega_2, \frac{y}{P_t}\Omega_2, \frac{z}{P_t}\Omega_2, \frac{z^5}{P_t^2}\Omega_2, \frac{yz^4}{P_t^2}\Omega_2, \text{ and } \frac{xz^4}{P_t^2}\Omega_2. \tag{5.3}$$

5.1.3 The action of monodromy on $H_1(X_b)$, thimbles, and recovering $H_2(Y)$

As X_b is a smooth quartic curve, it has genus 3 and the homology group $H_1(X_b)$ is free of rank 6. We assume we have a (primitive) period matrix of $H_1(X_b)$ given in the basis (5.3) for $H^1_{\mathrm{DR}}(X_b)$ and some basis $\eta_1, \dots, \eta_6$ of $H_1(X_b)$ which needs not be specified. We first aim at computing the action of $\pi_1(\mathbb{P}^1 \setminus \{t_1 \dots, t_{36}\}, b)$ on $H_1(X_b)$.

First we compute the simple direct loops $\ell_1, \dots, \ell_{36}$ around the critical values $t_1, \dots, t_{36}$, such that the composition $\ell_{36} \dots \ell_1$ is the indirect loop around ∞. Then for each i we may compute the monodromy matrix $M_i \in GL_6(\mathbb{Z})$ of the action of monodromy along ℓ_i on $H_1(Y_b)$ in the basis $\eta_1, \dots, \eta_6$ (see Section 3.4). For instance, we find

$$M_1 = \begin{bmatrix} 1 & 0 & 1 & 1 & 2 & 2 \\ 0 & 1 & -1 & -1 & -2 & -2 \\ 0 & 0 & 2 & 1 & 2 & 2 \\ 0 & 0 & -1 & 0 & -2 & -2 \\ 0 & 0 & 1 & 1 & 3 & 2 \\ 0 & 0 & -1 & -1 & -2 & -1 \end{bmatrix} = I_6 + \begin{bmatrix} 1 \\ -1 \\ 1 \\ -1 \\ 1 \\ -1 \end{bmatrix} \cdot \begin{bmatrix} 0 & 0 & 1 & 1 & 2 & 2 \end{bmatrix}. \tag{5.4}$$

This decomposition is the one of Equation (3.25). We choose a generator $d_i \in H_1(\mathcal{X}_b)$ of the image of $M_i - I$ (the choice is up to a sign). This is the vector of the coordinates of the vanishing cycle δ_i at t_i in the basis of $H_1(X_b)$. We have for example $d_1 = (1, -1, 1, -1, 1, -1)$. We also pick a permuting cycle, i.e. a preimage p_i of d_i through $M_i - I$, so that $d_i = M_i p_i - p_i$. For instance $p_1 = (0, 0, 1, 0, 0, 0)$. We then have an explicit understanding of the thimble $\Delta_i \in H_2(\mathcal{Y}_+, \mathcal{X}_b)$ as the extension $\tau_{\ell_i}(p_i)$ of p_i along ℓ_i. These thimbles freely generate $H_2(\mathcal{Y}_+, \mathcal{X}_b)$, and we have the 36×6 integer matrix B of the border map

$$\tilde{\delta}\colon H_2(\mathcal{Y}_+, \mathcal{X}_b) \to PH_1(\mathcal{Y}_b) : \Delta_i \mapsto \delta_i, \tag{5.5}$$

as per (3.27). This matrix, given in Fig. 5.1, has full column rank, and its kernel gives us a basis for $H_2(\mathcal{Y}_+)/H_2(\mathcal{X}_b)$, which has rank 30.

In order to recover $\mathcal{T}(\mathcal{Y})$, we need to quotient by the extensions of cycles in $H_1(\mathcal{X}_b)$ along the loop around ∞, which we recall is simply the composition $\ell_{36} \cdot \dots \cdot \ell_1$. The matrix T_i of the

$$\begin{pmatrix}
1 & 1 & 1 & 1 & 0 & -2 & 1 & 1 & -2 & 1 & 1 & 3 & 0 & -2 & 2 & -3 & 1 & 1 & 1 & 1 & 1 & -3 & 0 & 1 & 0 & 1 & 0 & 0 & 1 & -2 & 1 & 1 & 0 & 1 & 0 & 0 \\
-1 & -1 & -2 & -1 & 0 & 2 & -1 & 0 & 1 & -1 & 0 & -2 & 1 & 1 & 0 & 1 & 0 & 0 & 0 & 0 & -1 & 1 & 2 & 1 & 1 & 0 & 0 & 0 & -1 & 1 & -2 & -1 & 0 & 0 & 1 & 0 \\
1 & -1 & 1 & 0 & 2 & 0 & 0 & 0 & 0 & -1 & -1 & 1 & 1 & -1 & 1 & -1 & 1 & 1 & 1 & 1 & 1 & -2 & 2 & 0 & 2 & 2 & 2 & 1 & 1 & -1 & -1 & -1 & 1 & -1 & -1 & 1 \\
-1 & -1 & -2 & 0 & 1 & 2 & -1 & 1 & 0 & -1 & 0 & -1 & 2 & -1 & 2 & -1 & 1 & 1 & 1 & 1 & -1 & -1 & 4 & 2 & 2 & 1 & 1 & 1 & -1 & 0 & -3 & -1 & 0 & 0 & 1 & 1 \\
1 & 2 & 2 & 0 & -1 & -2 & 2 & -1 & 0 & 2 & 0 & 1 & -3 & 1 & -2 & 1 & -1 & -1 & -1 & -1 & 1 & 0 & -4 & -1 & -2 & -1 & -1 & -1 & 1 & -1 & 3 & 1 & 0 & 0 & 0 & -1 \\
-1 & -1 & -1 & 0 & 0 & 1 & -1 & 0 & 0 & -1 & 0 & -1 & 1 & 0 & 0 & 0 & 0 & 0 & 0 & 0 & -1 & 1 & 1 & 0 & 0 & 0 & 0 & 0 & -1 & 1 & -1 & 0 & 0 & 0 & 0 & 0
\end{pmatrix}$$

Figure 5.1: *The 6×36 matrix B of the border map $\tilde{\delta} : H_2(\mathcal{Y}_+, \mathcal{Y}_b) \to PH_1(\mathcal{Y}_b)$. Each column corresponds to the coordinates of a vanishing cycle at a critical point in the undetermined basis of $PH_1(\mathcal{X}_b)$.*

extension map $\tau_{\ell_i} : H_1(X_b) \to H_2(\mathcal{Y}, \mathcal{X}_b)$ in the bases $\beta_1, \ldots, \beta_6$ of $H_1(\mathcal{Y}_b)$ and $\Delta_1, \ldots, \Delta_{36}$ of $H_n(\mathcal{Y}, \mathcal{X}_b)$ is given by equation (3.26). For instance, we have

$$T_1 = \begin{bmatrix} 0 & 0 & 1 & 1 & 2 & 2 \\ 0 & 0 & 0 & 0 & 0 & 0 \\ \vdots & & & & & \vdots \\ 0 & 0 & 0 & 0 & 0 & 0 \end{bmatrix} \in \mathbb{Z}^{36\times 6}\,. \tag{5.6}$$

Using equation (3.29), we may then compute the matrix T_∞ of the extension map $\tau_\infty \colon H_1(\mathcal{X}_b) \to H_2(\mathcal{Y}, \mathcal{X}_b)$, given in Fig. 5.2.

$$\begin{pmatrix}
0 & 1 & 0 & 1 & 0 & 0 & 0 & 0 & 1 & 0 & -1 & 0 & 1 & 0 & 0 & 0 & 0 & 0 & 0 & 0 & 0 & 1 & 0 & 0 & 0 & 1 & 0 & -1 & 0 & -1 & 0 & 0 & 0 & 1 & 0 & 0 \\
0 & 1 & -1 & 2 & 0 & 0 & 0 & 0 & 0 & 1 & -2 & 0 & 1 & -1 & -1 & 1 & 1 & 1 & 1 & 1 & 1 & 2 & 0 & -1 & 0 & 1 & 0 & -2 & 0 & -1 & 0 & -1 & 1 & 2 & 1 & 0 \\
1 & 0 & -1 & 1 & -1 & 0 & 0 & 0 & 0 & 1 & -1 & -1 & 0 & 0 & 0 & 0 & 1 & 1 & 1 & 1 & 0 & 1 & 0 & -1 & -1 & 0 & 1 & -1 & 0 & -1 & 0 & -1 & 1 & 1 & 0 & 0 \\
1 & -1 & 0 & 0 & 0 & -1 & -1 & 0 & 0 & 0 & 1 & -1 & -1 & 1 & 0 & 0 & 1 & 1 & 1 & 1 & 0 & 0 & 0 & 0 & -1 & -1 & 0 & 0 & -1 & -1 & 0 & 0 & 0 & -1 & 0 & 1 \\
2 & 0 & -1 & 1 & 0 & -1 & -1 & 1 & 0 & 1 & 0 & -2 & 0 & 0 & -1 & 1 & 2 & 2 & 2 & 2 & 0 & 1 & 1 & -2 & -2 & 0 & 0 & -2 & -1 & -2 & 1 & -1 & 1 & 0 & 1 & 1 \\
2 & 1 & 0 & 0 & 0 & -1 & 0 & 2 & 1 & 1 & 0 & -2 & 1 & 0 & 0 & 1 & 1 & 1 & 1 & 1 & -1 & 1 & 2 & -2 & -2 & 1 & 0 & -2 & -1 & -2 & 1 & 0 & 1 & 0 & 0 & 0
\end{pmatrix}$$

Figure 5.2: *The transpose of the 36×6 matrix T_∞ of the extension map $\tau_\infty \colon H_1(\mathcal{X}_b) \to H_2(\mathcal{Y}_+, \mathcal{Y}_b)$. Each line corresponds to the coordinates of an extension along the equator in the basis of thimbles $\Delta_1, \ldots, \Delta_{36}$.*

We may then compute a supplement (as a $\mathbb{Z}$-module) of the image of T_∞ in the kernel of B, which has rank $36 - 6 - 6 = 24$. This gives a description of $\mathcal{T}(\mathcal{Y})$ as integer linear combinations of thimbles, given as 24 vectors of $\mathbb{Z}^{36}$. We may compute a basis $e_1, \ldots, e_{24}$ of this space. For instance we compute $e_2 = \Delta_2 - \Delta_{31} - \Delta_{35} - \Delta_{36}$.

5.1.4 Integrating forms

Let $\pi \colon \mathcal{Y} \to \mathcal{X}$ denote the canonical projection. As we know the periods of $\mathcal{X}_b$, we may compute the integral of the pullback of a primitive cohomology form $\operatorname{Res}\omega_j \in PH^2_{\mathrm{DR}}(\mathcal{X})$ along the thimbles $\int_{\Delta_i} \pi^* \operatorname{Res}\omega_j$ using methods detailed in Section 4.1. To recover the integral along an extension, it is sufficient to take the corresponding linear combinations of integrals along thimbles. For instance

$$\begin{aligned} \int_{e_2} \pi^* \operatorname{Res}\omega_j &= \int_{\Delta_2} \pi^* \operatorname{Res}\omega_j - \int_{\Delta_{33}} \pi^* \operatorname{Res}\omega_j - \int_{\Delta_{35}} \pi^* \operatorname{Res}\omega_j - \int_{\Delta_{36}} \pi^* \operatorname{Res}\omega_j \\ &= i1.718796454505093\ldots \quad \text{with 139 digits of precision.} \end{aligned} \tag{5.7}$$

This allows us to recover the full pairing $\mathcal{T}(\mathcal{Y}) \times PH^2_{\mathrm{DR}}(\mathcal{X}) \to \mathbb{C}$.

5.1.5 Recovering $PH_2(\mathcal{X})$

To recover $PH_2(\mathcal{X})$, we need to remove the 3 differences of blowup cycles in $H_2(\mathcal{Y})$, i.e. $E_i - E_1$ for $i \in \{2,3,4\}$. To identify them in $\mathcal{T}(\mathcal{Y})$ we can simply take the right kernel of the 21×24 period matrix $\left(\int_{e_j} \pi^* \operatorname{Res} \omega_i\right)$.

5.2 Explicit examples and benchmarking

In this section we analyse the performance of our algorithm to compute the periods of certain smooth quartic K3 surfaces. In particular we compare with the other existing method of Sertöz (2019) `numperiods` for the case of hypersurfaces. The reason why we are interested in K3 surfaces is twofold: they are Calabi-Yau manifolds, and they are the first case where `numperiods` struggles in the generic case.

`numperiods` relies on the deformation of a pencil of hypersurfaces along a path and analytically continues the period matrix using the Picard–Fuchs equations — much like we do in section Section 3.3 to compute the monodromy. Thus it is most efficient on families of K3 surfaces where the Picard–Fuchs equation has low order and degree. They start from the *Fermat K3 surface* $V(W^4 + X^4 + Y^4 + Z^4)$ for which the period matrix is known exactly thanks to Pham (1965) and Sertöz (2019), with entries given in terms of values of Gamma functions. When trying to compute the periods of quartic K3 surfaces given by generic quartic polynomials (i.e., with many monomials), the Picard–Fuchs equations can become quite wild, and computation time becomes an obstruction.

5.2.1 Benchmarking

Expected timings

Table 5.1 shows the time taken on a laptop to compute the periods of X for different dimensions and degrees, as well as the obtained precision. Each line of Table 5.1 corresponds to the computation of a single hypersurface $X = V(P)$, with $P = \sum_{m \in \mathcal{M}_{n,d}} a_m m$ where $\mathcal{M}_{n,d}$ is the set of monomial of degree d of $\mathbb{Q}(X_0, \dots, X_n)$, and a_m are random integer coefficients chosen uniformly between -20 and 20. These timings were obtained on an Apple Macbook Pro M1, using all 10 cores.

The column $|\Sigma|$ corresponds to the number of critical values of the fibration. This has an impact on the number of edges on which the Picard–Fuchs operators need to be integrated, and thus on the computational cost. More precisely, as the integration edges follow the Voronoi graph of the critical points, the number of edges is at most $3|\Sigma| - 6$ (Preparata & Shamos, 1985, Cor. 5.2).

The column $\operatorname{rk} PH^n(X)$ corresponds to the number of Picard–Fuchs operators that need to be integrated to recover the full period matrix of X, see Section 3.2.

The columns $\deg \mathcal{L}$ and $\operatorname{ord} \mathcal{L}$ correspond to the degree and order of these operators. More precisely let $\mathcal{L}$ be one of these Picard–Fuchs operators, corresponding to a form $\omega = \operatorname{Res} \frac{A}{P^k}$, as per Section 3.1. The order of $\mathcal{L}$ is $\operatorname{rk} PH^{n-1}(X_b) + 1$, and is the same for all forms. In contrast, the degree $\deg \mathcal{L}$ changes depending on the form — therefore a range is given instead of a single value[3]. The numbers in the column $\deg \mathcal{L}$ are lower and higher bounds for this degree for a specific P.

In the case of dimension greater than 2, the exceptional divisors of the modification were not identified. For quartic surfaces and cubic threefold, only the periods necessary to describe the

[3]It seems from experiments that the degree increases with the pole order k of ω. As the filtration with respect to this pole order coincides with the Hodge filtration (P. A. Griffiths, 1969), this implies that the degrees of the Picard–Fuchs operators of the holomorphic forms are the lowest. Thus the holomorphic periods are conveniently the less computationally expensive periods to compute.

n	d	$\|\Sigma\|$	$\mathrm{rk}\, PH^n(X)$	$\deg \mathcal{L}$	$\mathrm{ord}\, \mathcal{L}$	Time	Precision (dec. digits)
1	3	6	2	10-30	3	10 sec.	300
2	3	12	6	60	3	3 min.	300
3	3	24	10	110-320	7	8 hours*	260
1	4	12	6	30-80	4	8 min.	350
2	4	36	21	170-800	7	1 hour*	300
1	5	20	12	70-170	5	7 hours	270

*only the periods necessary for describing the Hodge structure were computed (see Section 5.2.1)

Table 5.1: *Data on the computation of hypersurfaces of degree d in $\mathbb{P}^{n+1}(\mathbb{C})$. $|\Sigma|$ is to the number of critical values of the fibration. $\mathrm{rk}\, H^n(X)$ is the size of the period matrix. $\mathrm{ord}\, \mathcal{L}$ and $\deg \mathcal{L}$ are the order and degree of the differential operators arising in the computation. Time is the* real *time, running on 10 cores. Precision is the number of correct decimal digits obtained.*

Hodge structure were computed (this corresponds to respectively 1 and 5 forms). This is typically what we are interested in when computing periods. Note that, the recovered data is not sufficient to continue the induction and access higher dimensional varieties — for this, the full period matrix is required.

Comparison with `numperiods` on quartic surfaces

The algorithm consists of 4 main steps:

- Computing the fundamental group of $\mathbb{P}^1 \setminus \Sigma$;
- Computing the Picard–Fuchs operators;
- Computing the monodromy matrices of the Picard–Fuchs operator;
- Recovering the action of monodromy and reconstructing the homology.

In practice, most of the time is spent on the third step. In the case of the computation of the periods of a quartic surface, the algorithm spends less than 1 second on step 4, around 20 seconds on step 1 and 2, and around 10 hours on step 3.

The algorithm of Sertöz (2019) is implemented in the package `numperiods`[4] (Lairez & Sertöz, 2019). In order to compare the efficiency of both methods, we show the time taken by `numperiods` to compute the periods of K3 surfaces defined by quartic polynomials of the form $F + P$, where $F = x^4 + y^4 + z^4 + w^4$ defines the Fermat quartic surface, and P is a polynomial with n monomials, with n ranging from 0 to 5. These examples were run on a single core, on a cluster with 500 Gb of memory, and for at most 48 hours each. Timings for specific cases are given in Table 5.2. In all but five of the 100 examples for $n \in \{4, 5\}$, the computation with `numperiods` could not be carried out, either because the memory usage exceeded the allocated 500 Gb, or because the computation lasted longer than the allocated 48 hours.

In total the CPU time for the computation of the periods of 204 quartic surfaces was measured using `lefschetz-family` with an input precision of 1500 bits. The average time taken was 9 hours, 56 minutes and 46 seconds. In practice, the package `lefschetz-family` makes use of several cores for the computation of the monodromy matrices of the Picard–Fuchs operators, which can greatly speed up the computation.

[4] https://gitlab.inria.fr/lairez/numperiods

P	`numperiods`	`lefschetz-family`	$\operatorname{ord}\mathcal{L}$	$\deg\mathcal{L}$
0	< 1 s	384 min.	–	–
$2x^2zw$	4 s	574 min.	3	4
$-2y^3z - 4z^2w^2$	2 min.	510 min.	5	38
$-xyzw + 4xzw^2 - 2y^4$	25 min.	607 min.	7	110
$y^3z + z^4 + y^3w + x^2zw$	346 min.	635 min.	14	591
$4xyz^2 - 5x^2zw - 4xw^3 - 4zw^3$	> 2880 min.	494 min.	21	?
$-2x^2w^2 - 4y^2w^2 - 2yzw^2 + 2yw^3$	> 500 Gb	543 min.	21	?
$x^4 - 4y^2z^2 - 5xz^2w + 2yz^2w + xyw^2$	> 500 Gb	538 min.	14	?

Table 5.2: *Comparison of CPU time necessary for the computation of the periods of the quartic surface defined by $x^4+y^4+z^4+w^4+P$, using `numperiods` and `lefschetz-family`. The columns $\operatorname{ord}\mathcal{L}$ and $\deg\mathcal{L}$ record the order and the degree of the coefficients of the Picard–Fuchs differential equation that `numperiods` integrates. The periods of the Fermat hypersurface are hard-coded in `numperiods`, which explains the instantaneous computation for $P = 0$.*

5.2.2 An application: Picard rank of families of quartic surfaces

In this section we explain how to use our algorithm to obtain certain algebraic invariants of quartic surfaces. Notably we compute the generic Picard rank of families of quartic surfaces (§§5.2.2 and 5.2.2), we check that two quartic surfaces are isomorphic to each other (§5.2.2), and give equations for quartic surfaces for each possible Picard rank (§5.2.2). These examples allow us to test our algorithm against known results.

Given a smooth quartic surface of $\mathbb{P}^3$, we may recover its Picard rank thanks to the numerical evaluation of some of its periods. Such a variety is a K3 surface. Its middle cohomology group $H^2(X)$ has rank 22, and its canonical bundle is trivial: there is a unique holomorphic form ω, up to scaling. The kernel of the map $\gamma \mapsto \int_\gamma \omega$ is a sublattice of $H_2(X)$ called the *Néron–Severi group* of X. The rank of this lattice is called the *Picard rank* (or *Picard number*, or *Néron–Severi rank*) of X.

The LLL algorithm (Lenstra et al., 1982) can be used to heuristically recover this kernel from high-precision numerical approximations of the periods. This computation is not certified and can fail in two ways, in principle. First, the algorithm may miss integer relations if the number of digits in the coefficients is not smaller than the number of significant digits computed in the periods. Second, it may recover fake integer relations reflecting a numerical coincidence that a higher precision computation would detect. In practice, we never observed these phenomena. See (Lairez & Sertöz, 2019) for a discussion of these issues.

Throughout the following examples, we used the following method. The holomorphic 2-form of a given quartic $\mathcal{X} = V(P)$ can be identified as the residue of the only irreducible rational form of $H^3(\mathbb{P}^3 \setminus X)$ with pole order 1 (P. A. Griffiths, 1969, Eq. 8.6). Explicitly the periods are given by $\int_\gamma \frac{\Omega_3}{P}$, with Ω_3 the volume form of $\mathbb{P}^3$ and $\gamma \in H_3(\mathbb{P}^3 \setminus \mathcal{X})$. We may then use the steps up to 5 of Section 4.3 to compute a basis of $\mathcal{T}(\mathcal{Y})$. We then compute the periods of the holomorphic form on this basis with the methods of Section 4.1. This yields 24 numerical approximations of complex numbers $\alpha_i \in \mathbb{C}$. Cycles on which the periods vanish induce integer linear relations between these numbers. Of these relations, three come from the exceptional divisors of the blowup $\pi\colon \mathcal{Y} \to \mathcal{X}$ (Section 4.2.1). As the Néron–Severi lattice is characterised by the vanishing of the periods, we may use these relations to compute it. All in all, the Picard rank $\rho(\mathcal{X})$ of $\mathcal{X}$ is given by

$$\rho(X) = 22 - \dim_{\mathbb{Q}} \langle \alpha_1, \ldots, \alpha_{24} \rangle \ . \tag{5.8}$$

We can apply the LLL algorithm to compute $\dim_{\mathbb{Q}} \langle \alpha_1, \dots, \alpha_{24} \rangle$ and heuristically recover the Picard rank.

Altogether the holomorphic periods of 530 smooth quartic surfaces were computed for the results presented in this section. The computations were run on a cluster, using 32 cores. The average time needed to compute the holomorphic periods of one quartic surface was around 40 minutes, ranging from 16 minutes up to 13 hours. The median time was 28 minutes. The computation took longer than 90 minutes for only 24 surfaces. It should be noted that the cause of lengthy computations seems to stem from the choice of the fibration $X \dashrightarrow \mathbb{P}^1$ rather than be intrinsic to the surface itself. Indeed, the limiting factor is the integration step, and the cases where the computation takes a lot of time seem to always be due to the integration on one single pathological edge. In all the cases we looked at closely, picking another generic fibration reduced the computation time, to around the expected 40 minutes. However, we have for now no way to choose a fibration that is well adapted to the computation of a given surface *a priori*.

Families studied by Bouyer

In this section we numerically verify the Picard ranks of the generic elements of the families of quartic surfaces of $\mathbb{P}^3$ given by Bouyer (2018, Theorem 4.9). These families are generated by polynomials of the form

$$\begin{aligned} [A,B,C,D,E] \stackrel{\text{def}}{=} {} & A(x^4+y^4+z^4+w^4) + Bxyzw + C(x^2y^2+z^2w^2) \\ & + D(x^2z^2+y^2w^2) + E(x^2w^2+y^2z^2), \end{aligned} \tag{5.9}$$

with 5 parameters A, B, C, D and E. More precisely, the families are given respectively by polynomials $[A,B,C,D,E]$, $[A,(DE-2AC)/A,C,D,E]$, $[A,0,C,D,2AC/D]$, $[A,B(2A-B)/A,B,B,B]$ and $[A,0,C,0,0]$. The theorem of Bouyer states that the generic Picard rank of these families are respectively 16, 17, 18, 19 and 19.

To generate elements of these 5 families, we simply pick integers A,B,C,D,E randomly in the interval $[-100,100]$ and consider the quartics defined by the above polynomials. If these quartics are smooth we may compute the Picard rank as above. Otherwise we pick other values for A,B,C,D,E.

We checked that the values our method yields for the Picard rank coincide with the values given by the theorem for the varieties corresponding to 56 sets of values for A,B,C,D,E. This gives numerical evidence of the results of Bouyer (2018).

We found singular examples were the Picard rank was not generic, for $[A,B,C,D,E]$ and $[A,(DE-2AC)/A,C,D,E]$ with $(A,B,C,D,E) = (49,92,-51,19,-51)$. The corresponding polynomials are

$$\begin{aligned} [A,B,C,D,E] = {} & 49x^4 - 51x^2y^2 + 49y^4 + 19x^2z^2 - 51y^2z^2 + 49z^4 + 92xyzw \\ & - 51x^2w^2 + 19y^2w^2 - 51z^2w^2 + 49w^4\,, \end{aligned} \tag{5.10}$$

and

$$\begin{aligned} [A,(DE-2AC)/A,C,D,E] = {} & 49x^4 - 51x^2y^2 + 49y^4 + 19x^2z^2 - 51y^2z^2 + 49z^4 \\ & + \frac{4029}{49}xyzw - 51x^2w^2 + 19y^2w^2 - 51z^2w^2 + 49w^4\,. \end{aligned} \tag{5.11}$$

The Picard ranks were 1 higher than the generic value for their respective families, i.e. 17 and 18.

Defining polynomial	Picard number
$x^3y + y^3z + y^3w + z^3w + xw^3$	≤ 2
$xy^3 + z^4 + x^3w + y^2zw + xw^3$	≤ 2
$x^4 + y^3z + xz^3 + x^3w + yw^3$	≤ 2
$y^3z + xyz^2 + xz^3 + x^3w + yw^3$	≤ 3
$x^3y + y^3z + z^3w + z^2w^2 + xw^3$	≤ 3
$x^2y^2 + x^3z + yz^3 + y^3w + xw^3$	≤ 18
$xy^3 + x^3z + xyzw + z^3w + yw^3$	≤ 19

Table 5.3: *The* 7 *missing quartics.*

5-nomial quartics

In Heal et al. (2022), the authors used the package `numperiods` to investigate the periods quartic K3 surfaces defined by elements of the set V_5 of smooth polynomials that are the sum of five distinct monomial with coefficient 1. Using deep-learning methods to guess efficient paths for deformation, they managed to compute the periods of all but 7 quartics. Reaching these missing quartics proved to be computationally too expensive using direct deformation techniques. Using `crystalline_obstruction` (Costa & Sertöz, 2021), a number theoretical method to bound the Picard rank, they computed the upper bounds for these missing quartics. In the other cases, the bound provided by `crystalline_obstruction` matched the estimate given by the LLL algorithm using numerical approximation of the periods with 300 digits of accuracy. This is summed up in Table 5.3, which is reproduced from Heal et al. (2022, Table 12.)

Using `lefschetz-family`, we were able to compute the periods of these quartic surfaces with 300 digits of accuracy, in about 40 minutes each. Using LLL, we find that the Picard ranks also match the upper bound computed using `crystalline_obstruction`, as was the case for the other quartics of V_5.

Picard rank of symmetric polynomials

In this section we compute the Picard rank of families of quartic surfaces defined by a symmetric polynomial. The defining equation of a quartic in $\mathbb{P}^3$ is a homogeneous polynomial in 4 variables, say x, y, z and w. We consider the families of polynomials that are symmetric in some of these variables. Up to a permutation of the variables, there are 4 such families:

1. polynomials symmetric in all the variables,
$$\forall \sigma \in \mathfrak{S}_{\{x,y,z,w\}} \quad P(x,y,z,w) = P(\sigma(x), \sigma(y), \sigma(z), \sigma(w))\,,$$
2. polynomials symmetric in three variables, say x, y and z,
$$P(x,y,z,w) = P(x,z,y,w) = P(y,x,z,w) = P(y,z,x,w) = P(z,x,y,w) = P(z,y,x,w)$$
3. polynomials where x and y are symmetric, as well as z and w
$$P(x,y,z,w) = P(y,x,z,w) = P(x,y,w,z) = P(y,x,w,z)\,,$$
4. and polynomials where x and y are symmetric
$$P(x,y,z,w) = P(y,x,z,w)\,.$$

A basis of the vector space of such polynomials is given by products of elementary symmetric polynomials. We may thus generate *a priori* generic (i.e. with minimal Picard rank) elements of the family by picking random coefficients as in the previous section. In practice we pick random integer coefficients in the interval $[-5, 5]$.

Doing so, we observe respectively

1. a Picard rank of 17 for 113 elements, 18 for one element, and 19 for one element,
2. a Picard rank of 14 for 100 elements, and 15 for one element,
3. a Picard rank of 12 for 107 elements,
4. a Picard rank of 8 for 114 elements.

This leads us to conjecture that the generic Picard ranks of these families are respectively 17, 14, 12 and 8.

Remark 42. *Alice Garbagnati pointed out that lower bounds on the Picard rank follow from properties of K3 surfaces with automorphisms. These bounds match the heuristic computation of the rank we obtained numerically. More precisely, the automorphisms of $\mathbb{P}^3$ that permute the coordinates induce automorphisms of the K3 surfaces of the aforementioned families. Denote σ such an automorphism and σ^* the induced isometry on $H_2(S)$. Depending on the nature of the automorphism, either the transcendental lattice is included in $H_2(X)^{\sigma^*}$ (the sublattice fixed by σ^*) or $H_2(X)^{\sigma^*}$ is included in the Néron–Severi lattice. The ranks of $H_2(X)^G$ for all finite group actions G are known (Xiao, 1996; Nikulin, 1979; Artebani et al., 2011; Hashimoto, 2012), and this yields lower bounds for the Picard ranks. However, the question of rigorously proving that the lower bounds match the Picard ranks seems to be still open.*

Two isomorphic rank 2 smooth quartic surfaces in $\mathbb{P}^3$

Oguiso (2017, Thm. 1.4) gives an example of two isomorphic smooth quartic K3 surfaces S_1 and S_2, that are isomorphic as abstract varieties but not Cremona equivalent (i.e. there is no birational automorphism of $\mathbb{P}^3$ inducing an isomorphism $S_1 \simeq S_2$). Defining equations f_1 and f_2 for S_1 and S_2 are given by

$$\begin{aligned} f_1 = {} & x^3y + x^2y^2 - xy^3 + x^3z + 2x^2yz - xy^2z - y^3z + x^2z^2 - xyz^2 - 2y^2z^2 - yz^3 - z^4 \\ & + x^3w - 2xy^2w - 2xyzw - xz^2w + yz^2w + xyw^2 - y^2w^2 - z^2w^2 + xw^3 + yw^3 \end{aligned} \tag{5.12}$$

and

$$\begin{aligned} f_2 = {} & x^4 + 3x^3z - x^2yz + 3x^2z^2 - 4xyz^2 - y^2z^2 + xz^3 - 3yz^3 - x^2yw + 2xy^2w \\ & + y^3w - 2x^2zw - 2xyzw + 3y^2zw - 3xz^2w - 3yz^2w - 2z^3w + 4xyw^2 \\ & + 2y^2w^2 + 3yzw^2 - z^2w^2 + 2xw^3 + 2yw^3 + zw^3 + w^4 \end{aligned} \tag{5.13}$$

The goal of this section is to present a method allowing one to numerically verify that these two surfaces are indeed isomorphic.

A *Hodge isometry* between two varieties X and Y is a morphism $X \to Y$ that induces an isometry of the homology groups $H_2(X) \simeq H_2(Y)$ that respects the Hodge decomposition on the complexifications $H_2(X, \mathbb{C})$ and $H_2(Y, \mathbb{C})$. When X is a K3 surface, its Hodge decomposition is determined entirely by the holomorphic periods (indeed $H^{2,0}(X)$ has rank 1 and is the complex conjugate of $H^{0,2}(X)$).

By the global Torelli theorem for K3 surfaces (Huybrechts, 2016, Thm. 5.3), it is sufficient to find a Hodge isometry between the second homology groups of two K3 surfaces to prove that they are isomorphic. In order to recover such an isometry, we proceed in the following way.

Using the methods presented in this chapter, we compute the holomorphic period vectors of S_i in some basis of homology $\gamma_1^i, \dots, \gamma_{22}^i$ of $H_2(S_i)$ for $i = 1, 2$. This allows to (heuristically) recover the Néron–Severi sublattice $\mathrm{NS}(S_i)$, which we find has rank 2. The transcendental lattice $\mathrm{Tr}(S_i)$ is then simply the orthogonal complement of $\mathrm{NS}(S_i)$ in $H_2(S_i)$. The lattice $\mathrm{NS}(S_i) \oplus \mathrm{Tr}(S_i)$ is a full rank sublattice of $H_2(S_i)$, which may have positive index. In order to find a Hodge isometry, we look for an isometry between these sublattices that extends to an isometry between the full homology lattices.

More explicitly, let ω_1 and ω_2 be the holomorphic forms of S_1 and S_2 respectively, $\gamma_1^1, \dots, \gamma_{22}^1 \in H_2(S_1)$ and $\gamma_1^2, \dots, \gamma_{22}^2 \in H_2(S_2)$ bases of cohomology. Let I_1, I_2 be the intersection matrices in these bases, and $\pi_1 = (\int_{\gamma_j^1} \omega_1)_{1 \le j \le 22}$ and $\pi_2 = (\int_{\gamma_j^2} \omega_2)_{1 \le j \le 22}$ the row vectors of the periods of the holomorphic form. Then a Hodge isometry is the data of a matrix $A \in GL_{22}(\mathbb{Z})$ and a scalar $\lambda \in \mathbb{C}$ such that

$$\pi_2 A = \lambda \pi_1 \text{ and } {}^t A I_2 A = I_1 \,. \tag{5.14}$$

Let $N_i \in \mathbb{Z}^{22\times 2}$ be the coordinate matrix of a basis of the Néron–Severi group $\mathrm{NS}(S_i)$ and $T_i \in \mathbb{Z}^{22\times 20}$ be the coordinate matrix of a basis of the transcendental lattice $\mathrm{Tr}(S_i)$. As these sublattices of $H_2(S_i)$ are algebraic invariants, we have the identities

$$AT_1 = T_2 B \text{ and } AN_1 = N_2 C \tag{5.15}$$

for some invertible matrices $B \in GL_{20}(\mathbb{Z})$ and $C \in GL_2(\mathbb{Z})$.

Then $\lambda \pi_1 T_1 = \pi_2 A T_1 = \pi_2 T_2 B$. In particular, coefficient wise we have

$$\lambda (\pi_1 T_1)_i = \sum_j (\pi_2 T_2)_j B_{ji} \,, \tag{5.16}$$

which allows us to recover the integers B_{ji} using the LLL algorithm. We find that $\lambda = 1$ with the choice $\omega_i = \mathrm{Res}(\Omega / f_i)$.

Furthermore

$$ {}^t C^t N_2 I_2 N_2 C = ^t N_1^t A I_2 A N_1 = ^t N_1 I_1 N_1 \,. \tag{5.17}$$

This yields 4 quadratic equations in the coefficients of C, to which we may find integer solutions. There are infinitely many solutions to this system, and not all yield a Hodge isometry — they only do if the corresponding A is an invertible integer matrix.

Indeed we have

$$A \left(\begin{array}{c|c} T_1 & N_1 \end{array} \right) = \left(\begin{array}{c|c} T_2 & N_2 \end{array} \right) \left(\begin{array}{c|c} B & 0 \\ \hline 0 & C \end{array} \right) , \tag{5.18}$$

and thus

$$A = \left(\begin{array}{c|c} T_2 & N_2 \end{array} \right) \left(\begin{array}{c|c} B & 0 \\ \hline 0 & C \end{array} \right) \left(\begin{array}{c|c} T_1 & N_1 \end{array} \right)^{-1} \in GL_{22}(\mathbb{Z}) \,. \tag{5.19}$$

We pick solutions for C and check whether they satisfy this condition. We then verify that the conditions of (5.14) are also satisfied. Using this method, we found that there is indeed a Hodge isometry between S_1 and S_2 up to high precision, which confirms that they are isomorphic.

An explicit equation of a smooth quartic K3 surface with given Picard rank

In this section we provide complements to Table 6.1 of Lairez and Sertöz (2019), for which examples of defining equations of quartic surfaces of Picard rank 2, 3 and 5 were missing. Additionally, we have verified the known entries of this table using the method presented in this thesis.

Defining polynomial	**Picard number**
$wx^3 + w^3y + y^4 + xz^3 + z^4$	1
$-x^2y^2 + xy^3 - y^4 + x^3z + x^2yz - xy^2z - y^3z + xyz^2 - y^2z^2 + xz^3 - yz^3 + x^3w$ $-x^2yw - xy^2w - y^2zw - z^3w - x^2w^2 - xyw^2 + y^2w^2 + yzw^2 + yw^3 - zw^3$	2
$x^4 - y^4 + z^4 - w^4 + (x-y)(z+w)yw - (x+y)(z-w)y^2$	3
$x^3y + z^4 + y^3w + zw^3$	4
$5x^4 + x^3y - xy^3 - 5y^4 + x^3z + x^2yz - xy^2z - y^3z + x^2z^2 + 2xyz^2 + 3y^2z^2 + 2xz^3 + 2yz^3$ $+2z^4 - x^3w + x^2yw + xy^2w - y^3w + x^2zw - y^2zw - 2xz^2w + 2yz^2w + 2z^3w$ $-2x^2w^2 - 2xyw^2 - 2y^2w^2 - 2xzw^2 - 2yzw^2 + 2z^2w^2 + 2xw^3 - 2yw^3 - 2zw^3 - 4w^4$	5
$x^3y + y^4 + z^3w + yw^3 + zw^3$	6
$w^3x + x^4 + wx^2z + x^3z + xy^2z - y^3z + wxz^2 + x^2z^2 - xz^3 + z^4$	7
$x^3y + z^4 + y^3w + xw^3 + w^4$	8
$w^4 + wx^2y + y^4 + x^3z - xy^2z + z^4$	9
$x^3y + z^4 + y^3w + w^4$	10
$w^4 + x^4 + x^2y^2 + y^4 - w^3z -^2 xy^2z + x^2z^2 + z^4$	11
$x^3y + y^4 + z^3w + x^2w^2 + w^4$	12
$w^4 +^3 x^4 + wy^3 + y^2z^2 + wz^3 +^2 xz^3$	13
$x^3y + y^4 + z^3w + yw^3 + w^4$	14
$x^3y + y^3z + z^4 + xy^2w + zw^3$	15
$x^3y + y^4 + z^3w + xyw^2 + y^2w^2 + w^4$	16
$x^3y + y^4 + z^4 + x^2w^2 + zw^3$	17
$x^3y + x^3z + y^3z + yz^3 + w^4$	18
$x^3y + z^4 + y^3w + xyzw + xw^3$	19
$x^3y + z^4 + y^3w + xw^3$	20

Table 5.4: *Example polynomial for each Picard number. The new rows are Picard numbers 2, 3 and 5.*

In addition to the example(s) of Section 5.2.2, Picard rank 2 smooth quartic K3 surfaces were found by testing generic polynomials with coefficients in $\{-1, 0, 1\}$. Following the construction of the proof of Oguiso (2012, Thm. 1.7), we may construct an equation of a smooth quartic surface with Picard rank 3. We also stumbled upon a rank 5 example, completing the missing entries. The completed table can be found in Table 5.4.

Such polynomials are too large (in terms of the number of monomials) for the Picard rank to be recovered using the previous method of Sertöz (2019) with current numerical integration software. Using the SageMath implementation of the algorithm presented in this thesis, we were able to numerically recover the Picard rank of these smooth quartic K3 surfaces in less than an hour each on a laptop.

5.2.3 An example from Feynman integrals: the Tardigrade Graph

The methods presented here allowed the study of the geometry of a parametrised Feynman integral corresponding to the Tardigrade graph. The associated Feynman integral is a relative period integral in the sense of Bloch et al. (2006) and Brown (2017) for a family of singular quartic surfaces defined by the Feynman graph in Fig. 5.3, as argued in Bourjaily et al. (2020), Bourjaily et al. (2019) and characterised completely in Doran, Harder, Pichon-Pharabod, et al. (2023). This example goes beyond the scope of this section, as the quartic surfaces associated to this graph are not smooth. It also shows that our algorithm manages examples from physics that were previously out of reach.

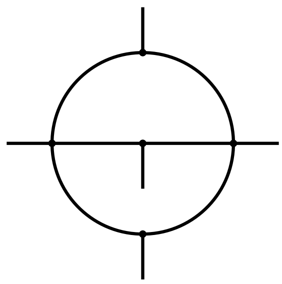

Figure 5.3: *The tardigrade graph*

The Tardigrade graph corresponds to a family of K3 surfaces given as the minimal resolution of a family of generically singular quartic surfaces in $\mathbb{P}^3$. For example, one element of this family, on which the computation was performed, is the quartic defined by the equation derived in Doran, Harder, Pichon-Pharabod, et al. (2023, §8)

$$\begin{aligned}
&6124x^4 - 24782692x^3y + 24962401977x^2y^2 - 20842243972xy^3 + 4331388844y^4 + 6124w^4\\
&\quad + 13827992x^3z - 27919677996x^2yz - 119291704836xy^2z + 50444249752y^3z\\
&\quad + 7840306116x^2z^2 - 1895725740xyz^2 + 168749562396y^2z^2 + 38842829528xz^3\\
&\quad + 168487393048yz^3 + 48321305644z^4 - 101996680x^3w + 204653103868x^2yw\\
&\quad - 85803990572xy^2w + 10300568y^3w - 115176640844x^2zw - 460049503942xyzw\\
&\quad - 18769272012y^2zw - 311785995116xz^2w - 108990818964yz^2w - 62891049316z^3w\\
&\quad + 417760330428x^2w^2 - 126779372xyw^2 + 10306692y^2w^2 + 179497287052xzw^2\\
&\quad + 37592148yzw^2 + 22845754953z^2w^2 - 101996680xw^3 + 12248yw^3 - 22389124zw^3\,.
\end{aligned} \tag{5.20}$$

Using a variation on the methods presented in this chapter, of which we give an overview below, we were able to recover algebraic invariants of this family, namely

1. its generic Picard rank, 11,
2. the Picard lattice, i.e. the kernel of the holomorphic period map $\gamma \mapsto \int_\gamma \omega$,
3. and an embedding of the Picard lattice in the standard K3 lattice.

The quartic surfaces considered generically have 4 nodal singularities. We want to obtain the periods of their minimal desingularisation. Despite the presence of singularities, we may still consider a Lefschetz fibration of these varieties and compute the monodromy matrices around the critical values. From these monodromy matrices, we recover the monodromy representation of a morsification of the singular quartic surface which yields a description of its homology. The homology of the morsification of the singular quartic is isometric to that of its desingularisation. Therefore this allows us to compute a description of the homology of the K3 surface. We can then integrate the holomorphic form following Section 4.1. This shows that we may use the effective Picard–Lefschetz theory presented in this thesis to recover the homology of hypersurfaces with nodal singularities.

In practice, however, in an effort to reduce the runtime, we may instead consider an elliptic fibration of the K3 surface directly. This has two main benefits:

- The order of the Picard–Fuchs equations that need to be integrated diminishes from 7 to 3 (as the genus of the homology of the fibre goes from 3 for a quartic curve to 1 for an elliptic curve). This greatly decreases the runtime of the computation down from one hour to less than a minute.
- We do not need to consider a modification of the K3 surface, which means there are no superfluous exceptional divisors to remove.

In order to obtain an elliptic fibration of the K3 surface, we project the K3 surface away from one of its singular points. This yields a double cover of $\mathbb{P}^2$ ramified along a sextic curve. Up to a change of variable, the defining equation of this sextic curve can be made quartic in one of the variables. Taking another variable as a parameter, we obtain an affine equation of the form $y^2 = p(x,t)$ with p quartic in x, which gives an elliptic fibration of the K3 surface parametrised by t. This fibration has 17 singular fibres, two of which are I_4 fibres, one is an I_2 and the rest are I_1's as per the Kodaira classification of singular fibers of elliptic surfaces (Kodaira (1963), see also Table 6.1 below). We identify the type of the singular fibres by looking at their monodromy matrices. Passing again to a morsification of the fibration, we are able to recover the homology and perform the integration. Further details about this computation are given by Doran, Harder, Pichon-Pharabod, et al. (2023, Appendix B).

In the next chapter, we will detail a general method for computing the homology and periods of elliptic surfaces.

Chapter 6

Application: Elliptic surfaces

As a second application of the theory detailed in the previous chapters, we deal with the case of elliptic surfaces. Elliptic surfaces are surfaces equipped with a fibration by elliptic curves, which in some sense makes them the easiest non-trivial surfaces to deal with. Indeed, the middle homology group of elliptic curves has rank 2, which is the lowest possible exhibiting possibly non-trivial monodromies. As in the case of hypersurfaces our goal will be to reduce to the case of a Lefschetz fibration. However in this setting we do not have the leisure of choosing the fibration: it is given as input. We will resort to using morsifications. We will see that this is always possible thanks to a result of Moishezon (1977) In fact we will also see that the singular fibres an elliptic surface can have are sufficiently well behaved that we can avoid explicitly realising the deformation. This greatly simplifies the algorithm and its implementation.

The work of this chapter is based on Pichon-Pharabod (2024).

6.1 Elliptic curves

In this section we recall certain facts about complex elliptic curves that are relevant to this text. Complex projective algebraic curves have the topology of a closed oriented real 2-manifolds. In particular their topology is characterised by a single integer: their *genus*. The most trivial example is the projective line, which is a topological sphere, i.e., has genus 0. The next step is genus 1: this is the realm of elliptic curves.

Definition 22. *An* elliptic curve *is an algebraic curve of genus* 1*.*

One way to realise an elliptic curve E is as a projective hypersurface, i.e., given by a unique equation in $\mathbb{P}^2$. The degree-genus formula links the degree d of a smooth curve to its genus g:

$$g = \frac{(d-1)(d-2)}{2}\,. \tag{6.1}$$

From this we may see that elliptic curves can equally be characterised as curves of degree 3. In fact, E is birationally equivalent to a curve defined by a *(reduced) Weierstrass equation*:

$$y^2 = x^3 + ax + b, \qquad a, b \in \mathbb{C}\,. \tag{6.2}$$

Elliptic curves exhibit various interesting properties. The first one is that their set of rational points has a canonical group structure (assuming it is non-empty), called the *Mordell–Weil* group $E(\mathbb{Q})$. This makes elliptic curves the baby case for abelian varieties.

The second interesting property is that their holomorphic bundle has rank 1. Indeed, the middle cohomology group has rank $2g = 2$, and thus the Hodge decomposition imposes $h^{1,0} = h^{0,1} = 1$. In the coordinates above the holomorphic is generated by $\omega = \frac{\mathrm{d}x}{y}$. In particular it is non-vanishing. This makes elliptic curves the baby case for Calabi-Yau varieties.

These two concepts are related by the following observation. Let E be an elliptic curve, let $\Lambda = \pi_1\mathbb{Z} + \pi_2\mathbb{Z}$ be the lattice of periods of ω, and define

$$E \to \mathbb{C}/\Lambda : P \mapsto \left[\int_O^P \omega\right] \tag{6.3}$$

As ω is holomorphic, this map is well defined. It turns out that is defines an isomorphism both analytically and algebraically: the group structure is preserved.

The first homology group $H_1(E)$ of an elliptic curve has rank 2. Its intersection pairing is antisymmetric and unimodular, and thus given in a certain basis by

$$I = \begin{pmatrix} 0 & 1 \\ -1 & 0 \end{pmatrix}. \tag{6.4}$$

Definition 23. *A basis γ_1, γ_2 of $H_2(E)$ is said to be* symplectic *if the above matrix I is the intersection matrix $(\langle\gamma_i, \gamma_j\rangle)_{i,j}$ of this basis.*

6.2 Elliptic surfaces

In this section, we recall the definition of an elliptic surface, as well as related notions that are useful to our discussion, notably the action of monodromy and Kodaira's classification of singular fibres. For further reading on elliptic surfaces, we recommend Schütt and Shioda (2010) and Miranda (1989).

Definition 24. *Let V be a complex curve. An* elliptic surface over V *is an complex surface S along with a proper surjective map $f: S \to V$ such that*

- *for all but finitely many $t \in V$, the fibre $F_t = f^{-1}(t)$ is a smooth genus 1 complex curve (i.e., an elliptic curve);*
- *no fibre contains a smooth rational curve of self-intersection -1.*

The second condition is there to ensure that the surface is relatively minimal, as such rational curves can always be blown down. We denote by Σ the finite set of values $t \in V$ over which the fibre F_t is not a smooth elliptic curve.

In the following, we consider an elliptic surface $f: S \to \mathbb{P}^1$ over $V = \mathbb{P}^1$. We will use the shorthand $S/\mathbb{P}^1$ to designate S together with the map $f: S \to \mathbb{P}^1$.

Definition 25. *A* section *of $S/\mathbb{P}^1$ is a map $\pi: \mathbb{P}^1 \to S$ such that $f \circ \pi = \mathrm{id}_V$.*

Sections of S are in bijection with $\mathbb{C}(t)$-points on the generic fibre E, which is an elliptic curve over $\mathbb{C}(t)$. Indeed, given a section π, the intersection of its image with the generic fibre $\operatorname{im}\pi \cap E$ yields a point in E. Conversely, given a point $P \in E(\mathbb{C}(t))$, its specialisation to any smooth fibre yields a point of the fiber. The closure Γ of the union of all these points yields a birational morphism $f|_\Gamma : \Gamma \to \mathbb{P}^1$. The inverse of this map gives the section associated to P, which we denote $\bar{P}$.

Throughout this chapter, we will only consider elliptic surfaces with section. We will notably fix a section O of S, which we call the *zero section.* It will serve as the zero of the group of rational points $E(\mathbb{C}(t))$ of the generic elliptic curve, as well as the generator of the $H_0(F_b)$ piece of the filtration of Theorem 22. Furthermore, to avoid the trivial case of a product $E \times \mathbb{P}^1$, we require in the rest of this text that the elliptic surface has at least one singular fibre.

Type	M_T	Minimal normal factorisation	Euler characteristic of the fibre
$I_\nu, \nu \geq 1$	$\begin{pmatrix} 1 & \nu \\ 0 & 1 \end{pmatrix}$	U^ν	ν
II	$\begin{pmatrix} 1 & 1 \\ -1 & 0 \end{pmatrix}$	VU	2
III	$\begin{pmatrix} 0 & 1 \\ -1 & 0 \end{pmatrix}$	VUV	3
IV	$\begin{pmatrix} 0 & 1 \\ -1 & -1 \end{pmatrix}$	$(VU)^2$	4
$I_\nu^*, \nu \geq 0$	$\begin{pmatrix} -1 & -\nu \\ 0 & -1 \end{pmatrix}$	$U^\nu(VU)^3$	$\nu + 6$
II^*	$\begin{pmatrix} 0 & -1 \\ 1 & 1 \end{pmatrix}$	$(VU)^5$	10
III^*	$\begin{pmatrix} 0 & -1 \\ 1 & 0 \end{pmatrix}$	$VUV(VU)^3$	9
IV^*	$\begin{pmatrix} -1 & -1 \\ 1 & 0 \end{pmatrix}$	$(VU)^4$	8

Table 6.1: *The singular fibre types of the Kodaira classification, representatives of their* $\mathrm{SL}_2(\mathbb{Z})$ *conjugacy class of the monodromy matrix, and the minimal normal factorisation of this representative in terms of the* I_1*-type matrices* $U = \left(\begin{smallmatrix} 1 & 1 \\ 0 & 1 \end{smallmatrix}\right)$ *and* $V = \left(\begin{smallmatrix} 1 & 0 \\ -1 & 1 \end{smallmatrix}\right)$.

6.2.1 The Kodaira classification

Kodaira provides a classification of the singular fibres of an elliptic fibration Kodaira (1963): Let $\sigma \in \Sigma$ be a critical value and ℓ be the counter-clockwise simple loop around σ pointed at b. As stated in the previous section, the monodromy action ℓ_* is represented by a matrix $M \in \mathrm{SL}_2(\mathbb{Z})$ in a symplectic basis of $H_1(F_b)$. The $\mathrm{SL}_2(\mathbb{Z})$-conjugation class of M determines the type of the singular fibre.

Furthermore the monodromy matrix has to be *unipotent*, i.e., there exist integers $r, s \in \mathbb{Z}$ such that $(M^r - 1)^s = 0$ (see Landman (1973)). The conjugacy classes of $SL_2(\mathbb{Z})$ unipotent matrices are classified in two infinite families I_ν and I_ν^*, $\nu \in \mathbb{N}$ and six classes II, III, IV, II^*, III^* and IV^*. Representatives M_T of these conjugacy classes are given in Table 6.1 (which is a reproduction of Cadavid and Vélez (2009, Table 1)), along with a factorisation as a product of I_1-type monodromy matrices which will prove useful in Section 6.4, and the Euler characteristic of the fibre. Lefschetz fibres are fibres of type I_1. These singular fibres have been extensively studied — for further reading on this topic, we recommend Esole (2017, Chap. 7).

6.3 Homology and periods of elliptic surfaces

In this section, we discuss means to recover the full homology lattice from the knowledge of the monodromy matrices of an elliptic fibration. Let us first fix some notations. Let $f\colon S \to \mathbb{P}^1$ be an elliptic fibration.

- F_v denotes the fibre above $v \in \mathbb{P}^1$. We will also use this notation for the homology class of F_v in $H_2(S)$ when there is no ambiguity;
- O denotes the zero section of $f\colon S \to \mathbb{P}^1$;
- $c_1, \dots, c_r \in \mathbb{P}^1$ denote the critical values of f, and $\Sigma = \{c_1, \dots, c_r\}$;
- m_v denotes the number of irreducible components of the fibre F_v;
- Θ_0^v denotes the *zero component* of F_v, i.e., the irreducible component intersecting the zero section.
- $\Theta_1^v, \dots, \Theta_{m_v-1}^v$ denote the irreducible components of F_v that are orthogonal to O;
- $\mathcal{T} = \mathcal{T}(S, F_b) \subset H_2(S, F_b)$ denotes the image of extension maps. For a basis $\ell_1, \dots, \ell_{r-1}$ of $\pi_1(\mathbb{P}^1 \setminus \Sigma, b)$, we have $\mathcal{T} = \bigoplus_{i=1}^{r-1} \operatorname{im} \tau_{\ell_i}$ as a direct consequence of (2.5);

Several cycles in $H_2(S)$ are distinguished in that their associated holomorphic periods (that is, periods of holomorphic forms) are directly computable, see Section 6.4.1 below. In the next paragraph, we define a lattice $\operatorname{Prim}(S) \subset H_2(S)$ of such cycles. When the fibration is Lefschetz, $\operatorname{Prim}(S)$ coincides with the full homology lattice $H_2(S)$. In general, however, $\operatorname{Prim}(S)$ may be a proper sublattice of $H_2(S)$. Nevertheless, we will show in Section 6.4.1 that $\operatorname{Prim}(S)$ always has full rank. In particular, all the periods of S can be recovered from the periods of $\operatorname{Prim}(S)$.

More precisely, the periods associated to singular components and the section are 0. Furthermore, we can use the methods of Chapter 3 to compute the periods of extensions. We call such cycles *primary* and define $\operatorname{Prim}(S)$ as follows:

Definition 26. *The* primary lattice $\operatorname{Prim}(S)$ *is the sublattice of $H_2(S)$ generated by extensions, fibre components and the zero section:*

$$\operatorname{Prim}(S) = \phi^{-1}(\mathcal{T}) \oplus \langle O \rangle \oplus \left(O^\perp \cap H_2(\pi^{-1}(\Sigma))\right), \tag{6.5}$$

where $\phi\colon H_2(S) \to H_2(S, F_b)$ is the inclusion.

Remark 43. *Although not apparent in the notation,* $\operatorname{Prim}(S)$ *depends on the fibration of the surface, and not solely on S.*

Note that the first term is isomorphic to $(\mathcal{T} \cap \ker \delta) \oplus \langle F_b \rangle$ per Lemma 10. Furthermore $\pi^{-1}(\Sigma)$ is the disjoint union of the singular fibres. Thus a basis of the last term is given by the Θ_i^v's where v ranges over Σ and i from 1 to $m_v - 1$.

In this chapter, we will adapt the methods developed in Chapter 2 in order to recover an effective description of the homology and compute the holomorphic periods. This case differs from the case of hypersurfaces and complete intersections in two major ways:

- the fibration is part of the input data. In particular, it needs not be a Lefschetz fibration, and we will thus need to make use of morsifications to recover the full homology.
- we do not have a description of the (primitive) cohomology in terms of the cohomology of the complement through the Leray residue. Nevertheless, we can recover a description of the holomorphic forms of the elliptic surface in a way that is convenient for integration thanks to work of Stiller (1987), see Section 6.5.1.

The following sections are dedicated to elucidating these difficulties. But first, let us already specify the self-intersection of the section, as mentioned in Lemma 25.

Lemma 44. $\langle O, O \rangle = -(\operatorname{rk} H_2(S) + 2)/12$

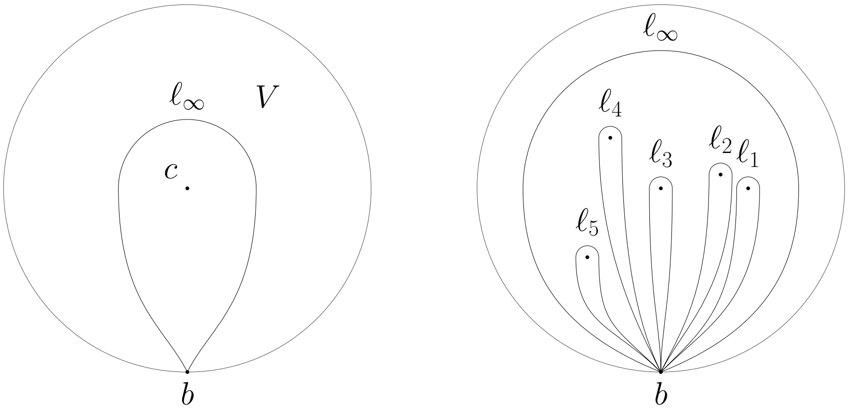

Figure 6.1: *The morsification of a neighbourhood of a single critical value.* Left: *A neighbourhood V of a single critical value of the elliptic fibration f, along with a chosen basepoint b. The homotopy group $\pi_1(V \setminus \{c\}, b)$ is generated by the counterclockwise loop ℓ_∞.* Right: *The neighbourhood after morsification. The critical fibre has split into five Lefschetz fibres. The homotopy group $\pi_1(V \setminus \Sigma)$ is generated by the 5 counterclockwise loops $\ell_1, \dots, \ell_5$. Thus $H_2(f^{-1}(V), F_b)$ has rank 5 — it follows from Table 6.1 that the original singular fibre was of type I_5. Furthermore we see that $\tau_{\ell_\infty} = \tau_{\ell_5 \dots \ell_1}$.*

Proof. By Schütt and Shioda (2010, Section 8.6), $-\langle O, O\rangle$ is equal to the arithmetic genus χ and by Schütt and Shioda (2010, Theorem 6.10), $\chi = \frac{e}{12}$, where $e = \operatorname{rk} H_0(S) - \operatorname{rk} H_1(S) + \operatorname{rk} H_2(S) - \operatorname{rk} H_3(S) + \operatorname{rk} H_4(S)$ is the topological Euler characteristic. As S is projective $\operatorname{rk} H_0(S) = \operatorname{rk} H_4(S) = 1$ and $\operatorname{rk} H_1(S) = \operatorname{rk} H_3(S) = 0$ by Lemma 21. □

6.4 Morsifications of elliptic surfaces

As mentioned in Section 2.3, morsification allow to use of the reconstruction of the homology from the monodromy representation of Lefschetz fibrations to obtain information about the homology of non-Lefschetz fibrations.

We start by the following theorem of Moishezon (1977), which guarantees the existence of a morsification of any elliptic surface.

Theorem 45 (Moishezon (1977, Thm. 8))**.** *Let $S \to V$ be an elliptic surface. There exists a morsification $\tilde{S} \to V \times D \to D$ of S. Moreover, the number of singular fibres of $\tilde{S}_u$ for $u \in D \setminus \{0\}$ does not depend on u.*

Remark 46. *In our setting, the existence of a section prevents the possibility of multiple fibres mentioned in Moishezon (1977).*

We will apply this result to neighbourhoods of each critical value to obtain local morsifications. For $c \in \Sigma$, define D_c a disk around c in $\mathbb{P}^1$ such that $b \notin D_c$ Let ℓ_c be a path connecting b to a point $b_c \in \partial D_c$. Assume that for $c \neq c'$, $D_c \cap D_{c'} = \emptyset$ and the interior of ℓ_c and $\ell_{c'}$ do not intersect. Let $\infty \notin \bigcup_{c \in \Sigma} D_c \cup \{b\}$, identify $\mathbb{C} = \mathbb{P}^1 \setminus \{\infty\}$, and let $S^* = f^{-1}(\mathbb{C})$. Define $T_c = f^{-1}(D_c)$ and $F_{b_c} = f^{-1}(b_c)$. With these new notations, Lemma 12 yields

$$\bigoplus_{c \in \Sigma} H_*(T_c, F_{b_c}) \to H_*(S^*, F_b)\,. \tag{6.6}$$

Note that $T_c \to D_c$ is an elliptic surface over D_c with a single singular fibre. In this setting, the type of the singularity is entirely determined by its monodromy, and so is the topology of its morsification. In particular, we will see that it is not necessary to explicitly realise the morsification to recover its monodromy representation.

Local morsification

Let $V \subset \mathbb{P}^1$ be a disk in $\mathbb{P}^1$ and consider an elliptic surface $S \to V$ with a single singular fibre. Let c denote the critical value and b a regular value on the boundary of V. Fix a symplectic basis of $H_1(F_b)$ and let M_∞ be the monodromy matrix around c in this basis. From Theorem 45, there exists a morsification of $S \to V$

$$\begin{tikzcd} \tilde{S} \arrow[r, "\tilde{f}"] \arrow[rr, bend right, dashed, "\eta"'] & V \times D \arrow[r, "p"] & D \end{tikzcd} \quad . \tag{6.7}$$

Let $t \neq c$ and $S' = \tilde{S}_t = \eta^{-1}(t)$. Then $S' \to V_t$ is a Lefschetz fibration. Denote by r its number of singular fibres and by Σ its set of critical values.

Lemma 47. *Following the terminology of Cadavid and Vélez (2009), the number r of singular fibres of $S' \to D$ is the number of factors in the minimal normal factorisation of M_T (see Table 6.1). Let $G_r \dots G_1$ be this factorisation. Let $A \in \mathrm{SL}_2(\mathbb{Z})$ be a matrix such that $M_\infty = AM_TA^{-1}$. Then there is a distinguished basis of $\pi_1(D \setminus \Sigma_t, b)$ such that the corresponding monodromy matrices $M_1, \dots, M_r$ are given by $M_i = AG_iA^{-1}$.*

Proof. The first part is simply the observation that

$$r = \chi(S) = \chi(S') = \sum_{v \in \Sigma} \chi(F_v)\,, \tag{6.8}$$

and $\chi(F_v) = 1$ for every v as F_v is of type I_1. For the second part, let $\ell_1, \dots, \ell_r$ be a distinguished basis of $\pi_1(D \setminus \Sigma, b)$. Then the result is a direct application of Cadavid and Vélez (2009, Thm.19), as Hurwitz moves on the product $M_r \dots M_1$ can be achieved by the action of a braid on $\pi_1(D \setminus \Sigma, b)$, see (2.2). □

Remark 48. *As shown by Cadavid and Vélez (2009, Thm. 21), the choice of the factorisation of M_T as a product of I_1 monodromy matrices does not matter. We could equivalently take any such minimal factorisation, such as the ones in Naruki (1987, Table 5).*

Pick such a distinguished basis $\ell_1, \dots, \ell_r$ of $\pi_1(D \setminus \Sigma, b)$ and let $\Delta_1, \dots, \Delta_r$ be the corresponding thimbles. Then the trivialisation of $\tilde{S}$ through η yields an isomorphism $H_2(S, F_b) \simeq H_2(S', F'_b) = \bigoplus_{i=1}^r \mathbb{Z}\Delta_i$. We conclude with two lemmas linking extensions and components of singular fibres of $f\colon S \to \mathbb{P}^1$ to this basis of thimbles.

Lemma 49. *Let ℓ_∞ be the simple loop around c pointed at b. Then*

$$\tau_{\ell_\infty} = \sum_{i=1}^{r} \tau_{\ell_i} \circ {\ell_{i-1}}_* \circ \cdots \circ {\ell_1}_*\,. \tag{6.9}$$

Proof. For $t \in D$, let Σ_t be the set of critical values of $\tilde{S}_t \to D$. Define $\tilde{\Sigma} = \bigcup_{t \in D} \Sigma_t \times \{t\}$. $\tilde{\Sigma}$ is an analytic set of $V \times D$ and the projection onto D is a finite morphism of degree r, totally ramified at c. Clearly, ℓ_∞ and $\ell_r \dots \ell_1$ have the same homotopy class in $\pi_1((V \times D) \setminus \tilde{\Sigma})$. The lemma is then a direct application of (2.5). □

Lemma 50. *The inclusion of the singular components of F_0 in $H_2(S, F_b)$ coïncides with the kernel of the boundary map:*

$$\bigoplus_{i=1}^{m_c-1} \langle \Theta_i^c \rangle = \ker\left(\delta : H_2(S', F_b') \to H_1(F_b')\right) . \tag{6.10}$$

In particular, $r = m_c$ if F_c has type I_{m_c} and $m_c + 1$ otherwise.

Proof. The direct inclusion is clear. The rank of this kernel is $r-1$ in the case of fibres of type I_ν and $r-2$ in the other cases. Therefore, if the mentioned equality holds, the last statement follows.

Let us detail the proof of the equality in the case of a fibre of type I_3. Per Table 6.1, its morsification splits it into 3 fibres of type I_1, for each of which the monodromy matrix is (up to a global conjugation) U. There are thus 3 thimbles, the restriction of the boundary map to these thimbles has rank 1, and the kernel thus has rank $3-1=2$. The intersection matrix of (the lift in $H_2(S)$ of) this kernel is computed using the methods of Section 2.2.3 and equal to

$$\begin{pmatrix} -2 & -1 \\ -1 & -2 \end{pmatrix}, \tag{6.11}$$

and it is thus a sublattice of discriminant 3. As this coincides with the discriminant of the sublattice generated by the singular components (Kodaira, 1963), and as one is contained in the other, these sublattices are equal. A similar direct computation gives the same result for each possible fibre type. □

An illustration of the effects of a morsification is provided in Fig. 6.1.

6.4.1 Global homology and periods

We are now ready to give an algorithm for computing $H_2(S)$ (with its lattice structure) from the monodromy representation of the fibration $S \to \mathbb{P}^1$.

Note that per Lemma 50 the sublattice generated by the singular components of a given singular fibre is explicitly identified in this description of homology; and per Lemma 49, the extensions of $\mathcal{T} \cap \ker\delta$ are also explicitly identified.

To conclude this section, we provide a way to compute the periods of certain 2-forms on this basis of homology. Let $\omega \in H^2(S)$ and assume that $\omega = \omega_t \wedge \mathrm{d}t$ for some 1-form $\omega_t \in H^1(S)$, where t denotes the dependance on a coordinate of $\mathbb{P}^1$. Then the integral of ω on an extension can be obtained as a path integral of a period of the elliptic fibre via the observation that

$$\int_{\tau_\ell(\eta)} \omega = \int_\ell \left(\int_{\eta_t} \omega_t \right) \mathrm{d}t \,, \tag{6.12}$$

where $\eta_t \in H_1(F_t)$ is the unique deformation of $\eta \in H_1(F_b)$ along ℓ. In particular, it is possible to recover the periods of ω on $\mathcal{T}$ with high precision from the Picard–Fuchs equation of ω_t using numerical integration methods with quasilinear algorithmic complexity with respect to precision alone van der Hoeven (1999) and Mezzarobba (2010). In practice, we rely on the implementation provided in SageMath by Mezzarobba (2016) in the *ore_algebra* package (Kauers et al., 2015). For further details on the computation of periods on thimbles, see Lairez et al. (2024, §3.7).

As the fibre components are localised in a single fibre, the periods of ω on a fibre component are all zero. The following lemma shows that this information, i.e., the periods on extension and fibre components, is sufficient to recover the full period mapping.

Lemma 51. *The primary lattice* $\mathrm{Prim}(S)$ *has full rank.*

Algorithm 1 Homology of elliptic surface

Input: the monodromy matrices $M_1, \dots, M_r \in \mathrm{SL}_2(\mathbb{Z})$ in a distinguished basis of $\pi_1(\mathbb{P}^1 \setminus (\Sigma \cup \{\infty\}))$
Output: a description of $H_2(S)$ with its lattice structure

$N \leftarrow []$
for $1 \le i \le r$ decreasing **do**
  Find $A \in SL_2(\mathbb{Z})$ and T such that $M_i = AM_TA^{-1}$ ▷ See Table 6.1 for M_T
  for W in the minimal normal factorisation of M_T **do**
    Append AWA^{-1} to N
for M_i in N **do**
  Compute $d_i \in \mathbb{Z}^{2\times 1}$ and $m_i \in \mathbb{Z}^{1\times 2}$ such that $M_i = I_2 + d_i m_i$.
  $T_i \leftarrow (-1)^{n-1} \left(\begin{array}{c} \mathbf{0} \\ \hline m_i \\ \hline \mathbf{0} \end{array} \right)$, where m_i is the i-th line.
$B \leftarrow \left(\begin{array}{c|c|c} d_1 & \cdots & d_r \end{array} \right)$
$T_\infty \leftarrow T_1 + T_2M_1 + T_3M_2M_1 + \cdots + T_rM_{r-1}\cdots M_1$
$k \leftarrow \ker B$
$i \leftarrow \operatorname{im} T_\infty$
$H \leftarrow k/i$
H is identified to the subspace of $H_2(S^*)/H_2(F_b)$ generated by extensions. The (representatives of) vectors of H are the coordinates in the basis of thimbles of $H_2(S^*, F_b)$.

Proof. For each $c \in \Sigma$, $H_2(T_c, F_{b_c})_{\mathbb{Q}} = (\ker \delta_c)_{\mathbb{Q}} \oplus (\operatorname{im} \tau_c)_{\mathbb{Q}}$. Furthermore, $\mathcal{T} = \bigoplus_{c\in\Sigma} \operatorname{im} \tau_c$. For a $\mathbb{Z}$-module A, denote by $A_{\mathbb{Q}}$ the tensor product $A \otimes \mathbb{Q}$. From Lemma 50 and Lemma 12, we have that

$$\begin{aligned}(\mathcal{T} \cap \ker \delta)_{\mathbb{Q}} \oplus \bigoplus_{\substack{c\in\Sigma \\ 1\le i\le m_c-1}} \langle \Theta_i^c \rangle_{\mathbb{Q}} \\ &= (\ker \delta)_{\mathbb{Q}} \cap \bigoplus_{c\in\Sigma} (\operatorname{im} \tau_c)_{\mathbb{Q}} \oplus (\ker \delta_c)_{\mathbb{Q}} , \\ &= (\ker \delta)_{\mathbb{Q}} .\end{aligned} \tag{6.13}$$

Lemma 10 allows to conclude. □

Let $\mathcal{B} = (\eta_1, \dots, \eta_s, F_b, O)$ be the basis of $H_2(S)$ obtained from Algorithm 1 and let

$$\mathcal{B}' = (\Gamma_1, \dots, \Gamma_t, \Theta_1, \dots, \Theta_{s-t}, F_b, O) \tag{6.14}$$

be a basis of $\mathrm{Prim}(S)$, such that for each i, $\Gamma_i \in \mathcal{T} \cap \ker \delta$ is an extension and $\Theta_i \in \ker \delta_c$ for some $c \in \Sigma$ is a fibre component. Over $\mathbb{Q}$, $\mathcal{B}'$ is also a basis of $H_2(S)_{\mathbb{Q}}$, and the matrix of change of basis $M_{\mathcal{B}'\to\mathcal{B}} \in \mathrm{GL}_{s+2}(\mathbb{Q})$ has integer coefficients and can be computed with Lemma 49 and Lemma 50.

Using the methods of Lairez et al. (2024, §3.7), we may numerically compute the periods $\int_{\Gamma_i} \omega$. Furthermore, the periods $\int_{\Theta_i} \omega$, $\int_{F_b} \omega$ and $\int_O \omega$ are all zero as the cycles of integration are all algebraic, see Lefschetz's theorem on $(1,1)$ classes. Let $\pi_{\mathcal{B}} = \left(\int_\gamma \omega \right)_{\gamma\in\mathcal{B}}$ be the vector of periods of ω on a basis $\mathcal{B}$. Then

$$\pi_{\mathcal{B}'} = \left(\int_{\Gamma_1} \omega, \dots, \int_{\Gamma_t} \omega, 0, \dots, 0 \right) \tag{6.15}$$

and

$$\pi_{\mathcal{B}} = M_{\mathcal{B}' \to \mathcal{B}}^{-1} \pi_{\mathcal{B}'} \,. \tag{6.16}$$

6.5 Recovering algebraic invariants of elliptic surfaces

In this section, we expalin how to compute explicit embeddings of the Néron–Severi lattice in the description of $H_2(S)$ given in the previous section. We then use this to recover the Mordell–Weil group, and the lattice structure of its torsion-free part, the Mordell–Weil lattice.

We start by recalling generalities about these lattices.

Definition 27. *The* Néron–Severi lattice $NS(S)$ *is the sublattice of* $H_2(S)$ *generated by classes of divisors. Its rank is called the* Picard rank *or* Picard number *or* Néron–Severi rank.

Definition 28. *The* trivial lattice $\mathrm{Triv}(S)$ *is the sublattice of* $\mathrm{NS}(S)$ *generated by the zero section and the fibre components. Its orthogonal complement is the* essential lattice $L(S) = \mathrm{Triv}(S)^{\perp}$.

Definition 29. *The* Mordell–Weil group $E(\mathbb{C}(t))$ *of the elliptic curve* $E/\mathbb{C}(t)$ *is the group of its* $\mathbb{C}(t)$*-rational points.*

As mentioned in the beginning of Section 6.2, sections of $S \to \mathbb{P}^1$ are in bijection with $E(\mathbb{C}(t))$. The following lemma shows that the group structure of $E(\mathbb{C}(t))$ coïncides with the lattice structure of $H_2(S)$ modulo the trivial lattice.

Theorem 52 (Schütt and Shioda (2010, Thm 6.5))**.** *The map* $P \mapsto \bar{P} \mod \mathrm{Triv}(S)$ *is an isomorphism from* $E(\mathbb{C}(t))$ *to* $\mathrm{NS}(S)/\mathrm{Triv}(S)$.

In particular, this equips the torsion-free part of the Mordell–Weil group with a lattice structure, inherited from the lattice structure on $\mathrm{NS}(S) \subset H_2(S)$. More precisely, the orthogonal projection of $NS(S)_{\mathbb{Q}} = \mathrm{NS}(S) \otimes \mathbb{Q}$ onto $L(S)_{\mathbb{Q}} = L(S) \otimes \mathbb{Q}$ defines a map $\phi\colon E(\mathbb{C}(t)) \to L(S)_{\mathbb{Q}}$. The kernel of this map is the torsion subgroup, and thus ϕ equips $E(\mathbb{C}(t))/E(\mathbb{C}(t))_{tor}$ with a rational lattice structure.

Definition 30. *The* Mordell–Weil lattice $\mathrm{MWL}(S)$ *of* S *is the resulting lattice* $-E(\mathbb{C}(t))/E(\mathbb{C}(t))_{tor}$.

Remark 53. *The minus sign means we are taking the opposite of the naturally induced pairing — this is so the lattice is positive definite instead of negative definite.*

For further reading on this topic, we recommend Schütt and Shioda (2010).

6.5.1 The cohomology of elliptic surfaces

Let ω be a holomorphic 2-form on S. As an element of $H^0(S, \Omega_S^2)$, it can be written as

$$\omega = f(t)\omega_t \wedge \mathrm{d}t \,, \tag{6.17}$$

where $\omega_t \in H^1(E)$ is a rational section of the holomorphic 1-form bundle of the generic fibre, and $f \in \mathbb{Q}(t)$ is a rational function. This representation is well adapted to the integration algorithm of Chapter 3. Of course the converse is not true: not every rational function f will yield a holomorphic 2-form on S. In fact the rational functions for which this is true are very tightly controlled by the *Picard–Fuchs equation* Λ of ω_t – that is, the minimal differential equation satisfied by ω_t with respect to the connection inherited from the derivation on $\mathbb{C}(t)$ through the fibration over $\mathbb{P}^1$, see Section 3.2 for its computation.

The following result of Stiller (1987) gives a way to compute rational functions $f_1, \ldots, f_r \in \mathbb{Q}(t)$ such that:

- $f_i(t)\omega_t \wedge \mathrm{d}t$ defines a holomorphic 2-form on S;
- and $f_1(t)\omega_t \wedge \mathrm{d}t, \ldots, f_r(t)\omega_t \wedge \mathrm{d}t$ is a basis of $H^{2,0}(S)$.

Theorem 54 (Stiller (1987, §3)). *There is a divisor $\mathfrak{A}_0$ on $\mathbb{P}^1$ depending only on Λ such that if $Z \in \mathcal{L}(\mathfrak{A}_0)$ (the linear system associated to $\mathfrak{A}_0$), then $\frac{Z}{W}\omega_t \wedge \mathrm{d}t$ is a holomorphic 2-form on S, where $W \in \mathbb{Q}(t)$ is the Wronskian of Λ. Furthermore the map $\mathcal{L}(\mathfrak{A}_0) \to H^{2,0}(S)$ is an isomorphism.*

An algorithm for computing $\mathfrak{A}_0$ is given in Stiller (1987, §3), and we recall it here for convenience. Assume that the Picard–Fuchs equation Λ has order two[1], or equivalently that ω_t and its derivative generate the full space of 1-forms of the generic fibre. In particular at any point $p \in \mathbb{P}^1$, the space of local solutions in a slit neighbourhood of p is generated by two solutions, that are locally of the form

$$(t-p)^q(h_1(t-p)\log(t-p) + h_2(t-p))\,, \tag{6.18}$$

with $q \in \mathbb{Q}$, h_1 and h_2 two holomorphic functions in a neighbourhood of 0. Let $r \leq s$ be the respective leading exponents of these two solutions. Then the order of $\mathfrak{A}_0$ at p is

$$\operatorname{ord}_p \mathfrak{A}_0 = \begin{cases} -\lfloor s \rfloor - 3 \text{ if } p = \infty \\ -\lfloor s \rfloor + 1 \text{ otherwise} \end{cases} \tag{6.19}$$

In particular, if p is a finite regular point of Λ, $\operatorname{ord}_p \mathfrak{A}_0 = 0$, meaning we can consider solely the singular points of Λ. For further reading on the topic, we recommend Stiller (1987) and Doran and Kostiuk (2023, §4.3).

The local exponents of Λ can be obtained symbolically from the operator (see Frobenius (1873) and Mezzarobba (2010, §4) for instance), and we thus have a method to compute a basis of the holomorphic 2-forms of S, with a presentation that is well suited for the integration methods of the periods mentioned in Section 6.4.1.

6.5.2 Computing the Néron–Severi lattice

We now focus on the computation of an invariant of elliptic surfaces — the *Mordell–Weil lattice*. The first step towards computing it is to compute the Néron–Severi lattice $NS(S)$. By Lefschetz's $(1,1)$ theorem P. Griffiths and Harris (1978, §1.2), it is entirely characterised as the kernel of the holomorphic period mapping.

Theorem 55 (Lefschetz (1,1) theorem). *Let $\omega_1, \ldots, \omega_s$ be a basis of the space of holomorphic 2-forms of S, $H^{2,0}(S)$, and consider the period map $\pi\colon H_2(S) \to \mathbb{C}^s, \gamma \mapsto (\int_\gamma \omega_1, \ldots, \int_\gamma \omega_s)$. Then*

$$NS(S) = \ker \pi\,. \tag{6.20}$$

We compute this kernel heuristically using the LLL method. In order to do this we need two things: a basis of $H^{2,0}(S)$ and numerical approximations of the associated periods.

We can thus compute high precision numerical approximations of the holomorphic periods of S. The Néron–Severi group can be heuristically computed by recovering integer linear relations between these periods. Indeed, let α_i be integers. Then

$$\int_{\sum_i \alpha_i\gamma_i} \omega = \sum_i \alpha_i \left(\int_{\gamma_i} \omega\right) = 0 \text{ for all } \omega \in H^{2,0}(S) \tag{6.21}$$

if and only if the cycle $\sum_i \alpha_i\gamma_i \in \mathrm{NS}(S)$, where the γ_i's form a basis of $H_2(S)$. Thus integer linear relations between the holomorphic period vectors $(\int_{\gamma_i} \omega_1, \ldots, \int_{\gamma_i} \omega_s)$ are in bijection with $NS(S)$.

[1]This may happen when S is an isotrivial elliptic surface. In that case, the author does not know of a way to identify the holomorphic form.

In order to recover these linear relations, we use the LLL algorithm. This computation is not certified, and may fail in two ways: the algorithm may miss integer relations with large coefficients, or may recover "fake" linear relations that hold up to very high precision. More precisely, the algorithm provides a sublattice $\Lambda \subset H_2(X)$ and positive numbers B, N and ε that depend on precision such that

1. $\Lambda = \mathrm{NS}(X)$; or
2. $\mathrm{NS}(X)$ is not generated by elements of the form $\sum_i \alpha_i\gamma_i$ with $\sum_i \alpha_i^2 \le B$; or
3. There exists $\sum_i \alpha_i\gamma_i \notin \mathrm{NS}(X)$ such that

$$\sum_j \left|\sum_i \alpha_i \int_{\gamma_i} \omega_j\right|^2 \le \varepsilon^2 \qquad \text{and} \qquad \sum_i \alpha_i^2 \le N^2 \,. \tag{6.22}$$

In practice, for 300 recovered decimal digits of precision for the periods of an ellipticK3surface (which was obtained in a few seconds in all the cases that we tried), we find $B \simeq 10^{132}$, $N = 3$, and $\varepsilon \simeq 10^{-271}$. For further discussion on these issues, see Lairez and Sertöz (2019).

6.6 Explicit example: an elliptic curve with high Mordell–Weil rank over $\mathbb{Q}$

In this section we detail the workings of our algorithm on an explicit example. A SageMath worksheet reproducing the results mentioned here is available at *example_paper_elliptic.ipynb*[2]. The elliptic surface S we consider is an elliptic K3 with Picard rank 19 used in Elkies and Klagsbrun (2020, §9) (with $u = 5$ in their notations) to find the elliptic curve with highest known Mordell–Weil rank over $\mathbb{Q}$ for which the Mordell–Weil torsion subgroup is $\mathbb{Z}/2\mathbb{Z}$. Its defining equation in projective coordinates is

$$X^3 + 4A(t)X^2Z + 512B(t)XZ^2 = Y^2Z \tag{6.23}$$

where

$$A(t) = 93273t^4 + 58840t^3 + 102618t^2 + 35680t + 14485 \tag{6.24}$$

and

$$\begin{aligned} B(t) = &-8590032t^8 - 78412620t^7 + 17011856t^6 + 241822775t^5 - 19459741t^4 - 127136490t^3 \\ &+16161642t^2 + 15406335t - 2083725 \end{aligned} \tag{6.25}$$

The homology lattice of S

This elliptic fibration has 16 singular fibres above points $c_1, \dots, c_{16}$. We pick a basepoint b as well as a distinguished basis $\ell_1, \dots, \ell_{16}$ of $\pi_1(\mathbb{C}^1 \setminus \{c_1, \dots, c_{16}\}, b)$. The corresponding monodromy matrices in a chosen symplectic basis γ_1, γ_2 of the homology of the fibre are given by

$$\begin{gathered} M_1 = \begin{pmatrix} 7 & 9 \\ -4 & -5 \end{pmatrix}, \quad M_i = \begin{pmatrix} 1 & 1 \\ 0 & 1 \end{pmatrix} \text{ for } i = 2, 3, 15 \\ M_i = \begin{pmatrix} 3 & 1 \\ -4 & -1 \end{pmatrix} \text{ for } i = 4, 9, 11, 12, \text{ and} \\ M_i = \begin{pmatrix} 3 & 2 \\ -2 & -1 \end{pmatrix} \text{ for } i = 5, 6, 7, 8, 10, 13, 14, 16. \end{gathered} \tag{6.26}$$

[2] https://nbviewer.org/urls/gitlab.inria.fr/epichonp/eplt-support/-/raw/main/example__paper__elliptic.ipynb

Computing the $\mathrm{SL}_2(\mathbb{Z})$ conjugation class of these matrices, one finds that eight fibres (those for which the monodromy matrix is M_5) are I_2 fibres, and the remaining eight are Lefschetz, i.e., of type I_1. Indeed, we have

$$M_5 = AM_{I_2}A^{-1} \text{ with } A = \begin{pmatrix} 1 & 0 \\ 1 & 1 \end{pmatrix} \in \mathrm{GL}_2(\mathbb{Z})\,. \tag{6.27}$$

Per the minimal normal factorisation of Table 6.1, $M_{I_2} = U^2$. Therefore in a morsification S' of S, there is a distinguished basis $\ell'_1, \dots, \ell'_{24}$ of $\pi_1(\mathbb{C} \setminus \Sigma', b)$ consisting of $8 + 8 \times 2 = 24$ elements, where Σ' is the set of critical values of the morsification, and such that the associated monodromy matrices are given by

$$\begin{aligned} M'_1 = \begin{pmatrix} 7 & 9 \\ -4 & -5 \end{pmatrix}, \quad M'_i &= \begin{pmatrix} 1 & 1 \\ 0 & 1 \end{pmatrix} \text{ for } i = 2, 3, 22, \\ M'_i &= \begin{pmatrix} 3 & 1 \\ -4 & -1 \end{pmatrix} \text{ for } i = 4, 13, 16, 17, \text{ and} \\ M'_i &= \begin{pmatrix} 2 & 1 \\ -1 & 0 \end{pmatrix} = AUA^{-1} \text{ for all other } i. \end{aligned} \tag{6.28}$$

We may then use the methods of Lairez et al. (2024, §§3, 5) to compute an effective basis $\Gamma_1, \dots, \Gamma_{22}$ of the homology of S' in terms of the thimbles $\Delta'_1, \dots, \Delta'_{24}$, the fibre class and the zero section. For instance, we find that a non trivial homology class is given by $\Delta'_2 - \Delta'_{22}$: as $M'_2 = M'_{22}$, this relative homology class has empty boundary and thus lifts to a class in $H_2(S')$. It is non-trivial as $\ell'_{22}{\ell'}_2^{-1}$ is non-trivial in $\pi_1(\mathbb{P}^1 \setminus \Sigma')$.

With this description, the singular components coming from an I_2 fibre of S above a critical value c can be obtained as the kernel of the thimbles of critical points flowing together at c. More explicitly, the component of the fibre above c_5 is the homology class corresponding to the lift of $\Delta'_5 - \Delta'_6$.

Furthermore, extensions of S can also be described in this basis. For example

$$\tau_{\ell_6^{-1}\ell_5}(\gamma_2) = \tau_{\ell_8^{-1}\ell_7^{-1}\ell_6\ell_5}(\gamma_2) = \Delta_5 + \Delta_6 - \Delta_7 - \Delta_8\,. \tag{6.29}$$

All in all we obtain the coordinates of a basis of $\mathrm{Prim}(S)$ in the basis of $H_2(S)$ obtained from the morsification S'. From the Picard–Fuchs equation of the surface, we recover using Theorem 54 that the space of holomorphic forms of S is generated by

$$\omega = \mathrm{Res}\,\frac{1}{P_t} \wedge \mathrm{d}t\,. \tag{6.30}$$

From then on, we can compute the periods on the primary lattice, and recover the full period mapping using the coordinates computed above. For example, we find that the holomorphic period of the first element of the basis of homology we computed is

$$\int_{\Gamma_1} \omega = -0.0007064447191\cdots - i0.0002821239749\cdots\,, \tag{6.31}$$

with certified precision bounds of around 150 digits.

Using the LLL algorithm, we find that the Néron–Severi lattice has rank 19 as expected. Finally the Mordell–Weil group is obtained as the quotient of the Néron–Severi lattice by the trivial lattice. We find

$$\mathrm{MW}(S) \simeq \mathbb{Z}^9 \times \mathbb{Z}/2\mathbb{Z}\,. \tag{6.32}$$

It should be noted that the result of Elkies and Klagsbrun (2020, §9) is stronger than what we have computed here. First our approach for computing the Néron–Severi group is heuristic as it relies on the LLL algorithm — in particular it is not a certified computation, and thus does not provide a proof. Secondly we have merely shown a result for the Mordell–Weil group over $\mathbb{C}(t)$[3], whereas Elkies and Klagsbrun (2020) shows that this computation holds over $\mathbb{Q}$ for one of the fibres.

[3]or rather over $\bar{\mathbb{Q}}(t)$.

Chapter 7

Ramified double covers of projective space

It is possible to adapt with minor modifications the case of hypersurfaces dealt with in Chapter 4 to deal with double covers of a projective space ramified along a smooth hypersurface. In fact the Griffiths-Dwork reduction is exactly the same up to a shift in the degree of the monomials being kept. Of particular interest are K3 surfaces obtained as double covers of $\mathbb{P}^2$ ramified along a sextic curve — so called *K3 surfaces of degree 2*. In this case, the method yields the K3 surface as a blow-down of the total space of a genus 2 fibration, where the fibres are double cover of $\mathbb{P}^1$ ramified at 6 points — i.e., hyperelliptic curves of degree 6.

In particular, the Picard–Fuchs equations that needs to be integrated to recover the monodromy representation of the surface have order 6. Because of this, the method is sufficient to compute the full period matrix of the K3 surface (i.e., not just the holomorphic periods) in a few hours on a laptop. Although this has not yet been tried, this means that we may recover the monodromy representation of threefolds obtained as double cover of $\mathbb{P}^3$ along a sextic surface, provided we are able to integrate the order 22 Picard–Fuchs equation of this fibration.

The content of this section is ongoing work.

7.1 Cohomology of ramified double covers of projective space

Let $x_0, x_1, \dots, x_n$ be projective coordinates of $\mathbb{P}^n$, and let P be a homogeneous polynomial of even degree $2dl$ in the x_i's such that $V(P)$ is a smooth hypersurface. Let $\mathcal{X}$ be the double cover of $\mathbb{P}^n$ ramified along $V(P)$. $\mathcal{X}$ can be defined as a hypersurface in weighted projective space $\mathbb{P}^{n+1}_{d,1\dots,1}$, with defining equation

$$\mathcal{X} : F = w^2 - P(x_0, \dots, x_n) = 0\,, \tag{7.1}$$

where w is the variable of weight d.

7.1.1 Weighted projective space

The space $\mathbb{P}^{n+1}_{d,1\dots,1}$ can be defined as the quotient

$$\mathbb{P}^{n+1}_{d,1\dots,1} \overset{\text{def}}{=} \mathbb{C}^{n+2}/\sim \tag{7.2}$$

where $\sim$ is the equivalence relation given by

$$(w, x_0, \dots, x_n) \sim (\lambda^d w, \lambda x_0, \dots, \lambda x_n) \text{ for all } \lambda \in \mathbb{C}\,. \tag{7.3}$$

There is an embedding $\mathbb{P}^{n+1}_{d,1\dots,1} \to \mathbb{P}^{n+1}$ given by the map

$$[w : x_0 : \cdots : x_n] \mapsto [w : x_0^d : \cdots : x_n^d]\,. \tag{7.4}$$

A generalisation of the work of P. A. Griffiths (1969) is done in I. Dolgachev (1982, §4.2) to obtain a description of the primitive cohomology of hypersurfaces in terms of residues of rational functions when the ambient space is a weighted projective space. In particular, as stated in Cox and Katz (1999, §5.3), it is possible to extend Griffiths-Dwork reduction to this case. In fact, as we will see in the next section, the reduction in the unweighted case is sufficient to recover the primitive cohomology of double covers.

7.1.2 Griffiths-Dwork reduction for double covers

In this section we develop the simplifications that can be made to Griffiths-Dwork reduction in the case of hypersurfaces. We recall that Griffiths-Dwork reduction is what allows us to compute a basis of the primitive cohomology of the variety, as well as deduce the Picard–Fuchs equation that need to be integrated to obtain both the monodromy representation and numerical values of the periods. As we will now see, there is no need for a specific implementation of the reduction in the weighted case, as it can be deduced from the usual unweighted reduction exposed in Section 3.1.

First, we see that every rational fraction class has a representative with no w in the numerator. Indeed, $2w = \partial_w(w^2+P)$ is in the Jacobian ideal. More precisely, let $k \in \mathbb{N}$ and $A \in \mathbb{C}[xw, \mathbf{x}]^{\mathbf{d}}_{2kg-n-3}$. Write $A = A_0 + wA_1 + w^2A_2$ with $\deg_w A_i = 0$ for $i = 0, 1$. Then

$$\frac{A}{F^k} = \frac{A_0}{F^k} + \frac{1}{2}\frac{2wA_1}{F^k} + \frac{A_2}{F^{k-1}} + \frac{PA_2}{F^k} = \frac{A_2}{F^{k-1}} + \frac{A_0 + PA_2}{F^k} - \frac{1}{2(k-1)}\partial_w \frac{A_1}{F^{k-1}}\,. \tag{7.5}$$

Clearly $\deg_w A_2 = \deg_w A - 2$ and thus the degree in w of the numerators strictly decreases when applying this reduction. Thus iterating it we obtain the claim above.

Furthermore, in the case where P is smooth, the Griffiths-Dwork reduction coincides with the reduction for the curve itself. Indeed

$$\frac{A\partial_{x_i}P}{F^k} = -\frac{1}{k-1}\frac{\partial_{x_i}A}{F^{k-1}} + \frac{1}{k-1}\partial_{x_i}\frac{A}{F^{k-1}} \tag{7.6}$$

The only thing that changes is the degree of the volume form ($2 + n + 1$ instead of $n + 1$), and thus the monomials that represent a basis of the cohomology. The reduction itself is exactly the same.

Working out Picard–Fuchs equations for hyperelliptic curves

We now deal with the base case for double covers, which are *hyperelliptic curves* given as double covers of $\mathbb{P}^1$ ramified along $2d$ points.

The family of zero-dimensional fibres is given by $\mathcal{X}_t = V(F)$ in $\mathbb{P}^1_{d,1}$, with $F = w^2 - P(t)x^{2d}$ for some degree $2d$ univariate polynomial P. The fibre consists of 2 points, and the associated periods are respectively $\pm\frac{1}{2i\pi}$. By Griffiths-Dwork reduction, the possible monomials representing 1-forms are of the form x^k for some $k < 2d - 1$ and with $k = 2di - (d + 1) = d(2i - 1) - 1$ for some $k \in \mathbb{N}$. It follows that there is a unique such monomial, x^{d-1}. This is expected, as

$\dim PH^0(\mathcal{X}_b) = \dim H_0(\mathcal{X}_b) - 1 = 1$. We then have for a rational function $r(t)$:

$$\partial_t \frac{r(t)x^{d-1}}{F} = \frac{r'(t)x^{d-1}}{F} - \frac{r(t)P'(t)x^{3d-1}}{F^2} \tag{7.7}$$

$$= \frac{r'(t)x^{d-1}}{F} - \frac{r(t)P'(t)\frac{1}{2dP(t)}x^d\partial_x F}{F^2} \tag{7.8}$$

$$= \frac{r'(t)x^{d-1}}{F} - \frac{r(t)P'(t)x^d}{2dP(t)}\frac{\partial_x F}{F^2} \tag{7.9}$$

$$= \frac{r'(t)x^2}{F} - \frac{r(t)P'(t)}{2P(t)}\frac{x^{d-1}}{F} + \partial_x\left(\frac{r(t)P'(t)}{2dP(t)}\frac{x^d}{F}\right) \tag{7.10}$$

so that $\partial_t\omega_t = \left(\frac{r'(t)}{r(t)} + \frac{P'(t)}{2P(t)}\right)\omega_t$ where $\omega_t = \operatorname{Res}\frac{r(t)x^{d-1}}{F}\Omega_0$.

7.2 An explicit example: double covers of $\mathbb{P}^2$ ramified along a smooth sexctic

Let $P = x^6 + y^6 + z^6$ and define the surface $\mathcal{X} = V(w^2 + P) \subset \mathbb{P}^3_{2,1,1,1}$ as the double cover of $\mathbb{P}^2$ ramified along $V(P)$. It is a smooth sextic K3 surface. Its middle cohomology group thus has rank 22 and its holomorphic subgroup has rank 1. In this section, we give an explicit description of the computation of the periods of $\mathcal{X}$.

A static SageMath worksheet reproducing the computations of this section can be found at *Fermat_periods.ipynb*[1]. The computation of this notebook took under 3 minutes on a laptop.

7.2.1 Constructing the Lefschetz fibration

Let $\lambda = x+y$ and $\mu = y-z$, and for $t \in \mathbb{P}^1$, define $H_t = V(\lambda - t\mu)$. This defines a hyperplane pencil $\{H_t\}_{t\in\mathbb{P}^1}$ in $\mathbb{P}^2$ with axis $A = V(\lambda,\mu)$. Then the modification of $\mathcal{Y}$ along $\mathcal{X}$ is the blowup of X along A which resolves the indeterminacies of the rational map $\frac{\lambda}{\mu} : \mathcal{X} \dashrightarrow \mathbb{P}^1$ into a map $f\colon \mathcal{Y} \to \mathbb{P}^1$. The fibre $f^{-1}(t)$ is isomorphic to $\mathcal{X}_t \overset{\text{def}}{=} \mathcal{X} \cap H_t$. The defining equation for $\mathcal{X}_t$ when $t \neq \infty$ is

$$w^2 + P_t = w^2 + ((y-z)*t - y)^6 + y^6 + z^6\,. \tag{7.11}$$

The map f has 30 critical values $t_1, \dots, t_{30}$. We chose a basepoint b and a value which will serve as ∞, both regular.

7.2.2 Computing cohomology

The primitive cohomology $PH^2(\mathcal{X})$ is computed thanks to the Griffiths–Dwork reduction (see Section 3.1). In comparison to the hypersurface case, we are keeping monomials of degree $6k-6$ $PH^2(\mathcal{X})$ has rank 21 and a basis is given by the residues of rational forms

$$\frac{1}{w^2+P}\Omega_3, \frac{A_1}{(w^2+P)^2}\Omega_3, \dots, \frac{A_{19}}{(w^2+P)^2}\Omega_3, \frac{x^4y^4z^4}{(w^2+P)^3}\Omega_3 \in H^3(\mathbb{P}^3_{3,1,1,1}\setminus\mathcal{X})\,, \tag{7.12}$$

where $A_1, \dots, A_{19}$ are all the monomials of degree 6 in x, y, z with exponents at most 4, and $\Omega_3 = w\mathrm{d}x\mathrm{d}y\mathrm{d}z - x\mathrm{d}w\mathrm{d}y\mathrm{d}z + y\mathrm{d}w\mathrm{d}x\mathrm{d}z - z\mathrm{d}w\mathrm{d}x\mathrm{d}y$ is the volume form of $\mathbb{P}^3_{3,1,1,1}$ (which has degree 6). The 21 monomials 1, $x^4y^4z^4$ and $A_1, \dots, A_{19}$ are all the monomials whose degree is a multiple of 6

[1] https://nbviewer.org/urls/gitlab.inria.fr/epichonp/eplt-support/-/raw/main/double_cover_periods.ipynb

and that are not divisible by the leading term of any element of the Jacobian ideal of $w^2 + P$, which is in this case, the monomial ideal $\langle w, x^5, y^5, z^5\rangle$.

Similarly, a basis of $\mathcal{H}$, defined as the space of sections of $PH_1(\mathcal{X}_t)$ (which, since 1 is odd, is just $H_1(\mathcal{X}_t)$) is given by the residues of the forms

$$\frac{z}{w^2+P_t}\Omega_2,\ \frac{y}{w^2+P_t}\Omega_2,\ \frac{z^7}{(w^2+P_t)^2}\Omega_2,\ \text{and}\ \frac{yz^6}{(w^2+P_t)^2}\Omega_2. \tag{7.13}$$

7.2.3 The action of monodromy on $H_1(\mathcal{X}_b)$, thimbles, and recovering $H_2(\mathcal{Y})$

As $\mathcal{X}_b$ is a double cover of $\mathbb{P}^1$ with simple ramification at 6 points, it is a hyperelliptic curve of genus 2 and the homology group $H_1(\mathcal{X}_b)$ is free of rank 4. We assume we have a (primitive) period matrix of $H_1(\mathcal{X}_b)$ given in the basis (7.13) for $H^1_{\mathrm{DR}}(\mathcal{X}_b)$ and some basis $\eta_1,\dots,\eta_6$ of $H_1(\mathcal{X}_b)$ which needs not be specified. We first aim at computing the action of $\pi_1(\mathbb{P}^1 \setminus \{t_1 \dots, t_{36}\}, b)$ on $H_1(\mathcal{X}_b)$.

First we compute the simple direct loops $\ell_1,\dots,\ell_{36}$ around the critical values $t_1,\dots,t_{36}$, such that the composition $\ell_{36}\dots\ell_1$ is the indirect loop around ∞. Then for each i we may compute the monodromy matrix $M_i \in GL_6(\mathbb{Z})$ of the action of monodromy along ℓ_i on $H_1(\mathcal{X}_b)$ in the basis $\eta_1,\dots,\eta_6$ (see Section 3.4). Doing so for every i, we obtain the monodromy representation given in Fig. 7.3. One may check that the product of these matrices (in reversed order, because we chose the convention that monodromy acts on the left) is the identity. Furthermore, all these monodromy matrices are of Lefschetz type, i.e., of the form (3.25). For instance, we find

$$M_1 = \begin{pmatrix} 1 & 0 & 0 & 0\\ 0 & 1 & 0 & 0\\ 0 & 0 & 2 & 1\\ 0 & 0 & -1 & 0\end{pmatrix} = I_4 + \begin{bmatrix}0\\0\\1\\-1\end{bmatrix}\cdot\begin{bmatrix}0 & 0 & 1 & 1\end{bmatrix} \tag{7.14}$$

We choose a generator $d_i \in H_1(\mathcal{X}_b)$ of the image of $M_i - I_4$ (the choice is up to a sign). This is the vector of the coordinates of the vanishing cycle δ_i at t_i in the basis of $H_1(\mathcal{X}_b)$. We have for example $d_1 = (0, 0, 1, -1)$. We may further check that this coincides with the Picard–Lefschetz formula (2.15), where here δ_1 is $\eta_3 - \eta_4$ and the intersection product in the basis $\eta_1,\dots,\eta_4$ is given by the matrix

$$\begin{pmatrix} 0 & 1 & 1 & 1\\ -1 & 0 & 1 & 1\\ -1 & -1 & 0 & 1\\ -1 & -1 & -1 & 0\end{pmatrix}. \tag{7.15}$$

We also pick a permuting cycle, i.e. a preimage p_i of d_i through $M_i - I_4$, so that $d_i = M_i p_i - p_i$. For instance $p_1 = (0, 0, 1, 0)$. We then have an explicit understanding of the thimble $\Delta_i \in H_2(\mathcal{Y}_+, \mathcal{X}_b)$ as the extension $\tau_{\ell_i}(p_i)$ of p_i along ℓ_i. These thimbles freely generate $H_2(\mathcal{Y}_+, \mathcal{X}_b)$, and we have the 30×4 integer matrix B of the border map

$$\tilde\delta\colon H_2(\mathcal{Y}_+, \mathcal{X}_b) \to PH_1(\mathcal{Y}_b) : \Delta_i \mapsto \delta_i\,, \tag{7.16}$$

as per (3.27). This matrix, given in Fig. 7.1, has full column rank, and its kernel gives us a basis for $H_2(\mathcal{Y}_+)/H_2(\mathcal{X}_b)$, which has rank 30.

In order to recover $\mathcal{T}(\mathcal{Y})$, we need to quotient by the extensions of cycles in $H_1(\mathcal{X}_b)$ along the loop around ∞, which we recall is simply the composition $\ell_{36}\cdot\dots\cdot\ell_1$. The matrix T_i of the extension map $\tau_{\ell_i} : H_1(X_b) \to H_2(\mathcal{Y}, \mathcal{X}_b)$ in the bases $\beta_1,\dots,\beta_6$ of $H_1(\mathcal{Y}_b)$ and $\Delta_1,\dots,\Delta_{30}$ of

$$\begin{pmatrix} 0&0&0&1&1&1&0&1&0&0&0&0&1&1&0&1&1&0&1&1&0&1&1&1&0&0&1&1&1&1 \\ 0&1&0&-1&-1&0&0&-1&0&1&1&1&-1&-1&0&-1&-1&0&0&0&1&-1&-1&-1&1&0&-1&-1&0&-1 \\ 1&-1&1&1&1&0&1&1&1&-2&-1&0&1&1&1&1&1&1&-1&0&-1&1&1&1&-1&1&1&1&0&1 \\ -1&0&-1&0&-1&0&-1&0&-1&1&0&0&-1&0&-1&-1&0&-1&0&0&1&-1&0&-1&0&-1&0&-1&0&-1 \end{pmatrix}$$

Figure 7.1: *The 4×30 matrix B of the border map $\tilde{\delta} : H_2(\mathcal{Y}_+, \mathcal{Y}_b) \to PH_1(\mathcal{Y}_b)$. Each column corresponds to the coordinates of a vanishing cycle at a critical point in the undetermined basis of $PH_1(\mathcal{X}_b)$.*

$H_n(\mathcal{Y}, \mathcal{X}_b)$ is given by equation (3.26). For instance, we have

$$T_1 = \begin{bmatrix} 0 & 0 & 1 & 1 \\ 0 & 0 & 0 & 0 \\ \vdots & & & \vdots \\ 0 & 0 & 0 & 0 \end{bmatrix} \in \mathbb{Z}^{30\times 6}\,. \tag{7.17}$$

Using equation (3.29), we may then compute the matrix T_∞ of the extension map $\tau_\infty : H_1(\mathcal{X}_b) \to H_2(\mathcal{Y}, \mathcal{X}_b)$, given in Fig. 7.2.

$$\begin{pmatrix} 0&0&0&0&1&-1&0&-1&-1&0&-1&0&-1&1&1&0&0&1&0&0&0&-1&-1&1&-1&1&0&1&1 \\ 0&1&-1&1&2&-1&0&-1&-1&0&-1&-1&-1&1&1&0&0&1&-1&0&0&0&-1&-1&1&0&0&-1&2&1 \\ 1&2&-1&0&1&0&-1&0&-1&0&-1&-1&0&1&1&1&-1&0&-1&-1&0&-1&0&-1&0&1&0&-1&2&1 \\ 1&1&0&0&1&0&0&-1&-1&1&-1&-1&-1&2&1&1&0&1&0&-1&-1&-1&-1&-2&0&0&1&-1&2&1 \end{pmatrix}$$

Figure 7.2: *The transpose of the 30×4 matrix T_∞ of the extension map $\tau_\infty : H_1(\mathcal{X}_b) \to H_2(\mathcal{Y}_+, \mathcal{Y}_b)$. Each line corresponds to the coordinates of an extension along the equator in the basis of thimbles $\Delta_1, \dots, \Delta_{30}$.*

We may then compute a supplement (as a $\mathbb{Z}$-module) of the image of T_∞ in the kernel of B, which has rank $30 - 4 - 4 = 22$. This gives a description of $\mathcal{T}(\mathcal{Y})$ as integer linear combinations of thimbles, given as 22 vectors of $\mathbb{Z}^{30}$. We may compute a basis $e_1, \dots, e_{22}$ of this space. For instance we compute $e_1 = \Delta_1 - \Delta_{26}$.

7.2.4 Integrating forms

Let $\pi \colon \mathcal{Y} \to \mathcal{X}$ denote the canonical projection. As we know the periods of $\mathcal{X}_b$, we may compute the integral of the pullback of a primitive cohomology form $\operatorname{Res}\omega_j \in PH^2_{\mathrm{DR}}(\mathcal{X})$ along the thimbles $\int_{\Delta_i} \pi^* \operatorname{Res}\omega_j$ using methods detailed in Section 4.1. To recover the integral along an extension, it is sufficient to take the corresponding linear combinations of integrals along thimbles. For instance

$$\begin{aligned} \int_{e_2} \pi^* \operatorname{Res}\omega_j &= \int_{\Delta_1} \pi^* \operatorname{Res}\omega_j - \int_{\Delta_{26}} \pi^* \operatorname{Res}\omega_j \\ &= 1.1703796777538011543627129 \cdots - i2.0271570660156736602115757 5\ldots \\ &\qquad \text{with 284 digits of precision.} \end{aligned} \tag{7.18}$$

This allows us to recover the full pairing $\mathcal{T}(\mathcal{Y}) \times PH^2_{\mathrm{DR}}(\mathcal{X}) \to \mathbb{C}$.

7.2.5 Recovering $PH_2(\mathcal{X})$

To recover $PH_2(\mathcal{X})$, we need to remove the 3 differences of blowup cycles in $H_2(\mathcal{Y})$, i.e. $E_i - E_1$ for $i \in \{2, 3, 4\}$. To identify them in $\mathcal{T}(\mathcal{Y})$ we can simply take the right kernel of the 21×24 period matrix $\left(\int_{e_j} \pi^* \operatorname{Res} \omega_i\right)$.

$$\begin{pmatrix} 1 & 0 & 0 & 0 \\ 0 & 1 & 0 & 0 \\ 0 & 0 & 2 & 1 \\ 0 & 0 & -1 & 0 \end{pmatrix}, \begin{pmatrix} 1 & 0 & 0 & 0 \\ 0 & 2 & 1 & 0 \\ 0 & -1 & 0 & 0 \\ 0 & 0 & 0 & 1 \end{pmatrix}, \begin{pmatrix} 1 & 0 & 0 & 0 \\ 0 & 1 & 0 & 0 \\ 0 & 0 & 2 & 1 \\ 0 & 0 & -1 & 0 \end{pmatrix}, \begin{pmatrix} 1 & 0 & 0 & 1 \\ 0 & 1 & 0 & -1 \\ 0 & 0 & 1 & 1 \\ 0 & 0 & 0 & 1 \end{pmatrix}, \begin{pmatrix} 2 & 1 & 1 & 1 \\ -1 & 0 & -1 & -1 \\ 1 & 1 & 2 & 1 \\ -1 & -1 & -1 & 0 \end{pmatrix},$$

$$\begin{pmatrix} 1 & 1 & 1 & 1 \\ 0 & 1 & 0 & 0 \\ 0 & 0 & 1 & 0 \\ 0 & 0 & 0 & 1 \end{pmatrix}, \begin{pmatrix} 1 & 0 & 0 & 0 \\ 0 & 1 & 0 & 0 \\ 0 & 0 & 2 & 1 \\ 0 & 0 & -1 & 0 \end{pmatrix}, \begin{pmatrix} 1 & 0 & 0 & 1 \\ 0 & 1 & 0 & -1 \\ 0 & 0 & 1 & 1 \\ 0 & 0 & 0 & 1 \end{pmatrix}, \begin{pmatrix} 1 & 0 & 0 & 0 \\ 0 & 1 & 0 & 0 \\ 0 & 0 & 2 & 1 \\ 0 & 0 & -1 & 0 \end{pmatrix}, \begin{pmatrix} 1 & 0 & 0 & 0 \\ 0 & 2 & 0 & -1 \\ 0 & -2 & 1 & 2 \\ 0 & 1 & 0 & 0 \end{pmatrix},$$

$$\begin{pmatrix} 1 & 0 & 0 & 0 \\ 0 & 2 & 1 & 0 \\ 0 & -1 & 0 & 0 \\ 0 & 0 & 0 & 1 \end{pmatrix}, \begin{pmatrix} 1 & 0 & 0 & 0 \\ -1 & 1 & 1 & 1 \\ 0 & 0 & 1 & 0 \\ 0 & 0 & 0 & 1 \end{pmatrix}, \begin{pmatrix} 2 & 1 & 1 & 1 \\ -1 & 0 & -1 & -1 \\ 1 & 1 & 2 & 1 \\ -1 & -1 & -1 & 0 \end{pmatrix}, \begin{pmatrix} 1 & 0 & 0 & 1 \\ 0 & 1 & 0 & -1 \\ 0 & 0 & 1 & 1 \\ 0 & 0 & 0 & 1 \end{pmatrix}, \begin{pmatrix} 1 & 0 & 0 & 0 \\ 0 & 1 & 0 & 0 \\ 0 & 0 & 2 & 1 \\ 0 & 0 & -1 & 0 \end{pmatrix},$$

$$\begin{pmatrix} 2 & 1 & 1 & 1 \\ -1 & 0 & -1 & -1 \\ 1 & 1 & 2 & 1 \\ -1 & -1 & -1 & 0 \end{pmatrix}, \begin{pmatrix} 1 & 0 & 0 & 1 \\ 0 & 1 & 0 & -1 \\ 0 & 0 & 1 & 1 \\ 0 & 0 & 0 & 1 \end{pmatrix}, \begin{pmatrix} 1 & 0 & 0 & 0 \\ 0 & 1 & 0 & 0 \\ 0 & 0 & 2 & 1 \\ 0 & 0 & -1 & 0 \end{pmatrix}, \begin{pmatrix} 2 & 2 & 1 & 0 \\ 0 & 1 & 0 & 0 \\ -1 & -2 & 0 & 0 \\ 0 & 0 & 0 & 1 \end{pmatrix}, \begin{pmatrix} 1 & 1 & 1 & 1 \\ 0 & 1 & 0 & 0 \\ 0 & 0 & 1 & 0 \\ 0 & 0 & 0 & 1 \end{pmatrix},$$

$$\begin{pmatrix} 1 & 0 & 0 & 0 \\ -1 & 1 & 0 & 0 \\ 1 & 0 & 1 & 0 \\ -1 & 0 & 0 & 1 \end{pmatrix}, \begin{pmatrix} 2 & 1 & 1 & 1 \\ -1 & 0 & -1 & -1 \\ 1 & 1 & 2 & 1 \\ -1 & -1 & -1 & 0 \end{pmatrix}, \begin{pmatrix} 1 & 0 & 0 & 1 \\ 0 & 1 & 0 & -1 \\ 0 & 0 & 1 & 1 \\ 0 & 0 & 0 & 1 \end{pmatrix}, \begin{pmatrix} 2 & 1 & 1 & 1 \\ -1 & 0 & -1 & -1 \\ 1 & 1 & 2 & 1 \\ -1 & -1 & -1 & 0 \end{pmatrix}, \begin{pmatrix} 1 & 0 & 0 & 0 \\ 0 & 2 & 1 & 0 \\ 0 & -1 & 0 & 0 \\ 0 & 0 & 0 & 1 \end{pmatrix},$$

$$\begin{pmatrix} 1 & 0 & 0 & 0 \\ 0 & 1 & 0 & 0 \\ 0 & 0 & 2 & 1 \\ 0 & 0 & -1 & 0 \end{pmatrix}, \begin{pmatrix} 1 & 0 & 0 & 1 \\ 0 & 1 & 0 & -1 \\ 0 & 0 & 1 & 1 \\ 0 & 0 & 0 & 1 \end{pmatrix}, \begin{pmatrix} 2 & 1 & 1 & 1 \\ -1 & 0 & -1 & -1 \\ 1 & 1 & 2 & 1 \\ -1 & -1 & -1 & 0 \end{pmatrix}, \begin{pmatrix} 1 & 1 & 1 & 1 \\ 0 & 1 & 0 & 0 \\ 0 & 0 & 1 & 0 \\ 0 & 0 & 0 & 1 \end{pmatrix}, \begin{pmatrix} 2 & 1 & 1 & 1 \\ -1 & 0 & -1 & -1 \\ 1 & 1 & 2 & 1 \\ -1 & -1 & -1 & 0 \end{pmatrix}$$

Figure 7.3: *The monodromy representation of the genus 2 fibration of the double cover of $\mathbb{P}^2$ ramified along $V(x^6 + y^6 + z^6)$.*

7.3 Application: double covers along sums of 3, 4, or 5 monomials

To demonstrate the applicability of our method, we follow the endeavours of Lairez and Sertöz (2019) and Heal et al. (2022) in investigating families of K3 surfaces defined by equations with a certain number of monomials.

Definition 31. *Let V_k denote the set of smooth homogeneous sextics on three variables that are expressed as the sum of k distinct monomials with coefficients equal to 1. For example,*

$$V_3 = \{x^6 + y^6 + z^6, x^6 + y^6 + xz^5, x^6 + y^5z + xz^5, x^6 + y^5z + yz^5, x^5y + y^5z + xz^5\} \tag{7.19}$$

We were able to compute the holomorphic periods of all elements of V_3, V_4 and V_5 with around 120 decimal digits of precision, in an average time of 2 minutes and 40 seconds each, on a laptop. There are 28 monomials of degree 6 on 3 variables. Thus there are $\binom{28}{5} = 98\,280$ quartics to consider in V_5. The symmetric group on three elements $\mathfrak{S}_3$ acts on V_k by permuting the variables. Of course, polynomials differing only by a permutation of the variables define the same K3 surface, and it is thus sufficient to consider their class under this action. There are only $16\,536$ $\mathfrak{S}_3$ classes in of sextic with 5 monomials, and of these classes, only 855 define smooth sextics. Similarly there are 5 classes in V_3 (enumerated in (7.19)) and 78 in V_4.

Picard rank	1	2	3	4	5	6	7	8	9	10	11	12	13	14	15	16	17	18	19	20
V_3	0	1	0	0	0	0	0	0	0	0	0	0	0	1	0	0	0	0	0	3
V_4	11	27	2	0	0	7	0	2	2	9	1	1	0	6	0	2	3	2	3	0
V_5	254	359	41	1	1	38	0	6	41	58	13	8	3	14	1	5	9	2	0	0

Table 7.1: *The frequencies of Picard ranks among the $\mathfrak{S}_3$ classes of V_3, V_4 and V_5*

The frequencies of Picard ranks for these classes for each family are listed in Table 7.1. Interestingly, Picard rank 7 is absent from this table. Furthermore there are more rank 2 examples than rank 1 — and this remains true when considering individual polynomials rather than their $\mathfrak{S}_3$ classes.

We also give in Table 7.2 example polynomials for the Picard ranks that were reached, much like Table 5.4.

7.3.1 The endomorphism ring of K3 surfaces

Finally, we also provide the frequency of the defining polynomial of the *transcendental endomorphism field*, as another example of an invariant of the K3 surfaces that may be recovered from the holomorphic periods. Let $\mathcal{X}$ be a projective K3 surface.

Definition 32. *The* endomorphism ring *of $\mathcal{X}$ is the ring of morphisms of Hodge structure $H^2_{\mathrm{DR}}(\mathcal{X}) \to H^2_{\mathrm{DR}}(\mathcal{X})$.*

Remark 56. *This definition does not impose any compatibility with the polarisation of the Hodge structure.*

As the Hodge filtration on $H^2_{\mathrm{DR}}(\mathcal{X})$ is entirely characterised by the integrals $\int_{\gamma_i} \omega_{\mathcal{X}}$ of the holomorphic 2-form $\omega_{\mathcal{X}}$ on a basis of cycles $\gamma_1, \ldots, \gamma_{22}$, this definition may be expressed in terms of the holomorphic period vector

$$w' = \left(\int_{\gamma_1} \omega_{\mathcal{X}}, \ldots, \int_{\gamma_{22}} \omega_{\mathcal{X}} \right). \tag{7.20}$$

Lemma 57. *The endomorphism ring of $\mathcal{X}$ is identified to the ring of linear maps $e : \mathbb{Z}^{22} \to \mathbb{Z}^{22}$ such that there exists $\lambda \in \mathbb{C}^*$ satisfying $e_{\mathbb{C}}(w') = \lambda w'$ (where $e_{\mathbb{C}} : \mathbb{C}^{22} \to \mathbb{C}^{22}$ is the complexification of e).*

As explained in Section 5.2.2, algebraic curves contained in $\mathcal{X}$ are identified to cycles on which the integral of the holomorphic 2-form vanishes. Such cycles give rise to endomorphisms of the Hodge structure that are in some way trivial as they do not relate to the transcendental entries of the period vector. In particular, it is pertinent to consider the restriction of endomorphism to a complement of these cycles in $H_2(\mathcal{X}) \simeq \mathbb{Z}^{22}$. We recall that $\mathrm{NS}(\mathcal{X})$ is the Néron–Severi group of $\mathcal{X}$, consisting of algebraic 1-cycles, and $\rho(\mathcal{X})$ is the rank of $\mathrm{NS}(\mathcal{X})$, the Picard rank. We thus define the *transcendental*

Defining polynomial	**Picard number**
$w^2 + xy^5 + x^5z + y^3z^3 + xz^5$	1
$w^2 + x^6 + y^5z + xz^5$	2
$w^2 + x^5y + xy^5 + x^3y^2z + z^6$	3
$w^2 + x^5y + y^6 + x^3yz^2 + x^3z^3 + xz^5$	4
$w^2 + x^5y + y^6 + x^4z^2 + x^2yz^3 + xz^5$	5
$w^2 + x^4y^2 + x^5z + y^5z + z^6$	6
–	7
$w^2 + x^5y + y^5z + y^2z^4 + xz^5$	8
$w^2 + x^5y + y^6 + x^2z^4 + z^6$	9
$w^2 + x^6 + y^5z + x^2z^4 + z^6$	10
$w^2 + x^5y + xy^5 + x^3yz^2 + z^6$	11
$w^2 + x^6 + y^6 + z^6 + x^2yz^3$	12
$w^2 + x^6 + y^6 + z^6 + x^2y^4 + x^4z^2$	13
$w^2 + x^6 + y^6 + xz^5$	14
$w^2 + x^6 + y^6 + z^6 + x^4yz + xyz^4$	15
$w^2 + x^6 + y^6 + z^6 + x^4y^2$	16
$w^2 + x^6 + y^6 + z^6 + x^4yz$	17
$w^2 + x^5y + x^3y^3 + xy^5 + z^6$	18
$w^2 + x^6 + y^6 + z^6 + x^3y^3$	18
$w^2 + x^6 + y^6 + z^6 + x^2y^2z^2$	19
$w^2 + x^6 + y^6 + z^6$	20

Table 7.2: *Example equations defining degree 2 K3 surfaces in $\mathbb{P}^{3,1,1,1}$ for each Picard number (except 7).*

endomorphism ring to be the morphisms of the transcendental lattice $\mathrm{Tr}(\mathcal{X}) = \mathrm{NS}(\mathcal{X})^\perp \subset H_2(\mathcal{X})$. Let $\eta_1, \dots, \eta_{22-\rho(\mathcal{X})}$ be a basis of $\mathrm{Tr}(\mathcal{X})$ and define $w = \left(\int_{\eta_1} \omega_{\mathcal{X}}, \dots, \int_{\eta_{22-\rho(\mathcal{X})}} \omega_{\mathcal{X}}\right)$.

Definition 33. *The* transcendental endomorphism ring *is the ring of endomorphisms e of* $\mathrm{Tr}(\mathcal{X}) \simeq \mathbb{Z}^{22-\rho(\mathcal{X})}$ *for which there is $\lambda \in \mathbb{C}^*$ such that $e_{\mathbb{C}}(w) = \lambda w$.*

Remark 58. *Again, we do not impose any compatibility with the lattice structure of* $\mathrm{Tr}(\mathcal{X})$.

We now expose methods of Lairez and Sertöz (2019) to compute this invariant from the period vector. From now on, we will no longer make the distinction between e and $e_{\mathbb{C}}$ to ease the notations. In order to find such e's, notice that we have the equivalence

$$\exists \lambda \in \mathbb{C}^*,\, e(w) = \lambda w \iff (w \cdot e(w))w = (w \cdot w)e(w)\,, \tag{7.21}$$

where $(\ \cdot\ )$ denotes any non-degenerate bilinear pairing on $\mathbb{Z}^{22-\rho(\mathcal{X})} \times \mathbb{Z}^{22-\rho(\mathcal{X})} \simeq \mathrm{Tr}(\mathcal{X}) \times \mathrm{Tr}(\mathcal{X})$ — for instance the canonical dot product $(\eta_i \cdot \eta_j) = \delta_{ij}$.

In terms of matrices, we are looking for $(22 - \rho(\mathcal{X})) \times (22 - \rho(\mathcal{X}))$ integer matrices N such that

$$(w^t N w)w = (w^t w)Nw\,, \tag{7.22}$$

which is a linear condition on N. In particular we may use the LLL algorithm (Lenstra et al., 1982) to heuristically recover such matrices N given a numerically approximation of w. In practice, however, these relations involve too many (r^2, which may be up to $21^2 = 441$) entries, and the precision we typically compute for w (300 digits) is not sufficient.

P(t)	1	2	3	4	5	6	7	8	9	10	11	12	13	14	15	16	17	18	19	20
$t-1$	265	360	43	1	1	1	0	0	43	60	14	0	3	3	1	5	12	1	3	0
t^2-t+1	0	0	0	0	0	40	0	8	0	0	0	9	0	17	0	2	0	3	0	3
$t^4-t^3+t^2-t+1$	0	26	0	0	0	4	0	0	0	7	0	0	0	0	0	0	0	0	0	0
$t^8-t^7+t^5-t^4+t^3-t+1$	0	0	0	0	0	1	0	0	0	0	0	0	0	1	0	0	0	0	0	0
$t^{20}-t^{15}+t^{10}-t^5+1$	0	1	0	0	0	0	0	0	0	0	0	0	0	0	0	0	0	0	0	0

Table 7.3: *The distribution of the defining equation $P(t)$ such that the endomorphism field is defined by $\mathbb{Q}[t]/(P(t))$, for the Σ_3-classes in V_3, V_4 and V_5. Notice that the field is always cyclotomic.*

Instead we detail here a finer algorithm for computing this invariant, which is in fact the one Lairez and Sertöz (2019) have implemented in `numperiods`[2] (Lairez & Sertöz, 2019) and `PeriodSuite`[3]. The trick is to proceed coordinate by coordinate. Let $N \in M_{22-\rho(\mathcal{X})}(\mathbb{Z})$, and denote by $N_1, \dots, N_{22-\rho(\mathcal{X})}$ its rows. Similarly denote by $w_1, \dots w_{22-\rho(\mathcal{X})}$ the coordinates of w. Let $2 \le i \le 22 - \rho(\mathcal{X})$ and consider

$$\begin{pmatrix} N_1 \cdot w & w_1 \\ N_i \cdot w & w_i \end{pmatrix}. \tag{7.23}$$

This 2×2 matrix is singular if and only if $(N_1 \cdot w, N_i \cdot w)$ is proportional to (w_1, w_i), and if and only if its determinant vanishes. As this determinant is linear in the entries of N_1 and N_i, we may find heuristically a basis of pairs of integer vectors (N_1, N_i) that satisfy this condition using LLL. Denote by Λ_i the sublattice of $\mathbb{Z}^{22-\rho(\mathcal{X})}$ generated by the admissible N_1's for a specific i.

Then we see that if N satisfies the condition (7.22), then

$$N_1 \in \bigcap_{i=2}^{22-\rho(\mathcal{X})} \Lambda_i\,. \tag{7.24}$$

[2]https://gitlab.inria.fr/lairez/numperiods
[3]https://github.com/emresertoz/PeriodSuite

Conversely, for any N_1 in this sublattice, there exists for every i a unique[4] N_i such that there exists a $\lambda \in \mathbb{C}^*$ satisfying

$$N_1 \cdot w_1 = \lambda w_1 \text{ and } N_i \cdot w_i = \lambda w_i \,. \tag{7.25}$$

Of course λ is determined by N_1 and independent of N_i. In particular, we see that

$$\begin{pmatrix} N_1 \\ \hline \vdots \\ \hline N_{22-\rho(\mathcal{X})} \end{pmatrix} \cdot w = \lambda w \,, \tag{7.26}$$

i.e., $N \cdot w = \lambda w$, and the linear map e induced by N is therefore a morphism of Hodge structure. The algorithm consists thus of three steps:

1. For every $2 \leq i \leq 22 - \rho(\mathcal{X})$, compute a basis of admissible pairs of vectors (N_1, N_i) using the LLL algorithm.

2. Compute a basis $N_{1,1}, \ldots, N_{1,r}$ of intersection of the Λ_i's.

3. For each $1 \leq j \leq r$, let N^j be the square matrix of size $22 - \rho(\mathcal{X})$ for which the rows are the $N_{i,j}$'s for $1 \leq i \leq 22 - \rho(\mathcal{X})$.

Let E be the transcendental endomorphism ring of $\mathcal{X}$, and denote $E_{\mathbb{Q}} = E \otimes \mathbb{Q}$. Then there is a map $\phi\colon E_{\mathbb{Q}} \to \mathbb{C}$ defined by $e(\omega_{\mathcal{X}}) = \phi(e)\omega_{\mathcal{X}}$. It is an injective ring morphism. In particular $E_{\mathbb{Q}}$ is a number field (Huybrechts, 2016, Corollary 3.3.6), called the *endomorphism field* of $\mathcal{X}$. In fact $E_{\mathbb{Q}}$ is either totally real or a CM-field (Zarkhin, 1983). In Table 7.3, we list the number fields that appeared among the classes of V_3, V_4 and V_5. Interestingly, we only encountered cyclotomic fields.

7.4 Beyond smooth ramification

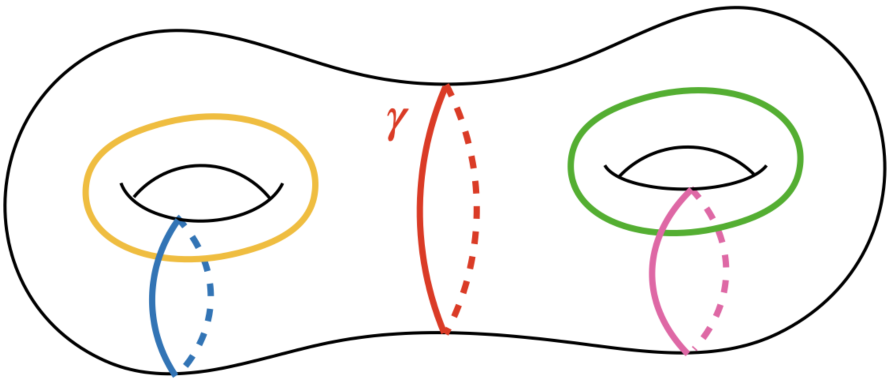

Figure 7.4: *The Dehn twist around the red loop γ leaves the standard symplectic homology basis of the genus 2 curve invariant (composed of the cycles of the other colours) as their representatives do not intersect the homology class of γ.*

In order to be able to generalise this approach to double covers of projective space ramified along hypersurfaces with singularities, a few points need to be addressed. First, for varieties of

[4] N_i is unique because if there was another such vector N_i', then $(N_i - N_i') \cdot w$ would be zero — i.e., there would a nontrivial integral relation between the coordinates of w.

dimension greater than 2, there might be different relatively minimal resolution of the singularities that appear — in particular there is a choice to be made here, so the problem is not well-posed.

For surfaces, there is a unique such minimal model (Lipman, 1969; Brieskorn, 1966). In this case, one may wonder whether an approach similar to the case of non-Lefschetz fibrations given in the case of elliptic surfaces in Section 6.4. However, contrary to the elliptic case, the morsification might not necessarily be determined entirely by the monodromy representation of the surface. A Kodaira-like classification of singular fibres in the case of genus 2 fibrations was initially worked out in Ogg (1966) and Iitaka (1967) independently. This list was later completed in Namikawa and Ueno (1973), along with equation for pencils of genus 2 curves realising each possible type. In Sakalli and Horn-Morris (2023), the authors give factorisation of conjugacy class of degenerations of genus 2 curves into Dehn twists. However it is, to my knowledge, not known if this factorisation is unique, as it is in the case of genus 1 as shown in Cadavid and Vélez (2009). There are singular fibres of families of genus 2 curves around which the (homological) monodromy is trivial (see type $[I_0\text{-}I_0\text{-}m]$, Namikawa and Ueno (1973)). Concretely, consider the Dehn twist with respect to the loop γ in Fig. 7.4, so that the singular fibre consists of two elliptic curves kissing at one point. As γ does not intersect the standard symplectic basis of $H_2(\mathcal{X})$, the action of monodromy on the homology is trival. However, it is not guaranteed that such degenerations can appear in fibration of smooth surfaces. In any case, this should not be much of an obstruction: an effective workaround would be to consider an explicit realisation of the morsification. Such an endeavour is in essence carried out in Section 8.2.2.

Part II

Perspectives

Chapter 8

Applications in homological mirror symmetry

In this chapter, we demonstrate the applicability of the methods we have developed to certain constructions coming from mirror symmetry. Homological mirror symmetry predicts relations between the symplectic geometry and holomorphic geometry of *mirror pairs* of Calabi–Yau manifolds. In particular in this context the Doran-Harder-Thompson conjecture predicts a link between certain types of degenerations of Calabi–Yau manifolds and fibration structures on the mirror side. The methods developed in this thesis allow to investigate the fibered Calabi–Yau manifolds, and this is the topic of this chapter in two settings: the case of degenerations of K3 surfaces, and of Fano threefolds.

The content of Section 8.1 is based on ongoing work with Charles F. Doran. The content of Section 8.2 is based on ongoing work with Charles F. Doran and Andrew Harder. The content of Section 8.3 is based on ongoing work with Charles F. Doran and Alan Thompson.

8.1 Fibration structure of mirrors of Fano threefolds

In Doran, Harder, Katzarkov, et al. (2023), the authors investigate the mirror symmetry of low rank Fano threefolds. The mirrors of these Fano threefolds are Landau–Ginzburg threefolds, which admit *Calabi-Yau compactification* by Przyjalkowski (2017). Concretely, this means the Landau–Ginzburg model can be realised by a fibration over $\mathbb{P}^1$ of which the generic fibres are quartic K3 surfaces. The polarisation of the K3 surfaces has to be Dolgachev–Nikulin dual (I. V. Dolgachev, 1996) to the Picard lattice of the original Fano threefold — in particular their ranks should add up to 20.

The work of Doran, Harder, Katzarkov, et al. (2023) produces explicit equations for these families of K3 surfaces, and identifies lines included in the K3 surfaces which in turn yield elliptic fibrations. Using this data, we can apply the methods of Chapter 6 to compute an effective basis of the homology of these K3 surfaces.

In this section, we report on the study of a large number of K3 surfaces appearing in Doran, Prebble, et al. (2023). In total, we considered 638 elliptic fibrations, of 85 K3 surfaces. The average time for the computation of the holomorphic period vector of these elliptic surface with 150 digits of precision was 36 seconds. The result are summarized in Table 8.1.

We may note some disparities between the Picard rank we computed and the results of Doran, Harder, Katzarkov, et al. (2023). For example, for Family 2.33, we obtain a Picard rank of 19, compared to the expected 18. This is because the given quartic equation for this family corresponds

Family	Picard rank	Discriminant
2.2	18	−4
2.3	18	−4
2.4	18	−9
2.5	18	−9
2.6	19	12
2.7	18	−16
2.9	18	−17
2.10	18	−16
2.11	18	−13
2.12	19	20
2.13	18	−24
2.14	18	−25
2.15	18	−12
2.16	18	−20
2.17	18	−25
2.18	18	−16
2.19	18	−17
2.20	18	−29
2.21	19	28
2.22	18	−24
2.23	18	−16
2.24	18	−21
2.25	18	−16
2.26	18	−21
2.27	18	−17
2.28	18	−9
2.29	18	−16
2.30	18	−12
2.31	18	−13
2.32	19	12
2.33	18	−9
2.34	18	−9
2.35	18	−8
2.36	18	−5
3.1	19	12
3.2	17	16
3.3	18	−28
3.4	17	24
3.5	17	28
3.6	17	32
3.7	18	−36
3.8	17	34
3.9	18	−12
3.10	18	−40
3.11	17	28
3.12	17	36
3.13	19	30
3.14	17	18
3.15	17	34
3.16	17	30
3.17	18	−28
3.18	17	26
3.19	18	−24
3.20	18	−28
3.21	17	22
3.22	17	18
3.23	18	−28
3.24	17	22
3.25	18	−20
3.26	17	18
3.27	19	12
3.28	17	16
3.29	17	12
3.30	17	14
3.31	18	−12
4.1	19	24
4.2	17	44
4.3	18	−32
4.4	17	48
4.5	17	40
4.6	16	−39
4.7	19	34
4.8	18	−52
4.9	17	32
4.10	16	−31
4.11	17	28
4.12	16	−23
4.13	17	20
5.1	17	42
5.2	16	−44
5.3	18	−36
6.1	18	−25
7.1	18	−16
8.1	18	−9
9.1	18	−4

Table 8.1: *The generic Picard rank and discriminant of the Picard lattice of the families of Doran, Harder, Katzarkov, et al. (2023).*

to a specific Landau–Ginzburg model, which is not necessarily representative of the full moduli space. To check this, we can consider the general Laurent polynomial for the Landau–Ginzburg model for Family 2.33 which is given in Doran, Harder, Katzarkov, et al. (2023, §5.2):

$$p_{a,b} = x + y + z + \frac{x}{z} + \frac{a}{xy} + b\,. \tag{8.1}$$

In order to recover the quartic equation, we multiply $p_{a,b} - \lambda$ by xyz and homogenise in w:

$$x^2yz + xy^2z + xyz^2 + x^2yw + azw^3 + (b-\lambda)xyzw\,. \tag{8.2}$$

We notice that the line $x = w = 0$ lies in this quartic, thus it admits an elliptic fibration, obtained by replacing w by tx and dividing by x:

$$xyz + y^2z + yz^2 + tx^2y + at^3zx^2 + (b-\lambda)txyz\,. \tag{8.3}$$

The example computed in Table 8.1 was the one of Doran, Harder, Katzarkov, et al. (2023, §B.33), corresponding to $a = b = 0$ and $\lambda = 3/2$. Taking instead the different values $\lambda = 5$, $b = 0$ and $a = 2$, for example, we can proceed with the computation of the holomorphic periods of the elliptic surface and thus recover the Picard rank, which we find is equal to the expected 18. We also note that the discriminant is the same as the one of Table 8.1, i.e., -9.

8.1.1 The monodromy representation of the Fano threefolds

Using the braid computation method of Chapter 10, we may recover the monodromy representation of the K3-fibered compactified Landau–Ginzburg mirrors of the Fano threefold from the monodromy representation of the various elliptic K3 surfaces which constitute its fibre. We have tried to do so with the elliptic fibrations obtained from the line divisors in the K3 surfaces. In many cases, the computation of the (pseudo-)braid along one single edge lasted longer than 1 minute and was halted. Nevertheless, we were able to carry out the braid computation for the monodromy representation of at least one fibration for all the 87 families of K3 surfaces with a line divisor, except families 2.15 and 3.21.

This way, we may compute the matrices of the monodromy action on the transcendental lattice of the K3 surface. In particular we are able to recover certain 3-cycles as extensions of transcendental cycles.

For example, for the family 2.2, there are 4 finite critical values c_1, c_2, c_3, c_4, and the monodromy representation given a distinguished basis around these critical values for a basis of the transcendental cycles are given by

$$\begin{pmatrix} 1 & 1 & 3 & -2 \\ 0 & 1 & 2 & 2 \\ 0 & 0 & 1 & -2 \\ 0 & 0 & 0 & -1 \end{pmatrix}, \begin{pmatrix} -2 & 3 & 3 & 3 \\ 2 & -1 & -2 & -2 \\ -2 & 2 & 3 & 2 \\ -1 & 1 & 1 & 2 \end{pmatrix}, \begin{pmatrix} -1 & 1 & 3 & 1 \\ -4 & 3 & 6 & 2 \\ 0 & 0 & 1 & 0 \\ 4 & -2 & -6 & -1 \end{pmatrix}, \begin{pmatrix} 1 & 0 & 0 & -1 \\ 0 & 1 & 0 & 4 \\ 0 & 0 & 1 & -2 \\ 0 & 0 & 0 & -1 \end{pmatrix}. \tag{8.4}$$

We see that the last three monodromy matrices are of Lefschetz type. As a sanity check, we may also see that these monodromy matrices preserve the intersection product, which in this basis of the transcendental lattice is given by

$$\begin{pmatrix} -2 & 4 & -2 & -1 \\ 4 & -6 & 4 & 4 \\ -2 & 4 & -2 & -2 \\ -1 & 4 & -2 & -2 \end{pmatrix}. \tag{8.5}$$

In fact, this determines the intersection product up to a sign. Furthermore, using another elliptic fibration of the same K3 surface, we find the monodromy matrices

$$\begin{pmatrix} -2 & -1 & 2 & 1 \\ -3 & 0 & 0 & -1 \\ -2 & 0 & 1 & 0 \\ 0 & 0 & -2 & -1 \end{pmatrix}, \begin{pmatrix} 1 & 0 & 0 & 0 \\ 0 & 1 & 0 & 0 \\ 3 & 1 & -1 & 0 \\ -3 & -1 & 2 & 1 \end{pmatrix}, \begin{pmatrix} 0 & -3 & 2 & 1 \\ 0 & 1 & 0 & 0 \\ -1 & -3 & 3 & 1 \\ 3 & 9 & -6 & -2 \end{pmatrix}, \begin{pmatrix} 1 & 0 & 0 & 0 \\ 1 & 0 & 0 & 1 \\ 1 & -1 & 1 & 1 \\ -1 & 1 & 0 & 0 \end{pmatrix}. \tag{8.6}$$

Comparing the periods, we may find the matrix of the change of basis between the two representations of the transcendental lattice:

$$\begin{pmatrix} -1 & -1 & 2 & 1 \\ 0 & 1 & -2 & -1 \\ 0 & 1 & -3 & -2 \\ 0 & 2 & -2 & -1 \end{pmatrix}. \tag{8.7}$$

We then check that up to conjugation by this change of basis, the monodromy representations are the same.

Using the methods of Section 3.5 we recover 2 cycles as extensions of transcendental cycles of the K3 fibre along loops in $\mathbb{C} \setminus \{c_1, c_2, c_3, c_4\}$. This data is an algebraic invariant of the Fano threefold. To our knowledge, this is the first computational method allowing the access to such data.

8.2 Degenerations of K3 surfaces

We are interested in studying the degeneration of K3 surfaces via the Lefschetz fibrations obtained in Chapter 4. Let us first expose the setting, mostly following Kondo (1985).

Definition 34. *A* semi-stable degeneration of K3 surfaces *is a map $\pi\colon \mathcal{X} \to D$ from a threefold $\mathcal{X}$ to a disk D, such that*

- *the fibres $\mathcal{X}_t = \pi^{-1}(t)$ are smooth K3 surfaces for $t \neq 0$;*
- *the central fibre $\mathcal{X}_0 = \pi^{-1}(0)$ is a divisor with normal crossing;*
- *$\mathcal{X}_0$ does not have components with multiplicity.*

A degeneration of K3 surfaces is weakly Kähler *if there exists a bimeromorphic map $\mathcal{X} \to \mathcal{X}'$ to a Kähler manifold, which is biholomorphic on $\mathcal{X} \setminus \mathcal{X}_0$.*

Similar to the Kodaira classification for elliptic curves, singular fibres in families of K3 surfaces have been classified by work of Kulikov (1977), Persson (1977), and Persson and Pinkham (1981). This classification is summarised in the following theorem of Kondo (1985).

Theorem 59 (Kondo, 1985, Theorem 1.5, attributed to Kulikov, 1977)**.** *Let $\pi\colon \mathcal{X} \to D$ be a weakly Kähler semi-stable degeneration of algebraic K3 surfaces. Then the central fibre $\mathcal{X}_0 = \pi^{-1}(0)$ is one of the following three types:*

- ***Type I**: a smooth K3 surface*
- ***Type II**: a union of surfaces $V_1 \cup \cdots \cup V_n$, where V_1 and V_n are rational surfaces, $V_2, \ldots, V_{n-1}$ are elliptic ruled surfaces and $V_i \cap V_j$ is an elliptic curve when $j = i + 1$ and empty otherwise.*
- ***Type III**: a union of rational surfaces $V_1 \cup \cdots \cup V_n$, where $V_i \cap V_j$ are smooth rational curves.*

The goal of this chapter is to showcase how the methods presented in this thesis can be used to investigate the degeneration in an effective manner. We first look at a type *III* degeneration of quartic K3 surfaces, and then at a type *II* degeneration of degree 2 K3 surfaces.

8.2.1 Type *III* degeneration

We consider the 1-parameter family of K3 surfaces obtained from the pencil generated by the Fermat quartic surface and a union of 4 hyperplanes:

$$\mathcal{X}_t : t(x^4 + y^4 + z^4 + w^4) + (1-t)xyzw\,. \tag{8.8}$$

The central fibre is the union of the four hyperplanes $x = 0$, $y = 0$, $z = 0$ and $w = 0$. These hyperplanes intersect pairwise in a line, and any triplet intersects at a single point. We thus have 4 distinguished singular points corresponding to each choice of the three hyperplanes

We obtain a fibration of the quartic K3 surfaces $\mathcal{X}_t$ by the pencil of hyperplanes $x + y + z = u(y - z + w)$, which, for generic values of t and in particular in a neighbourhood of $t = 0$, is Lefschetz.

The critical values of the map $\mathcal{X}_t \dashrightarrow \mathbb{P}^1$ obtained from this hyperplane pencil are the roots in u of a bivariate polynomial $P(u, t)$. We may compute $P(t, \cdot)$ for fixed t, and by evaluation-interpolation methods we are also able to recover the full polynomial P. P has degree 36 in u (as is expected as a Lefschetz fibration by genus 3 curves of a K3 surface has 36 singular fibres), and degree 21 in t. When t is set to 0, P factors into

$$\begin{aligned} P(0,u) = c(u-1)^3u^3(u+1)^3(1+u^4)\left(1+(u-1)^4\right)\left(1+(u+1)^4\right) \\ \times(1+6u^2+u^4)(1-4u+6u^2-4u^3+2u^4)(1+4u+6u^2+4u^3+2u^4)\,, \end{aligned} \tag{8.9}$$

where c is a rational coefficient. Notice that this polynomial only has degree 33 — this is because three of the roots diverge to infinity. Furthermore, note that for generic rational values of t, $P(t, u)$ is irreducible.

We can see that there are 4 clusters of 3 confluent fibres, at 1, 0, -1 and ∞, which correspond to the triple points. Furthermore, the quartic terms can be associated to pairs of the triple points: for example $(1 + u^4)$ corresponds to the points 0 and ∞. The geometrical interpretation of these quadruple of critical values is less clear. These clusters are represented in Fig. 8.1

We may compute the monodromy representation of the fibration in a neighbourhood of any of the triplet of critical values. for example, for one of these clusters, we find the monodromy representation

$$\begin{pmatrix} 1 & 0 & 0 & 0 & 2 & 2 \\ 0 & 1 & 0 & 0 & 0 & 0 \\ 0 & 0 & 1 & 0 & 0 & 0 \\ 0 & 0 & 0 & 1 & 0 & 0 \\ 0 & 0 & 0 & 0 & 2 & -1 \\ 0 & 0 & 0 & 0 & 1 & 0 \end{pmatrix}, \begin{pmatrix} -3 & 4 & 8 & 0 & -8 & 12 \\ 0 & 1 & 0 & 0 & 0 & 0 \\ 0 & 0 & 1 & 0 & 0 & 0 \\ -2 & 2 & 4 & 1 & -4 & 6 \\ 5 & -5 & -10 & 0 & 11 & -15 \\ 2 & -2 & -4 & 0 & 4 & -5 \end{pmatrix}, \begin{pmatrix} -1 & 2 & 4 & 0 & -2 & 4 \\ 0 & 1 & 0 & 0 & 0 & 0 \\ 0 & 0 & 1 & 0 & 0 & 0 \\ -2 & 2 & 4 & 1 & -2 & 4 \\ 4 & -4 & -8 & 0 & 5 & -8 \\ 1 & -1 & -2 & 0 & 1 & -1 \end{pmatrix}. \tag{8.10}$$

These monodromy matrices are given in a symplectic basis for the space of 1-cycles of the fibre, i.e., in this basis the intersection product is given by

$$\begin{pmatrix} 0 & -1 & 0 & 0 & 0 & 0 \\ 1 & 0 & 0 & 0 & 0 & 0 \\ 0 & 0 & 0 & -1 & 0 & 0 \\ 0 & 0 & 1 & 0 & 0 & 0 \\ 0 & 0 & 0 & 0 & 0 & -1 \\ 0 & 0 & 0 & 0 & 1 & 0 \end{pmatrix} \tag{8.11}$$

We thus recover the vanishing cycles

$$v_1 = (0,\, 0,\, 0,\, 0,\, 1,\, 1)^t\,, v_2 = (1,\, 1,\, 0,\, -2,\, 5,\, 2)^t\,, v_3 = (1,\, 1,\, 0,\, -2,\, 4,\, 1)^t\,. \tag{8.12}$$

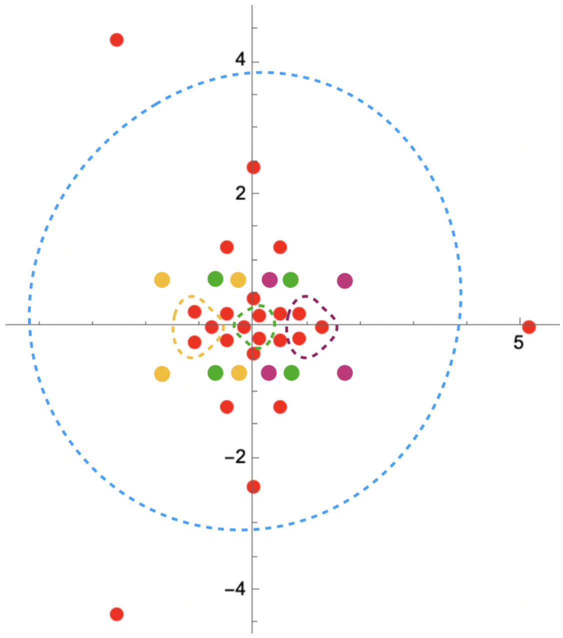

Figure 8.1: *The critical values of the fibration of $\mathcal{X}_c$ for $c = 10^{-5}$. We have identified the four clusters of three critical values merging together in the dashed curves (the blue dashed curve corresponds to the cluster at ∞, and the critical values in the cluster are really those outside of the circle). We have also colour-coded the three quadruples of critical values arrange in squares corresponding to the pairs of clusters consisting of a finite cluster and the cluster at ∞.*

We have the relation $v_1 + v_2 = v_3$ and the intersection pairing between v_1 and v_2 is

$$\begin{pmatrix} 0 & 3 \\ -3 & 0 \end{pmatrix}. \tag{8.13}$$

The same computation yields the same result for the other clusters. Comparing the vanishing cycles from one cluster to another, as well as the other critical values, is dependant on a choice of a connecting path. Nevertheless, doing so for a certain choice, we find that different clusters give different embeddings of this rank 2 lattice into the full rank 6 lattice of the full first homology group of the fibre.

More precisely, we consider a disk containing two clusters and the corresponding quadruplet of critical values. The vanishing cycles of the critical values are given, in order, by

$$\begin{pmatrix} 2 \\ 1 \\ 0 \\ -1 \\ 1 \\ 0 \end{pmatrix}, \begin{pmatrix} 1 \\ 2 \\ 0 \\ -1 \\ 0 \\ 0 \end{pmatrix}, \begin{pmatrix} 4 \\ 5 \\ 0 \\ -3 \\ 1 \\ 0 \end{pmatrix}, \begin{pmatrix} 1 \\ 1 \\ 0 \\ -1 \\ 1 \\ 0 \end{pmatrix}, \begin{pmatrix} 1 \\ 1 \\ 0 \\ -1 \\ 1 \\ 0 \end{pmatrix}, \begin{pmatrix} 0 \\ 0 \\ 0 \\ 0 \\ 1 \\ 1 \end{pmatrix}, \begin{pmatrix} 1 \\ 1 \\ 0 \\ -2 \\ 5 \\ 2 \end{pmatrix}, \begin{pmatrix} 1 \\ 1 \\ 0 \\ -2 \\ 4 \\ 1 \end{pmatrix}, \begin{pmatrix} 1 \\ 1 \\ 0 \\ -1 \\ 1 \\ 0 \end{pmatrix}, \begin{pmatrix} 1 \\ 1 \\ 0 \\ -1 \\ 1 \\ 0 \end{pmatrix} \tag{8.14}$$

The first three correspond to one of the cluster, the next two to two of the four orbiting points, the next three correspond to the other cluster and the last 2 to the last two orbiting values. We can see that the vanishing cycles at the orbiting critical values are all equal to $v_{\text{orb}} = (1, 1, 0, -1, 1, 0)^t$. Let $v_1^1 = (2, 1, 0, -1, 1, 0)^t$ and $v_2^1 = (1, 2, 0, -1, 0, 0)^t$ be a basis of the span of the vanishing cycles at the first cluster, and similiarly $v_1^2 = (0, 0, 0, 0, 1, 1)^t$ and $v_2^2 = (1, 1, 0, -2, 4, 1)^t$ for the second cluster. Then $\langle v_1^1, v_2^1, v_1^2, v_2^2\rangle$ has rank 4, and v_{orb} lies primitively in $\frac{1}{4}\langle v_1^1, v_2^1, v_1^2, v_2^2\rangle$.

Such intersection products are relevant because they provide information about the *Fukaya category* (Seidel, 2008) of the K3 surface. The methods described here provide an effective way of computing certain data pertaining to this category. Fukaya categories are relevant in mirror symmetry, as we shortly explain in Section 8.3.3.

8.2.2 Type *II* degeneration

We consider the 1-parameter family of degree 6 K3 surfaces obtained as double covers of $\mathbb{P}^2$ ramified along a sextic, given by the equation in $\mathbb{P}^3_{3,1,1,1}$

$$\mathcal{X}_t = w^2 - t(x^6 + y^6 + z^6) - (1-t)(x^3 + y^3 + z^3)\,. \tag{8.15}$$

The central fibre consists of two copies of $\mathbb{P}^2$ glued along the Fermat elliptic curve $V(x^3 + y^3 + z^3)$ — in particular this is a type *II* degeneration.

We take the projection $\mathbb{P}^2 \dashrightarrow \mathbb{P}^1$ given by the hyperplane pencil $H_u : x + y = u(y - z)$ The generic fibre is a hyperelliptic curve of degree 6, i.e., a genus 2 curve (see Chapter 7). Similarly to the quartic case, we may compute the bivariate polynomial P giving the critical values. It has degree 30 in u (as expected) and degree 7 in t, and is irreducible. When evaluated at the singular fibre $t = 0$, it factorises in the following way

$$\begin{aligned} P(0,u) = (4u^6 + 24u^4 + 24u^2 - 3)^2(u^6 + 6u^4 + 9u^2 + 3)(u^6 - 3u^5 + 15u^4 - 6u^3 + 9u + 3) \\ \times(u^6 + 3u^5 + 15u^4 + 6u^3 - 9u + 3)\,. \end{aligned} \tag{8.16}$$

We notably see that 6 pairs (c_1, c_2) of critical values merge, as represented in Fig. 8.2.

We may compute the intersection product of the vanishing cycles in a local monodromy representation in a neighbourhood of at these critical values. That is, we can choose $U \subset \mathbb{P}^1$ such that these critical values are in U and stay in U as $t \to 0$. We can then choose a basepoint $b \in U$ and simple loops ℓ_1, ℓ_2 around the two confluent critical values c_1, c_2 in $\pi_1(U \setminus \{c_1, c_2\}, b) \subset \pi_1(\mathbb{P}^1 \setminus \Sigma, b)$. Then the intersection matrix of the vanishing cycles at c_1 and c_2 along these simple loops is given by

$$\begin{pmatrix} 0 & -2 \\ 2 & 0 \end{pmatrix} \tag{8.17}$$

regardless of the pair of points considered.

8.3 Allowable loops of elliptic fibration of M-polarised K3 surfaces

The simplest occurence of Type *II* degenerations of K3 surfaces is that of *Tyurin degenerations*, where $n = 2$ (in the notations of Theorem 59) and the K3 degenerates into the union of two rational surfaces glued along an elliptic curve.

Let $\mathcal{X} \to \mathbb{P}^1$ be an elliptic K3 surface and denote Σ its set of critical values. For homological mirror symmetric reasons, we are interested in loops $\ell : [0,1] \to \mathbb{P}^1 \setminus \Sigma$ satisfying the following conditions:

- ℓ is not self-intersecting; in particular it separates $\mathbb{P}^1$ in two disks. We denote by D_1 and D_2 these two regions.

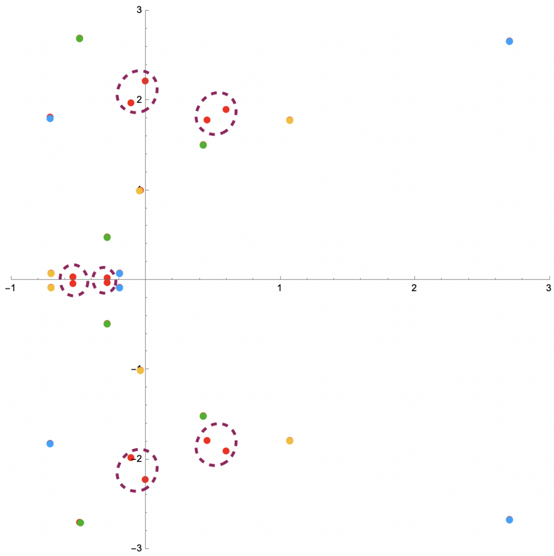

Figure 8.2: *The critical values of the fibration of $\mathcal{X}_c$ for $c = 1/100$ in the complex plane. We have identified the six clusters of two critical values merging together in the dashed curves. We have also colour-coded the roots of the other three degree* 6 *factors of the factorisation* (8.16)*.*

- the action of monodromy along ℓ on the fiber at $\ell(0) = \ell(1)$ is of the type I_{12-e}, i.e., has $\mathrm{SL}_2(\mathbb{Z})$ conjugation class
$$\begin{pmatrix} 1 & 12-e \\ 0 & 1 \end{pmatrix}, \tag{8.18}$$
where e is the Euler characteristic of the elliptic surface obtained by the restriction to one of the D_i's.

Such loops are called *allowable* — they are related to the elliptic curve along which the rational surfaces are glued in Tyurin degenrations, see Giovenzana and Thompson (2024). We then wish to check whether the cycle obtained by extending the invariant vector of ℓ_* along ℓ lies (up to a multiple of the fibre) in the transcendental lattice of the K3 surface, and whether it does so primitively.

Let $\mathcal{X} \to \mathbb{P}^1$ be an elliptically fibered K3 surface with polarisation $M = H \oplus (-E_8) \oplus (-E_8)$. The following theorem realizes the family of M-polarized K3 surface as a family of quartic surfaces in $\mathbb{P}^3$.

Theorem 60 (Clingher et al., 2009, Theorem 3.1)**.** *An M-polarised K3 surface $\mathcal{X}$ is isomorphic for the quartic surface $\mathcal{X}_{a,b,c}$ in $\mathbb{P}^3$ defined by the equation*

$$Q(a,b,d) : y^2zw - 4x^3z + 3axzw^2 + bzw^3 - 12(dz^2w^2 + w^4) = 0 \tag{8.19}$$

for some $a, b, d \in \mathbb{C}$. Furthermore, the isomorphism class of $\mathcal{X}_{a,b,d}$ is determined by the fundamental invariants *a^3/d and b^2/d*

The two lines $x = w = 0$ and $z = w = 0$ lie in $\mathcal{X}_{a,b,c}$. In particular, for generic values of a, b, d, the K3 surface has two distinct elliptic fibrations, which we call the *standard* fibration and *alternate* fibration respectively.

In this chapter, we realise the elliptic fibrations of M-polarised K3 surfaces as multiple covers of rational surfaces with 3 singular fibres. Before we proceed to the study of these elliptic fibrations, let us recall facts about rational elliptic surfaces with few singular fibres. Because any three points in $\mathbb{P}^1$ can be sent to $\{0, 1, \infty\}$ by a Möbius transformation, there is a unique rational surface with this fibre configuration. More generally, the moduli space of elliptic surfaces with an admissible configuration of four fibres of a given type is 1-dimensional. The full classification of such rational surfaces was computed in Herfurtner (1991).

8.3.1 The standard fibration

The standard elliptic fibration is the one given by $z = w = 0$. It is given by the equation

$$bt^3Z^3 - \frac{1}{2}t^4Z^3 + 3at^2XZ^2 - \frac{1}{2}dt^2Z^3 + tY^2Z - 4X^3 = 0\,. \tag{8.20}$$

It has four I_1 fibres and two II^* fibres.

Lemma 61. *The standard fibration of $\mathcal{X}_{a,b,d}$ is the double cover of the rational elliptic surface with three fibres of type I_1, I_1 and II^*, ramified at two generic points.*

This rational surface is the seventh entry in Table 3 of Herfurtner (1991) with the parameter ρ_4 set to 1 (indeed, the confluence of a IV fibre with an I_0^* fibre yields a type II^* fibre). In particular, after a Möbius transformation setting the II^* fibre at ∞, it is realised by the equation

$$Y^2Z = 4X^3 - (3t^4 + 36t^3 - 78t^2 + 36t + 3)XZ^2 - (t^6 - 36t^5 + 69t^4 - 69t^2 + 36t - 1)Z^3\,. \tag{8.21}$$

We then pullback to obtain the double cover with the change of variable $u = c_1t + c_0 + \frac{c_{-1}}{t}$, such that $u = \infty$ when t is either 0 or ∞. It is then sufficient to find values for c_1, c_0, c_{-1} for which the fibres match those of the standard elliptic fibration of $\mathcal{X}_{a,b,d}$. This amounts to having matching discriminants, and we find that this happens whenever

$$a = 16\,, \quad c_1 = \frac{1}{128}\,, \quad c_0 = -\frac{b}{64}\,, \quad c_{-1} = \frac{d}{128}\,. \tag{8.22}$$

Note that although this solution specifies the value of a, the fundamental invariants of Theorem 60 are still free to take any value and thus this covers all possible isomorphism class of the K3 surfaces. This proves Lemma 61.

From this presentation, we can obtain information about the elliptic K3 surface. First, the fibres come in pairs with equal monodromy. Furthermore, we may partition $\mathbb{P}^1$ into two open disks and an equator, with each disk corresponding to each copy of the rational surface. In particular, the action of monodromy along the equator coincides with the monodromy along a loop around the two ramification points of the double cover. As the two points are generic, this monodromy is trivial. Finally, the Euler characteristic of the rational surface is $e = 12$, and thus trivial monodromy corresponds the type of (8.18). Thus the loop tracing the equator satisfies the properties we are after.

Of course, it is possible to also add any of the I_1 fibres in one of the copies. Indeed, then the monodromy will be equal to that of the fibre, and the Euler characteristic will have shifted by 1. All in all we find 3 such loops up to the $\mathbb{Z}/2\mathbb{Z}$ reflection coming from the double cover.

Let us first focus on the equator. As the monodromy is trivial, in this case we have not only one, but two possible extensions. Nevertheless, we find that whatever 1-cycle is being extended, it yields a 2-cycle lying primitively in the transcendental lattice.

For the other loops, there is only a single invariant 1-cycle. However, extending along the loop yield the same result as extending it along the equator. Indeed by formula (2.5), we have

$$\tau_{\ell_{I_1}\ell_{\text{equator}}} = \tau_{\ell_{I_1}}(\ell_{\text{equator}*}\gamma) + \tau_{\ell_{\text{equator}}}(\gamma) \tag{8.23}$$

and

$$\tau_{\ell_{I_1}}(\ell_{\text{equator}*}\gamma) = \tau_{\ell_{I_1}}(\gamma) = 0\,, \tag{8.24}$$

where ℓ_{I_1} is the loop around the I_1 and ℓ_{equator} the one along the equator.

Explicitly, the monodromy representation in a given symplectic basis of the first homology group of the fibre with a given distinguished basis of $\pi_1(\mathbb{P}^1 \setminus \Sigma)$ is

$$M_1 = M_4 = \begin{pmatrix} 1 & 1 \\ 0 & 1 \end{pmatrix}, \quad M_2 = M_5 = \begin{pmatrix} 1 & 0 \\ -1 & 1 \end{pmatrix}, \quad M_3 = M_6 = \begin{pmatrix} 0 & -1 \\ 1 & 1 \end{pmatrix} \tag{8.25}$$

This description is schematized in Fig. 8.4.

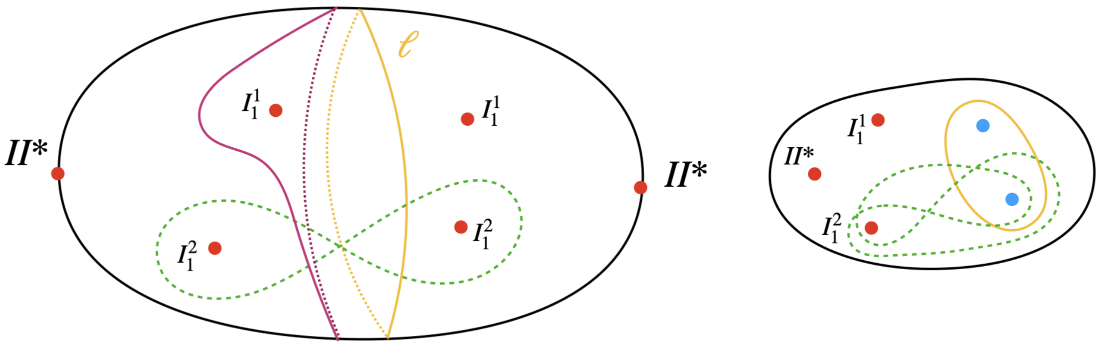

Figure 8.3: *A schematic representation of the standard elliptic fibration of an M-polarised K3 surface (left) as the double cover of a rational surface (right). The elliptic K3 surface, has 6 singular fibres represented in red. Two of type II^* and four of type I_1. The singular fibres come in pair stemming from the rational surface, represented below. The two ramification points in the rational surface are represented in blue. The loop ℓ is the lift of the orange loop in the elliptic surface around the ramification points. As these are generic, there is no ramification. The nontrivial extensions along the dashed path in green yields a transcendental cycle. The purple path is also a allowable path in the elliptic K3 surface. It is equivalent to the orange one in that any extension without boundary along this path is equal to an extension along ℓ.*

8.3.2 The alternate fibration

The alternate elliptic fibration is the one obtained using the line $x = w = 0$. It is given by the equation

$$-\frac{1}{2}t^4X^3 + bt^3X^2Z + 3at^2X^2Z - \frac{1}{2}dt^2XZ^2 + tY^2Z - 4X^2Z = 0\,. \tag{8.26}$$

It has six I_1 fibres and one I_{12}^* fibre. In this model, the II^* fibres are above the points 0 and ∞.

Lemma 62. *The alternate fibration of $\mathcal{X}_{a,b,d}$ is the triple cover of the rational elliptic surface with three fibres of type I_1, I_1 and I_4^* with total ramification at the I_4^* fibre and simple ramification at three generic points.*

This rational surface is the first entry in Table 3 of Herfurtner (1991) with the parameter ρ_4 set to 1 (indeed, the confluence of a I_4 fibre with an I_0^* fibre yields a type I_4^* fibre). In particular, after a Möbius transformation setting the I_4^* fibre at ∞, it is realised by the equation

$$\begin{aligned}&\left(4X^3 - Y^2Z\right)t^6 + \left(-24X^3 + 6Y^2Z\right)t^5 + \left(60X^3 - 15Y^2Z - 192XZ^2\right)t^4 \\ &+ \left(-80X^3 + 20Y^2Z + 384XZ^2 + 512Z^3\right)t^3 + \left(60X^3 - 15Y^2Z - 48XZ^2\right)t^2 \\ &+ \left(-24X^3 + 6Y^2Z - 288XZ^2 - 576Z^3\right)t + 4X^3 - Y^2Z + 144XZ^2 = 0\,.\end{aligned} \tag{8.27}$$

We then pullback to realize the triple cover with the change of variable $t' = \alpha(t-x_1)(t-x_2)(t-x_3)$, so that there is total ramification at ∞. It is then sufficient to find values for c and the x_i's for which the fibres match those of the standard elliptic fibration of $\mathcal{X}_{a,b,d}$. This amounts to having matching discriminants, and we find that this happens under the conditions

$$a = \frac{2}{3}(x_1^2 + x_2^2 + x_3^2)\,, \quad b = 4x_1x_2x_3\,, \quad d = 2304\,, \quad u = -\frac{1}{12}\,, \quad x_1 + x_2 + x_3 = 0\,. \tag{8.28}$$

Again, although we have to specify the value of d, the invariants are still free to take any value and thus this covers all possible isomorphism class of the K3 surfaces. This proves Lemma 62.

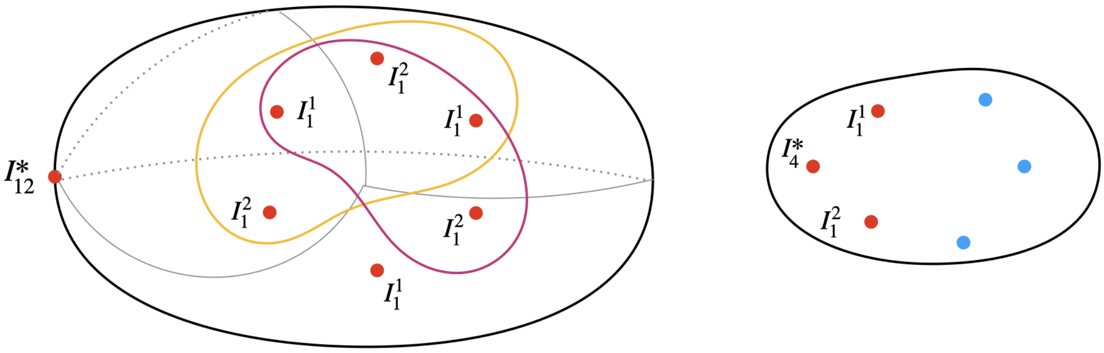

Figure 8.4: *A schematic representation of the alternate elliptic fibration of an M-polarised K3 surface as the triple cover of a rational surface. The elliptic surface, above, has 7 singular fibres represented in red: one of type I_{12}^* and six of type I_1. The I_1 fibres come in triplets stemming from the I_1's of the rational surface, represented on the right. The three generic ramification points in the rational surface are represented in blue, and there is also ramification at the I_4^* fibre. The orange and purple loops are allowable in the elliptic K3.*

From this presentation, we can obtain information about the elliptic K3 surface. The I_1 fibres come in triplets with equal monodromy which we may explicitly compute. Concretely, the monodromy representation in a given symplectic basis of the first homology group of the fibre with a given distinguished basis of $\pi_1(\mathbb{P}^1 \setminus \Sigma)$ is

$$M_1 = M_3 = M_5 = \begin{pmatrix} -2 & 9 \\ -1 & 4 \end{pmatrix}, \quad M_2 = M_4 = M_6 = \begin{pmatrix} 0 & 1 \\ -1 & 2 \end{pmatrix}, \quad M_7 = \begin{pmatrix} -1 & -12 \\ 0 & -1 \end{pmatrix} \tag{8.29}$$

The homotopy class of any loop in $\pi_1(\mathbb{P} \setminus \Sigma)$ is generated by the loops around the I_1 fibres. In particular, the monodromy along the any loop is a composition of the monodromy around the I_1 fibres. We may thus search for loops satisfying our property by finding products of the matrices M_1, M_2, M_1^{-1} and M_2^{-1} which are in the conjugacy class of (8.18) for some e. We did so for product of up to 10 terms. Apart from the obvious powers of the M_i's and their inverse, which would lead to trivial 2-cycles, the only such relations we have found is

$$M_2M_1M_2M_1 = M_4M_3M_2M_1 = \begin{pmatrix} 1 & -8 \\ 0 & 1 \end{pmatrix}, \tag{8.30}$$

as well as its inverse and their conjugation by any of the M_i. Thus a loop encircling any $e = 4$ consecutive I_1 fibres in the above monodromy representation yields a monodromy of the type of (8.18). In fact, one may show that these are the only allowable loops for this elliptic surface (although we will not do it in this text).

For each such loop ℓ we may then compute the extension along ℓ of the cycle γ invariant under the action of ℓ_*. We obtain that such 2-cycles are always primitive in the transcendental lattice, and that they generate the full transcendental lattice. This is represented in Fig. 8.4.

8.3.3 Perspectives

Homological mirror symmetry predicts that Calabi-Yau varieties come in pairs, with a relation between the symplectic geometry structure of the first variety to and the holomorphic structure of the other, and vice-versa. More precisely, for a mirror pair $(\mathcal{X}, \check{\mathcal{X}})$, it predicts an equivalence of categories between the *Fukaya caterogy* of $\mathcal{X}$ (Seidel, 2008) with the *bounded derived category of coherent sheaves* of $\check{\mathcal{X}}$ (Orlov, 2009). In this setting, the Doran-Thompson-Harder conjecture predicts that when a Calabi-Yau manifold $\mathcal{X}$ degenerates into the union of two quasi-Fano manifolds $\mathcal{X}_1 \cup_Z \mathcal{X}_2$ intersecting along a common anti-canonical smooth divisor Z, then one may reconstruct the mirror $\check{\mathcal{X}}$ of $\mathcal{X}$ by gluing the mirror Landau-Ginzburg models of $\mathcal{X}_1$ and $\mathcal{X}_2$, which equips $\check{\mathcal{X}}$ with a fibration by Calabi-Yau manifolds over $\mathbb{P}^1$. This conjecture was proven in the case of elliptic curves in Kanazawa (2017). For polarised K3 surfaces, recent work of Giovenzana and Thompson (2024) reduces the proof of this conjecture to a computational check, which involves finding the allowable loops in elliptic K3 surfaces. The methods developed in this thesis allow precisely to carry out these computations as shown on the examples above, and thus would in turn allow to provide the missing step to obtain a proof of this conjecture for polarised K3 surfaces.

Chapter 9

Numerical check of the Deligne conjecture for certain Calabi-Yau threefolds

We now turn to an application in arithmetic geometry. We aim to check the Deligne conjecture numerically on certain examples of Calabi-Yau threefolds. Deligne's conjecture, first formulated by Deligne (1979), is, in some sense, a generalisation of the Birch and Swinnerton–Dyer conjecture (Birch & Swinnerton-Dyer, 1965) for modular elliptic curves to higher dimensional Calabi–Yau manifolds.

In the case of hyperelliptic curves, Beilinson's conjecture (Beilinson, 1985), which can itself be seen as a generalisation of the Birch and Swinnerton–Dyer conjecture, was tested numerically in Dokchitser et al. (2006), and later to superelliptic (non-hyperelliptic) curves Neurohr (2018). In higher dimensions, Yang (2021) provides a numerical check of the Deligne conjecture for two Calabi–Yau threefolds, relying on work of Candelas et al. (2020). More recently, for certain $(1,1,1,1)$ hypergeometric motives, Golyshev (2023) provides a numerical check of the Beilinson conjecture.

The methods of this thesis allow to compute the periods of certain Calabi–Yau threefolds given as fibered products of elliptic surfaces, as we will now present in this section. This opens the door to the numerical check of the Deligne conjecture in many cases, provided we also know the values of L-functions.

The content of this chapter is ongoing work with Nutsa Gegelia and Duco van Straten.

9.1 Topology and periods of fibered product of elliptic surfaces

Let $f_1 : S_1 \to \mathbb{P}^1$ and $f_1 : S_2 \to \mathbb{P}^1$ be two elliptic surfaces. We may construct a threefold by taking their fibered product $\mathcal{X} = S_1 \times_{\mathbb{P}^1} S_2$. This threefold is by construction equipped with a fibration f over $\mathbb{P}^1$. For $t \in \mathbb{P}^1$ by $E_{it} = f_i^{-1}(t)$ the fiber of S_i above t. Then the fibre of this threefold is the surface $\mathcal{X}_t = f^{-1}(t) \simeq E_{1t} \times E_{2t}$.

By the Künneth formula, we thus have

$$H^2(\mathcal{X}_t) \simeq H^1(E_{1t}) \otimes H^1(E_{2t}) \oplus H^0(E_{1t}) \otimes H^2(E_{2t}) \oplus H^2(E_{1t}) \otimes H^0(E_{2t}) \,. \tag{9.1}$$

Note that $H^0(E_{it})$ and $H^2(E_{it})$ have trivial monodromy for $i = 1, 2$. Thus the only relevant part of the homology of the fibre is $H^1(E_{1t}) \otimes H^1(E_{2t})$, which has rank $2 \times 2 = 4$.

The periods of the fibre are easily obtained from those of E_1 and E_2 thanks to the formula

$$\int_{\gamma_1\times\gamma_2}\omega_1\otimes\omega_2=\int_{\gamma_1}\omega_1\int_{\gamma_2}\omega_2 \tag{9.2}$$

where $\omega_i \in H^1_{\mathrm{DR}}(E_{it})$ and $\gamma_i \in H_1(E_{it})$. In particular it is apparent that the Picard–Fuchs operator of $\omega_{1t}\otimes\omega_{2t}$ is simply the symmetric product $\mathcal{L}=\mathcal{L}_1 Ⓢ \mathcal{L}_2$ of the Picard–Fuchs operators $\mathcal{L}_i$ of ω_{it} — that is, the minimal operator annihilating the product of a solution of $\mathcal{L}_1$ and one of $\mathcal{L}_2$. In particular, if ω_{it} is cyclic for $i=1,2$, then $\mathcal{L}$ has order 4 and thus encodes the full action of monodromy on $H_2(E_{1t}\times E_{2t})$. Alternatively, the monodromy may also be recovered as the tensor product of the monodromies of S_1 and S_2.

When the critical locus of S_1 and S_2 are disjoint, this defines a smooth threefold. When the two surfaces are additionally relatively minimal rational elliptic surfaces, Schoen (1988) showed that the fibered product defines a smooth Calabi-Yau threefold. Furthermore, authorising certain types of singular fibres to coincide, it is shown in Kapustka and Kapustka (2009) that the possibly singular threefold admits a *small resolution* into a Calabi–Yau threefold.

9.1.1 The cohomology of $\mathcal{X}$ and Deligne's period

We recall the general setting, mostly following Golyshev and Van Straten (2023) for the exposition and context. All the elliptic surfaces we will consider are rational surfaces with 3 or 4 singular fibres. The fibered product we will consider are Calabi-Yau threefolds with middle Hodge numbers $(1,1,1,1)$ — so-called $(1,1,1,1)$-*motives*.

We will be interested not only in the fibered product, but in a family of such threefolds which we may define from two given elliptic surfaces. For $u\in\mathbb{C}$, consider the map $i_u^*:\mathbb{P}^1\to\mathbb{P}^1$ defined by $t\mapsto u/t$ and define $S_1\times_u S_2 \stackrel{\text{def}}{=} S_1\times_{\mathbb{P}^1} i_{u*}(S_2)$. Then in Golyshev and Van Straten (2023) the authors show that the 1-parameter family $\{\mathcal{X}^u\}_{u\in\mathbb{P}^1}$, where $\mathcal{X}^u$ is the small resolution of $S_1\times_u S_2$ is a flat family of smooth Calabi-Yau threefolds of Hodge numbers $(1,1,1,1)$.

Before we can define Deligne's period, let us introduce some notation. The complex conjugation $c\in\mathrm{Gal}(\mathbb{C}/\mathbb{R})$ induces an involution c_* of $H_3(\mathcal{X})$. We denote by $H_3^+(\mathcal{X})$ the invariant sublattice under this involution, that is the kernel of $c_*-\mathrm{id}$. It has rank 2, and we denote by γ_1^+,γ_2^+ an integral basis of this space When ω is defined over $\mathbb{Q}$, such cycles can be identified by the fact that their periods are real. In particular we may heuristically recover these cycles numerically by finding integer linear relations between the imaginary parts of a basis of the periods. Similarly, we define $H_3^-(\mathcal{X})$ the kernel of $c_*+\mathrm{id}$, the space of imaginary cycles, and denote a basis as γ_1^-,γ_2^-. Of course $H_3^+(\mathcal{X})$ and $H_3^-(\mathcal{X})$ are in direct sum — however, in all the cases we checked, they only generate a non-primitive full rank sublattice of $H_3(\mathcal{X})$.

Recall the Hodge filtration $\mathcal{F}^3\subset\mathcal{F}^2\subset\mathcal{F}^1\subset\mathcal{F}^0=H^3_{\mathrm{DR}}(\mathcal{X})$. From $h^{3,0}=h^{2,1}=1$ we directly obtain that $\dim H^3_{\mathrm{DR}}(\mathcal{X})=4$ and $\dim\mathcal{F}^i=4-i$ — in particular $\dim\mathcal{F}^2=2$. We can now define *Deligne's period.*

Definition 35. Deligne's period c^+ *is the determinant of the period map restricted* $H_3^+(\mathcal{X})\times\mathcal{F}^2\to\mathbb{C}$ *in an integral basis of* $H_3^+(\mathcal{X})$ *and a rational basis of* $\mathcal{F}^2$.

Remark 63. *Deligne's period is thus only defined up to a rational number, depending on the choice of the bases of* $H_3^+(\mathcal{X})$ *and* $\mathcal{F}^2$.

We now explain how to obtain a Hodge basis of $H^3_{\mathrm{DR}}(\mathcal{X})$. We obtain this by following the ideas of Stiller (1987). We will consider global sections of $\mathcal{H}^2(E_{1t}\times E_{2t})$ of the form $\omega_t=c(t)\omega_{1t}\otimes\omega_{2t}$ where ω_{it} is a global section of $\mathcal{H}^{1,0}(E_{it})$ and $c(t)\in\mathbb{Q}(t)$. The trick is to find a rational coefficient

c such that this form does not have residues anywhere. In all the cases we have considered, this can be done by taking $c(t) = t^i$ a power of t, such that the local exponents of the Picard–Fuchs equation of ω_t are "minimal". Then $\omega_t \wedge \mathrm{d}t$ defines a holomorphic form ω on $\mathcal{X}$.

To then complete this into a Hodge basis of $H^3_{\mathrm{DR}}(\mathcal{X})$, we consider the embedding of $\mathcal{X}$ into the family $\{\mathcal{X}^u\}$. We may compute the Gauss-Manin connection explicitly using the methods of Section 3.2. In particular by Griffiths transversality we obtain.

$$H^{3,0}(\mathcal{X}_u) = \mathcal{F}^3 = \langle \omega \rangle \,, \tag{9.3}$$
$$\mathcal{F}^2 = \langle \omega, \partial_u \omega \rangle \,, \tag{9.4}$$
$$\mathcal{F}^1 = \langle \omega, \partial_u \omega, \partial_u^2 \omega \rangle \,, \tag{9.5}$$
$$H^3(\mathcal{X}_u) = \mathcal{F}^0 = \langle \omega, \partial_u \omega, \partial_u^2 \omega, \partial_u^3 \omega \rangle \,. \tag{9.6}$$

Lemma 64. *Deligne's period is given by*

$$c^+ = \begin{vmatrix} \int_{\gamma_1^+} \omega & \int_{\gamma_1^+} \partial_u \omega \\ \int_{\gamma_2^+} \omega & \int_{\gamma_2^+} \partial_u \omega \end{vmatrix} \,. \tag{9.7}$$

9.2 L-functions and Deligne's conjecture

The Deligne conjecture is a generalisation to higher dimensions of the Birch-Swinnerton-Dyer conjecture, which relates the real holomorphic period of an elliptic curve to a certain arithmetic invariant, its *L-function.* The goal of this section is to provide a statement of Deligne's conjecture in our setting, and to expose numerical evidence for Deligne's conjecture that we can derive from the computations of the previous section.

9.2.1 L-functions

Broadly, L functions are certain meromorphic functions carrying arithmetic information about a motive. They stem from analytic continuation of L-series, which are Dirichlet series that converge on the upper complex half-plane.

In the setting we are considering, the L-function takes the form of an infinite product over the prime numbers p

$$L(\mathcal{X}, s) = \prod_{p \text{ prime}} F_p(p^{-s})^{-1} \tag{9.8}$$

where the F_p are certain polynomials called *Euler factors.* They are obtained as the characteristic polynomial of the action of the geometric p-Frobenius on the ℓ-adic cohomology group $H^3_{\text{ét}}(\mathcal{X}, \mathbb{Q}_\ell)$ (which we did and will not define in this text):

$$F_p(t) = \det\left(1 - t \, \mathrm{Frob}_p \,|_{H^3_{\text{ét}}(\mathcal{X}, \mathbb{Q}_\ell)}\right) \,. \tag{9.9}$$

Conjectural methods for computing the Euler factors, and thus values of L-functions were developed in Candelas et al. (2021). I am thankful to Nutsa Gegelia for providing the numerical values of the L-functions of the following examples.

9.2.2 Numerical check of Deligne's conjecture

We are now able to state Deligne's conjecture in the context we are interested in.

Conjecture 1 (Deligne's conjecture)**.** *The ratio $L(\mathcal{X}, 2)/c^+$ is a rational number.*

Fibered product	ratio	c(t)
$A \times_1 A$	-2^{-4}	1
$A \times_1 B$	$2^2 \cdot 3^{-2}$	t^2
$A \times_1 c$	3^{-1}	t^5
$A \times_1 d$	2^{-2}	t^5
$B \times_1 B$	$2^8 \cdot 3^{-5}$	t^2
$B \times_1 c$	$-2^5 \cdot 3^{-3}$	t^5
$A \times_{-1} A$	-2^{-4}	1
$A \times_{-1} B$	$2^2 \cdot 3^{-2}$	t^2
$A \times_{-1} b$	2^{-5}	1
$A \times_{-1} c$	3^{-1}	t^5
$A \times_{-1} f$	$-2 \cdot 3^{-1}$	t^5
$B \times_{-1} B$	$2^8 \cdot 3^{-4}$	t^2
$B \times_{-1} c$	$2^6 \cdot 3^{-3}$	t^5

Table 9.1: *$L(\mathcal{X}, 2)\pi^2/c^+$ for Calabi-Yau threefolds of Hodge type $(1,1,1,1)$. The obtained ratios are only recovered numerically with tens of digits of precision (depending on $\mathcal{X}$). Note that c^+ is only defined up to the square of a rational number.*

The rational elliptic surfaces we consider are the following:

$$\begin{aligned}
&A : (-x^2z - yz^2)t - x^3 - xyz + y^2z = 0\\
&B : 64z^3t^3 - 48xz^2t^2 + 12x^2zt - x^3 - x^2z + y^2z = 0\\
&b : (-x^2z - xyz - yz^2)t - x^3 - xyz + y^2z = 0\\
&c : z^3t^6 - 3xz^2t^4 + 2yz^2t^3 + 3x^2zt^2 - 3xyzt - x^3 + xyz + y^2z = 0\\
&d : 8z^3t^6 - 8z^3t^5 + (4xz^2 + z^3)t^4 + 2x^2zt^2 - 4xyzt - x^3 + xyz + y^2z = 0\\
&f : 54z^3t^6 - 27z^3t^5 + 9z^3t^4 + (9yz^2 - z^3)t^3 - 3xyzt - x^3 + xyz + y^2z = 0
\end{aligned}$$

The small resolution of the fibered product between certain pairs of these surfaces define smooth Calabi-Yau threefold. Among these, we were able to compute a numerical approximation of the L-value and compare with the computation of the Deligne period obtained with our method.

This is presented in Table 9.1. We also included the rational coefficient $c(t)$ necessary to find the holomorphic form. The rational ratios are subject to a choice of the holomorphic form up to a rational factor, and thus only defined up to the square of a rational number. Nevertheless, intriguingly, we find rational coefficients with only 2 and 3 in their prime decomposition.

In many cases, while the resulting threefold is indeed Calabi–Yau and we were able to compute Deligne's period, we found that the L-values was zero. In this case, Deligne's conjecture no longer applies, but Beilinson's conjecture predicts a similar relation between Deligne's period and the value of the L-function, but also involving the determinant of a height pairing of arithmetic nature, Beilinson's heights. Obtaining a way to evaluate this determinant would allow for the numerical check of Beilinson's conjecture for these threefolds.

Chapter 10

Braids and monodromy

In this chapter, we provide an alternative way of computing the action of monodromy on the homology. We will not attempt to formalise the results stated here, only to provide insights into the computational aspects.

In short: We have a tower of fibration $\mathcal{X}_{t,t'} \subset \mathcal{X}_b \subset \mathcal{X}$ where $\mathcal{X}_t$ is the generic fibre of the modification $\mathcal{Y}$ of $\mathcal{X}$ and similarly for $\mathcal{X}_{t,t'}$ and $\mathcal{Y}_t \to \mathcal{X}_t$. The monodromy with respect to t acts on the level of the fundamental group of the punctured base of the fibration $\mathcal{Y}_t \to \mathbb{P}^1$. This monodromy can be lifted to recover the action of monodromy on extensions of $\mathcal{Y}_t$, i.e. $H_{n-1}(\mathcal{Y}_b, \mathcal{X}_{b,b'})$ for some generic basepoints b and b'. To compute the monodromy, we encode an element ℓ of the fundamental group of the punctured base of $\mathcal{Y}_t \to \mathbb{P}^1$ as a word related to a covering tree of its critical values. As the parameter t varies, we may track the way the topology of this graph changes, and we may compute how the word changes accordingly. Doing this iteratively along a loop ℓ' we obtain a new word which describes precisely the homotopy class of the monodromy of ℓ along the loop ℓ'.

The content of this chapter is ongoing work, joint with Alexandre Guillemot and Pierre Lairez.

10.1 Braids

Let $n \geq 2$.

Definition 36. *The* Artin braid group on n strands is group A_n *is the group on* $n-1$ *characters* $\sigma_1, \ldots, \sigma_{n-1}$ *subject to the relations*

$$\sigma_i\sigma_{i+1}\sigma_i = \sigma_{i+1}\sigma_i\sigma_{i+1} \text{ for } 1 \leq i \leq n-1 \tag{10.1}$$

and

$$\sigma_i\sigma_j = \sigma_j\sigma_i \text{ for } i-j \geq 2\,. \tag{10.2}$$

Braids can equivalently be characterised as elements of the fundamental group of the space of configurations.

Definition 37. *The* space of ordered configuration *of* n *points* C_n^{ord} *in the complex plane is the topological space*

$$C_n^{ord} = \{(c_1, \ldots, c_n) \in \mathbb{C}^n \mid c_i \neq c_j \text{ for } i \neq j\} \subset \mathbb{C}^n\,, \tag{10.3}$$

equipped with the subspace topology.

The symmetric group on n elements $\mathfrak{S}_n$ acts on C_n^{ord} by permuting the coordinates.

Definition 38. *The* space of (unordered) configuration *of n points C_n in the complex plane is the quotient of C_n by $\mathfrak{S}_n$*

$$C_n = C_n^{ord}/\mathfrak{S}_n \tag{10.4}$$

equipped with the quotient topology.

Via this characterisation, we can see that braids act on the fundamental group of the disk D punctured at n points $c_1, \ldots, c_n$ pointed at a point $b \in \partial D$. More precisely, if $\ell_1, \ldots, \ell_n$ is a distinguished basis of $\pi_1(\mathbb{C} \setminus \{c_1, \ldots, c_n\}, b)$, the braid σ_i acts by a *Hurwitz move* which sends $\ell_1, \ldots, \ell_n$ to the distinguished basis

$$\ell_1, \ldots, \ell_{i-1},\ \ell_{i+1},\ \ell_{i+1}\ell_i\ell_{i+1}^{-1},\ \ell_{i+2}, \ldots, \ell_n\,; \tag{10.5}$$

similarly, σ_i^{-1} sends it to

$$\ell_1, \ldots, \ell_{i-1},\ \ell_i^{-1}\ell_{i+1}\ell_i,\ \ell_i,\ \ell_{i+2}, \ldots, \ell_n\,. \tag{10.6}$$

This is depicted in Fig. 10.1. In particular, one may see that braids preserve the product $\ell_n\ell_{n-1}\cdots\ell_1$. Furthermore, a simple loop ℓ_i is always sent to the conjugate $\rho^{-1}\ell_j\rho$ of another simple loop. In fact, this characterises the automorphisms of the fundamental group that come from braids.

Lemma 65 (Artin, 1947, Theorem 15)**.** *An automorphism f of the free group F_n on n elements $\ell_1, \ldots, \ell_n$ comes from a braid if an only if*

- *$f(\ell_i)$ is conjugate to some $f(\ell_j)$ for $i = 1, \ldots, n$;*
- *$f(x_n \ldots x_1) = x_n \ldots x_1$.*

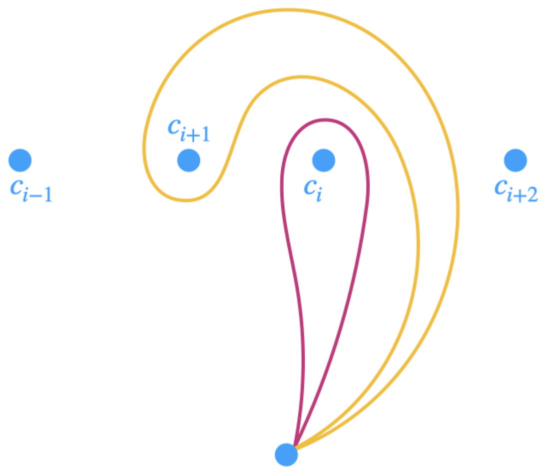

Figure 10.1: *The generator σ_i acts on $\pi_1(\mathbb{C} \setminus \{c_1, \ldots, c_n\}, b)$ by transposing c_i and c_{i+1} anticlockwise. This distorts the simple loops around c_i and c_{i+1} in the way depicted in this figure. The simple loops around the other critical values are unchanged.*

10.1.1 Action on monodromy representation

The idea is the following. We recall the notations of Chapter 4. Let $\mathcal{Y} \subset \mathbb{P}^N \times \mathbb{P}^1$ be such that the projection $\mathcal{Y} \to \mathbb{P}^1$ is a fibration by complete intersections. Denote by Σ its set of critical values and choose a basepoint $b \notin \Sigma$. The fibre $\mathcal{X}_t$ above a generic value $t \notin \Sigma$ is itself a projective variety in $\mathbb{P}^N$. We choose a pencil of hyperplanes $\{H_u\}_{u\in\mathbb{P}^1}$ of $\mathbb{P}^N$ and obtain, after taking the modification $\mathcal{Y}_t$ of $\mathcal{X}_t$, a fibration $g_t : \mathcal{Y}_t \to \mathbb{P}^1$. Denote by Σ_t critical values of g_t. Finally, choose a point $b' \notin \Sigma_b$.

Lemma 66. *Σ_t is the set of roots in u of a polynomial $p(t,u)$, of which the coefficients are polynomials in t.*

Definition 39. *Let* Crit *be the union of the set of roots of the discriminant* $\mathrm{discr}_u\, p(t,u)(u-b')$ *of $p(t,u)(u-b')$ and of the leading coefficient of p. In particular, $p(t,u)$ has precisely $r = \deg_u p$ roots whenever $t \notin$* Crit*, and b' is never a critical value of $\mathcal{X}_t \to \mathbb{P}^1$.*

In particular when $t \notin \mathrm{Crit}$, then Σ_t defines a configuration in $\mathbb{C}_n$. Thus, if $\ell : [0,1] \to \mathbb{P}^1 \setminus \mathrm{Crit}$ is a loop pointed at b, it lifts to an element of the fundamental group of C_n, and thus induces a braid $\sigma \in A_n$.

From this braid we may recover the monodromy action on extensions by the following observation. Let $\ell \in \pi_1(\Sigma_b, b')$ and $\gamma \in H_{n-2}(\mathcal{X}_{bb'})$, so that $\tau_\ell(\gamma)$ defines a relative homology class in $H_{n-1}(\mathcal{Y}_b)$, where $\mathcal{Y}_b$ is the modification of $\mathcal{X}_b$. Fix a representative $w : [0,1] \to \mathbb{P}^1 \setminus \Sigma_b$, $w(0) = w(1) = b'$ of ℓ. Then w also defines a map to $\mathbb{P}^1 \setminus \Sigma_t$ for t sufficiently close to b.

Thus if ℓ' is a path connecting b to t, ℓ' induces a map

$$\pi_1(\mathbb{P}^1 \setminus \Sigma_b, b') \to \pi_1(\mathbb{P}^1 \setminus \Sigma_t, b')\,. \tag{10.7}$$

By iterating this step and deforming the representatives w to stay away from Σ_t, we find that a loop $\ell' \in \pi_1(\mathbb{P}^1 \setminus \mathrm{Crit}, b)$ induces a homomorphism

$$\ell'_* : \pi_1(\mathbb{P}^1 \setminus \Sigma_b, b') \to \pi_1(\mathbb{P}^1 \setminus \Sigma_b, b')\,. \tag{10.8}$$

Similarly to Chapter 2, the map $(\mathcal{Y} \cap H_{b'} \times \mathbb{P}^1) \to \mathbb{P}^1 \setminus \mathrm{Crit}$ is a locally trivial fibration by Ehresmann's lemma, and the fibre above t is $\mathcal{X}_{tu}$. In particular ℓ' also induces a monodromy action.

$$\ell'_* : H_{n-2}(\mathcal{X}_{bb'}) \to H_{n-2}(\mathcal{X}_{bb'})\,. \tag{10.9}$$

Lemma 67. *ℓ' induces a monodromy action ℓ'_* on extensions of $\mathcal{X}_b \to \mathbb{P}^1$, given by the formula*

$$\ell'_*(\tau_\ell(\gamma)) = \tau_{\ell'_*\ell}(\ell'_*\gamma)\,. \tag{10.10}$$

Similarly, the monodromy along $\ell'_*\ell$ is given by the equation

$$(\ell'_*\ell)_*\,(\gamma) = \ell'_*(\ell_*({\ell'_*}^{-1}\gamma))\,. \tag{10.11}$$

Remark 68. *One may check the compatibility of these formulae, i.e., that monodromy and extensions* commute *(in a broad sense) with the monodromy along ℓ'.*

In the case of hypersurfaces, we may simplify this expression by choosing a convenient hyperplane pencil $\{H_u\}_{u\in\mathbb{P}^1}$. Concretely, recall that the fibre of the modification $\mathcal{Y}$ above t is given by $\mathcal{X} \cap H'_t$ for a pencil of hyperplanes $\{H'_t\}_{t\in\mathbb{P}^1}$ in $\mathbb{P}^{N+1}$. Then we may choose $\{H_u\}_{u\in\mathbb{P}^1}$ to be such that $H_{b'}$ is the axis $H_{b'} = A$ of $\{H'_t\}_{t\in\mathbb{P}^1}$ in $H'_t \simeq \mathbb{P}^1$. Then for all t,

$$\mathcal{X}_{bb'} = \mathcal{X}'\,, \tag{10.12}$$

where $\mathcal{X}' = \mathcal{X} \cap A$ is the exceptional locus. In particular, this implies that the action of monodromy along ℓ' on $H_{n-2}(\mathcal{X}_{bb'})$ is trivial.

In general, we may deduce the action of ℓ' on $H_{n-2}(\mathcal{X}_{bb'})$ from its action on $\pi_1(\mathbb{P}^1 \setminus \Sigma_b)$ up to sign, because of Schur's lemma. Indeed (10.11) tells us that up to a change of basis, the monodromy representations $\ell \mapsto \ell_*$ and $\ell \mapsto (\ell'_*\ell)_*$ are the same. The former is given as input data and the latter can be computed using (2.2), assuming we know a representation of $\ell'_*\ell$ in the basis of $\pi_1(\mathbb{P}^1 \setminus \Sigma_b, b')$. Such a representation can be obtained from the braids induced by the movement of Σ_t as t moves along ℓ', using (10.5), (10.5) and (2.2).

10.1.2 Link to parabolic cohomology

The methods presented here are not fundamentally new. In the dual setting of the cohomology, algorithms for computing the *parabolic cohomology* of a variation of local systems were already given in Dettweiler and Wewers (2006a, 2006b). In fact the parabolic cohomology coincides precisely with the lattice of extensions of $\mathcal{X}$ introduced in. The difference is that instead of considering n-cycles, they consider n-cocycles given by $\langle \gamma, \cdot \rangle : H_n(\mathcal{X}) \to \mathbb{Z}$. One may check that the spaces E_g and H_g in Dettweiler and Wewers (2006b, Section 1.2) coincide with respectively the combination of thimbles that are extensions around infinity, and combinations of thimbles without boundaries. In particular, the space $W_g = H_g/E_g$ coincides with $\mathcal{T}(\mathcal{Y})$.

10.2 Computing braids

We now provide an algorithm for computing braids. Let $P(u,t)$ be a bivariate polynomial of degree n in u, define Crit as above, and let ℓ be a loop in $\mathbb{C} \setminus \mathrm{Crit}$. We assume we are able to track the roots in u of P as t: that is, for every $t \in [0,1]$, we are able to compute a tuple $(c_1(t), \ldots, c_n(t)) \in \mathbb{C}^n$ such that

- $P(\ell'(t), c_i) = 0$ for all i and
- c_i it continuous.

Such paths may be computed in a certified manner with software such as SIROCO (Marco-Buzunariz & Rodríguez, 2016), or more recently Guillemot and Lairez (2024).

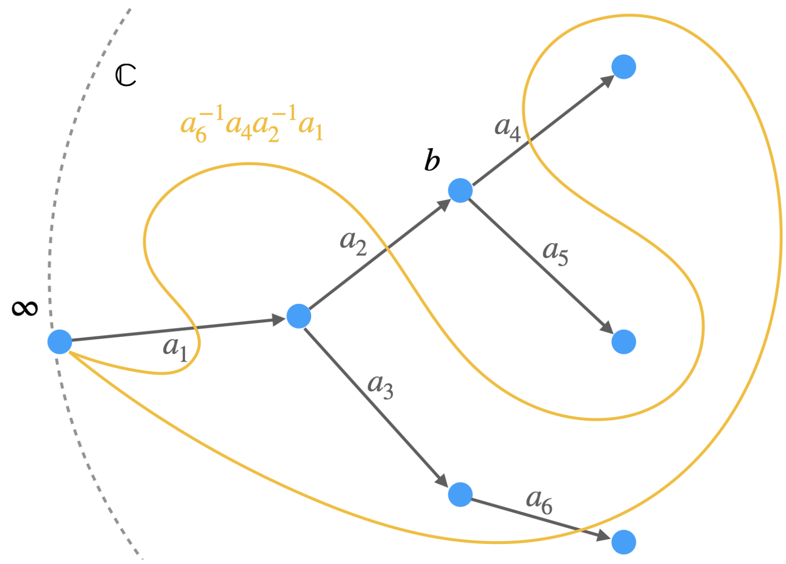

Figure 10.2: *The representation of elements of the fundamental group $\pi(\mathbb{C} \setminus \Sigma_b \cup \{b'\})$ in terms of the edges of a tree. The orange loop intersects the edge a_6, then a_4, then a_2 and finally a_1 and loops back to b. Its homotopy class thus corresponds to the word $a_6^{-}1a_4a_2^{-1}a_1$. The powers keep track of the orientation of the intersection.*

We then compute the braids by computing their action on the fundamental group of $\mathbb{C} \setminus \Sigma_b$. More precisely, let T be a minimal covering tree of $\Sigma_b \cup \{b', \infty\}$, such that ∞ is a leaf. We label the edges of T by letters $a_1, \ldots, a_{n+1}$ of the free group F_{n+1} on $n+1$ elements. Furthermore we choose an orientation of the edges. We can do so canonically by orienting the edges away from

∞ Then every element of $\pi_1(\mathbb{C} \setminus \Sigma_b, \infty)$ can represented by a word in F_{n+1}, the letters of which correspond to the edges of T it intersects. This is schematized in Fig. 10.2.

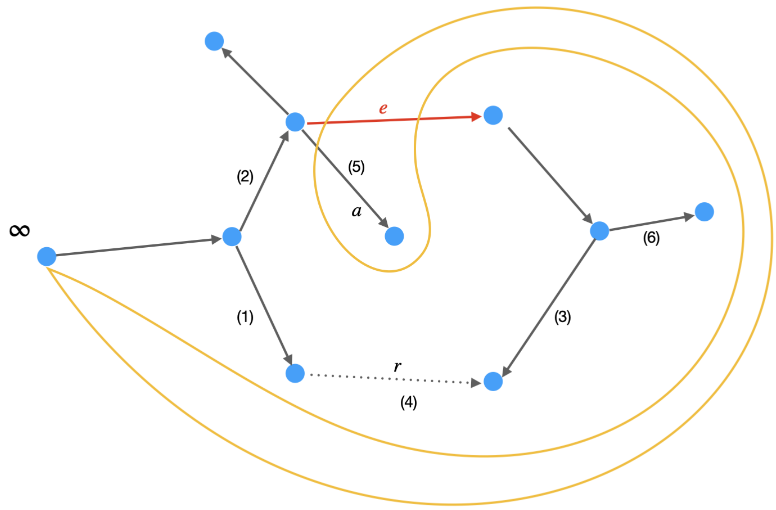

Figure 10.3: *The change of the topology of a minimal tree. Adding the red edge creates a cycles, and the edges of the old tree may have 6 possible configurations with respect to that cycle. Note that the orientation of the edges on the right changes when replacing the dotted edge by the red one. As an example if we consider the loop represented by the edge a in the old tree, its corresponding homotopy class is the orange loop, and the word of this homotopy class in the new tree is* eae^{-1}

Then, as the points of Σ_b move around, the graph will move accordingly, and will eventually no longer be minimal. When this happens, we get rid of the long edges and add shorter edges to recover yet again a minimal graph. We do this in steps, removing and adding only one edge at a time. In particular, adding an edge creates a cycle in the graph. In order to compute the braiding action, we need to keep track of how the homotopy classes represented by $a_1, \ldots, a_{n+1}$ vary with the modification of the topology of the graph. There are 6 possible configurations that one should consider with respect to the created cycles, which are depicted in Fig. 10.3. Let T^- be T with the edge removed, T^+ with the edge added and C the cycle of T^+. The configurations are characterised by

1. The edge is in C, in the same component of T^- as ∞, after the point closest to ∞ when going clockwise.
2. The edge is in C, is in the same component of T^- as ∞, before the point closest to ∞ when going clockwise.
3. The edge is in C, is in the component of T^- not containing ∞.
4. The edge is the one being removed.
5. The edge is not in C, and contained in the component of $\mathbb{P}^1 \setminus C$ not containing ∞.
6. The edge is not in C, and contained in the component of $\mathbb{P}^1 \setminus C$ containing ∞.

Furthermore, depending on the orientation of the cycle (when going clockwise from the point closest to ∞, do we encounter first the edge that gets removed or the one that gets added?) the transformation rules also differ. Denote by e the edge that is added and by r the edge that is removed. Then, when removing r and adding e in Fig. 10.3, the transformation rules in the six different cases are given by:

1. $a \mapsto ae$
2. $a \mapsto e^{-1}a$
3. $a \mapsto a^{-1}e$
4. $r \mapsto e$
5. $a \mapsto e^{-1}ae$
6. $a \mapsto a$

When removing e and adding r, the transformation rules are:

1. $a \mapsto ar^{-1}$
2. $a \mapsto ra$
3. $a \mapsto ra^{-1}$
4. $e \mapsto r$
5. $a \mapsto rar^{-1}$
6. $a \mapsto a$

By computing these graphs for points along the path ℓ' and tracking the way their topology changes, assuming the steps are small enough, we are able to recover the action of monodromy along ℓ' on $\pi_1(\mathbb{P}^1 \setminus \Sigma_b \cup \{b\}, \infty)$. To recover the action of $\pi_1(\mathbb{P}^1 \setminus \Sigma_b, b')$, it is sufficient to find how monodromy along ℓ' affects a path connecting ∞ to b'. This can be read from the action of monodromy along ℓ' on a simple loop $\ell_{b'} \in \pi_1(\mathbb{P}P^1 \setminus \Sigma_b \cup \{b'\}, \infty)$ around b'. Indeed, braids act by conjugation on simple loops, and therefore we have that

$$\ell'_* \ell_{b'} = \sigma^- 1 \ell_{b'} \sigma \tag{10.13}$$

for a certain $\sigma \in \pi_1(\mathbb{P}^1 \setminus \Sigma_b)$, and we have that a path p connecting ∞ to b' is deformed to $p\sigma^{-1}$.

Puting all of this together, we are able to recover the action of monodromy of $\pi_1(\mathbb{P}^1 \setminus \Sigma, b)$ on $\pi_1(\mathbb{P}^1 \setminus \Sigma_b, b')$ described in Section 10.1.1, which in turns allows to recover the action of monodromy on $H_n(\mathcal{X}_b, \mathcal{X}')$

Bibliography

Artebani, M., Sarti, A., & Taki, S. (2011). K3 surfaces with non-symplectic automorphisms of prime order. With an appendix by Shigeyuki Kondō. *Mathematische Zeitschrift*, *268*(1-2), 507–533. https://doi.org/10.1007/s00209-010-0681-x

Artin, E. (1947). Theory of braids. *Annals of Mathematics. Second Series*, *48*, 101–126. https://doi.org/10.2307/1969218

Beilinson, A. A. (1985). Higher regulators and values of L-functions. *Journal of Soviet Mathematics*, *30*, 2036–2070. https://doi.org/10.1007/BF02105861

Beukers, F., & Peters, C. a. M. (1984). A family of K3 surfaces and $\zeta(3)$. *1984*(351), 42–54. https://doi.org/10.1515/crll.1984.351.42

Birch, B. J., & Swinnerton-Dyer, H. P. F. (1965). Notes on elliptic curves. II. *Journal für die Reine und Angewandte Mathematik*, *218*, 79–108. https://doi.org/10.1515/crll.1965.218.79

Bloch, S., Esnault, H., & Kreimer, D. (2006). On Motives Associated to Graph Polynomials. *Communications in Mathematical Physics*, *267*(1), 181–225. https://doi.org/10.1007/s00220-006-0040-2

Bloch, S., Kerr, M., & Vanhove, P. (2015). A Feynman integral via higher normal functions. *Compositio Mathematica*, *151*(12), 2329–2375. https://doi.org/10.1112/S0010437X15007472

Booker, A. R., Sijsling, J., Sutherland, A. V., Voight, J., & Yasaki, D. (2016). A database of genus-2 curves over the rational numbers. *LMS Journal of Computation and Mathematics*, *19*(A), 235–254. https://doi.org/10.1112/S146115701600019X

Bostan, A., Lairez, P., & Salvy, B. (2013). Creative telescoping for rational functions using the griffiths: Dwork method. *Proceedings of the 38th International Symposium on Symbolic and Algebraic Computation*, 93–100. https://doi.org/10.1145/2465506.2465935

Bourjaily, J. L., McLeod, A. J., Vergu, C., Volk, M., von Hippel, M., & Wilhelm, M. (2020). Embedding Feynman integral (Calabi-Yau) geometries in weighted projective space. *Journal of High Energy Physics*, *2020*(1), 78. https://doi.org/10.1007/JHEP01(2020)078

Bourjaily, J. L., McLeod, A. J., von Hippel, M., & Wilhelm, M. (2019). Bounded Collection of Feynman Integral Calabi-Yau Geometries. *Physical Review Letters*, *122*(3), 031601. https://doi.org/10.1103/PhysRevLett.122.031601

Bouyer, F. (2018). The Picard group of various families of $(\mathbb{Z}/2\mathbb{Z})^4$-invariant quartic K3 surfaces. *Acta Arithmetica*, *186*, 61–86. https://doi.org/10.4064/aa170718-7-3

Brieskorn, E. (1966). Über die Auflösung gewisser Singularitäten von holomorphen Abbildungen. *Mathematische Annalen*, *166*(1), 76–102. https://doi.org/10.1007/BF01361440

Brown, F. (2017). Feynman amplitudes, coaction principle, and cosmic Galois group. *Communications in Number Theory and Physics*, *11*(3), 453–556. https://doi.org/10.4310/CNTP.2017.v11.n3.a1

Bruin, N., Sijsling, J., & Zotine, A. (2019). Numerical computation of endomorphism rings of Jacobians. *The Open Book Series*, *2*(1), 155–171. https://doi.org/10.2140/obs.2019.2.155

Cadavid, C. A., & Vélez, J. D. (2009). Normal factorization in $\mathrm{SL}(2, \mathbb{Z})$ and the confluence of singular fibers in elliptic fibrations. *Beiträge zur Algebra und Geometrie*, *50*(2), 405–423.

Candelas, P., de la Ossa, X., Elmi, M., & van Straten, D. (2020). A one parameter family of Calabi-Yau manifolds with attractor points of rank two. *Journal of High Energy Physics*, *2020*(10), 74. https://doi.org/10.1007/JHEP10(2020)202

Candelas, P., de la Ossa, X., & van Straten, D. (2021). Local Zeta Functions From Calabi-Yau Differential Equations. https://doi.org/10.48550/arXiv.2104.07816

Carlson, J., Müller-Stach, S., & Peters, C. (2017). *Period Mappings and Period Domains* (2nd ed.). Cambridge University Press. https://doi.org/10.1017/9781316995846

Chudnovsky, D. V., & Chudnovsky, G. V. (1989). Transcendental methods and theta-functions. In L. Ehrenpreis & R. Gunning (Eds.), *Proceedings of Symposia in Pure Mathematics* (pp. 167–232). American Mathematical Society. https://doi.org/10.1090/pspum/049.2/1013173

Chudnovsky, D. V., & Chudnovsky, G. V. (1990). Computer Algebra in the Service of Mathematical Physics and Number Theory. In *Computers in Mathematics*. CRC Press.

Clingher, A., Doran, C. F., Lewis, J., & Whitcher, U. (2009). Normal forms, K3 surface moduli, and modular parametrizations. In *Groups and symmetries. From Neolithic Scots to John McKay. Selected papers of the conference, Montreal, Canada, April 27–29, 2007.* (pp. 81–98). American Mathematical Society (AMS).

Costa, E., Mascot, N., Sijsling, J., & Voight, J. (2019). Rigorous computation of the endomorphism ring of a Jacobian. *Mathematics of Computation*, *88*(317), 1303–1339. https://doi.org/10.1090/mcom/3373

Costa, E., & Sertöz, E. C. (2021). Effective obstruction to lifting Tate classes from positive characteristic.

Cox, D., & Katz, S. (1999). *Mirror Symmetry and Algebraic Geometry* (Vol. 68). American Mathematical Society. https://doi.org/10.1090/surv/068

Cucker, F., Krick, T., & Shub, M. (2018). Computing the homology of real projective sets. *Foundations of Computational Mathematics*, *18*(4), 929–970. https://doi.org/10/gd2sm7

Cynk, S., & van Straten, D. (2019). Periods of rigid double octic Calabi–Yau threefolds. *Annales Polonici Mathematici*, *123*, 243–258. https://doi.org/10.4064/ap180608-23-10

Deconinck, B., & van Hoeij, M. (2001). Computing Riemann matrices of algebraic curves. *Physica D: Nonlinear Phenomena*, *152–153*, 28–46. https://doi.org/10.1016/S0167-2789(01)00156-7

Deligne, P. (1979). Values of L-functions and periods of integrals
Published: Automorphic forms, representations and L-functions, Proc. Symp. Pure Math. Am. Math. Soc., Corvallis/Oregon 1977, Proc. Symp. Pure Math. 33, No. 2, 313-346 (1979).

de Rham, G. (1931). Sur l'analysis situs des variétés à n dimensions. *Journal de Mathématiques Pures et Appliquées. Neuvième Série*, *10*, 115–200.

Dettweiler, M., & Wewers, S. (2006a). Variation of local systems and parabolic cohomology. *Israel Journal of Mathematics*, *156*, 157–185. https://doi.org/10.1007/BF02773830

Dettweiler, M., & Wewers, S. (2006b). Variation of parabolic cohomology and Poincaré duality. In *Groupes de Galois arithmétique et différentiels* (pp. 145–164). Société Mathématique de France.

Di Rocco, S., Eklund, D., & Gäfvert, O. (2020). Sampling and homology via bottlenecks.

Dokchitser, T., de Jeu, R., & Zagier, D. (2006). Numerical verification of beilinson's conjecture for K_2 of hyperelliptic curves. *Compositio Mathematica*, *142*(2), 339–373. https://doi.org/10.1112/S0010437X05001892

Dolgachev, I. V. (1996). Mirror symmetry for lattice polarized K3 surfaces. *Journal of Mathematical Sciences (New York)*, *81*(3), 2599–2630. https://doi.org/10.1007/BF02362332

Dolgachev, I. (1982). Weighted projective varieties. In J. B. Carrell (Ed.), *Group Actions and Vector Fields* (pp. 34–71). Springer Berlin Heidelberg. https://doi.org/10.1007/BFb0101508

Donagi, R. (1983). Generic torelli for projective hypersurfaces.

Doran, C. F., Harder, A., Katzarkov, L., Ovcharenko, M., & Przyjalkowski, V. (2023). Modularity of Landau-Ginzburg models.

Doran, C. F., Harder, A., Pichon-Pharabod, E., & Vanhove, P. (2023). Motivic geometry of two-loop Feynman integrals.

Doran, C. F., & Kostiuk, J. (2023). Geometric variations of local systems and elliptic surfaces. *Israel Journal of Mathematics*, *258*(1), 1–79. https://doi.org/10.1007/s11856-023-2466-z

Doran, C. F., Prebble, J., & Thompson, A. (2023). Normal Forms and Tyurin Degenerations of K3 Surfaces Polarised by a Rank 18 Lattice.

Ehresmann, C. (1951). Les connexions infinitésimales dans un espace fibré différentiable Published: Centre Belge Rech. Math., Colloque Topologie, Bruxelles, du 5 au 8 juin 1950, 29-55 (1951).

Elkies, N. D., & Klagsbrun, Z. (2020). New rank records for elliptic curves having rational torsion. In *ANTS XIV. Proceedings of the fourteenth algorithmic number theory symposium, Auckland, New Zealand, virtual event, June 29 – July 4, 2020* (pp. 233–250). Mathematical Sciences Publishers (MSP). https://doi.org/10.2140/obs.2020.4.233

Elsenhans, A.-S., & Jahnel, J. (2022). Real and complex multiplication on K3 surfaces via period integration.

Esole, M. (2017). Introduction to Elliptic Fibrations. In A. Cardona, P. Morales, H. Ocampo, S. Paycha, & A. F. Reyes Lega (Eds.), *Quantization, Geometry and Noncommutative Structures in Mathematics and Physics* (pp. 247–276). Springer International Publishing. https://doi.org/10.1007/978-3-319-65427-0_7

Ferguson, H., & Bailey, D. (1992). A Polynomial Time, Numerically Stable Integer Relation Algorithm.

Fité, F., Kedlaya, K. S., Rotger, V., & Sutherland, A. V. (2012). Sato-Tate distributions and Galois endomorphism modules in genus 2. *Compositio Mathematica*, *148*(5), 1390–1442. https://doi.org/10.1112/S0010437X12000279

Frobenius, G. (1873). Über die Integration der linearen Differentialgleichungen durch Reihen. *1873*(76), 214–235. https://doi.org/10.1515/crll.1873.76.214

Giovenzana, L., & Thompson, A. (2024). Degenerations and Fibrations of K3 Surfaces: Lattice Polarisations and Mirror Symmetry.

Giusti, M., Lecerf, G., & Salvy, B. (2001). A Gröbner free alternative for polynomial system solving. *Journal of Complexity*, *17*(1), 154–211. https://doi.org/10.1006/jcom.2000.0571

Golyshev, V. (2023). On L-derivatives and biextensions of calabi-yau motives.

Golyshev, V., & Van Straten, D. (2023). Congruences via fibered motives. *Pure and Applied Mathematics Quarterly*, *19*(1), 233–265. https://doi.org/10.4310/PAMQ.2023.v19.n1.a9

Griffiths, P. A. (1969). On the Periods of Certain Rational Integrals: I. *Annals of Mathematics*, *90*(3), 460–495. https://doi.org/10.2307/1970746

Griffiths, P., & Harris, J. (1978). Principles of algebraic geometry Published: Pure and Applied Mathematics. A Wiley-Interscience Publication. New York etc.: John Wiley & Sons. XII, 813 p. £ 29.60; $ 58.00 (1978).

Griffiths, P. A. (1968). Periods of Integrals on Algebraic Manifolds, I. (Construction and Properties of the Modular Varieties). *American Journal of Mathematics*, *90*(2), 568–626. https://doi.org/10.2307/2373545

Grothendieck, A. (1966). On the de rham cohomology of algebraic varieties. *Publications Mathématiques de l'Institut des Hautes Études Scientifiques*, *29*(1), 95–103. https://doi.org/10.1007/BF02684807

Guillemot, A., & Lairez, P. (2024). Validated numerics for algebraic path tracking.

Haraoka, Y. (2020). *Linear Differential Equations in the Complex Domain: From Classical Theory to Forefront* (Vol. 2271). Springer International Publishing. https://doi.org/10.1007/978-3-030-54663-2

Harder, A., & Thompson, A. (2015). The Geometry and Moduli of K3 Surfaces. https://doi.org/10.1007/978-1-4939-2830-9_1

Hartshorne, R. (1977). *Algebraic geometry* (Vol. 52). Springer, Cham.

Hashimoto, K. (2012). Finite symplectic actions on the K3 lattice. *Nagoya Mathematical Journal*, *206*, 99–153. https://doi.org/10.1215/00277630-1548511

Håstad, J., Just, B., Lagarias, J. C., & Schnorr, C. P. (1989). Polynomial time algorithms for finding integer relations among real numbers. *SIAM Journal on Computing*, *18*(5), 859–881. https://doi.org/10.1137/0218059

Hatcher, A. (2002). *Algebraic topology*. Cambridge University Press.

Heal, K., Kulkarni, A., & Sertöz, E. C. (2022). Deep learning Gauss-Manin connections. *Advances in Applied Clifford Algebras*, *32*(2), 41. https://doi.org/10.1007/s00006-022-01207-1

Herfurtner, S. (1991). Elliptic surfaces with four singular fibres. *Mathematische Annalen*, *291*(2), 319–342. https://doi.org/10.1007/BF01445211

Hirzebruch, F. (1956). Der Satz von Riemann-Roch in Faisceau-theoretischer Formulierung: Einige Anwendungen und offene Fragen.

Huybrechts, D. (2016). *Lectures on K3 Surfaces* (1st ed.). Cambridge University Press. https://doi.org/10.1017/CBO9781316594193

Iitaka, S. (1967). *On the degenerates of a normally polarized abelian variety of dimension 2 and an algebraic curve of genus 2 (in japanese)* (Doctoral dissertation). University of Tokyo.

Kanazawa, A. (2017). Doran-Harder-Thompson conjecture via SYZ mirror symmetry: Elliptic curves. *SIGMA. Symmetry, Integrability and Geometry: Methods and Applications*, *13*, paper 024, 13. https://doi.org/10.3842/SIGMA.2017.024

Kapustka, G., & Kapustka, M. (2009). Fiber products of elliptic surfaces with section and associated Kummer fibrations. *International Journal of Mathematics*, *20*(4), 401–426. https://doi.org/10.1142/S0129167X09005339

Katz, N. M., & Oda, T. (1968). On the differentiation of De Rham cohomology classes with respect to parameters. *Journal of Mathematics of Kyoto University*, *8*(2), 199–213. https://doi.org/10.1215/kjm/1250524135

Kauers, M., Jaroschek, M., & Johansson, F. (2015). Ore Polynomials in Sage. In J. Gutierrez, J. Schicho, & M. Weimann (Eds.), *Computer Algebra and Polynomials: Applications of Algebra and Number Theory* (pp. 105–125). Springer International Publishing. https://doi.org/10.1007/978-3-319-15081-9_6

Kodaira, K. (1963). On compact analytic surfaces. III. *Annals of Mathematics. Second Series*, *78*, 1–40. https://doi.org/10.2307/1970500

Kondo, S. (1985). Type II degeneration of K3 surfaces. *Nagoya Mathematical Journal*, *99*, 11–30. https://doi.org/10.1017/S0027763000021462

Kostiuk, J. (2018). Geometric Variations of Local Systems.

Kulikov, V. S. (1977). Degenerations of K3 surfaces and Enriques surfaces. *Mathematics of the USSR. Izvestiya*, *11*, 957–989. https://doi.org/10.1070/IM1977v011n05ABEH001753

Lairez, P., Pichon-Pharabod, E., & Vanhove, P. (2024). Effective homology and periods of complex projective hypersurfaces.

Lairez, P., & Sertöz, E. C. (2019). A Numerical Transcendental Method in Algebraic Geometry: Computation of Picard Groups and Related Invariants. *SIAM Journal on Applied Algebra and Geometry*, *3*(4), 559–584. https://doi.org/10.1137/18M122861X

Lamotke, K. (1981). The topology of complex projective varieties after S. Lefschetz. *Topology*, *20*(1), 15–51. https://doi.org/10.1016/0040-9383(81)90013-6

Landman, A. (1973). On the Picard-Lefschetz Transformation for Algebraic Manifolds Acquiring General Singularities. *Transactions of the American Mathematical Society*, *181*, 89–126. https://doi.org/10.2307/1996622

Lefschetz, S. (1924). *L'analysis situs et la géométrie algébrique*. Gauthier-Villars et cie.

Lenstra, A. K., Lenstra, H. W., & Lovász, L. (1982). Factoring polynomials with rational coefficients. *Mathematische Annalen*, *261*(4), 515–534. https://doi.org/10.1007/BF01457454

Lipman, J. (1969). Rational singularities, with applications to algebraic surfaces and unique factorization. *Publications mathématiques de l'IHÉS*, *36*(1), 195–279. https://doi.org/10.1007/BF02684604

Marco-Buzunariz, M. Á., & Rodríguez, M. (2016). SIROCCO: A Library for Certified Polynomial Root Continuation. In G.-M. Greuel, T. Koch, P. Paule, & A. Sommese (Eds.), *Mathematical Software – ICMS 2016* (pp. 191–197). Springer International Publishing. https://doi.org/10.1007/978-3-319-42432-3_24

Mather, J. (2012). Notes on Topological Stability. *Bulletin of the American Mathematical Society*, *49*(4), 475–506. https://doi.org/10.1090/S0273-0979-2012-01383-6

Mezzarobba, M. (2010). NumGfun: A package for numerical and analytic computation with D-finite functions. *Proceedings of the 2010 International Symposium on Symbolic and Algebraic Computation*, 139–145. https://doi.org/10.1145/1837934.1837965

Mezzarobba, M. (2016). Rigorous Multiple-Precision Evaluation of D-Finite Functions in SageMath. https://doi.org/10.48550/arXiv.1607.01967

Miranda, R. (1989). *The basic theory of elliptic surfaces. Notes of lectures.* ETS Editrice.

Moishezon, B. (1977). *Complex Surfaces and Connected Sums of Complex Projective Planes* (Vol. 603). Springer. https://doi.org/10.1007/BFb0063355

Molin, P., & Neurohr, C. (2019). Computing period matrices and the Abel-Jacobi map of superelliptic curves. *Mathematics of Computation*, *88*(316), 847–888. https://doi.org/10.1090/mcom/3351

Morse, M. (1929). The Foundations of the Calculus of Variations in the Large in m-Space (First Paper). *Transactions of the American Mathematical Society*, *31*(3), 379–404. https://doi.org/10.2307/1989523

Namikawa, Y., & Ueno, K. (1973). The complete classification of fibres in pencils of curves of genus two. *Manuscripta Mathematica*, *9*, 143–186. https://doi.org/10.1007/BF01297652

Naruki, I. (1987). On Confluence of Singular Fibers in Elliptic Fibrations. *Publications of the Research Institute for Mathematical Sciences*, *23*(2), 409–431. https://doi.org/10.2977/prims/1195176546

Narumiya, N., & Shiga, H. (2001). The mirror map for a family of K3 surfaces induced from the simplest 3-dimensional reflexive polytope. https://doi.org/10.1090/crmp/030/13

Neurohr, C. (2018). *Efficient integration on Riemann surfaces & applications* (Doctoral dissertation).

Nikulin, V. V. (1979). Finite automorphism groups of Kählerian surfaces of type K3. *Trudy Moskovskogo Matematicheskogo Obshchestva*, *38*, 75–137.

Niyogi, P., Smale, S., & Weinberger, S. (2008). Finding the homology of submanifolds with high confidence from random samples. *Discrete & Computational Geometry*, *39*(1), 419–441. https://doi.org/10/b7qcdg

Oaku, T., & Takayama, N. (1999). An algorithm for de Rham cohomology groups of the complement of an affine variety via D-module computation. *Journal of Pure and Applied Algebra*, *139*(1-3), 201–233. https://doi.org/10/dqgzc6

Ogg, A. P. (1966). On pencils of curves of genus two. *Topology*, *5*(4), 355–362. https://doi.org/10.1016/0040-9383(66)90027-9

Oguiso, K. (2012). Smooth quartic K3 surfaces and Cremona transformations, II. https://doi.org/10.48550/arXiv.1206.5049

Oguiso, K. (2017). Isomorphic Quartic K3 Surfaces in the View of Cremona and Projective Transformations. *Taiwanese Journal of Mathematics*, *21*(3), 671–688. https://doi.org/10.11650/tjm/7833

Orlov, D. (2009). Derived categories of coherent sheaves and triangulated categories of singularities. In *Algebra, arithmetic, and geometry. In honor of Y. I. Manin on the occasion of his 70th birthday. Vol. II* (pp. 503–531). Birkhäuser. https://doi.org/10.1007/978-0-8176-4747-6_16

Persson, U. (1977). *On degenerations of algebraic surfaces* (Vol. 189). American Mathematical Society (AMS). https://doi.org/10.1090/memo/0189

Persson, U., & Pinkham, H. (1981). Degeneration of Surfaces with Trivial Canonical Bundle. *Annals of Mathematics*, *113*(1), 45–66. https://doi.org/10.2307/1971133

Pham, F. (1965). Formules de Picard-Lefschetz généralisées et ramification des intégrales. *Bulletin de la Société Mathématique de France*, *93*, 333–367. https://doi.org/10.24033/bsmf.1628

Pichon-Pharabod, E. (2024). A semi-numerical algorithm for the homology lattice and periods of complex elliptic surfaces over the projective line.

Preparata, F. P., & Shamos, M. I. (1985). *Computational Geometry.* Springer. https://doi.org/10.1007/978-1-4612-1098-6

Przyjalkowski, V. V. (2017). Calabi-Yau compactifications of toric Landau-Ginzburg models for smooth Fano threefolds. *Sbornik: Mathematics*, *208*(7), 992–1013. https://doi.org/10.1070/SM8838

Sakalli, S., & Horn-Morris, J. V. (2023). Singular fibers in algebraic fibrations of genus 2 and their monodromy factorizations.

Schoen, C. (1988). On fiber products of rational elliptic surfaces with section. *Mathematische Zeitschrift*, *197*(2), 177–199. https://doi.org/10.1007/BF01215188

Schütt, M., & Shioda, T. (2010). Elliptic surfaces. In *Algebraic geometry in East Asia – Seoul 2008. Proceedings of the 3rd international conference "Algebraic geometry in East Asia, III", Seoul, Korea, November 11–15, 2008* (pp. 51–160). Mathematical Society of Japan.

Seidel, P. (2008). Fukaya Categories and Picard–Lefschetz Theory. https://doi.org/10.4171/063

Sertöz, E. C. (2019). Computing Periods of Hypersurfaces. *Mathematics of Computation*, *88*(320), 2987–3022. https://doi.org/10.1090/mcom/3430

Shiga, H. (1979). One attempt to the K3 modular function I. *Annali della Scuola Normale Superiore di Pisa - Classe di Scienze*, *6*(4), 609–635.

Stiller, P. (1987). The Picard numbers of elliptic surfaces with many symmetries. *Pacific Journal of Mathematics*, *128*(1), 157–189. https://doi.org/10.2140/pjm.1987.128.157

Swierczewski, C. (2017). Abelfunctions: A library for computing with Abelian functions, Riemann surfaces, and algebraic curves.

The Sage Developers. (2023). SageMath, the Sage Mathematics Software. https://doi.org/10/gr8dhc

Torelli, R. (1913). Sulle varietà di \emphJacobi. *Accademia dei Lincei, Rendiconti, V. Serie*, *22*(2), 98–103, 437–441.

Tretkoff, C. L., & Tretkoff, M. D. (1984). Combinatorial group theory, Riemann surfaces and differential equations. In *Contributions to group theory* (pp. 467–519). AMS. https://doi.org/10/fzq8bb

van der Hoeven, J. (1999). Fast evaluation of holonomic functions. *Theoretical Computer Science*, *210*(1), 199–215. https://doi.org/10.1016/S0304-3975(98)00102-9

Voisin, C. (2002). *Hodge theory and complex algebraic geometry. I. Translated from the French by Leila Schneps* (Vol. 76). Cambridge University Press.

Xiao, G. (1996). Galois covers between K3 surfaces. *Annales de l'institut Fourier*, *46*(1), 73–88. https://doi.org/10.5802/aif.1507

Yang, W. (2021). Deligne's conjecture and mirror symmetry. *Nuclear Physics B*, *962*, 115245. https://doi.org/10.1016/j.nuclphysb.2020.115245

Zarkhin, Y. G. (1983). Hodge groups of K3 surfaces. *Journal für die Reine und Angewandte Mathematik*, *341*, 193–220. https://doi.org/10.1515/crll.1983.341.193